Scuola di dottorato

Università DEGLI STUDI DI MILANO-BICOCCA

Department of Materials Science

PhD program in Materials Science and Nanotechnology Cycle XXXV

Curriculum in Materials Technology

NEW FUNCTIONALISATION APPROACHES OF LIGNOCELLULOSIC FEEDSTOCK TO OBTAIN NEW REINFORCING FILLERS TAILORED TO RUBBER COMPOUNDS

Ferruti Federica Maria Camilla

Registration number 860922

Industrial tutor: Dr. Luca Giannini

Supervisor: Prof. Luca Zoia

Coordinator: Prof. Marco Bernasconi

ACADEMIC YEAR 2021/2022

TABLE OF CONTENTS

ABBREVIATION LIST

Materials, reagents and solvents

Abbreviation	Meaning
6PPD	*N*-(1,3-dimethylbutyl)-N'-phenyl–1,4-benzenediamine
AC	acetone
AL	herbaceous alkaline lignin
APTES	(3-aminopropyl)triethoxysilane
BR	butadiene rubber
CB	carbon black
CBS	*N*-Cyclohexylbenzothiazol-2-sulphenamide
$Cr(acac)_3$	chromium-(III) acetylacetonate
DMSO	dimethyl sulfoxide
e-HNDI	*endo*-*N*-hydroxy-5-norbornene-2,3-carboximide
EA	ethyl acetate
ET	ethanol
G	guaiacyl unit
GlyIns	glycidylated insoluble fraction
GlySol	glycidylated soluble fraction
H	p-hydroxyphenyl unit
HW	hardwood lignin
HKL	hardwood kraft lignin
Ins	insoluble fraction
*i*PrOH	isopropanol
IR	synthetic polyisoprene rubber
KL	kraft lignin
LNPs	lignin nanoparticles
NR	natural rubber
S	syringyl unit
SBR	styrene-butadiene rubber
SKL	softwood kraft lignin
Sol	soluble fraction
SW	softwood lignin
TEMS	γ-methacryloyl propyl triethoxy silane
TESPD	bis(triethoxysilylpropyl)disulfide supported on CB
TESPT	bis[3-(triethoxysilyl)propyl]tetrasulphide
THF	tetrahydrofuran
VA	vinyl acetate
VM	vinyl methacrylate

Analytical techniques

Abbreviation	Meaning
FT-IR / ATR	Fourier Transform Infrared Spectroscopy / Attenuated Total Reflectance
DLS	Dynamic Light Scattering
GPC	Gel Permeation Chromatography
NMR	Nuclear Magnetic Resonance
RPA	Rubber Process Analyzer
SEM	Scanning Electron Microscopy

Parameters and units

Abbreviation	Meaning
CD	crosslink density
E-factor	environmental factor
e-HNDI	*endo*-*N*-hydroxy-5-norbornene-2,3-carboximide solution
E'	storage dynamic modulus
E"	loss dynamic modulus
G'	shear storage modulus
G"	shear loss modulus
G*	complex modulus
MH	moment highest referred to the torque
MH-ML	difference between moment highest and moment lowest
ML	moment lowest referred to the torque
Mn	number average molecular weight
Mw	weight average molecular weight
MW	molecular weight
PDI	polydispersity index
phr	parts per hundred rubber
T90	time needed by the torque to reach 90 % of the maximum value
tanδ	hysteresis, dumping factor
T_g	glass transition temperature
TS2	time taken by the torque to increase by 2 units above ML value

Institutes

Abbreviation	Meaning
ASTM	American Society of Testing Materials
ECHA	European Chemical Agency

SYNOPSIS

Rubber products are commonly employed in a wide variety of industries including tyre manufacturing, packaging, engineering and construction. The mechanical performances of rubber itself are unsatisfactory for the desired applications so their improvement is necessary. This enhancement is commonly obtained by vulcanisation and addition of reinforcing fillers in the elastomeric matrix. The former ensures the formation of a crosslinked polymeric network resulting in an improvement in elasticity. The latter is known to reinforce the rubber matrix by restricting its mobility.

The most popular reinforcing filler is carbon black.[1] However, its use is associated with health and environmental concerns. For this reason, many tyre manufacturers are concentrating their efforts in replacing carbon black with more sustainable alternatives. In this regard, Pirelli has set its sustainability goals to minimise impacts on people and environment while maximising performances.[2] Their ambitions include the increment of renewable materials and the simultaneous reduction of fossil-based compounds in tyre formulations. In this frame, the present research project dealt with the development of sustainable reinforcing fillers for rubber compounds in alternative to fossil-based technologies with a particular focus on lignin. Lignocellulosic feedstocks are the most abundant biomass on Earth and their use is going to play a crucial role in the transition to a biobased economy. The valorisation of this resource is particularly challenging when it comes to lignin. The term *lignin* identifies a class of aromatic biopolymers with heterogenous structures depending on the botanical source and isolation process. Of particular relevance is the kraft process which is responsible for about 85% of the world lignin production. Despite its availability at industrial scale, the structural complexity of this isolated, *i.e.*, technical lignin has hampered its conversion into value-added products and the rational design of functional materials. However, the concerns about toxicity and environmental concerns related to the use of fossil-based materials are eliciting investigations regarding the use of renewable resources, including lignin(s). This material could be considered as a valid alternative to carbon black in rubber compounds due to its good physical-chemical and mechanical properties, comprising a high antioxidant activity and a useful thermal stability.[3] Its combination with an elastomeric matrix, however, requires overcoming the poor compatibility between the two materials related to the amphiphilic character of lignin, *i.e.*, both of natural and of isolated, technical lignins, which results into strong self-interactions. So, it was necessary to modify lignin in order to improve the number and quality of its interaction with rubber resulting in a reinforcing effect.[4,5] To ensure the desired reinforcement, two strategies were explored in the present work. The former dealt with the functionalisation of lignin hydroxyl groups ensuring the formation of covalent bonds between lignin and the rubber matrix during vulcanisation.[6] The latter consisted in the formulation of lignin into nanoparticles designed to exhibit unique properties due to their high surface to volume ratio. For both processes, it was necessary to both set up and scale up procedures to furnish consistent batches of lignin-based material suitable for the formulation of rubber compounds. The

dynamic-mechanical behavior of a variety of composites including modified lignin were assessed in order to explore the possibility to employ these systems in tyre formulations.

A novel methodology was set up for the functionalisation of isolated technical lignin aiming at its compatibilisation and binding with the rubber matrix. The procedure consisted in the mechanochemical esterification of lignin in the presence of a base as activator and enol ester as acyl donor. Mechanochemistry allowed running reactions in the absence of solvents, taking advantage of mechanical energy to trigger chemical transformations, avoiding organic solvents, limiting work-up procedures and reducing wastes with respect to wet chemistry syntheses. The use of an enol ester instead of more conventional acyl donors, *i.e.*, anhydrides and acyl chlorides, was associated to a high atom efficiency and the avoidance of halogenated reagents.[7] The driving force for the formation of the desired ester relied on the release of an enol as the leaving group which easily tautomerised to the corresponding ketoform, leaving no free nucleophile and making the reaction irreversible.[8] Different acyl donors were screened to select the most reactive ones and a variety of bases were investigated as activators for the reaction. Kraft lignin was selected for its high abundancy. The functionalised lignin was incorporated in different rubber compounds in partial or complete substitution of conventional fillers. The dynamo mechanical properties of these composites were assessed, along with their tensile behaviour.

The structural heterogeneity of lignin required a deeper investigation of its structure and a refinement. One of the most popular refinement of lignin structure into narrowly polydisperse portions relies on organic solvent extraction.[9] This technique allows for the isolation of fractions whose properties, including molecular weight distribution and functional group content, could be tuned as a function of the physicochemical characteristics of the solvent. An innovative analytic procedure combining GPC and fluorescence allowed assessing the homogeneity of phenolic distribution as a function of molecular weight in fractions isolated by solvent extraction. These analyses proved that the extraction procedure was effective in isolating groups of macromolecules which were homogeneous in terms of phenol distribution alongside the molecular weight ranges.[10]

A strategy to enhance the reinforcing effects of fillers in polymeric composites involves nanometric sizes. Nanomaterials are associated to higher surface-to-volume ratios than the corresponding micrometric counterpart. This feature allows for the immobilisation of a large portion of matrix which thus resists to mechanical solicitations and displays different behaviours than the bulk material.[11] Lignin nanoparticles (LNPs) were produced by a scalable procedure commonly referred to as solvent shifting.[12] Analytical investigations about solvent-extracted fractions guided the choice of specific lignin fractions for the development of LNPs with peculiar features. The innovative procedure allowed valorising the entire starting kraft lignin in a material efficient manner. It was possible to produce LNPs which proved dimensionally stable in a broad pH range 4.5-12.0 where lignin normally aggregates or dissolves.[13] The

same approach allowed preparing LNPs with a surface-specific covalent functionalisation, an achievement never attempted in literature, to the best of our knowledge. Surface-functionalised LNPs were employed for the development of performance-competitive adhesives for aminated glass surfaces, as such paving way for a new class of lignin-based functional materials. Both alkaline stable and surface-functionalised LNPs were included in rubber compounds to evaluate their reinforcing effects as unique fillers and in partial substitution of carbon black.

The thesis is outlined as follows.

The *Introduction* chapter offers a review of the background with a particular focus on tyre technology, needs for a transition to a biobased economy, lignocellulosic feedstock and strategies employed to valorise lignin as an alternative reinforcing filler for tyre compounds.

The *Experimental section* is devoted to the materials and methods employed during the experimental work for synthesis and characterisation of materials and data elaboration. The chapter was structured into different subsections describing: analytics of lignin-based materials; synthetic procedures for the mechanochemical modification of lignin; functionalisation and formulation of lignin nanoparticles; rubber compounding; characterisation of rubber composites.

The chapter dedicated to *Results and discussion* reports the findings of the investigation. This section included the study of: mechanochemical compatibilisation of lignin with rubber and evaluation of the effects on the mechanical performances of rubber composites; structural characteristics of softwood and hardwood kraft lignins and their fractions with a particular focus on phenolic group distribution as a function of molecular weight; synthesis and modification of lignin nanoparticles and evaluation of the effects on the mechanical performances of rubber nanocomposites.

The conclusive chapter sums up the main results and states the conclusion of the research.

References

[1] D. E. Hall, J. C. Moreland, *Rubber Chem. Technol.* **2001**, *74*, 525.

[2] Group Industrial Plan sustainability targets, .

[3] N. A. Mohamad Aini, N. Othman, M. H. Hussin, K. Sahakaro, N. Hayeemasae, *Front. Mater.* **2020**, *6*.

[4] P. Frigerio, L. Zoia, M. Orlandi, T. Hanel, L. Castellani, *BioResources* **2014**, *9*, 1387.

[5] D. Barana, S. D. Ali, A. Salanti, M. Orlandi, L. Castellani, T. Hanel, L. Zoia, *ACS Sustain. Chem. Eng.* **2016**, *4*, 5258.

[6] D. K. Setua, M. K. Shukla, V. Nigam, H. Singh, G. N. Mathur, *Polym. Compos.* **2000**, *21*, 988.

[7] M. Paravidino, U. Hanefeld, *Green Chem.* **2011**, *13*, 2651.

[8] F. A. Carey, R. J. Sundberg, *Advanced Organic Chemistry: Part A: Structure and Mechanisms*, Springer Science & Business Media, **2007**.

[9] A. Tagami, C. Gioia, M. Lauberts, T. Budnyak, R. Moriana, M. E. Lindström, O. Sevastyanova, *Ind. Crops Prod.* **2019**, *129*, 123.

[10] A. Salanti, M. Orlandi, H. Lange, F. Ferruti, L. Zoia, *ACS Sustain. Chem. Eng.* **2022**, *10*, 11680.

[11] A. Papon, K. Saalwächter, K. Schäler, L. Guy, F. Lequeux, H. Montes, *Macromolecules* **2011**, *44*, 913.

[12] S. Beisl, A. Miltner, A. Friedl, *Int. J. Mol. Sci.* **2017**, *18*, 1244.

[13] M. H. Sipponen, H. Lange, M. Ago, C. Crestini, *ACS Sustain. Chem. Eng.* **2018**, *6*, 9342.

INTRODUCTION

1 Tyres

1.1 Historical background

The first pneumatic tyre was patented by Robert Thomson in 1845. Unluckily, the first air-filled tyres lacked durability, so solid rubber tyres dominated the market until 1887, when John Boyd Dunlop patented a pneumatic tyre for bicycles, the most common vehicle of the time. Subsequently, pneumatic tyres became more and more popular thanks to technological improvements as reinforcement. In the so-called bias-ply tyres it was provided by a metal carcass embedded in the structure; in steel belted radial tyres it was afforded by steel along with nylon, rayon or polyester fibres (in 1948). Cross-ply tyres were outclassed by radial tyres which presented reduced heat build-up, lower rolling resistance and superior longevity. At the time, Michelin in France, Bridgestone in Japan, Pirelli in Italy, and Continental in Germany were the biggest radial tyre manufacturers. Because of its relatively high cost, this technology reached the U.S.A. only later, when the market demand had increased and its superiority in durability and gas mileage had become evident. [1]- [3]

In 1974, Pirelli introduced the wide radial tyre whose sidewalls reduced height could couple with the increasing power available on cars. [4]Further evolution in radial technology has allowed the development of contemporary automotive tyres which are used in a wide variety of vehicles including automobiles, trucks, buses, tractors, industrial vehicles, bicycles, motor bicycles, wheelchairs, and airplanes. In 2015 more than 3 billion tyres were produced, and the market is in expansion. [5] Independently on the possible evolutions in the transportation sector involving fuels, tyres are expected to go on being an essential component in vehicles. The increasing automobile demand and production by growing economies, especially in Asia, have been spurring producers to develop more sustainable solutions to face the growing need for raw materials, the environmental impact of manufacture and use along with the disposal of increasing amounts of exhausted products. Governments and companies are taking action toward technical and business model innovation in order to reduce environmental impact, especially lowering CO_2 emissions, waste production, water supply etc. and using renewable resources. [6], [7]

1.2 Functions, structure and components

Tyre structure has evolved during the years resulting in the highly engineered, complex product known today. Tyres are complex composites comprising a variety of components, each of them exerting a specific function. Tyres must provide manifold functions: load-carrying capacity, cushioning and dampening, steering response, cornering force, driving and braking torque transmission, dimensional

stability, abrasion resistance, minimum noise and vibration, and durability. All these mechanical properties are interrelated and finely tuneable by design: the decision to affect one parameter influences the others, either positively or negatively. [8]– [12]

Tyres are complex elastomer formulations comprising fibres, textiles, and steel cords. The structure of reinforcing fibers is described by the number, location, and dimensions of the various constituents used in their composition. Characteristics and performances of elastomer formulatons are determined by the nature of rubbers blended along with vulcanising agents, fillers, protective substances, and processing aids. Tyres performances can be evaluated considering three key parameters: the vehicle mission profile, mechanical properties and performances and, finally, aesthetics, comfort and behavioural features.

A pneumatic tyre comprises two main areas: tread, which is contact with the road, and casing, which supports the load and transmits power to tread. Both areas include manifold components, each of them contributing to the final properties of the tyre. Rubbery parts are composed of different elastomers blended with vulcanising agents, fillers, protective substances, and processing aids. In a radial tyre, these different rubber compounds act as a structural unit holding together all the components of tyre. Furthermore, they protect belts, steel or fabric breakers, steel beads, and textile, which provide the ultimate strength to the tyre. The so-called beads keep the tyre in position on the rim thus ensuring a stronger structure and better mechanical properties. [3] On top of the beads, there is a low-extensible belt which affords strength and protection to plies. Ply cords, either textile for passenger tyres or steel for truck tyres, extend from one bead to the other representing the primary reinforcing component of tyre casing. Above the belt, the tread comes into direct contact with the road so it must provide low rolling resistance, good wet skid, traction, abrasion resistance, cornering characteristics, high heat dissipation, and minimum generation of noise. Tread is usually a blend of natural rubber, styrene-butadiene rubber, and butadiene rubber compounded with silica, carbon black, vulcanising agents, and oils. The formulation of tread base is designed to afford low rolling resistance, good dissipation and good adhesion of tread with belts. Instead, tread shoulder (upper part of sidewalls) is responsible for the tread cornering performances and heat dissipation. Specific layers increase adhesion among all the tyre structural components. [13], [14]

1.3 Materials

Tyres include diverse constituents, each of them exerting a specific function. Tread compounds are designed to reduce rolling resistance and exalt abrasion resistance while offering excellent grip in dry and wet conditions, in a wide range of temperature. The use of blends of elastomers in the sidewalls must provide loading resistance and protection from environmental stresses. Innerliner compounds must abate

air loss. As a result, a tyre comprises many different rubber compounds, each of them formulated to afford specific features. Over 200 raw materials can be incorporated in a tyre but they can be grouped in a few main categories depending on their function: polymers, fillers, vulcanisation system, stabiliser system and special materials. [13] The most abundant fraction includes polymers, either synthetic or natural rubbers, which compose the matrix of compounds. [16] Rubber compounds show intriguing peculiar properties such as abrasion resistance, high elasticity, and damping features. An accurate selection of the rubber matrix can be coupled with the choice of suitable fillers in order to afford the final compound new properties such as impermeability, conductivity, etc., and, in the case of reinforcing fillers, better mechanical performances. [16] The features of the final compound depend not only on the nature of the filler used but also on its dispersion in and compatibility with the rubber matrix. Common fillers include carbon black, carbon nanotubes, silica, clay, and bio-nanofibers. [17]- [23] Other important components are vulcanising chemicals, responsible for the rate and efficiency of polymer crosslinking. Resins can be incorporated to promote adhesion between cords and rubber and improve reinforcement. Besides, antioxidants and antiozonants enhance stability, whereas plasticisers improve processability.

1.3.1 Polymers

Elastomers, commonly referred to as rubbers, are viscoelastic polymers able to regain their shape after deformation. They are composed of high molecular weight macromolecules connected either physically or chemically. The secret for shape recovery lies in the links among macromolecules which avoid macroscopic flow. Before the application of external forces, chains are randomly coiled in an equilibrium state of maximum entropy. Then, when an external force is applied to the specimen, macromolecules are uncoiled and align in the direction of the force, with a net loss of entropy. The presence of intermolecular links prevents macromolecules from slipping and allows the recovery of the original shape when the stress is released. [14] As a result, the polymer shows high elongation at break, high resilience, high elasticity, and low hardness. [16] The chemical structure of macromolecules influences the polymer physical properties. High molecular weights correspond to high entanglement degree and stiffness at high elongations. [24]– [26]

Restrictions in rotation along C-C single bonds along the polymer chain can cause increased stiffness, as occurs in polystyrene whose bulky side groups hinder bond rotation if compared to polyethylene. [28] Regular chemical structures result in a higher crystallinity. At high elongations, the alignment of polymer chains in the same direction as the applied force may induce increased crystallinity and, as a result, augmented stiffness. [29]- [31] Temperature changes influence thermal agitation and elastic properties of a

polymer: by decreasing temperature, stiffness increases until the polymer acquires a glassy state. Polymers experiment with augmented rigidity, hysteresis and internal viscosity at a temperature value referred to as glass transition temperature (T_g). The chemical structure of the polymer, in particular steric hindrance and number of side groups, influence T_g. To preserve rubbery-like macroscopic properties, elastomers must present a glass transition temperature (T_g) lower than working temperature: if T_g were higher, the polymer would result brittle and fragile.

Elastomers can be divided into two main categories: natural and synthetic rubbers. The first elastomeric material to be discovered was natural rubber, attained from the rubber tree (*Hevea brasiliensis*) latex. Although Europeans had known natural rubber since the 18th century, they started producing commercial goods only a century later and its applicability remained limited till the discovery of vulcanisation in 1839. [32] Only at the beginning of the 20th century, the synthetic equivalents of natural rubber were developed in Germany to keep up with the increasing demand and production of tyres. Since then, synthetic rubbers, produced from different monomers obtained by petroleum refining and cracking, have been employed to overcome the dearth of natural rubber supplies. Presently, about thirty distinct synthetic rubbers and eight kinds of natural rubber are included in tyre formulations. [33] Natural rubber accounts for the 46% of the total world rubber consumption. Remarkably, among synthetic rubbers, styrene butadiene rubber (SBR) is responsible for about 18% of the world rubber utilisation. [34]]

1.3.1.1 Natural Rubber

The chemical structure of natural rubber (NR) corresponds to that of linear *cis*–1,4-polyisoprene (Figure 1). Its number average molecular mass ranges from 10^5 to 10^6, presenting bimodal distribution and high polydispersity (2–10). Chain terminals include a few isoprene repeating units in *trans* configuration and a primary alcohol or a fatty acid ester as functional groups. [35] Glass transition temperature (T_g) lies around 200 K. [36]

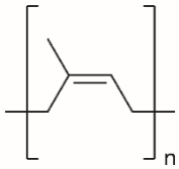

Figure 1. Repeat unit of *cis*–1,4-polyisoprene.

Natural rubber is attained in form of a stable aqueous suspension, commonly referred to as latex, from the sap of many plants (up to 2500 species). [35] Rubber tree (*Hevea brasiliensis*) is the most relevant source of NR from a commercial standpoint, although numerous alternatives, including Guayule (*P. argentatum*), Russian dandelion (*Taraxacum kok-saghyz*) and Canadian goldenrod (*S. canadensis*), have been studied as a

consequence of the general transition towards renewable feedstocks and the increasing demand of rubber. [37] Though *Hevea brasiliensis* is indigenous to Brasil, it is extensively cultivated in both tropical and subtropical areas. Currently, Malaysia, Indonesia, Thailand, China, and India are responsible for about 85 % of total world natural rubber production. [38]

Freshly tapped natural rubber latex is a colloidal system of micrometric, spherical particles dispersed in aqueous medium. The suspension is stabilised by the presence of proteins, phospholipids and other lipidic substances adsorbed on the particle surface forming a thin ~10 nm layer. NRL generally contains 30-40% in weight of solid particles, out of which up to 36% consists of natural rubber, the remaining fraction includes lipids (~3%) proteins (1-1,5%), sugars and soluble salts of calcium, magnesium, potassium, and copper. Newly exudated NRL is neutral but does not prove stable when exposed to air for long periods. Proteins contained in NRL present isoelectric points ranging from pH 4.0 to 4.6; exposure to air stimulates acidification and subsequently triggers coagulation. Commercial NRL is stabilised by adding ammonia which maintains an alkaline environment and hampers the proliferation of microorganisms. [39]- [41] Natural rubber presents terrific properties which cannot be equalled by synthetic counterparts. This is accordingly ascribed to its peculiar microstructure: the biological control over the living polymerisation results in 100% *cis* double bond configuration, defined molecular weight distributions and specific terminal functional groups and proteins. Recent studies have evidenced a correlation between the outstanding properties of natural rubber and the presence of calcium divalent cations which are supposed to promote ionic crosslinking by bridging two carboxylate groups belonging to different macromolecules. [42] Also strain induced crystallisation (SIC) contributes to the exceptional performances of natural rubber. When it is subjected to uniaxial stress, macromolecules tend to align along the direction of the applied force, thus producing nanometric crystalline domains which act as in situ generated fillers which provide additional physical crosslinking and, consequently, mechanical reinforcement. [43] Natural rubber presents other terrific properties which make it the ideal elastomer for tyre manufacture: high elasticity, resilience, low heat build-up, low hysteresis, good abrasion resistance, outstanding dynamic properties, and excellent processability. NR is also employed in the production of mechanical products, medical and health-related commodities, anti-vibration mountings, load-bearing components, flexible couplings. [44]

1.3.1.2 Synthetic Rubber

Synthetic rubbers have appeared in the 20th century as a reaction to the increasing demand for elastomers, lower processing costs and better materials performances for special applications. [45] Tyre manufacturing accounts for ~70% of the world consumption of synthetic rubber, [46] especially styrene-butadiene (SBR)

butadiene (BR), and polyisoprene (IR) rubbers. [47] All these elastomers are brought together by the presence in their backbone of chemical insaturations provided by the diene functionality of the monomer.

Styrene-butadiene rubber (SBR) is a random copolymer of styrene and 1,3- butadiene, industrially prepared by either emulsion or solution polymerisation. The copolymer typically consists of 75 % wt butadiene and 25 % wt styrene (butadiene to styrene molar ratio 6:1). Butadiene monomers can be inserted in the polymer chain in cis, trans or vinylic configuration of the double bond. This structural feature is difficult to be tuned during the synthesis, especially if it involves emulsion polymerisation. Nevertheless, SBR produced via emulsion method shows easier processability, higher tear and tensile strengths if compared to solution SBR. Due to its irregular structure, SBR is completely amorphous. If paralleled to NR, SBR vulcanizates present lower resilience and inferior resistance to fatigue, tearing, and cut; though, they show enhanced resistance towards abrasion, thermal ageing, and mechanical cleavage of the chains.

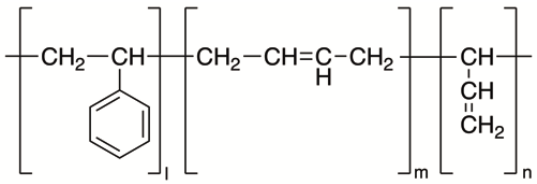

Figure 2. Repeat units typical of styrene butadiene rubber.

Along with SBR, butadiene rubber (BR) plays a key role in tyre manufacture. Industrial production of BR commonly involves solution polymerisation including the use of organometallic catalysts in order to control microstructure, yielding high selectivity for cis configuration of the double bond in the backbone (90-98%) and narrow molecular weight distributions. Polybutadiene is usually incorporated in blends with natural rubber to efficiently balance physical properties. [39], [49]

1.3.2 Vulcanisers

Vulcanisation is the chemical process responsible for the mechanical properties which make rubber so valuable a material. It was introduced by Charles Goodyear in 1839. [50] Unvulcanised rubber proves very soft and presents unsatisfactory physical properties such as sensitivity to extreme temperatures, swelling in solvents, poor resistance to light, and irreversible deformability after high strains. These features would be inadequate for the production of performing materials as tyres. Vulcanisation introduces intermolecular crosslinking which forms a three-dimensional mesh. Crosslinks may include a short chain of sulphur atoms, a single sulphur atom, a C-C single bond, a polyvalent organic radical, an ionic cluster,

or a polyvalent metal ion. At a molecular level, rubber macromolecules (whose number average molecular weight usually ranges between 100,000 and 500,000 Da) become chemically linked with junctures spaced 4,000–10,000 Da along the polymer chains.

This chain interconnection is responsible for enhanced elasticity, decreased plasticity and stickiness. [51] Other crucial features which affect the final performances of the material, such as tensile strength, dynamic modulus, hysteresis, and abrasion resistance are upgraded. In particular, hysteresis is a key parameter describing the deformation energy which is not stored or borne by the elastic network but converted to heat and it is inversely related to crosslinking degree. Conversely, tear strength, fatigue life, and toughness increase with small amounts of crosslinking, but they are reduced by further junctures formation. These parameters are directly proportional to breaking energy and hysteresis, so they reach an optimum at some intermediate crosslink density. They are also affected by the type of polymer and crosslink, kind and amount of filler, etc. [51], [52]

Moreover, dimensional stability is improved by vulcanisation and when crosslinking is thorough rubber goods cannot be solubilised in any solvent or remoulded. Hence, the final item has to be shaped before vulcanisation.

Relevant process parameters for vulcanisation are the so-called scorch time, namely the delay before crosslinking starts, the rate of vulcanisation after the scorch period and the final extent of crosslinking. Scorch time is essential to avoid undesired, premature vulcanisation before mixing, forming, and flowing in the mould are complete. When crosslinking starts, rapid progression is needed, and the interconnection degree must be controlled.

Vulcanisation of rubber compounds usually proceeds by heating the polymeric matrix mixed with the vulcanising system in a mould under pressure. Industrially, the process comprises the use of vulcanising agents, activators and accelerators. The most common vulcanising agents are based on either sulphur or peroxide.

1.3.2.1 Accelerated sulphur vulcanisation

Accelerated sulphur vulcanisation is the most common process, though its mechanism has not been exhaustively understood. For many applications, it is the only choice guaranteeing a delayed action necessary for processing, shaping, and forming before the creation of the intractable vulcanised network. It is used in the case of natural rubber (NR), synthetic isoprene rubber (IR), styrene-butadiene rubber (SBR), butadiene rubber (BR), nitrile rubber, chlorobutyl rubber, bromobutyl rubber, and ethylenepropylene-diene-monomer rubber. In accelerated sulphur vulcanisation, along with sulphur,

there are always at least one type of accelerator and one activator produced by the interaction of zinc oxide and a fatty acid. The latter form a salt able to create complexes with accelerators and reaction products generated between accelerators and sulphur.

Moreover, inhibitors preventing premature vulcanisation can be added to hamper undesired early crosslinking. Originally, sulphur vulcanisation proceeded by adding eight parts of elemental sulphur per 100 parts of rubber (phr) at 140 °C for 5 hours. Thanks to the addition of zinc oxide as an activator, a selected mixture of accelerators, vulcanisation times have been reduced to 1-3 minutes. Hence, sulphur vulcanisation without accelerators has no commercial relevance. Accelerators comprise organic compounds, either benzothiazoles, sulfenamides, dithiocarbamantes or secondary amines. Their interaction with sulphur results in the production of Ac-S_x-Ac monomeric polysulphides (Ac designates an organic radical derived from the accelerator) which later network with rubber yielding rubber-S_x-Ac polymeric polysulphides which further evolve into the final rubber-S_x-rubber crosslinks. Inorganic activators are usually added to improve accelerators activity, thus enhancing crosslinking efficiency. The presence of activators modifies the reaction path as shown in Scheme 1 for benzothiazole-accelerated sulphur vulcanisation in the presence of zinc oxide: after the initial formation of activator-accelerator adducts, rubber-S_x-Ac species are produced at higher rate but crosslinking results slower. In fact, zinc cation coordinates one of the sulphur atoms involved in the most labile S–S bond of the rubber-S_x-Ac species. As a result, a stronger S-S bond in the same polymeric polysulphide must be broken, that is the reason why crosslinking becomes slower. Conversely, the extent of interconnection is enhanced since less sulphur is used in each crosslink, that is polymeric chains result connected by shorter sulphur bridges.

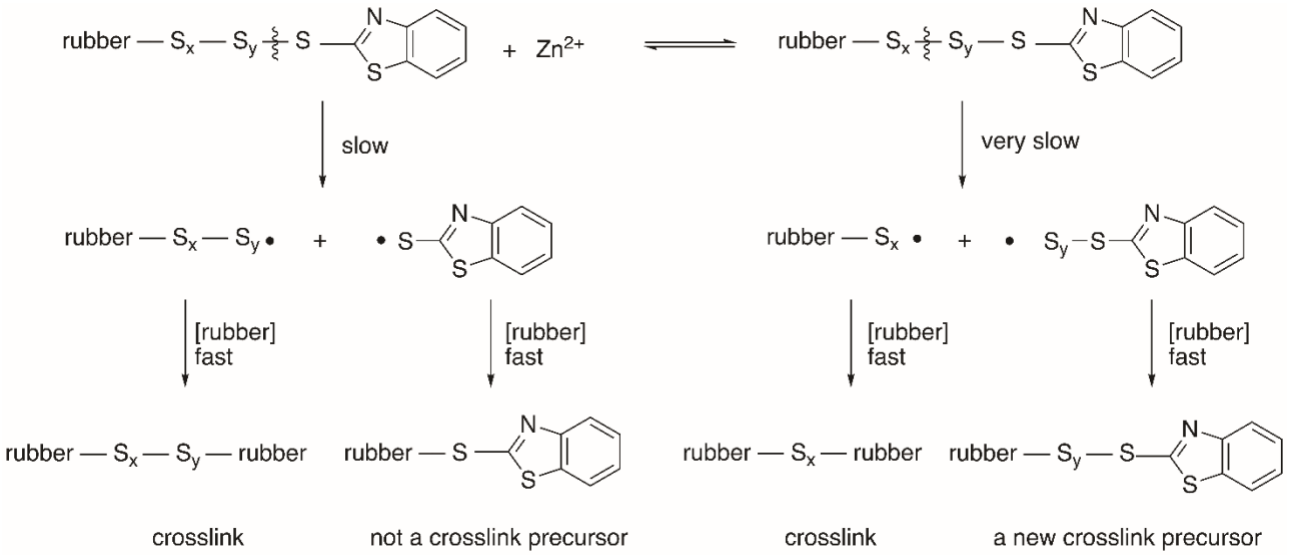

Scheme 1. Scheme for benzothiazole-accelerated sulphur vulcanisation in the presence of zinc oxide.

The final properties of vulcanizates can be finely tuned by modulating absolute and relative amounts of vulcanisers. When both sulphur and accelerator quantities are increased, higher crosslink degree thus stiffer compounds are obtained. Sulphur to accelerator ratio impacts on the average length of sulphur bridges, the number of rubber-S_x-Ac pendants, and the extent of intramolecular crosslinking. Conventional vulcanisation systems include high sulphur amounts and low accelerators quantities; this leads to long polysulphidic bridges interconnecting polymer chains. Conversely, efficient vulcanisation systems comprise limited sulphur amounts and higher accelerators extent. At optimum vulcanisation times, they mainly generate monosulphidic crosslinks and less chain modification. [49], [53]- [57]

1.3.2.2 Peroxide-induced vulcanisation

Peroxide-induced vulcanisation is a relatively less common alternative to the sulphur process. It comprises the decomposition of peroxide into free radicals which interact rubber chains by either hydrogen abstraction in allylic position or addition to double bond. The former mechanism is the predominant one in the case of isoprene rubber. The radical on the polymer chain can couple with another radical or, alternatively, react with a double bond of an adjacent chain. Independent of the mechanism (Scheme 2), as a result, a new C-C single bond is generated. In the latter case, the radical survives and can further react creating additional crosslinks. However, a polymeric radical can undergo chain scission with the generation of a vinyl moiety and a new polymeric radical.

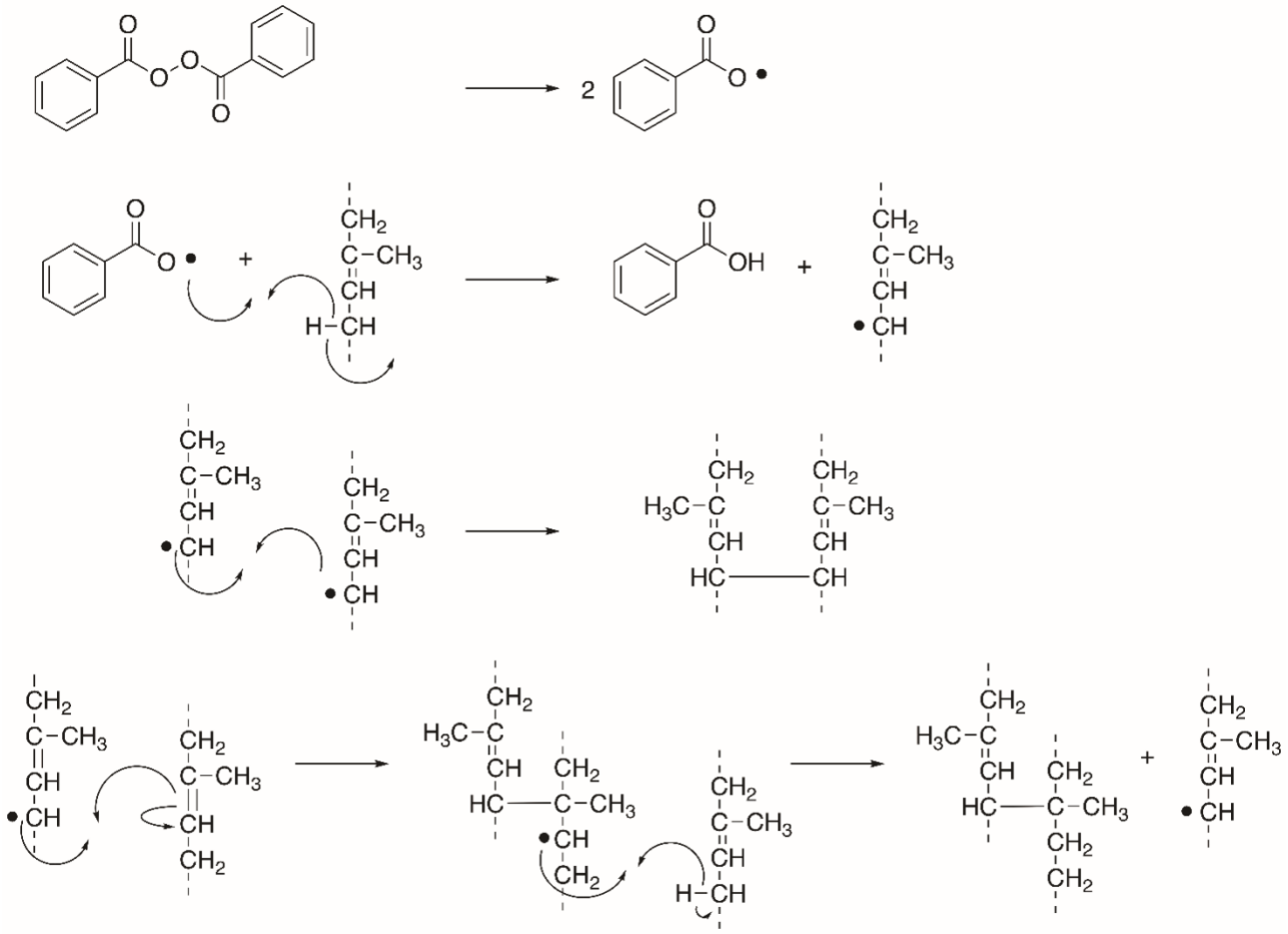

Scheme 2. Mechanism of peroxide-induced vulcanisation with dicumyl peroxide.

1.3.3 Fillers

Natural and synthetic rubbers cannot be considered as finite materials for conventional applications even after vulcanisation without any improvement of their mechanical properties, including wear resistance, hardness and toughness. [58] For this reason, fillers result to be the second ingredient in terms of abundancy in rubber compounds, after rubber itself. [59] Rubber compounds may include three main types of fillers classified on the basis of the physical properties they impart: non-reinforcing, semi-reinforcing and reinforcing fillers. Chalk powder, clay, and calcium carbonate are some examples of non-reinforcing filler whose purpose is to decrease the cost of the final product without any improvement of the properties. Conversely, reinforcing fillers, such as carbon black, silica, etc., enhance the mechanical properties of vulcanised rubber compounds such as tensile strength, modulus, stiffness, abrasion resistance, elongation at break, heat build-up, and rolling resistance. [60]– [62] They can additionally protect rubbers from heat, light or chemical degradation or they can improve gas permeability and, consequently, tyre pressure retention. This opens the way to the production of tyres with superior mechanical

performances. The reinforcing effect strongly depends on the intrinsic properties of the filler such as chemical composition, particle size, shape, structure, aspect ratio, surface area, surface chemistry, and density. [47], [63]]

The reinforcing effect of a filler is strongly affected by its particle size. The smaller the particle size, the higher the surface to volume ratio, the higher the rubber-filler interface extension, the better the mechanical reinforcement of the rubber compound. [64]– [66] The surface of a particulate is known to be correlated to the third power of the size of each single particle. Consequently, the formation of an extended interfacial area between filler and matrix is expected along with a large additional portion of immobilised rubber displaying different properties with respect to the bulk matrix. [67] The properties at the interface between filler and matrix deeply affect the macroscopic properties of the whole compound, so nanocomposites are regarded as intriguing materials for a wide variety of applications including biomedicine, catalysis, sensing, etc. Reinforcing fillers can be referred to as nanoparticles, nanofibers or nanoplates according to whether they present three, two or just one dimension in the nanoscale, respectively. Fillers larger than 1 μm usually do not exert any reinforcing effect. Moderate reinforcing is achieved for fillers with particle dimension raging from 100 nm to 1 μm. Excellent reinforcing action is guaranteed by fillers with particle size between 1 and 100 nm. [16]

At the interface, rubber and filler may interact either physically by Van der Waals forces, or chemically by polymer grafting on a filler opportunely functionalised at the surface. High particles surface areas correspond to a larger fraction of polymer chains adsorbed on the filler surface, commonly referred to as bound rubber (Figure 3). This means an enhanced restriction of chains mobility under strain and a consequent high reinforcement effect of rubber compounds. [16] Additionally, a portion of the polymeric matrix, called occluded rubber, can be wholly interlocked in the voids between the filler particle and thus be shielded from deformation, consequently increasing the effective fraction of the filler. [16], [68]- [70]

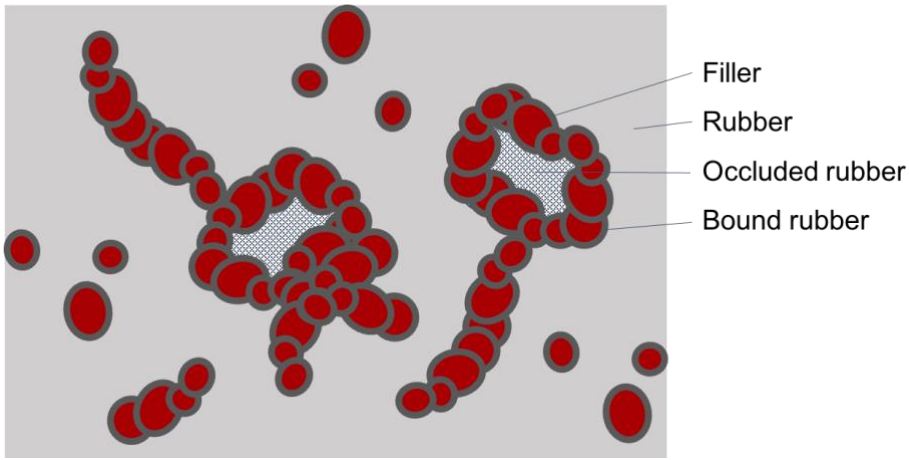

Figure 3. Schematic representation of a rubber reinforced by fillers.

The surface activity of the filler defines both filler-rubber and filler-filler interactions which significantly influence the viscoelastic behaviour of rubber compounds. [68], [71], [72] It can be enhanced by decorating the filler surface with functional groups showing a strong affinity and chemical reactivity toward the rubber matrix. [62], [73], [74] High surface activity reflects on strong rubber-filler interactions and, as a result, on high reinforcement effects. Filler-filler interactions are a key parameter defining the dispersion of filler particles in the polymeric matrix and consequently the extent of reinforcement. [75]– [77] Above a certain filler volume fraction defined as percolation threshold, filler particles become part of a three-dimensional network extended throughout the whole matrix. The complex behaviour of filled elastomers has been tentatively explained by many theories and models: hydrodynamic theory for the increase in viscosity, Payne effect for the non-linear viscoelastic behaviour as a result of the breakdown of filler aggregates, strain amplification for the presence of local strains higher than the applied one, weak and strong linkages, slippage at interface for the sliding of molecular chains under strain and subsequent redistribution of the stress, Büche model for the connection of filler particles by common rubber polymer chains and redistribution of the stress. Nonetheless, only a combination of these models can describe the complicated effects of elastomer reinforcement.

The morphological characteristics of filler particles are a critical parameter influencing the efficiency of reinforcement. Spherical filler particles usually form chainlike or branched superstructures which do not tear apart during the processing of rubber compounds and behave as additional reinforcing fillers which determine strain amplification effects in the deformable phase of the compound. [64], [78] Moreover, particle shape affects reinforcement: fillers with high aspect ratio (length to width ratio) show greater reinforcing effects than the spherical ones. In the case of particles endowed with high aspect ratio, the enhanced reinforcing effect is commonly ascribed to the higher surface area which reflects into wider contact area and adhesion between filler and elastomeric matrix and in a higher portion of bound rubber. [60]

Typical reinforcing fillers extensively employed in tyre manufacture are carbon black and silica.

1.3.3.1 Carbon black

Carbon black is the typical reinforcing filler for tyres and is essentially composed of almost pure elemental carbon arranged in imperfect graphitic layers stacked in spherical primary nanoparticles. These particles present a rough surface decorated by diverse functional groups as phenols, carboxylic acids, ketones, quinones and lactones (Figure 4). These chemical functionalities allow for the interaction of carbon black with curing agents and reactive sites of elastomer chains in composites. [79]– [81] The features of carbon black particles such as size, surface activity, and structure can be tuned according to the production conditions. As a result, a huge variety of carbon blacks are commercially available. The industrial

processes for carbon black synthesis are known as furnace black and thermal black processes, the former being the most common one. The furnace black process comprises the partial pyrolysis of heavy aromatic oils in vapour phase under controlled conditions to produce microscopic particles. Since particle size and surface area play a key role in the extent of reinforcement, these two properties have been selected by the American Society of Testing Materials (ASTM) for the classification of carbon blacks. The ASTM nomenclature format consists of an alphanumerical code comprising a letter, *i.e.*, N or S for normal or slow curing rate induced by the type of carbon black, followed by a single digit related to particle size, and two final digits randomly assigned. [82] Each carbon black affords peculiar features to rubber compounds so it must be attentionally selected to bestow the desired properties on the final material. The effect of carbon black characteristics on the physical properties of rubber compounds has been studied and some general trends have been elucidated. By increasing carbon black structure, fatigue resistance and cut growth are enhanced. Conversely, particle size, tear strength, abrasion resistance, and, unfortunately, heat build-up and hysteresis increase with the increase in particle size. Carbon black loading directly correlates with hardness, heat build-up, rolling resistance, and wet-skid features. Abrasion resistance, compound processability, and tensile strength reach an optimum at some intermediate loading value, then start decreasing. [17], [83]– [85]

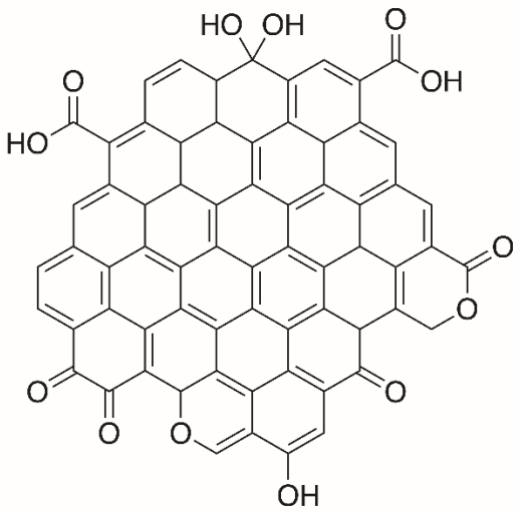

Figure 4. Representation of carbon black structure.

1.3.3.2 Silica

Silica is commonly employed as a reinforcing filler in rubber industry. Although at the beginning it was used as a non-reinforcing filler along with carbon black, later the introduction of silica-silane technology demonstrated the reinforcing ability of silica in elastomers. [86] Its reinforcing effect are similar to those

imparted by carbon black and, additionally, they bestow low hysteresis, a desired feature for tyres. The use of inorganic fillers is particularly advantageous because of the possibility to rolling resistance (up to 20%), thus enhancing the fuel efficiency of vehicles. However, it presents the disadvantages of relatively high cost and low compatibility with the elastomeric matrix. A niche process for silica production is flame pyrolysis, [76], [87] whereas the most common one is silica precipitation by controlled neutralisation of a diluted solution of sodium silicate. Two key parameters to obtain highly dispersible reinforcing silica by precipitation are both neutralisation and drying conditions. [76], [87], [88] Precipitated silica size originally ranges from 5 to 50 nm, later they are fused together by siloxane bonds to form aggregates (100-500 nm in size). The latter suffer from poor dispersibility in hydrophobic polymers due to the strong tendency to aggregation via hydrogen bonding, imparted by the presence of superficial silanol groups.

In order to enhance dispersion and filler-rubber compatibility, the surface of silica particles is functionalised with particular coupling agents, among which bis[3-(triethoxysilyl)propyl]tetrasulphide (TESPT) is the most common. This organosilane proves bifunctional: its triethoxysilyl moiety reacts with silanol groups exposed on silica surface, whereas the tetrasulfide function attacks polymer chains (Figure 5). As a result, silica-rubber compatibility is improved. [89] Hence, compatibilised silica fillers bestow enhancement in tear strength, wet traction, and hysteresis, and reduction in heat build-up, on a variety of rubber compounds included in tyres, industrials rubber goods and shoe soles. [90], [91]

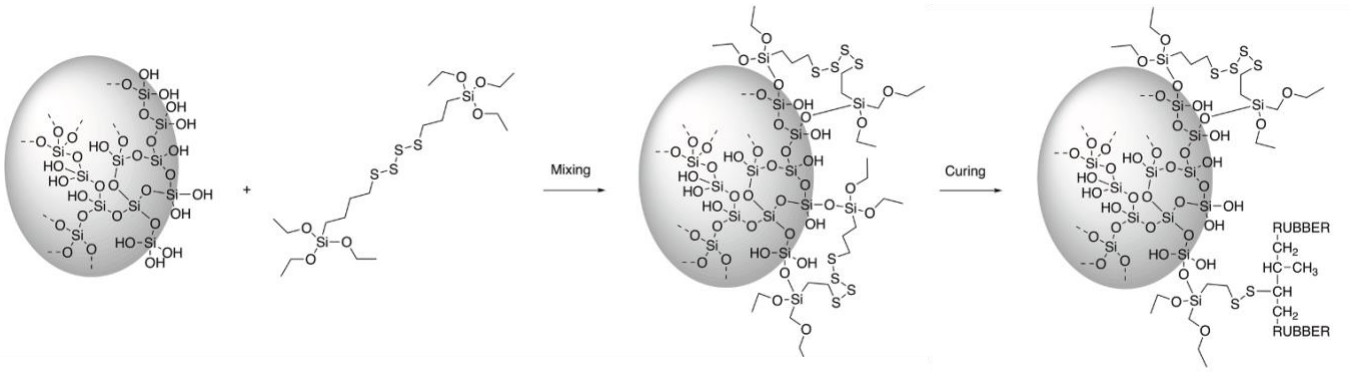

Figure 5. Functionalisation of surface silica particles with an organosilane coupling agent (TESPT).

1.3.3.3 Novel fillers

New fillers are presently under study to match and even outclass carbon black and silica for the production of high performing items. In this regard, particular attention is focused on nanomaterials able to further improve mechanical properties and barrier effect. Among them Polyhedral Oligomeric Silsesquioxanes (POSS) and Silica/Allumina nano-oxides impart low hysteresis at high temperatures favouring lower rolling resistance. Moreover, high aspect ratio nanofillers, including Carbon Nano Fibres

(CNF), Carbon Nano Tubes (CNT), Polymeric Nanofibers, Graphene (delaminated Graphite), Clays and Zirconium Phosphates, show particularly low percolation threshold and can afford excellent mechanical properties. [92], [93] Along with the desire for fillers capable of offering improved mechanical performances, a growing interest has been recently elicited by fillers produced from renewable resources. This could moderate the ecological footprint related to tyre manufacturing. Fillers obtained from renewable biomasses are intriguing not only for their carbon neutrality (which makes them incomparably more environmentally friendly than carbon black) but also for their large availability, low cost, safe, biodegradability, easy disposal, and reduced specific gravity. Some examples of renewable products examined as potential reinforcing fillers comprise cellulose, cellulose nanocrystals, starch nanocrystals, chitin nanowhiskers, bamboo fibres, rice husk fibres, rice husk ashes, lignin, biochar, pollens, and soy flour. [94]

1.3.4 Stabilisers

Ageing effects can alter organic polymer structures which are vulnerable to degradation determined by oxygen, ozone, light, heat, solvents, moisture, sulphur, dynamic fatigue and heavy metal contamination. Unsaturated elastomers, as natural and synthetic rubbers, are particularly vulnerable to oxidation and ozonation. They are also susceptible to heat because the energy required to generate a radical species on the basis of C=C double bonds is relatively low. Such anti-degradants must be added to unsaturated rubbers in order to preserve original properties and prevent embrittlement. Elastomers can be protected by different types of inhibitors, classified based on their mechanism of action: free radical chain stoppers, peroxide decomposers, light absorber, metal deactivators, and inhibitor regenerators.

Antioxidants are crucial to protect vulcanizates from oxidation by reacting with oxygen and free radicals. They are conventionally grouped in primary and secondary antioxidants, acting as chain terminators and as hydroperoxide decomposers, respectively. Conventional antioxidants comprise hindered phenols, aromatic amines, and hydroperoxide decomposing antioxidants. Contrariwise, antiozonants' mechanism of action has not been fully understood yet and four different theories have been formulated. The first one hypothesises the competitive reaction of antiozonants with rubber for ozone. The second one theorises the formation of a protective layer of ozonised antiozonant on the rubber surface, which results shielded from further attacks by ozone. The third one conjectures the reaction between antiozonants and ozonised rubber fragments in order to restore polymer chains. The last one theorises the formation of zwitterions from the ozonised products. Along with antioxidants and antiozonants, waxes in form of microcrystals and paraffin are usually added to compounds as protective agents.

1.3.5 Special Compounding Ingredients

Polymers, fillers, vulcanisers and stabilisers constitute the primary materials of rubber compounds. Along with them, other secondary ingredients are also added such as processing oils, plasticisers, colouring agents, and resins. To improve processability, it is useful to add processing oils which can be aromatic, naphthenic, or paraffinic. Recent studies have focused on the replacement of polycyclic aromatic hydrocarbons (PAHs) as processing oils in favour of less toxic, eco-friendly alternatives. Nonetheless, processing oils must have the right molecular composition, molecular weight, and viscosity which assure their compatibility with the elastomeric matrix. Additionally, plasticisers can be incorporated into rubber compounds to enhance flexibility. Their typical effects consist in the decrease in tensile strength and static modulus associated with an improvement in low-temperature flexibility and elongation at break. Furthermore, processing, resins, and tackifying resins can be added to upgrade tensile strength, tack, dispersion of filler, and resistance to fatigue and cut growth. [63], [104] Finally, colouring agents may be added for the aesthetics of the final rubber item.

2 A transition from fossil resources to renewable feedstocks for a sustainable economy

Currently, energy and a wide variety of chemicals and materials are industrially produced from fossil feedstocks. [105], [106] In the last decades, the large availability of relatively cheap crude oil has supported developing countries to rely on petrochemical sources to provide the growing population with consumer goods, energy and fuels.

The increasing demand for such commodities raises serious issues related to the depletion of fossil resources which are considered non-renewable for practical reasons since their generation takes millions of years. Moreover, the geopolitical instability of some of the major producing countries along with the exhaustion of fossil feedstocks is causing a price increase of the fuel which reflects in higher production, transportation, energy and commodities costs, in conclusion in a reduced cost-effectiveness of the use of this kind of reserves. [107] Since the industrial revolution, manifold environmental concerns have raised, all of them related to the use of fossil resources and their combustion for fuel production: the increase in carbon dioxide (from ~280 ppm before the industrial revolution to ~310 ppm in 1950 and ~400 ppm nowadays) and other greenhouse gasses levels in the atmosphere leading to global warming, the pervasive presence of microplastics due to plastic wastes decommissioning in waterways, the increase in nitrogen and phosphorous concentration in the soils caused by the widespread consumption of fertilisers, and the

presence of a permanent deposit of airborne particulates such as black carbon in sediments and glaciers. [108], [109]

Along with economic issues and stricter law requirements, environmental concerns such as the increasing levels of greenhouse gasses leading to global warming, fossil feedstocks medium-term exhaustion, and unsustainability of the use of non-renewable resources are stimulating investigations on alternative sources for energy and organic carbon. Biomass is regarded by experts as the only green, eco-friendly, and sustainable substitute for fossil feedstocks in the production of chemicals and liquid fuels. [106] Nevertheless, the switch from a petroleum-centred economy to one based on biomass requires an innovation since the well-established petrochemical technologies are not suitable for the transformation and utilisation of biomass derivatives. [105] The recalcitrance relative to the establishment of an alternative paradigm in energy and chemicals production lies in the complex interactions between industry, technology, science, markets, and policy [110] that reflects into higher production costs for biomass and depreciation of capital investments in conventional, petroleum-related technology. [111], [112]

Nonetheless, the extensive employment of renewable biomass for chemicals and fuel production presents controversial issues. One of them is the competition with food supply when edible biomass feedstocks, *e.g.*, sugars, starches and vegetable oils are used. Dedicated crops have to be set for biomass production at the expenses of virgin forests causing deforestation, global warming and biodiversity threatening concerns in some developing countries around the world. All these issues have spurred researchers to develop technologies to process abundant and cheap nonedible biomass for a sustainable production of fuels and chemicals without affecting food provisions or inducing changes in land use. The rational exploitation of renewable resources is known as biomass refinery. [113] [115] It aims at developing strategies to valorise all the components of vegetable and animal resources and residues, including forestry residues, manure, waste oils and fats, in an optimised way from a green, technical and economic standpoint without competing with food and feed production. The high oxygen content which discriminates biomass from petroleum feedstocks gives the former low volatility, high water solubility, high reactivity and low thermal stability. [117] All these features support the processing of biomass resources by catalytic aqueous-phase technologies at moderate temperatures. Unlike petroleum, biomass is renewable, abundantly available, and carbon neutral, being part of a closed cycle: the CO_2 released during the transformation of biomass into chemicals and fuels is recaptured by plants so transmuted into organic carbon and reconverted into biomass via photosynthesis in a process without net carbon emission. [107], [116] Manifold renewable resources can be exploited for the production of chemicals and fuels: polysaccharides (cellulose, starch, chitin, chitosan, hemicellulose), lignin, vegetable oils, sugars, pine resin derivatives (terpenes and rosin),

polycarboxylic acid, glycerol, and furans. Among them, lignocellulosic biomass including cellulose, hemicellulose and lignin is regarded as the most promising alternative to fossil resources thanks to its renewability, abundance, relative cheapness, and worldwide availability. [117]– [118] Many researches have explored and confirmed the huge potential of lignocellulosic sources for a sustainable production of chemicals, fuels, and value-added materials. [119]– [123] Lignocellulosic biomass is the perfect candidate for the sustainable replacement of fossil feedstocks because it is obtained from non-edible parts of plants and crops so there is no competition with food supplies, [124] as opposed to what happens during bioethanol production from starch and sugar crops. [125] Compared to other biomass, the lignocellulosic one can be produced in shorter times and lower costs improving the cost-effectiveness. Furthermore, it is a processing waste which is usually disposed in soil and landfill, triggering damages to the environment. On the contrary, it can be valorised for the production of value-added chemicals [126] though it is challenging. [116] The difficulties in lignocellulosic processing lie in a highly complex structure which reflects into high chemical recalcitrance and low enzymatic degradability, making pretreatments relatively expensive and energy consuming . [123] The manifold attractive features of this resource make it worth studying and developing new efficient pretreatment systems. [127]

3 Lignocellulosic feedstocks

The most abundant biomass is lignocellulose which approximately constitutes half plant matter produced via photosynthesis, [128]with a 200 billion metric tons yearly supply worldwide. [129]

Lignocellulose is a polymeric material present in plants mainly composed of carbohydrate polymers (cellulose and hemicellulose) and aromatic polymers (lignin and tannin). [130] These polymers are part of plant cell walls whose multilayer structure comprises cellulose microfibrils immersed in a hemicellulose-lignin matrix. [131]

The distribution of these components in plants cell wall, their relative content and three-dimensional structure depend on the vegetal source. [132] Generally, lignocellulose includes 35-50 % cellulose, 20-35 % hemicellulose, and 10-25 % lignin and other minoritarian components (oils, waxes and minerals). [133] Lignocellulose resistance to degradation is ascribable to cellulose high crystallinity, lignin hydrophobicity and encapsulation of cellulose into a hemicellulose-lignin matrix. [134]– [136] Its chemical recalcitrance and resistance to degradation increase processing cost for this feedstock compared to easily degradable edible biomass [105] but this resource is particularly attractive for its lack of competition with food supply. [124]

There exist three main categories of lignocellulosic biomasses showing relevance for industrial applications according to their vegetal source: hardwoods are so called because of their hard and durable wood and belong to angiosperms, also referred to as flowering plants, having seeds enclosed within an ovary (usually a fruit), flat leaves and usually a seasonal lifecycle; softwoods, denominated this way for their soft and workable wood, belong to gymnosperms, usually evergreen plants having needle-like leaves, and naked seeds found on scales, leaves or as cones; [137] herbaceous plants, also known as grasses, differ from the other categories for their flexible stem and can be either annual, biennial or perennial. [138], [139]

3.1 Cellulose

Cellulose is the major component of lignocellulose and the most abundant biomass in the biosphere accounting for $7.5 \cdot 10^{10}$ tons of annual production. [140] It is mainly produced by plants where, thanks to its fibrillar nature, it shows a structural function in association with lignin, hemicellulose and pectin. Cellulose is also produced by marine organisms, *i.e.*, tunicates, algae, fungi and bacteria.

Cellulose is a linear syndiotactic high molecular weight homopolymer: Its repeating unit is considered to be cellobiose, composed of anhydro-*D*-glucose (*D*-anhydroglucopyranose) rings linked by β–1,4-glycosidic bonds (Figure 6). The average degree of polymerisation of native cellulose ranges from 500 to 15000 glucose units depending on the vegetal source, making cellulose one of the longest bio-macromolecules in nature. [140]– [144] Chain ends are not chemically equivalent, one bearing a reducing hemiacetal functionality and the other presenting a non-reducing aliphatic hydroxyl group.

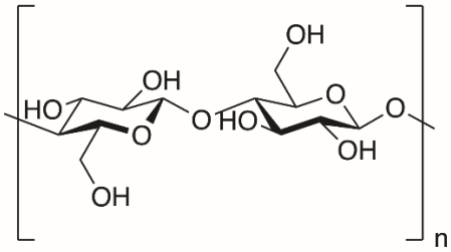

Figure 6. Cellulose structure.

Glucopyranose units present a chair conformation bearing hydroxyl groups in equatorial positions and hydrogen in axial ones. This conformation produces a linear extension of the chain. Laterally protruding hydroxyl groups dictate the supramolecular, hierarchical organisation of cellulose because of their ability to establish both intramolecular and intermolecular hydrogen bonds. These interactions force a close packing of cellulose which presents crystalline domains surrounded by less ordered, semi-crystalline and amorphous regions. Depending on the botanical source, extraction process and possible chemical modifications, cellulose can arrange into six different crystalline structures characterised by dissimilar

hydrogen bonding patterns. Though, native cellulose there are three most common crystalline allomorphs referred to as cellulose I_α, cellulose I_β, and para-crystalline cellulose. Hydrogen bonds impose a semi-rigid close packing, absence of a melting point and poor solubility in either water or traditional organic solvents. They also induce a microfibrillar structure endowed with high tensile strength which bestows rigidity on cell walls. [144] In particular, during biosynthesis, thirty-six distinct cellulose molecules form elementary fibrils which organise in microfibrils that, in turn, build cellulose fibres. This hierarchical structure depends on the biosynthesis conditions which are typical of each botanical source. [145]

Cellulose abundancy and renewability are attractive features which have extensively been employed in industrial scale production of paper and semi-synthetic films (cellophane), manufacture of cotton and synthetic textile fibres, e.g., rayon, which are used as active components in coatings, optical films, foodstuffs, pharmaceutics, cosmetics, additives in building materials etc. [146] Furthermore, the increasing interest for renewable materials and nanotechnology has inspired researchers to study cellulose conversion into biofuels and cellulose nanoparticles for the design of novel biomaterials and composites. [147]– [153]

3.2 Hemicellulose

Hemicellulose is the second most abundant polymer in the biosphere. It is a random copolymeric polysaccharide including as monomers pentose sugars (xylose and arabinose), hexose sugars (mannose, glucose and galactose,) and some sugar acid residues (4-*O*-methyl glucuronic acid and galacturonic acid). Its polymerisation degree is usually lower than that of cellulose, its chemical composition and architecture (either linear or branched) depend on the botanical source. Hemicelluloses from softwoods mainly contain glucommannans. On the other hand, hemicelluloses extracted from hardwoods and herbaceous plants typically include β-*D*-xylopyranose units connected by 1-4 bonds and can have a branched architecture bearing either monomeric or oligomeric pendants of different nature (arabinose, glucuronic acid or its 4-*O*-methyl ether, and acetic, ferulic, and *para*-coumaric acids). [154], [155]

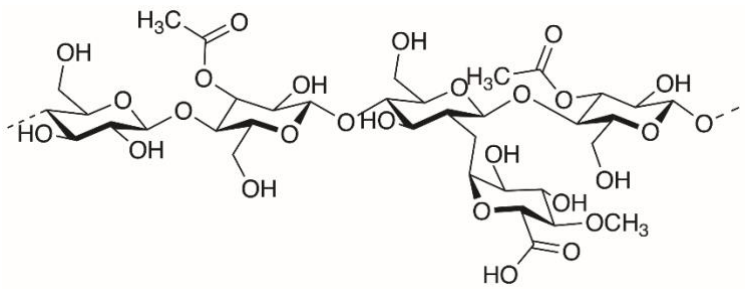

Figure 7. Partial molecular structure of hemicellulose.

Unlike cellulose, hemicellulose does not present any crystalline domains. Along with cellulose and lignin, it constitutes a complex structure responsible for the mechanical strength of plant cell walls and hemicellulose protection against hydrolysis. From a technological point of view, pretreatments are necessary to separate hemicellulose from lignin and cellulose, make it susceptible to hydrolysis and isolate its monomers as fundamental starting materials for the production of a lot of valuable chemicals. [156]

3.3 Lignin

Lignin is a three-dimensional, branched amorphous polymer consisting of methoxylated phenylpropane units. Its natural abundance has the same order of magnitude as that of cellulose and it constitutes the most copious renewable source for aromatic chemical production. Along with cellulose and hemicellulose, it forms a stiff composite that provides plant cell walls tensile strength and acts as a barrier to moisture controlling fluid flow and as a protection against biochemical attacks by inhibiting enzymatic degradation of other components. [157]

The biosynthesis of lignin is supposed to start from the conversion of phenylalanine into the three hydroxycinnamyl alcohols denoted as monolignols, *i.e.*, *para*-coumaryl, coniferyl and sinapyl alcohols. [158]–[160]

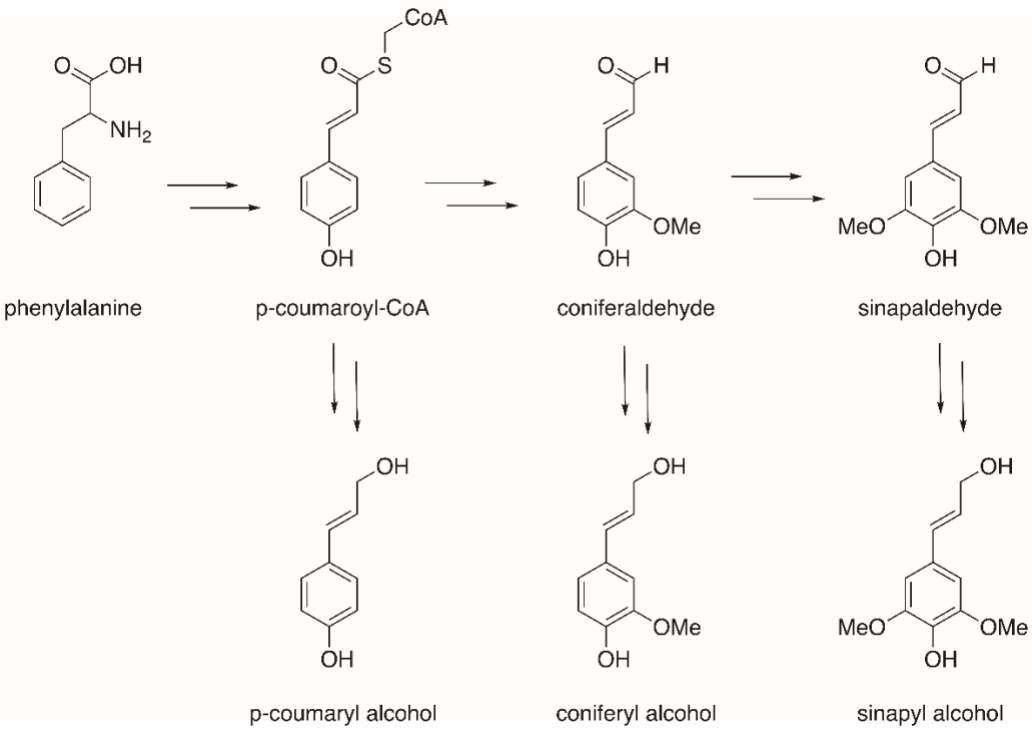

Figure 8. The main biosynthetic paths from phenylalanine to monolignols.

Free monolignols are relatively toxic and unstable, and they are stored and transported inside the cells in the form of monolignol glucosides, with the glycosylation occuring *via* the phenolic hydroxyl group. Their polymerisation results in the final lignin. Once incorporated into the macromolecular structure, the C_9 phenylpropane moieties are referred to as p-hydroxyphenyl (H, from coumaryl alcohol), guaiacyl (G, from coniferyl alcohol), and syringyl (S, from sinapyl alcohol) units. After the breaking of the glycosidic bond, the polymerisation is supposed to follow a chain polymerisation mechanism initiated by the oxidase-assisted oxidation of the phenolic hydroxyl groups. The ensuing free radicals couple with each other in a combinatorial fashion to produce a quinomethide intermediate. Subsequent hydrogen abstraction or nucleophilic attack by water, alcohols, or phenolic hydroxyl groups on the benzyl carbon of the intermediate restore the aromaticity of the benzene ring. The generated dimers are prone to further polymerisation. [130]

Although monolignols biosynthesis is controlled, lignification is supposed to follow the chemistry of radical coupling. If it were enzyme-assisted, lignin would be expected to be produced in a pure enantiomeric form. The racemic nature of lignin supports the hypothesis of random, uncontrolled lignification. [161] The absence of any stereo- or regio-control results in a high structural variability in lignin. Consequently, phenylpropane units are coupled through a variety of connections: β-*O*-4' and 5-5' linkages are the most abundant, comprising 50-60% and 20-25%, respectively of all bonds in lignin; 4-*O*-5', β-β', β-5', spirodienone, dibenzodioxocin, and phenylcoumaran are the other connections found in lignin, as depicted in Figure 9 and Figure 10. [162]

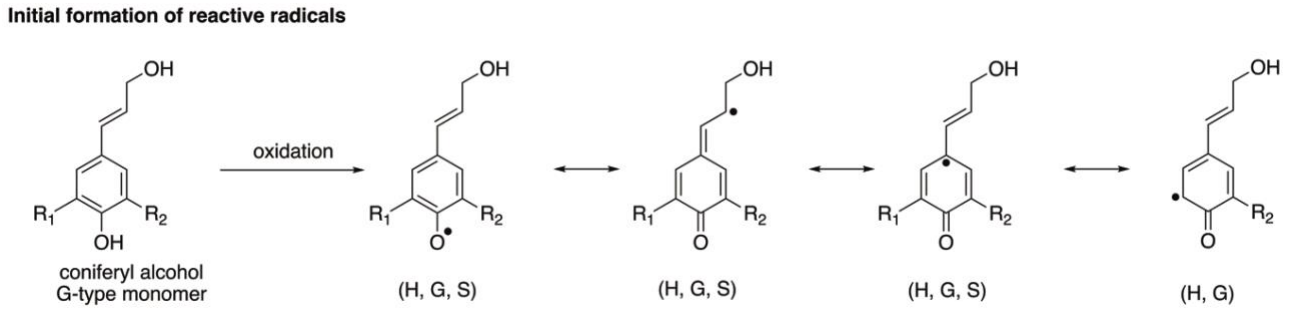

Figure 9. Initial formation of reactive radicals. Redrawn from reference. [162]

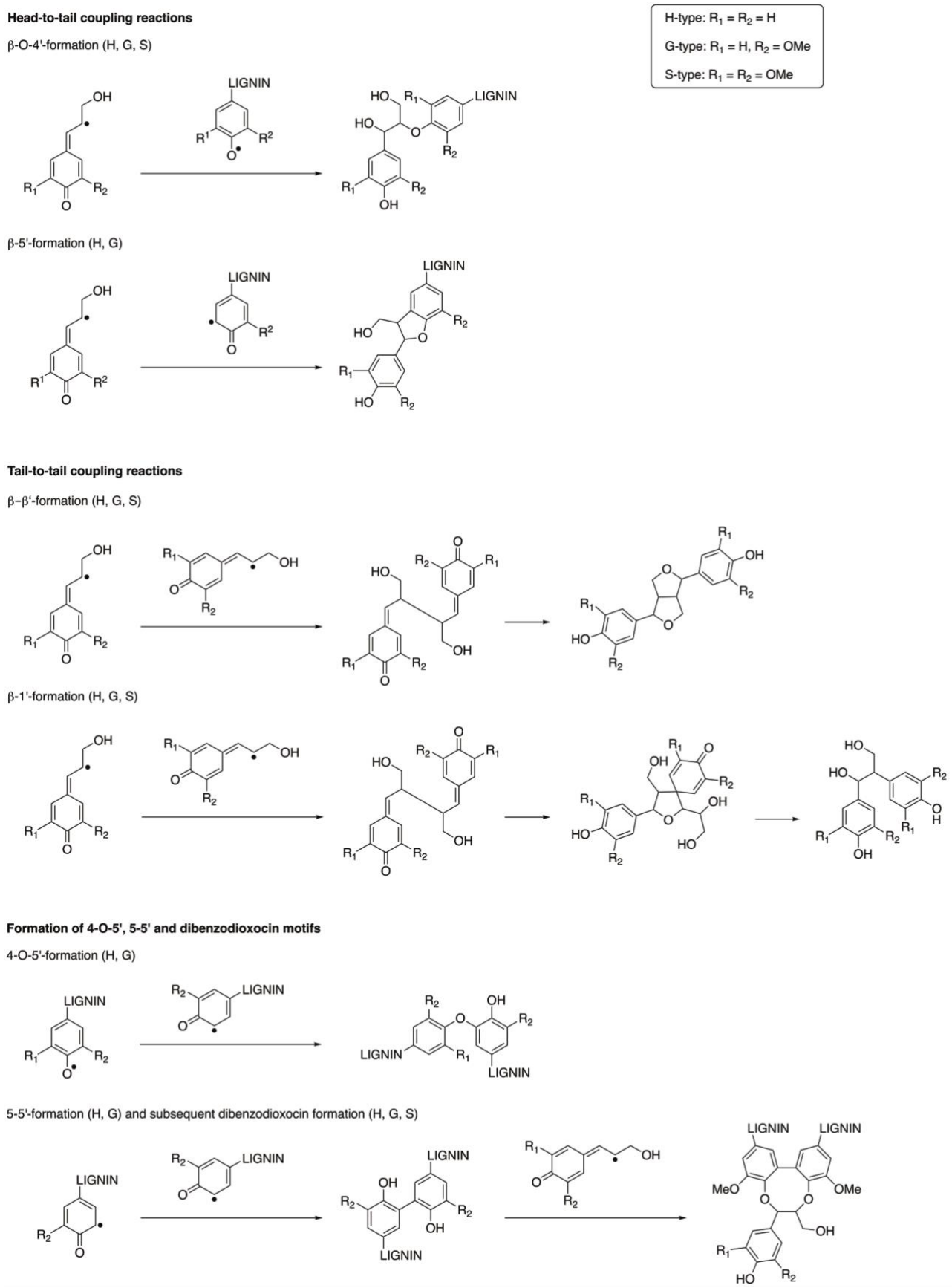

Figure 10. Formation of the most recurrent interunit connections found in lignin. Redrawn from reference. [162]

This structural variability is further magnified by the contribution of monolignols which varies depending on the botanical species, age and environmental conditions of the plant. [163] Generally, hardwood lignins contain sinapyl and coniferyl alcohols, softwood lignins are mostly composed by coniferyl alcohol, and herbaceous plants include all the three monomers. [160]

Differences in composition impact on the connectivity among fundamental units. For example, hardwood lignin is rich in S units which favour β-*O*-4 linkages whereas they hinder β–5' and 5-5' bonds. In softwood lignin, the predominance of G units makes β–5' and 5-5' linkages more frequent, at the expenses of other intermonomeric connections. Finally, herbaceous lignin comprises all three monomers in appreciable amounts, as it is for hardwoods (Table 1). [164]

Table 1. Average relative abundancy of interunit linkages and monomeric units inside lignin.

Type of linkage	Relative abundancy / %		Units	Relative abundancy / %		
	Softwood	Hardwood		Softwood	Hardwood	Herbaceous
β–*O*–4'	50	60	H	9	4	17
α–*O*-4'	5	7	G	91	33	49
β–5'	10	6	S	0	63	34
5–5'	10	5				
4–*O*–5'	4	7				
Other bonds	21	15				

Moreover, the degree of methoxylation of phenylpropane moieties heavily affects the macromolecular architecture of lignin. In particular, methoxy groups hinder the crosslinking among units thus reducing the extent of branching. [165], [166] The prevalence of highly methoxylated S units in hardwood lignin makes its structure generally linear, with a relatively low frequency of crosslinks. Conversely, softwood lignin results more branched due to the preponderance of G units which are prone to further radical coupling reactions in position 5, thus enhancing the potential connectivity. [167]

Lignocellulosic biomass presents a complex structure in which cellulose, hemicellulose and lignin are tightly entangled. In order to be exploited, these three main components must be divided. For this purpose, fractionation pre-treatments are essential in the processing of lignocellulose for most applications. [168]

Based on the type of source and desired product, different techniques, including mechanical, chemical and biological strategies, can be employed. The most relevant approaches are mechanical comminution,

pyrolysis, steam explosion, ammonia explosion, CO_2 explosion, ozonolysis, acid/alkaline hydrolysis, organosolv and biodegradation. [169] There also exist industrial processes based on different technologies. Traditionally, lignin has always been considered as a low-value coproduct in paper industry which considers cellulose as the desired product. Recently the new concept of biorefinery has caught on. According to this holistic approach, all the biomass components should be valorised and converted into valuable products. Whichever the case, lignin separation is the crucial step. Industrial processes insert impurities and alternative lignin structure: in particular, the cleavage of some ether and ester bonds results in a variation of both molecular weight and functional groups distribution. Impure, fragmented lignins isolated at industrial scale are usually referred to as technical lignins. The main industrial processes include sulphur-based or, alternatively, sulphur-free strategies, as reported in Scheme 3.

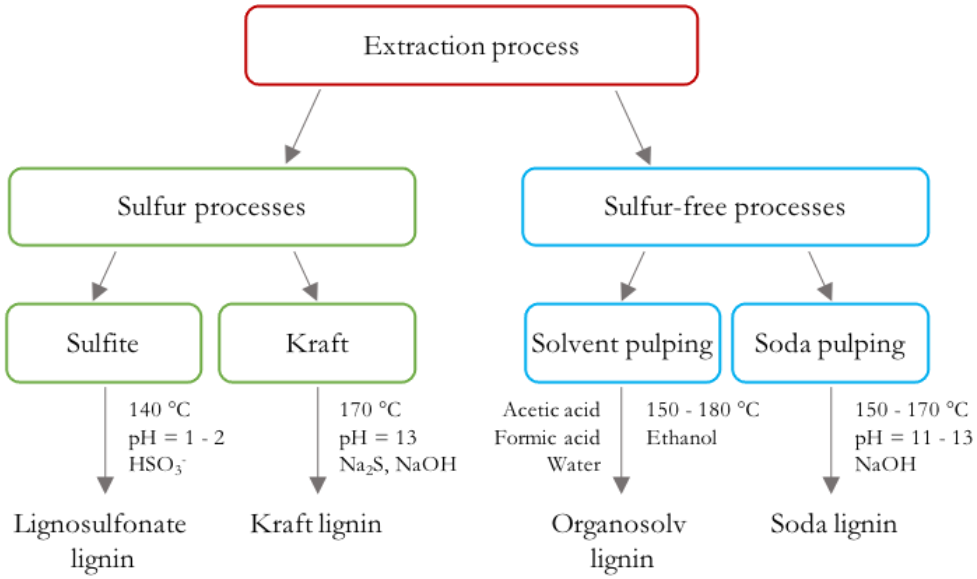

Scheme 3. Schematic representation of the main industrial processes for the production of technical lignins.

The most common procedure, denominated the kraft process, is widely used by pulp and paper industries, and is estimated to yearly generate $6 \cdot 10^5$ tons of lignin and to constitute about 85% of the world lignin production. [170] Cooking in an oxidative atmosphere induces sulphur incorporation (up to 2%), β-*O*-aryl bond cleavage and consequent increase in the amount of phenolic hydroxyl groups which are prone to induce the formation of condensed structures. Kraft pulping additionally induces the conversion of β-1' and β-5' into stilbene and aryl enol ether subunits. Lignin fragments, which result soluble in the alkaline, dark solution termed as black liquor, are then precipitated by the addition of a diluted solution of sulfuric acid and recovered. Kraft lignin generally shows a number average molecular weight ranging 1000-3000 Da with a polydispersity between 2 and 4. Kraft lignin produced during

papermaking is mainly burnt as a fuel and only 2% is isolated and sold. A structural representation of softwood kraft lignin is shown in Figure 11.

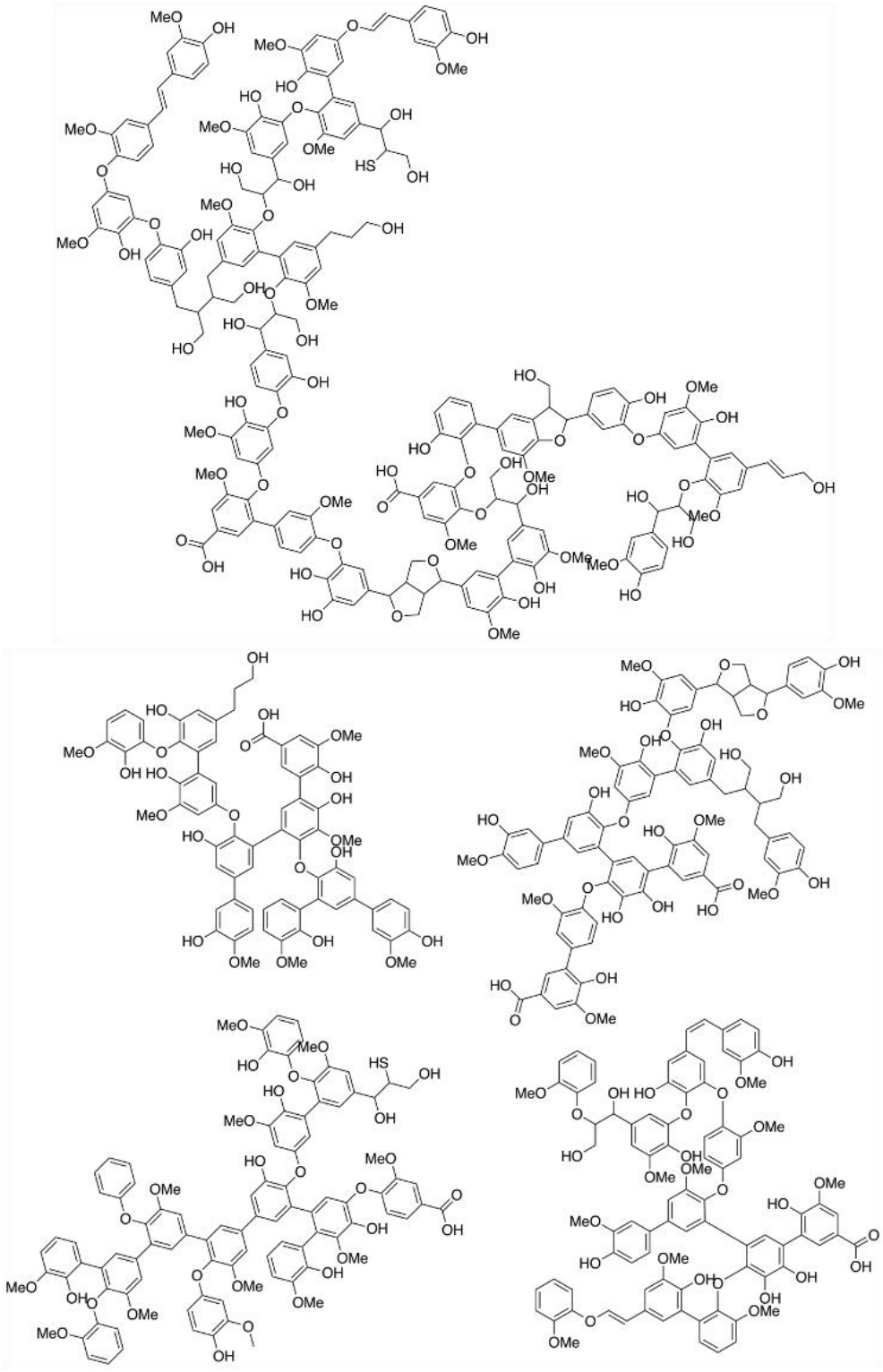

Figure 11. Schematic representation of softwood kraft lignin structure.

An alternative industrial strategy for the isolation of lignin is the sulphite process. During the cooking in the presence of HSO_3^- and SO_3^{2-}, half phenylpropanoid units result to be sulfonated and the ensuing product is a water-soluble polyelectrolyte. Lignosulfonates are then recovered as ammonium, sodium, magnesium or calcium salts. The sulphite process induces the cleavage of β-*O*-4 bonds and favours condensation reactions, resulting in a number average molecular weight between 1000 and 140000 Da, although the most common range is between 5000 and 20000 Da. Polydispersity is typically comprised between 4 and 9 and sulphur content commonly ranges between 3% and 8 %.
If compared to sulphur-based processes, the sulphur-free ones produce highly fragmented lignin with a chemical structure quite similar to the native one. Among them, soda or alkaline pulping allows recovering highly pure lignin which can be used in specific applications where the presence of sulphur would be a concern. Soda lignin may present high silicate and nitrogen contents. The presence of concentrated bases favours the cleavage of β-*O*-4 bonds and the isolation of low molecular weight lignin (1000-6000 Da). The organosolv process uses a mixture of organic solvents (including acetic/formic/organic peroxide acids and ethanol) and water. If compared to other technical lignins, the organosolv one proves more hydrophobic, less condensed, sulphur-free, and thus differently valuable. The average molecular weight is commonly less than 1000 Da with a polydispersity between 2.4 and 6.4. [130], [170]

Lignin is recognised to bear a wide variety of functional groups, *i.e.*, aliphatic and phenolic hydroxyls, carboxylic, carbonyl and methoxyl groups, which suggest the possibility for further chemical modification and lignin employment as a new chemical feedstock, especially for the synthesis of aromatic chemicals. Only 2% of lignin extracted throughout the world is presently exploited as a chemical raw material. Most lignin is considered as a waste product in the process of cellulose fibres isolation during which it undergoes chemical degradation into fragments (whose average molecular weight ranges from one thousand to tens of thousands) which are mostly combusted to provide energy. [171] Reproducibility is the most challenging issue in the use of lignin as a source of macromonomers for the synthesis of polyesters, polyurethanes or polyethers, as an additive in polymeric composites or as a precursor to carbon-based materials. Structural variability, inconstant molecular weight distribution, and the presence of impurities in technical lignin may cause variations in the properties of the final material. New biorefinery processes for lignin extraction have been developed to better control the features of low-molecular weight lignin fragments which are meant to be a source of macromonomers. [162] Currently, lignin, mainly in the form of lignosulphonates, is employed as a stabiliser for plastics and rubber, phenolic resins, dispersants, automotive brakes and wood panel products. [173] Additionally, it is object of study for its valorisation and production of aromatic chemicals, carbon fibres and thermoplastics. [174] Definitely, one of the most

intriguing challenges in lignin chemistry is the development of efficient, cheap, and green processes for both isolation and valorisation including chemical modifications. [175]

3.4 Lignin carbohydrate complexes (LCC)

In lignocellulosic biomass, cellulose, hemicellulose and lignin are tightly connected through either non-covalent interactions or covalent bonds which involve carbohydrates and lignin aromatic and aliphatic hydroxyls. [176] Covalent links are supposed to include ester and ether bonds as illustrated in Figure 12.

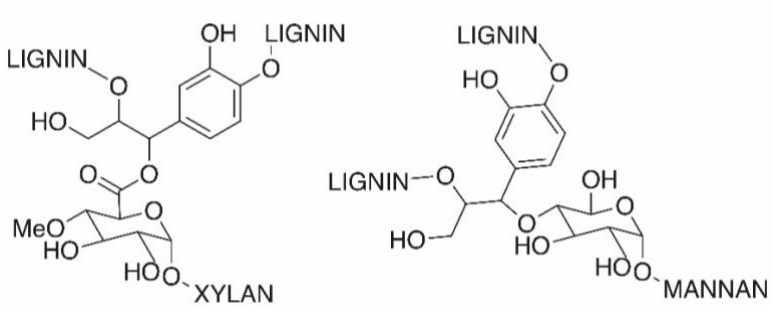

Figure 12. Examples of ester and ether bonds between lignin and carbohydrates.

3.5 Minor components

Lignocellulosic biomass includes minor components along with cellulose, hemicellulose and lignin. These constituents do not influence the feedstock properties and processability and mostly include small organic compounds such as extractives and mineral fractions, the so-called ashes comprising metal oxides. According to the botanical origin, extractives can constitute 2-25% of the dry mass of the source. They encompass alkanes, fatty alcohols, fatty acids, free and conjugated sterols, terpenoids, triglycerides and waxes. The lipophilic nature of these compounds may impact on fractionation processes. [177] Moreover, plant cell walls include other organic molecules such as starch, pectin and proteins. Conversely, ashes may contribute to 2–17% of the dry mass of the feedstock. They comprise different metal oxides such as SiO_2, Al_2O_3, Na_2O, K_2O, MgO and CaO. [178]

4 Valorisation of lignin as alternative reinforcing filler in the rubber industry

Lignin seems a promising alternative to carbon black in rubber industry. Lignin, especially kraft lignin deriving from paper and pulp industry, is available at industrial scale. It is a rather cheap material deriving from renewable resources. The use of lignin as bio-filler in rubber compounds has gained more and more attention due to concerns regarding the toxicity of carbon black on health and environment [179] So, lignin is being regarded as a valid alternative to carbon black due to its good physical chemical and mechanical properties, antioxidant activity and thermal stability. [180] However, incorporating lignin in a rubber matrix requires the overcome the scarce compatibility between the two materials due to the polarity of lignin molecules which result into strong self-interactions. As a consequence, lignin is often chemically modified to enhance its dispersion in the elastomeric matrix and improve its interfacial adhesion to the rubber macromolecules. The abundancy of functional groups in lignin, including aliphatic alcohols, phenols and carboxylic acids, suggest for the possibility for a chemical modification in order to enhance an appropriate compatibility with rubber matrix. [99] The reinforcing capacity of lignin strongly depends on strong interfacial adhesion with rubber matrix and particle size. [181] As a result, in order to improve the reinforcing effects of lignin, it is possible to functionalise lignin so that covalent bonds can be formed with rubber macromolecules during vulcanisation. [183]– [185] Another possibility to enhance the reinforcing effects of lignin could be to convert it into nanoparticles, which are known to display unique properties due to their high surface to volume ratio. A high surface area results into a high contact area with the elastomeric matrix and the immobilisation of a few nanometres thick portion of rubber which is stacked to the filler and resists to solvent dissolution. So, in the present research, both possibilities were explored with a particular attention on the development of sustainable and green approaches.

4.1 Mechanochemical functionalisation of lignin

In literature, many wet chemistry synthetic strategies have been reported for the chemical modification of lignin. The most targeted groups include aliphatic alcohols, phenols, and carboxylic acids. The most popular approaches comprise the use of organic solvents as reaction media, as such being affected by a high environmental impact and use of hazardous chemicals. [186], [187] However, mechanochemistry can be regarded as an alternative to run reactions in the solid state, taking advantage of mechanical energy to trigger chemical transformations. [182] As such, it is associated with the avoidance or saving of organic solvents, waste reduction, and up to quantitative yields thanks to an increase also due to the absence of extensive work-up procedures. [188], [189] Mechanochemistry relies on the intimate contact between

functionalising agents and substrate, and a high energy associated with shear and friction forces typical for the milling process. [190] Such milling proved to increase the surface area of the substrate and to be associated to an alteration of its reactivity, resulting in different reaction outcomes with respect to wet chemistry. [191]– [193] In fact, mechanochemistry is known to open synthetic possibilities which are commonly inaccessible to wet chemistry alternative procedures due to its power to induce an intimate contact between reagents, overcome solubility restrictions and provide mechanical energy to induce chemical reactions. [194]

The study of mechanochemistry applied to lignin is emerging as a new, yet underinvestigated, trend in research (Figure 13).

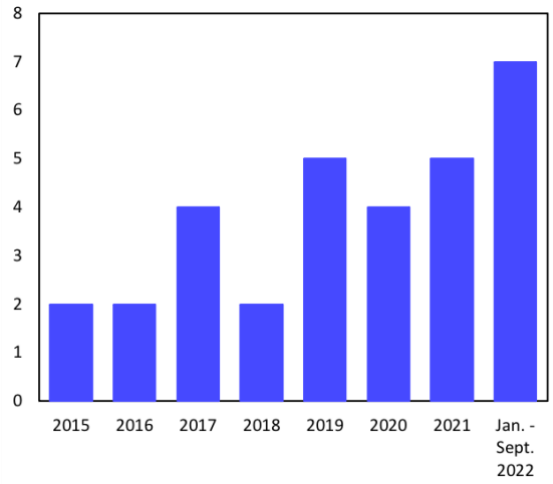

Figure 13. Bibliometrics of the keywords 'mechanochemistry' and 'lignin' in the period 2015 - Sept. 2022 (source: Scopus).

Mechanochemical modifications of lignin reported in literature include the reduction in particle size associated with milling, depolymerisation and chemical modification. Most works are focused on lignin fragmentation into lower molecular weight molecules to be used as platforms for the synthesis of new materials. [195]– [197] The structural complexity of lignin has caused, however, a focussing on the study of lignin model compounds in order to assess the possible interunit bonds which are susceptible to mechanochemical cleavage. [198]- [200] It is unfortunately very questionable to which extend insights gained on the basis of models can be extrapolated to predict how a lignin sample will behave, since the density of various functional groups in an oligomeric or polymeric lignin molecule cause chemically very different situations than encountered in a lignin model. Some studies have been devoted to the chemical functionalisation of lignin model compounds and only a few have been focused on lignin as substrate. In particular, attention has been attracted by the esterification of polar hydroxyl groups of lignin model compounds and lignin. The conversion of those functional groups into esters was achieved for lignin

model compounds by using non-cyclic or cyclic anhydrides as acylating agents and using an enzyme to catalyse the reaction. [201] However, this strategy presents drawbacks associated to poor atom efficiency and suffers from high environmental impact and use of hazardous chemicals. In addition, this approach prevented the possibility to recover the enzyme, which could not be reused for the production of further batches of functionalised lignin. In literature it has been described the possibility to functionalise organosolv lignin *via* mechanochemical transesterification using methyl oleate as acyl donor and KOH as catalyst. [202] This approach was reported to functionalise 25 % of hydroxyl groups. Starting from this reference, the present work aimed at functionalising lignin using acyl donors which could provide lignin with an activated double bond. The introduction of this functionality was expected to ensure a covalent bond of lignin to the rubber macromolecules, aiming at the mechanical reinforcement of compounds.

4.2 Nanolignin as reinforcing filler

Lignin nanoparticles (LNPs) are a new frontier in the field of nanomaterials which is driving more and more attention (Figure 14), aiming at the development of novel functional materials based on renewable sources.

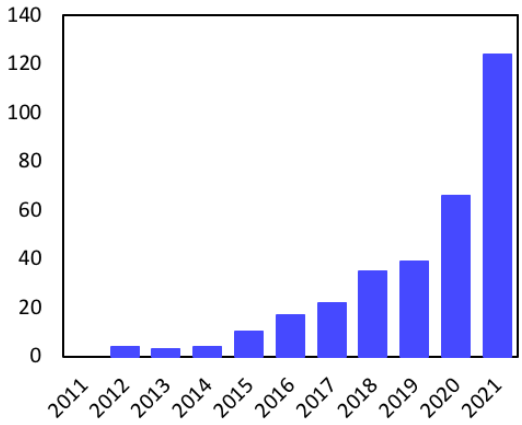

Figure 14. Bibliometrics of the keyword 'nanolignin' in the years 2011-2021 (source: Scopus).

Nanomaterials display unique properties related to their high surface area while their interactions depend on the surface chemistry. When included in polymeric compounds, they are known to exhibit superior reinforcing effects than the corresponding micrometric material due to their high contact area with the matrix. [203], [204] The large interface results in immobilisation of a portion of polymeric matrix which is stacked to the filler and resists to mechanical stresses. The nanoformulation of lignin could be inserted in the frame of this current knowledge in order to develop bio-based reinforcing fillers for rubber

compounds. LNPs may find application in a large variety of fields including nanomedicine, UV-blockers, antioxidants, reinforcement of polymers, electrodes. [205] However, the structural heterogeneity of lignin makes the production of nanomaterials challenging. [206] The main preparation procedures for nanolignin include:

- anti-solvent precipitation using water, acid solutions and supercritical CO_2 as antisolvent;
- physicochemical treatments as ultrasonication and homogenisation;
- other preparations as ice segregation-induced self-assembly, aerosol-slow synthesis and electrospinning of solutions. [207]

The most studied approaches for the formation of solid nanoparticles include anti-solvent precipitation. Solvent shifting includes the mixing of a lignin solution with an excess of antisolvent which is associated to the formation of nanoparticles due to their decreasing solubility. [208] Nanoparticles formed by solvent shifting display a spherical morphology due to minimisation of surface energy. The most popular technique involves the dissolution of lignin into a water-miscible organic solvent and the addition of excess water as antisolvent to induce nanoprecipitation. This method seems promising due to its possibility of scalability and tunability of nanoparticles dimensions by controlling volume and flow rate of both lignin solution and antisolvent, concentration of lignin solution. [209]

Nanolignin has demonstrated to create better interactions with polymeric matrixes than the corresponding micrometric material. [204] These enhanced interactions resulted in a reinforcing effect of nanolignin when blended with different polymers, including polylactic acid (PLA) [210], [211] and polyvinyl alcohol (PVA). [212] In preliminary studies, nanolignin demonstrated to display a strong interfacial interaction with natural rubber and have a positive impact on the mechanical properties of the composite. [100] This preliminary state of the art was considered as a promising starting point for the development of nanolignin-natural rubber compounds aiming at equalling or even improving the mechanical performances with respect to fossil-based fillers, *i.e.*, carbon black, while incrementing the content in bio-based materials in rubber composites for tyre industry.

References

[1] http://www.digitaltrends.com/cars/modern-tyre-technology-basics/

[2] http://www.jags.org/TechInfo/2001/05May01/tyres/historyoftyres.htm

[3] http://www.madehow.com/Volume–1/Tyre.html

[4] http://www.companieshistory.com/pirelli/

[5] https://rubberworld.com/global-tyre-market-forecast-to-produce-over-2-7-billion-tyres-by-2026

[6] https://corporate.pirelli.com/corporate/en-ww/investors/annual-report-download-2021

[7] https://www.bridgestone.com/responsibilities/library/pdf/sr2020.pdf

[8] B. Rodgers, *Rubber Compounding: Chemistry and Applications,* Marcel Dekker, 2004.

[9] J. E. Mark, B. Erman, F. R. Eirich, *Science and Technology of Rubber,* Elsevier Academic Press, 2005.

[10] A. K. Chandra, V. Bhandari, *Adv. Elastomers II*, Springer, Berlin, Heidelberg, **2013**, *55*, 183.

[11] D. J. Schuring, *Rubber Chem. Technol.* **1990**, *53*, 600.

[12] *Indian Rubber Institute., Rubber Engineering*, 1st ed., McGraw-Hill, New York, 1999.

[13] T. L. Ford, F. S. Charles, *Heavy Duty Truck Tyre Engineering*, SAE's 34th L. Ray Buckingdale Lecture, SP729, 1988.

[14] J. A. Davison, *Design and Application of Commercial Type Tyres*, SAE's 15th L. Ray Buckingdale Lecture, SP344, 1969.

[15] http://thetyredigest.michelin.com/an-unknown-object-the-tyre-materials

[16] J. L. Leblanc, *Prog. Polym. Sci.* **2002**, *27*, 627.

[17] W. M. Hess, W. K. Klamp, *Rubber Chem. Technol.* **1983**, *56,* 390.

[18] S. Hui, T. K. Chaki, S. Chattopadhyay, *J. Appl. Polym. Sci.* **2008***, 110,* 825.

[19] A. Bertora, M. Castellano, E. Marsano, M. Alessi, L. Conzatti, P. Stagnaro, G. Colucci, A. Priola, A. Turturro, *Macromol. Mater. Eng.*, **2011**, *296*, 455.

[20] M. Bhattacharya, M. Maiti, A. K. Bhowmick, *Rubber Chem. Technol.*, **2008**, *81*, 782.

[21] G. Ramorino, F. Bignotti, S. Pandini, T. Riccò, *Compos. Sci. Technol.*, **2009**, *69,* 1206.

[22] V. Favier, G. R. Canova, J. Y. Cavaillé, H. Chanzy, A. Dufresne, C. Gauthier, *Polym. Adv. Technol.*, **1995**, *6*, 351.

[23] M. A. S. Azizi Samir, F. Alloin, A. Dufresne, *Biomacromolecules*, **2005**, *6*, 612.

[24] R. Evans, *The Composition of a Tyre: Typical Components Creating markets for recycled resources*, 2006.

[25] https://rma.org/about-rma/rubber-faqs

[26] M. Guaita, F. Ciardelli, E. P. La Mantia, *Fondamenti di scienza dei polimeri*, Edizioni N., 2006.

[27] http://thetyredigest.michelin.com/an-unknown-object-the-tyre-materials

[28] H. Warson, *Appl. Synth. Resin Latices*, 2001, 1.

[29] M. Negahban, *Int. J. Solids Struct.* **2000**, *37*, 2811.

[30] L. E. Nielsen, F. D. Stockton, *J. Polym. Sci. Part A Gen. Pap.*, **1963**, *1*, 1995.

[31] A. T. Di Benedetto, *J. Polym. Sci. Part B Polym. Phys.* **1987**, *25*, 1949.

[32] L. R. G. Treloar, *Rubber Chem. Technol.* **1974**, *47*, 625.

[33] https://www.goodyear.eu/en_gb/consumer/learn/how-tyres-are-made.html

[34] https://www.european-rubber-journal.com/article/2065874/iisrp-publishes-worldwide-rubber-statistics-2017

[35] J. E. Puskas, E. Gautriaud, A. Deffieux, J. P. Kennedy, *Prog. Polym. Sci.* **2006**, *31*, 533.

[36] M. J. R Loadman, *J. Therm. Anal. Calorim.* **1985**, *30*, 929.

[37] J. B. van Beilen, Y. Poirier, *Trends Biotechnol.* **2007**, *25*, 522.

[38] Y. Hayashi, *Plant Biotechnol.* **2009**, *26*, 67.

[39] U. K. Niyogi, *Intros. to Fibre Sci. Rubber Technol.* **2007**.

[40] C. C. Ho, T. Kondo, N. Muramatsu, H. Ohshima, *J. Colloid Interface Sci.* **1996**, *178*, 442.

[41] J. Sansatsadeekul, J. Sakdapipanich, P. Rojruthai, *J. Biosci. Bioeng.* **2011**, *111*, 628.

[42] M. M. Rippel, F. Galembeck, *J. Braz. Chem. Soc.* **2009**, *20*, 1024.

[43] H. Zhang, A. K. Scholz, Y. Merckel, M. Brieu, D. Berghezan, E. J. Kramer, C. Creton, *J. Polym. Sci. Part B Polym. Phys.* **2013**, *51*, 1125.

[44] (a) J. A. Brydson, *Rubber Chemistry*, Applied Science Publishers, 1978; (b) A. N. Gent, *Engineering with Rubber: How to Design Rubber Components*, Hanser, Munich, 2001.

[45] M. Morton, *Rubber World* **1989**, *201*, 55.

[46] http://www.therubbereconomist.com/The_Rubber_Economist/Vehicle_and_tyre.html

[47] B. Rodgers, *Rubber Compounding: Chemistry and Applications*, Marcel Dekker, 2004.

[48] B. Rodgers, W. H. Waddell, S. Solis, W. Klingensmith, *Kirk-Othmer Encycl. Chem. Technol.*, John Wiley & Sons, Inc., Hoboken, NJ, USA, 2004.

[49] D. R. Tobergte, S. Curtis, *J. Chem. Info. Model.* **2013**, *53*, 1689.

[50] Charles Goodyear, US3633A, 1844.

[51] J. E. Mark, B. Erman, F. R. Eirich, *Science and Technology of Rubber*, Elsevier Academic Press, 2005.

[52] W. Hofmann, *Vulcanisation and Vulcanising Agents.*, Maclaren and Sons Ltd., London, 1967.

[53] P. Ghosh, S. Katare, P. Patkar, J. M. Caruthers, V. Venkatasubramanian, K. A. Walker, *Rubber Chem. Tech.* **2003**, *76*, 592.

[54] C. S. S. R. Kumar, A. M. Nijasure, *Resonance* **1997**, *2*, 55.

[55] A. Y. Coran, *J. Appl. Polym. Sci.* **2003**, *87*, 24.

[56] L. González, A. Rodríguez, J. L. Valentin, A. Marcos-Fernández, P. Posadas, *K. G. K.* **2005**, *58*, 638.

[57] G. Heideman, R. N. Datta, J. W. M. Noordermeer, B. van Baarle, *J. Appl. Polym. Sci.* 2005, *95*, 1388.

[58] A. N. Gent, *Engineering with rubber*, Hanser Publications, 2012.

[59] http://www.indiarubberdirectory.com/engineering/standard_rubber_formulations.asp

[60] B. B. Boonstra *Polymer* **1979,** *20*, 691.

[61] J. Fröhlich, W. Niedermeier, H.D. Luginsland, *Compos. Part A Appl. Sci. Manuf.* **2005,** *36*, 449.

[62] S. J. Park, K. S. Cho, *J. Colloid Interface Sci.* **2003,** *267*, 86.

[63] J. E. Mark, B. Erman, F. R. Eirich, *Science and Technology of Rubber*, Elsevier Academic Press, 2005.

[64] W. M. Hess, *Rubber Chem. Technol.* **1991,** *64,* 386.

[65] C. R. Herd, G. C. McDonald, W. M. Hess, *Rubber Chem. Technol.* **1992,** *65*, 107.

[66] D. Barnard, C. S. L. Baker, I. R. Wallace, *Rubber Chem. Technol.* **1985,** *58*, 740.

[67] S. Lowell, Joan E. Shields, Martin A. Thomas, Matthias Thommes, *Characterisation of Porous Solids and Powders: Surface Area, Pore Size and Density*, Kluwer Academic Publishers, **2004**.

[68] M. J. Wang, *Rubber Chem. Technol.* **1999**, *72*, 430.

[69] M. J. Wang, *Rubber Chem. Technol.* **1998**, *71,* 520.

[70] W. Niedermeier, J. Froehlich, H. Luginsland, *K. G. K.* **2002,** *55*, 356.

[71] A. R. Payne, R.E. Whittaker, *Rubber Chem. Technol.* **1971**, *44*, 440.

[72] I. Pliskin, N. Tokita, *J. Appl. Polym. Sci.* **1972**, *16*, 473.

[73] T. Vilgis, G. Heinrich, M. Kluepell, *Reinforcement of Polymer Nano-Composites: Theory, Experiments and Applications*, Cambridge University Press, 2009.

[74] J. J. Brennan, T. E. Jermyn, B. B. Boonstra, *J. Appl. Polym. Sci* **1964,** *8*, 2687.

[75] A.R. Payne, W.F. Watson, *Rubber Chem. Technol.* **196**3, *36*, 147.

[76] Y. Chevallier, J. Morawski, EP0157703A1, **1985**.

[77] L. R. Evans, W.H. Waddell, *K. G. K.* **1995**, *48*, 718.

[78] W. M. Hess, G. C. McDonald, E. Urban, *Rubber Chem. Technol.* **1973**, *46,* 204.

[79] D. S. Villars, *J. Am. Chem. Soc.* **1947**, *69*, 214.

[80] E. Papirer, V. T. Nguyen, J. B. Donnet, *Carbon N. Y.* **1978**, *16*, 141.

[81] D. Rivin, J. Aron, A. I. Medalia, *Rubber Chem. Technol.* **1968**, *41*, 330.

[82] ASTM D1765.

[83] J. O'Brien, E. Cashell, G.E. Wardell, V. J. McBrierty, *Macromolecules* **1976**, *9,* 653.

[84] A. P. Legrand, N. Lecomte, A. Vidal, B. Haidar, E. Papirer, *J. Appl. Polym. Sci.* **1992**, *46,* 2223.

[85] T. A. Vilgis, G. Heinrich, *Macromolecules* **1994**, *27*, 7846.

[86] R. Rauline, EP0501227A1, **1992**.

[87] A. P. Legrand, *The Surface Properties of Silicas*, John Wiley, **1998**.

[88] W. L. Hergenrother, J. Oziomek, W. M. Cole, US6180710B1, **2001**.

[89] U. Goerl, A. Hunsche, A. Mueller, H. G. Koban, *Rubber Chem. Technol.* **1997***, 70,* 608.

[90] M. P. Wagner, *Rubber Chem. Technol.* **1976***, 49*, 703.

[91] W. H. Waddell, L. R. Evans, *Rubber Chem. Technol.* **1996***, 69*, 377.

[92] K. W. Stöckelhuber, A. Das, R. Jurk, G. Heinrich, *Polymer* **2010**, *51*, 1954.

[93] P. Zhang, M. Morris, D. Doshi, *Rubber Chem. Technol.* **2016**, *89*, 79.

[94] A. F. Martins, L. L. Y. Visconte, R. C. R. Nunes, *K. G. K.* **2002**, *55*, 637.

[95] G. Siqueira, S. Tapin-Lingua, J. Bras, D. da Silva Perez, A. Dufresne, *Cellulose* **2011**, *18*, 57.

[96] H. Angellier, S. Molina-Boisseau, A. Dufresne *Macromolecules* **2005**, *38*, 9161.

[97] K. Gopalan Nair, A. Dufresne, *Biomacromolecules* **2003**, *4*, 657.

[98] A. Das, K. W. Stöckelhuber, R. Jurk, M. Saphiannikova, J. Fritzsche, H. Lorenz, M. Klüppel G. Heinrich, *Polymer* **2008**, *49*, 5276.

[99] P. Frigerio, L. Zoia, M. Orlandi, T. Hanel, L. Castellani, *BioResources* **2014**, *9*, 1387.

[100] C. Jiang, H. He, H. Jiang, L. Ma, D. M. Jia, *Express Polym. Lett.* **2013**, *7*, 480.

[101] S. C. Peterson, *J. Elastomers Plast.* **2012**, *44*, 43.

[102] O. O. Fadiran, J. C Meredith, *J. Mater. Chem. A* **2014**, *2*, 17031.

[103] V. K. Thakur, D. Grewell, M. Thunga, M. R. Kessler, *Macromol. Mater. Eng.* **2014**, *299*, 953.

[104] S. K. De, J. R. White, *Rubber Technologist's Handbook*, Rapra Technology Ltd, **2001**.

[105] J. C. Serrano-Ruiz, R. Luque, A. Sepúlveda-Escribano, *Chem. Soc. Rev.* **2011**, *40*, 5266.

[106] M. Alonso, J. Q. Bond, J. A. Dumesic, *Green Chem.* **2010**, *12*, 1493.

[107] E. Regnier, *Energy Econ.* **2007**, *29*, 405.

[108] W. Steffen, W. Broadgate, L. Deutsch, O. Gaffney, C. Ludwig, *Anthr. Rev.* **2015**, *2*, 81.

[109] W. Steffen, P. J. Crutzen; J. R. McNeill, *A. J. Hum. Environ.* **2007**, *36*, 614.

[110] V. Vandermeulen, M. Van der Steen, C. V. Stevens, G. Van Huylenbroeck, *Bioprod. Biorefining* **2012**, *6*, 453.

[111] A. J. Ragauskas, C. K. Williams, B. H. Davison, G. Britovsek, J. Cairney, C. A. Eckert, W. J. Frederick, J. P. Hallett, D. J. Leak, C. L. Liotta, J. R. Mielenz, R. Murphy, R. Templer and T. Tschaplinski, *Science* **2006**, *311*, 484.

[112] V. Dornburg, B. G. Hermann, M. Patel, *Environ. Sci. Technol.* **2008**, *42*, 2261.

[113] B. Kamm, P. R. Gruber, M. Kamm, *Biorefineries-Industrial Processes and Products*, Vols. 1&2, Wiley-VCH, Weinheim, **2006**.

[114] T. E. Amidon, C. D. Wood, A. M. Shupe, Y. Wang, M. Graves, S. Liu, *J. Biobased Mater. Bioenergy* **2008**, *2*, 100.

[115] G. M. Campbell, P. Vadlani, A. Azapagic, *Chem. Eng. Res. Special Issue on Biorefinery Innovations* **2009**, *87*, 1101.

[116] C. H. Zhou, X. Xia, C.X. Lin, D. S. Tong, J. Beltramini, *Chem. Soc. Rev.* **2011**, *40*, 5588.

[117] C. H. Zhou, J. N. Beltramini, Y. X. Fan, G. Q. Lu, *Chem. Soc. Rev.* **2008**, *37,* 527.

[118] G. W. Huber, S. Iborra, A. Corma, *Chem. Rev.* **2006**, *106,* 4044.

[119] C. Somerville, H. Youngs, C. Taylor, S. C. Davis, S. P. Long *Science* **2010**, *329*, 790.

[120] E. Taarning, C. M. Osmundsen, X. Yang, B. Voss, S. I. Andersen, C. H. Christensen, *Energy Environ. Sci.* **2011**, *4,* 793.

[121] P. Mäki-Arvela, I. Anugwom, P. Virtanen, R. Sjöholm, J. P. Mikkola, *Ind. Crops Prod.* **2010**, *32,* 175.

[122] N. Sun, H. Rodríguez, M. Rahman, R.D. Rogers, *Chem. Commun.* **2011**, *47,* 1405.

[123] A. Barakat, H. de Vries, X. Rouau, *Bioresour. Technol.* **2013**, *134*, 362.

[124] Y. Sun, J. Cheng, *Bioresour. Technol.* **2002**, *83*, 1.

[125] F. Cherubini, *Energy Convers. Manag.* **2010**, *51*, 1412.

[126] M. J. Taherzadeh, K. Karimi, *Int. J. Mol. Sci.* **2008**, *9,* 1621.

[127] D. M. Alonso, S. G. Wettstein, J. A. Dumesic, *Green Chem* **2013**, *15*, 584.

[128] T. Abbasi, S. A. Abbasi, *Renew. Sustain. Energy Rev.* **2010**, *14*, 919.

[129] Y. H. P. Zhang, *J. Ind. Microbiol. Biotechnol.* **2008**, *35*, 367.

[130] S. Laurichesse, L. Avérous, *Progress in Polymer Science 39*, **2014**, 1266.

[131] V. K. Thakur, M. K. Thakur, P. Raghavan, M. R. Kessler, *ACS Sust. Chem. Eng.* **2014**, *2,* 1072.

[132] A. Barakat, H. de Vries, X. Rouau, *Bioresour. Technol. 134*, **2013**, 362.

[133] B. Saha, C. T. Hou, *Handb. Ind. Catal.*, 1st ed., CRC Press, **2005**, 1.

[134] Mark B. O. Menges, *Encyclopedia of polymer science and engineering – Vol. 8*, John Wiley&Sons, 2nd Edition, **1987**.

[135] V. Urgatondo, M. Mitjans, M.P. Vinardell, *Industrial Crops and Products 30*, **2009**, 184.

[136] M. H. Hussin, A. A Rahim, M. N. M. Ibrahim, M. Yemloul, D. Perrin, N. Brosse, *Industrial Crops and Products* **2014**, *52,* 544.

[137] http://www.diffen.com/difference/Angiosperms_vs_Gymnosperms

[138] http://www.diffen.com/difference/Hardwood_vs_Softwood

[139] http://sbi3uiplantkingdom.weebly.com/week–12/herbaceous-vs-woody-plants

[140] D. Klemm, F. Kramer, S. Moritz, T. Lindstrom, M. Ankerfors, D. Gray, A. Dorris, Y. Habibi, L. Lucia, O. J. Rojas, *Angew. Chemie - Int. Ed.* **2009**, *50*, 5438.

[141] X. Qiu, S. Hu, *Materials (Basel)* **2013**, *6*, 738

[142] B. B. Hallac, A. J. Ragauskas, *Biofuels, Bioprod. Biorefining* **2011**, *5*, 215.

[143] M. Mutwil, S. Debolt, S. Persson, *Curr. Opin. Plant Biol.* **2008**, *11*, 252.

[144] S. Rebouillat, F. Pla, *J. Biomat. Nanobiotech.* **2013**, *4*, 165.

[145] R. M. Brown, J. *Macromol. Sci. Part A* **1996**, *33*, 1345.

[146] M. Rose, R. Palkovits, *Macromol. Rapid Commun.* **2011**, *32*, 1299.

[147] D. Klemm, H. Schmauder, T. Heinze, *Biopolymers* **2002**, *6*, 275.

[148] D. Klemm, B. Heublein, H. Fink, A. Bohn, *Ang. Ch. - Int. Ed.* **2005**, *44*, 3358.

[149] D. Klemm, F. Kramer, S. Moritz, *Angewandte Chemie International Edition* **2011**, *50*, 5438.

[150] X. Qiu, S. Hu, *Materials (Basel)* **2013**, *6,* 738.

[151] G. Siqueira, J. Bras, A. Dufresne, *Polymers (Basel)* **2010**, *2*, 728.

[152] R. J. Moon, A. Martini, J. Nairn, J. Simonsen, J. Youngblood, *Chem. Soc. Rev.* **2011**, *40*, 3941.

[153] S. Kalia, A. Dufresne, B. M. Cherian, B. S. Kaith, L. Avérous, J. Njuguna, E. Nassiopoulos, *Int. J. Polym. Sci.* **2011**, *2011*, 1.

[154] A. S. Mamman, J. M. Lee, Y. C. Kim, I. T. Hwang, N. J. Park, Y. K. Hwang, J. S. Chang, J. S. Hwang *Biofuels, Bioprod. Biorefining* **2008**, *2*, 438.

[155] X. Gao, R. Kumar, C. E. Wyman *Biotechnol. Bioeng.* **2014**, *111*, 1088.

[156] C.E. Wyman, *Biotechnol. Prog.* **2003**, *19*, 254.

[157] W. Boerjan, J. Ralph, M. Baucher, *Annu. Rev. Plant. Biol.* **2003**, *54*, 519.

[158] K. V. Sarkanen, C. H. Ludwig, *Lignin, Occurrence, Formation, Structure and Reactions,* Wiley/Interscience, New York, **1971**, 95.

[159] K. Freudenberg, A. C. Neish, *Constitution and biosynthesis of lignin*., Springer-Verlag, New York, **1968**, 47.

[160] E. Dorrestijn, L. J. J. Laarhoven, I. W. C. E. Arends, P. Mulder, *J. Anal. Appl. Pyrolysis* **2000**, *54*, 153.

[161] J. M. Finefield, D. H. Sherman, M. Kreitman, R. M. Williams, *Angew. Chem. Int. Ed. Engl.* **2012**, *51*, 4802.

[162] a. J. Zakzeski, P. C. A. Bruijnincx, A. L. Jongerius, B. M. Weckhuysen, *Chem. Rev.* **2010**, *110*, 3552. b. H. Lange, E. D. Bartzoka, C. Crestini, C. *Lignin Biorefinery: structure, pretreatment, and use*; in: M. Aresta, A. Dibenedetto, F. Dumeignil, *Biorefineries, an Introduction*; De Gruyter: Berlin, Boston, **2015**.

[163] A. Gandini, *Green. Chem.* 2011, *13*, 1061.

[164] A. U. Buranov, G. Mazza, *Ind. Crops Prod.* **2008**, *28*, 237.

[165] W. G. Glasser, R. A. Northey, T. P. Schultz, *Lignin: historical, biological, and materials perspectives.* ACS Symp. Ser., 742. Washington, DC, **1999**, 559.

[166] D. R. Ratnaweera, D. Saha, S. V. Pingali, N. Labbé, A. K. Naskar, M. Dadmun, *RSC Adv.* **2015**, *5*, 67258.

[167] D. S. Argyropoulos, L. Jurasek, L. Krištofová, Z. Xia, Y. Sun, E. Paluš, *J. Agr. Food Chem.* **2002**, *50,* 658.

[168] N. Mosier, C. Wyman, B. Dale, R. Elander, Y. Y. Lee, M. Holtzapple, M. Ladisch, *Bioresour. Technol.* **2005**, *96*, 673.

[169] Y. Sun, J. Cheng, *Bioresour. Technol.* **2002**, *83*, 1.

[170] A. G. Vishtal, A. Kraslawski, *BioResources* **2011**, *6*, 3547.

[171] J. Lora, *Monomers, Polymers and Composites from Renewable Resources Elsevier*, Amsterdam, **2008**, 225.

[172] M. N. Belgacem, A. Gandini, *Monomers, Polymers and Composites from Renewable Resources,* Elsevier, Amsterdam, **2008**.

[173] (a) J. H. Banoub, B. Benjelloun-Mlayah, F. Ziarelli, N. Joly, M. Delmas, *Rapid Commun. Mass Spectrom.* **2007**, *21*, 2867; (b) M. Delmas, *Chem. Eng. Technol.*, **2008**, *31*, 792.

[174] K. Biernat, P. L. Grzelak, *Biofuels - Status and Perspective*; InTech, **2015**.

[175] M. Kleinert, T. Barth, *Chem. Eng. Technol.* **2008**, *31*, 736.

[176] A. U. Buranov, G. Mazza, *Ind. Crops Prod.* **2008**, *28*, 237.

[177] G. Marques, J. C. del Río, A. Gutiérrez, A. *Bioresour., Technol.* **2010**, *101*, 260.

[178] D. Barana, A. Salanti, M. Orlandi, D. S. Ali, L. Zoia, *Ind. Crops Prod.* **2016**, *86*, 31.

[179] A. A. Basfar, M. M. Abdel-Aziz, S. Mofti, *Radiat. Phys. Chem.* **2002**, *63*, 81.

[180] N. A. Mohamad Ainim N. Othman, M. H. Hussin, K. Sahakaro, N. Hayeemasae, *Front. Mater.* **2020**, *6*, 329.

[181] C. Jiang, H. He, H. Jiang, L. Ma, D. M. Jia, *Express Polymer Letters* **2017**, *7*, 480.

[182] S. Dabral, M. Turberg, A. Wanninger, C. Bolm, J. G. Hernández, *Molecules* **2017**, *22*, 146.

[183] D. K. Setua, M. K. Shukla, V. Nigam, H. Singh, G. N. Mathur, *Polym. Compos.* **2000**, *21*, 988.

[184] V. K. Thakur, A. S. Singha, *Int. J. Polym. Anal. Charact.* **2010**, *15*, 471.

[185] C. Jiang, H. He, X. Yao, P. Yu, L. Zhou, D. Jia,, *J. Appl. Polym. Sci.* **2015**, *132*, 1.

[186] X. Zhao, Y. Zhang, M. Yang, Z. Huang, H. Hu, A. Huang, Z. Feng, *Polymers* **2018**, *10*, 907.

[187] M. Paravidino, U. Hanefeld, *Green Chem.* **2011**, *13*, 2651.

[188] M. J. Rak, T. Friščić, A. Moores, *Faraday Discuss.,* **2014**, *170*, 155.

[189] V. Strukil, M. D. Igrc, M. Eckert-Maksić, T. Friščić, *Chem. Eur. J.* **2012**, *18*, 8464.

[190] T. Friščić, C. Mottillo, H. M. Titi, *Angew. Chem. Int. Ed.* **2020**, *59*, 1018.

[191] J. G. Hernández, C. Bolm, *J. Org. Chem.* **2017**, *82*, 4007.

[192] H. Ashrafi, R. Emadi, R. Zamani Foroushani, *Adv. Powder. Technol.* **2015**, *26*, 1452.

[193] P. Pourghahramani, B. N. Akhgar *J. Ind. Eng. Chem.* **2015**, *25*, 131.

[194] J. L. Do, T. Friščić, *ACS Cent. Sci.* **2017**, *3*, 13.

[195] S. G. Yao, J. K. Mobley, J. Ralph, M. Crocker, S. Parkin, J. P. Selegue, M. S. Meier, *ACS Sustainable Chem. Eng.* **2018**, *6*, 5990.

[196] T. Kleine, J. Buendia, C. Bolm, *Green Chem.*, **2013**, *15*, 160.

[197] R. Behling, S. Valange, G. Chatel, *Green Chem.* **2016**, *18*, 1839.

[198] S. Dabral, H. Wotruba, J. G. Hernández, C. Bolm, *ACS Sustainable Chem. Eng.* **2018**, *6*, 3242.

[199] C. Sun, L. Zheng, W. Xu, A. V. Dushkin, W. Su, *Green Chem.* **2020**, *22*, 3489.

[200] C. Scimmi, L. Sancineto, C. Santi, *Int. J. Mol. Sci.* **2022**, *23*, 4378.

[201] U. Weißbach, S. Dabral, L. Konnert, C. Bolm, J. G. Hernández, *Beilstein J. Org. Chem.* **2017**, *13*, 1788.

[202] X. Guo, X. Junna, M. P. Wolcott, J. Zhang, *ChemistrySelect* **2016**, *1*, 3449.

[203] D. Dionisi, M. Beccari, S. Di Gregorio, M. Majone, M. P. Papini, G. Vallini, *J. Chem. Technol. Biotechnol. Int. Res. Process. Environ. Clean Technol.* 2005, *80*, 1306.

[204] S. S. Nair, S. Sharma, Y. Pu, Q. Sun, S. Pan, J. Y. Zhu, *ChemSusChem.* **2014**, *7*, 3513.

[205] W. D. H. Schneider, A. J. Pinheiro Dillon, M. Camassola, *Biotechnology Advances* **2021**, *47*, 107685

[206] S. Beisl, A. Miltner, A. Friedl, *Int. J. Mol. Sci.* **2017**, *18*, 1244.

[207] Z. Zhang, V. Terrasson, E. Guénin, *Nanomaterials* **2021**, *11*, 1336.

[208] F. R. Wurm, C. K. Weiss, *Front. Chem.* **2014**, *2*, 49.

[209] C. G. Conner, A. N. Veleva, V. N. Paunov, S. D. Stoyanov, O. D. Velev, *Part. Part. Syst. Charact.* **2020**, *37*, 2000122.

[210] W. Yang, E. Fortunati, F. Dominici, G. Giovanale, A. Mazzaglia, G. M. Balestra, J. M. Kenny, *Eur. Polym. J.* **2016**, *79*, 1.

[211] W. Yang, E. Fortunati, F. Dominici, J. M. M. Kenny, D. Puglia, *Eur. Polym. J.* **2015**, *71*, 126.

[212] W. Yang, J. S. Owczarek, E. Fortunati, M. Kozanecki, A. Mazzaglia, G. M. Balestra, G.M., J. M. Kenny, L. Torre, D. Puglia, *Ind. Crops Prod.* **2016**, *94*, 800.

EXPERIMENTAL SECTION

5 Materials

Solvents and reagents, unless otherwise indicated, were analytical-grade commercial products and used as received. Lignins here investigated included herbaceous alkaline lignin, hardwood kraft lignin. BIOPIVA™ 200 (UPM, Finland) softwood kraft lignin for mechanochemical esterification and rubber compounds, BIOPIVA™ 100 pine kraft lignin (UPM, Finland) for nanolignin for adhesives.

6 Analytical techniques

This section will present the main analytical techniques employed during the experimental work followed by technical specifications of the equipment and operational procedure details.

6.1 ^{1}H NMR spectroscopy

Lignin (25-30 mg) was dissolved in d_6-DMSO (0.750 mL) and spectra were registered by a Bruker Avance NMR spectrometer operating at 500.130 MHz (^{1}H).

6.2 ^{31}P NMR spectroscopy

The structural characterisation of lignin by ^{31}P NMR required the phosphitylation of hydroxyl-containing functional groups by the use of opportune derivatising agent as shown Scheme 4. After chemical modification and addition of an internal standard, it was possible to quantify aliphatic, carboxylic and phenolic functionalities, and even to distinguish among units deriving from the three monolignols: *p*-hydroxyl (H), guaiacyl (G), and syringyl (S). Characteristic signals are summarised in Table 2.

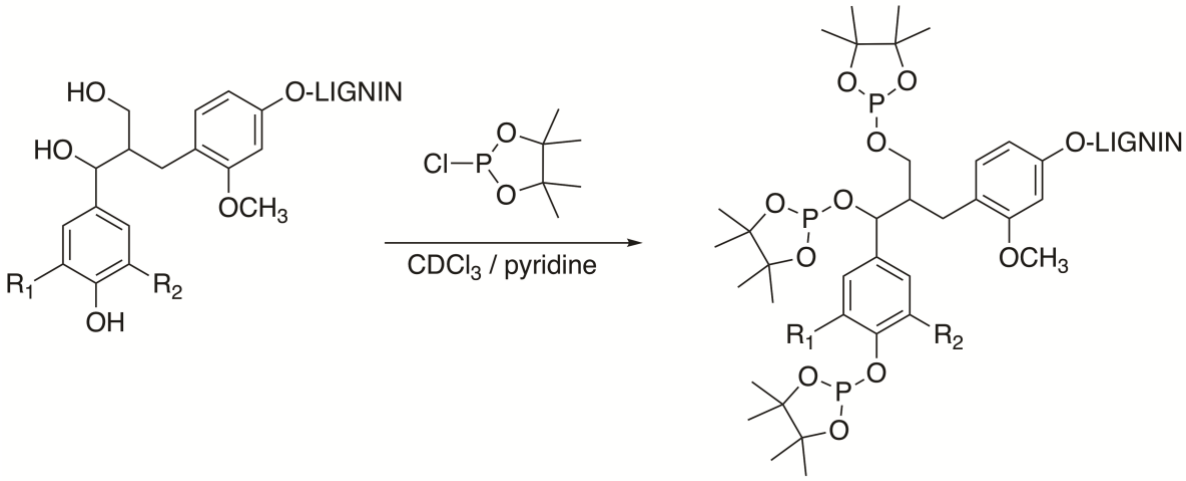

Scheme 4. Reaction of phosphytilation of lignin for the preparation of samples for ^{31}P NMR.

Samples were prepared by dissolving accurately weighed lignin samples (20 mg) in a pyridine-deuterated chloroform solution (1.6:1 v/v mL, 700 μL) containing 1 mg/mL of chromium-(III) acetylacetonate ($Cr(acac)_3$). Then 100 μL of *endo*-*N*-hydroxy-5-norbornene-2,3-carboximide solution (*e*-HNDI, 121.5 mM, $CDCl_3$/pyridine 4.5:0.5) was added, along with 100 mL of 2-chloro-4,4,5,5-tetramethyl–1,3,2-dioxaphospholane as the derivatising agent. [1] ^{31}P NMR spectra were recorded on opportunely phosphitylated lignin samples solubilised in a pyridine- deuterated chloroform (1.6:1 v/v) mixture. Analyses were performed on a Bruker Avance NMR spectrometer operating at 500.130 MHz (^{1}H).

Table 2. Typical chemical shifts and integration regions for lignin in a ^{31}P NMR spectrum (reproduced from reference [1]).

δ /ppm	**Assignment**
132.2	water adduct
133.5–136	carboxylic acids
137–138.5	*p*-hydroxy coumaryl phenols
138.5–140.5	guaiacyl phenols
140.5–144.5	condensed and syringyl phenols
145–150	aliphatic alcohols
151–152.5	internal standard *endo*-*N*-hydroxy-5-norbornene-2,3-carboximide
175	excess unreacted 2-chloro-4,4,5,5-tetramethyl–1,3,2-dioxaphospholane

6.3 Fourier Transform Infrared Spectroscopy (Attenuated Total Reflectance): FT-IR (ATR)

FT-IR spectroscopy allowed to characterise lignin and investigate relative modifications.

Spectra were recorded with a Nicolet iS10 spectrometer (Thermo Scientific) equipped with an ATR Smart device (total scan 32, range 4000–800 cm^{-1}, resolution 1 cm^{-1}).

6.4 Gel Permeation Chromatography (GPC) combined with UV detector

The molecular weight distribution of acetylated lignin samples was determined by gel permeation chromatography (GPC). GPC traces were obtained using a Waters 600 E liquid chromatography equipped with a HP1040 ultraviolet detector set at 280 nm. The mobile phase was tetrahydrofuran (THF). The operational conditions were: sample concentration 2 mg mL^{-1}; flow rate 1 mL min^{-1}; injection volume 20 µL (Rheodyne loop valve); column system composed by an Agilent PL gel 5 µm, 500 Å, and an Agilent PL gel 5 µm, 104 Å columns connected in series; temperature 25 °C. Polystyrene standards ($3 \cdot 10^6$–162 $g \cdot mol^{-1}$) from Polymer Laboratories were used for calibration. All samples were filtered through a 0.2 µm syringe Whatman filter before measurements.

Lignin acetylation was necessary to obtain a complete solubilisation in THF and compare the results with literature. Lignin (100 mg) was acetylated in a pyridine-acetic anhydride solution (1:1 v/v, 4 mL) kept at 40 °C overnight. Samples were stripped with ethanol toluene, and chloroform (3 x 25 mL each solvent), dried in vacuum and dissolved in THF for the analysis. [2]

6.5 Gel Permeation Chromatography (GPC) combined with fluorescence detector

The phenolic group distribution of lignin as a function of molecular weight was assessed on lignin samples submitted to dansylation for the selective fluorescent labelling of phenols. [2] Lignin (100 mg) and tetrabutylammonium bromide (5 mg) were dissolved in a 0.1 M carbonate buffer solution at pH 10 (20 mL) at 50 °C. Dansyl chloride (1.2 times the total phenolic content as calculated from ^{31}P NMR) solubilised in acetonitrile (10 mL) was added to the solution of lignin. The reaction was run for 90 min at 50 °C under vigorous stirring. The mixture was cooled down at room temperature. Then dansylated lignin was recovered by centrifugation and washed twice with acidic water after regeneration in cold acidic water (0.1 M HCl).

GPC traces were obtained on an Agilent 1260 Infinity liquid chromatography system, equipped with an autosampler (Agilent 1260 Vialsampler, injection volume 25 µL), an Agilent 1260 DA VL detector (set

at 280 nm) and an Agilent 1260 FL detector (λ excitation: 390 nm, λ emission: 550 nm for all samples). Different columns were in sequence: Agilent PLgel 5 μm (500 Å), Agilent PLgel 5 μm (1000 Å) and Agilent PLgel 5 μm (10000 Å). Samples of 1 mg·mL^{-1} were dissolved in tetrahydrofuran and the same solvent was used as eluent (Fluka 98 %) at a flow rate of 1 mL·min^{-1}. Polystyrene standards (3·10^6–162 g·mol^{-1}) were provided by Polymer Laboratories.

6.6 Chromatographic data elaboration

GPC coupled with UV (280 nm) detector was used to analyse acetylated lignin and gain information about the molecular weight distribution. GPC equipped with a fluorescence detector (excitation 390 nm, emission 550 nm) was employed for the assessment of phenolic distribution as a function of molecular weight in dansylated samples. Molar extinction coefficient and fluorescent intensity were assumed to be independent on molecular weight and structural surroundings of aromatic rings and dansylated groups. Chromatograms were then analysed as follows. [3]]

1. In GPC chromatograms of acetylated lignin, the representative weight fraction was assessed for each specific molecular weight (MW) range b⟶a including >10000 g·mol^{-1}; 10000-5000 g·mol^{-1}; 5000-3000 g·mol^{-1}; 3000-2000 g·mol^{-1}; 2000–1000 g·mol^{-1}; 1000-200 g·mol^{-1}. The calculations were performed by dividing the UV absorbance calculated over a specific MW range by the one associated to the whole MW distribution:

$$\frac{g_{lignin\ (b \rightarrow a)}}{g_{total\ lignin}} = \frac{\sum_{n=a}^{b} Abs(n)}{\sum_{n=200}^{10000} Abs(n)}$$

2. The fluorescence of the sample was corrected taking into account the effect of auto-fluorescence of lignin, related to the presence of aromatic structures like stilbenoids and phenylcumarones.

3. The UV profile of a generic dansylated sample was compared to the curve of the corresponding acetylated sample in order to estimate the variation in hydrodynamic volume of lignin after dansylation. The displacement towards higher MW influenced low MW species than the high MW ones. So, the integration range 1000-200 g·mol^{-1} in acetylated curves was turned into 1250-200 g·mol^{-1} for dansylated profiles to take into account this phenomenon. The other ranges were not submitted to any change.

4. The representative phenolic molar fraction associated to a specified molecular weight range was individuated by elaborating fluorescence signals. The same MW ranges were considered as in point 1. Since the auto-fluorescence of lignin was corrected, signals accounted only for the fluorescence of dansyl-labelled phenols. Phenolic molar fractions were calculated by dividing the fluorescence intensity calculated over a specific MW range by the one related to whole MW distribution:

$$\frac{mmol_{PhOH\ (b\rightarrow a)}}{mmol_{total\ PhOH}} = \frac{\sum_{n=a}^{b} Fluo(n)}{\sum_{n=200}^{10000} Fluo(n)}$$

Finally, the phenolic content over a specific MW range was calculated as follows:

$$\frac{mmol}{g} PhOH\ (b \rightarrow a) = \frac{mmol_{PhOH\ (b\rightarrow a)}}{g_{lignin\ (b\rightarrow a)}} = \frac{mmol_{PhOH\ (b\rightarrow a)}}{mmol_{total\ PhOH}} \cdot \frac{mmol_{total\ PhOH}}{g_{total\ lignin}} \cdot \frac{g_{total\ lignin}}{g_{lignin\ (b\rightarrow a)}}$$

where $\frac{mmol_{total\ PhOH}}{g_{total\ lignin}}$ was the quantification obtained by ^{31}P NMR analysis.

6.7 Dynamic Light Scattering (DLS)

The average hydrodynamic diameters of lignin particles were evaluated by dynamic light scattering (DLS). Measurements were carried out on a Malvern ZetaSizer Nano ZS instrument equipped with a 633 nm solid state He-Ne laser at a scattering angle of 173°, operating at 298 K. Disposable, plastic cuvettes with an optical path length of 1 cm were used. Lignin nanoparticle suspensions in distilled water were analysed. pH was set at the desired value by adding 1 M sodium hydroxide or 1 M hydrochloric acid directly into the cuvette. The refractive index and the viscosity of the solution were approximated to those of pure water at 298 K (1.33 and 0.8929 cP, respectively). The measurements were repeated at least three times, each repetition being the average of 10 scans of 60 s each.

6.8 Scanning Electron Microscopy (SEM)

Air-dried LNPs and disrupted glass joints were visualised by a scanning electron JSM-7000F microscope (JEOL, Japan) without any preparation of the sample. Air-dried LNPs obtained by dialytic solvent exchange and LNPs-rubber composites were sputtered with gold and graphite, respectively, and observed with a Zeiss Gemini microscope.

6.9 Specific surface area

Specific surface areas were determined by nitrogen physisorption using a Quantachrome Autosorb-1 apparatus according to BET and t-plot methods. Nanolignin samples were degassed at 80 °C overnight.

7 Chemical modification of lignin

7.1 Mechanochemical esterification of lignin - small scale procedure

In the optimised procedure, herbaceous alkaline or BIOPIVA™ 200 (UPM, Finland) softwood kraft lignin (dry content of 200 mg) and a base (NaOH, Na_2CO_3, K_2CO_3) were introduced in a 50 mL planetary ball mill grinding jar made of steel equipped with 10 balls of the same material (Ø 7 mm). The mixture was ground at 500 rpm for 30 min in a Retsch PM 100 planetary ball mill. The acyl donor (vinyl acetate, vinyl methacrylate, isopropenyl acetate) was introduced and the mixture was milled for additional 2 h. The content of the jar was transferred in a centrifuge tube with the help of deionised water. 0.1 m HCl was added to induce the neutralisation of lignin salt and the precipitation of the product which was recovered after centrifugation and two additional washes with water. Then, the product was dried by freeze-drying and isolated as a brownish powder.

7.2 Mechanochemical esterification of lignin - large scale procedure

In the optimised procedure, herbaceous alkaline or BIOPIVA™ 200 (UPM, Finland) softwood kraft lignin (dry content of 5 g) and a base (NaOH, Na_2CO_3) were introduced in a 250 mL planetary ball mill grinding jar made of steel equipped with balls of the same material (17 spheres Ø 7 mm, 2 spheres Ø 10 mm). The mixture was ground at 400 rpm for 30 min in a Retsch PM 100 planetary ball mill. The, the acyl donor (vinyl acetate, vinyl methacrylate) was introduced, and the mixture was milled for additional 4 h. The content of the jar was transferred in a centrifuge tube with the help of deionised water. 0.1 m HCl was added to induce the neutralisation of lignin salt and the precipitation of the product which was recovered after centrifugation and two additional washes with water. Then, the product was dried by freeze-drying and isolated as a brownish powder.

8 Preparation, reinforcement and functionalisation of lignin nanoparticles (LNPs)

8.1 Preparation of LNPs by nanoprecipitation via dialysis and reinforcement by enzymatic reaction

8.1.1 Preparation of colloidal suspensions of LNPs by nanoprecipitation via solvent polarity shift by dialysis

BIOPIVA™ 200 (UPM, Finland) dried softwood kraft lignin (37.5 mg) were solubilised in THF (25 mL) for 2 h at room temperature under magnetic stirring. The solution was inserted in a dialysis bag which was immerse in 250 mL of deionised water. The external water was changed frequently, THF was recovered by evaporation under reduced pression. Solvent exchange was run for 72 h. By solvent exchange, a water suspension of LNPs was formed with a final concentration 0.9 mg·mL^{-1}. [4]

8.1.2 Reinforcement of LNPs by enzymatical reaction

LNPs in the dispersed state were treated with laccase from *Trametes versicolor* (13.0 nkat·mg^{-1}, Sigma Aldrich) in a quantity to ensure 900 nkat(enzyme)/g(lignin). The reaction was run in an open vessel at room temperature overnight. [6] The reaction was quitted by thermal treatment at 80 °C for 10 min.

8.2 Preparation of LNPs by nanoprecipitation via direct mixing and reinforcement by epoxy chemistry

8.2.1 Solvent fractionation of lignin

Dried softwood kraft lignin (10 g) was dissolved in organic solvent (100 mL), i.e., ethyl acetate or ethanol, and vigorously stirred at room temperature for 3 h. The insoluble residue was recovered by filtration on a Büchner filter and dried at 45 °C for one night. [7] The solvent was removed from the soluble portion by evaporation under reduced pression.

8.2.2 Etherification of lignin fractions with epichlorohydrin: small scale

BIOPIVA™ 200 and 100 (UPM, Finland) softwood kraft lignins were etherified according to the following procedure. In a 250 mL one-necked round bottom flask equipped with a condenser, lignin (500 mg) was dissolved in a 50 % v/v mixture of acetone and water (75 mL) in the presence of sodium hydroxide (3 eq. the number of OH-groups of the lignin fraction). Then, epichlorohydrin (20 eq. the

number of -OH groups of the lignin fraction) was dropped into the solution and the reaction mixture was stirred at 50 °C for 5 h. The product precipitated upon addition of water (50 mL) and 0.1 m HCl until pH 3.5 was reached. [8] The desired product was recovered as a brownish powder by centrifugation, two washes with excess deionised water and freeze-drying.

8.2.3 Etherification of lignin fractions with epichlorohydrin: scale up

BIOPIVA™ 200 (UPM, Finland) softwood kraft lignin was etherified according to a procedure known in literature. In a 2 L one-necked round bottom flask equipped with a condenser, lignin (5 g) was dissolved in a 50 % v/v mixture of acetone and water (750 mL) in the presence of sodium hydroxide (3 eq. the number of OH-groups of the lignin fraction). Then, epichlorohydrin (20 eq. the number of -OH groups of the lignin fraction) was dropped into the solution and the reaction mixture was stirred at 50 °C for 5 h. The product precipitated upon addition of water (500 mL) and 0.1 m HCl until pH 3.5 was reached. The desired product was recovered as a brownish powder by centrifugation, two washes with excess deionised water and freeze-drying.

8.2.4 Preparation of colloidal suspensions of LNPs by nanoprecipitation via solvent polarity shift by direct mixing: small scale

LNPs were formulated by nanoprecipitation. BIOPIVA™ 200 and 100 (UPM, Finland) softwood kraft lignins (360 mg) were dissolved in a 3:1 % wt mixture of acetone and water (12 g) at room temperature for 2 h under vigorous stirring. Insoluble residues were removed by filtration on filter paper. Excess water (36 g, 3:1 % wt water/solution) was rapidly poured into the solution under vigorous stirring and nanoparticles instantaneously formed. Acetone was removed by evaporation under reduced pression. Large aggregates were removed by filtration on a filter paper. [9] In the case of LNPs prepared by recombining fractions, unmodified and epoxidised fractions were mixed according to their mass ratio in the original lignin.

8.2.5 Preparation of colloidal suspensions of LNPs by nanoprecipitation via solvent polarity shift by direct mixing: scale up

For the production of large LNPs with an average hydrodynamic diameter of 350 nm, BIOPIVA™ 200 (UPM, Finland) softwood kraft lignin (10 g of dried content) was solubilised in a 3:1 % wt acetone/water mixture (69 and 23 mL, respectively). Then, the solution was poured into excess water (920 mL) under vigorous stirring. The desired final concentration of 7 % wt was obtained by evaporation of excess solvent.

For the production of small LNPs with an average hydrodynamic diameter of 150 nm, lignin (10 g of dried content) was solubilised in a 3:1 % wt acetone/water mixture (375 and 125 mL, respectively). Then, the solution was poured into excess water (1250 mL) under vigorous stirring. The desired final concentration of 7 % wt was obtained by evaporation of excess solvent.

8.2.6 Reinforcement of LNPs by epoxy chemistry

LNPs in the dispersed state were cured by heating samples in a sealed vial at 105 °C for 16 h.

8.3 Application of reinforced LNPs by epoxy chemistry as adhesives for aminated glass

8.3.1 Sample preparation for adhesive tests

Microscope glass slides (26 mm x 76 mm, VWR) were firstly rinsed with distilled water, sonicated in acetone for 5 minutes and *i*PrOH for additional 5 minutes, and finally air dried. In a beaker, 3-aminopropyltriethoxysilane (10 mL) was dropwise added to a mixture (200 mL) of *i*PrOH/water 95:5 (v/v) at room temperature under vigorous stirring. When a whitish suspension was produces, glass slides were soaked in the suspension overnight. Then, glass slides were rinsed sonicated for 5 minutes and rinsed again with *i*PrOH, and finally air-dried. [10] Suspension of nanoparticles from BIOPIVA™ 100 (UPM, Finland) softwood kraft lignin (4.3 g L^{-1}, 50 µL) was placed on a 26 x 26 mm section (geometry requirements stated in ASTM D5868 for single-lap shear testing) of aminated glass. [11] Another aminated glass slide was placed on top and the system was cured at 105 °C for 16 h.

8.3.2 Shear mechanical test of adhesive strength

Glass joints were submitted to uniaxial shear mechanical tests an Instron 5960 universal testing machine (Instron, USA) with a 100 N load cell at a strain rate of 1 mm min^{-1} at 50% relative humidity at 25 °C. [12] The geometry of the sample met the requirements specified in ASTM D5868. [11] Further shear mechanical tests were accomplished by applying a load of growing weight to the glass joint with a grip. The relative results were reported as an average of three repetitions for each sample.

8.3.3 Environmental impact assessment

The environmental impact for the production of LNP-based adhesives was calculated in terms of *E*-factor and solvent demand. In details, the solvent demand was computed as an independent metric and excluded from the calculations of *E*-factor due to the different processing required for the treatment of solvents and non-volatile wastes. The overall *E*-factor is defined as the ratio between the mass of wastes (solvent excluded) divided by the mass of the final product. [13] The total mass of wastes could be defined

as the sum of the masses of input materials minus the masses of the product of each step *i* (1, 2,… N). [14]

$$E-factor = \frac{m_{total\ waste}}{m_{final\ product}} = \frac{\sum_{i=1}^{N} m_{input,i} - \sum_{i=1}^{N} m_{product,i}}{m_{product,N}}$$

The contribution of each step *i* to the overall *E*-factor was calculated as the ratio between the mass waste related to that stage and the mass of the final product.

$$E-factor_i = \frac{m_{waste,i}}{m_{final\ product}}$$

The overall solvent demand was esteemed as the ratio between the mass of the solvent for the entyre process and the mass of the final product.

$$Solvent\ demand = \frac{m_{total\ solvent}}{m_{final\ product}}$$

The contribution of each step *i* to the overall solvent demand was calculated as ratio between the mass of the solvent related to that stage and the mass of the final product.

$$Solvent\ demand_i = \frac{m_{solvent,i}}{m_{final\ product}}$$

9 Rubber compounding

This section describes the main procedures that were used to prepare rubber model compounds.
The rubber compounds were prepared with a small-sized Brabender mixer with an internal chamber of 50 mL and a fill factor of 0.9.

9.1 Preparation of NR / lignin masterbatches

9.1.1 NR / lignin masterbatch preparation by coagulation

9.1.1.1 Preparation of NR masterbatches including milled lignin

The preparation of NR / lignin masterbatches included the dissolution of a proper amount of milled BIOPIVA™ 200 (UPM, Finland) softwood kraft lignin in water (12 mL per gram of lignin) and the adjustment of pH to 10.5–11 by addition of NaOH aqueous solution. After 10 minutes stirring, the solution was gently poured in a beaker containing a proper amount of 60 % wt natural rubber latex. The resulting emulsion was stirred for 30 minutes and finally sulfuric acid was progressively added to induce coagulation which was evaluated by visual inspection. The paste was filtered off on a Büchner funnel, repeatedly washed in excess water until pH 6 was obtained. The thick paste was dried at 45 °C for approximately 60 hours. [15]

9.1.1.2 Preparation of NR masterbatches including functionalised lignin salt obtained by mechanochemical esterification

A proper amount of functionalised BIOPIVA™ 200 (UPM, Finland) softwood kraft lignin salt obtained by mechanochemical esterification with vinyl methacrylate associated with either NaOH or Na_2CO_3 was dispersed in water (12 mL per gram of lignin), then 37 % HCl was added in order to induce the neutralisation and precipitation of lignin. After centrifugation (4000 rpm, 7 min) and washing with excess water, functionalised lignin was retrieved as a wet powder. It was subsequently suspended in water (12 mL per gram of lignin) and pH was adjusted to 10.5–11 by adding NaOH aqueous solution. After 10 minutes stirring, the solution was gently poured in a beaker containing a proper amount of 60 % wt natural rubber latex. The resulting emulsion was stirred for 30 minutes and finally 25 % sulfuric acid was progressively added to induce coagulation which was evaluated by visual inspection. The paste was filtered off on a Büchner funnel, repeatedly washed with excess water until pH 6 was obtained. The thick paste was dried at 45 °C for approximately 60 hours.

9.1.2 Preparation of NR / lignin masterbatches by codrying

9.1.2.1 Preparation of NR masterbatches including milled lignin

The preparation of NR / softwood kraft lignin (BIOPIVA™ 200, UPM, Finland) masterbatches included the dispersion in water (12 mL per gram of lignin) of a proper amount of milled lignin. Then, pH was adjusted to 10.5–11 by adding NH_4OH aqueous solution. After 10 minutes stirring, the solution was gently poured in a beaker containing a proper amount of 60 % wt natural rubber latex. The resulting emulsion was stirred for 30 minutes and finally dried at 45 °C for approximately 60 hours.

9.1.2.2 Preparation of NR masterbatches including functionalised lignin salt obtained by mechanochemical esterification

A proper amount of functionalised lignin salt (BIOPIVA™ 200, UPM, Finland) obtained by mechanochemical esterification with vinyl methacrylate associated with either NaOH or Na_2CO_3 was dispersed in water (12 mL per gram of lignin), then 37 % HCl was added in order to induce the precipitation of lignin. After centrifugation (4000 rpm, 7 min) and washing with excess water, functionalised lignin was retrieved as a wet powder. It was then suspended in water (12 mL per gram of lignin) and pH was adjusted to 10.5–11 by adding NH_4OH aqueous solution. After 10 minutes stirring, the solution was gently poured in a beaker containing a proper amount of 60 % wt natural rubber latex. The resulting emulsion was stirred for 30 minutes and finally dried at 45 °C for approximately 60 hours.

9.1.2.3 Preparation of NR masterbatches including LNPs

Nanolignin (BIOPIVA™ 200, UPM, Finland) 7 % % wt suspension was poured into a beaker containing a proper amount of 60 % wt natural rubber latex kept under vigorous stirring. The mixture was stirred at room temperature for 30 minutes and finally dried at 45 °C for approximately 60 hours.

9.2 Formulation of rubber compounds

Rubber compounds were obtained by mixing several ingredients (fillers, vulcanisers, and antioxidants) in different elastomers with the Brabender internal chamber mixing following a procedure described below and schematised in Table 3.

In phase 1, temperature was set at 120 °C and rotor speed at 60 rpm. At first, rubber and, if required, NR/lignin masterbatch were progressively introduced in the mixer. Once the addition was over, the elastomer was homogenised for 1 minute. Then, other fillers (carbon black, silica) and compatibilisers (silanes) were added and mixed with the rubber for 2 minutes. Finally, protective agents [*N*-(1,3-dimethylbutyl)-*N*'-phenyl–1,4-benzenediamine, commonly known as 6PPD] and, if needed, activators (stearic acid, zinc oxide) were introduced and mixed for additional 2 minutes.

In phase 2, temperature was set at 80 °C and rotor speed at 45 rpm. The compound obtained in phase 1 was homogenised by kneading for 1 minute. Afterward, accelerators (*N*-cyclohexylbenzothiazol-2-sulphenamide, the so-called CBS) and vulcanisers (sulphur- or peroxide- based vulcanisers) were added and mixer for further 2 minutes.

Table 3. Mixing phases for rubber compounding.

PHASE	TEMPERATURE / °C	ROTOR SPEED / RPM	TIME / MIN	ACTION
1	120	60	0	load rubber and, if required, masterbatch
			1	add fillers and, if required, compatibilisers
			3	add protective agents and, if required, activators
			5	dump
2	80	45	0	load compound from phase 1
			1	add vulcanisers and, if required, accelerators
			3	dump

The amount of ingredients will be expressed in *phr* (parts per hundred rubber), a unit indicating the percentual mass ratio between the specific ingredient and the total rubber quantity in the formulation.

10 Characterisation of rubber compounds

10.1 Vulcanisation

Crosslinking was monitored throughout vulcanisation by using the RPA 2000 rubber process analyser supplied by Alpha Technologies. The rubber specimen is inserted in a heated cavity and is subjected to sinusoidal oscillations of the support. [16]

10.2 DMA / RPA - Dynamic Mechanical Analysis / Rubber Processing Analyzer

The tests were performed with a RPA 2000 Alpha Technologies rubber process analyser. This analysis provides information about the viscoelastic properties of compounds, data are recorded on both green and cured samples.

10.3 Tensile properties

Specimen for tensile tests were prepared as following:
Rubber compounds rest at room temperature for 24 h after being mixed. Afterwards, they were flattened into 8 mm thick sheets by a two-roll mill and cured in a hydraulic press at 170 °C, pressure 4.3 bar for 10 min. For each sheet three dumbbell shaped test specimens were die-cut and their thickness was measures. Tensile stresses at different elongation (10, 50, 100, and 300% elongation), tensile strength and elongation at break were assessed. Tensile analyses were accomplished using a Zwick/Roell tensile testing machine. The testing parameters complied with ISO 37 and UNI 6065 standards. Tests involved stretching specimens at constant speed till break. Data were reported as a means of three analyses, and the median sample was plotted.

Tensile properties take into account the behaviour of a material on which tensile forces are applied and provide information on the macroscopical mechanical properties of the material itself.
One of the most common plots which describes mechanical performances is stress - strain curves. During this test, a dumbbell- or ring- shaped sample is stretched increasing the deformation at constant rate. The tensile elastic modulus (E) is a measurement of the stiffness of the material and is defined as the stress (σ) required to elongate the specimen at a certain strain (ε): $E(\sigma) = \sigma/\varepsilon$.
Properties at failure are crucial parameters to be considered while describing the mechanical properties of a material. The ultimate tensile strength is the force per unit area needed to break the specimen and provides information on the ability of the material to resist loads. The ultimate elongation (also referred to as elongation at break) is the maximum extension the material can withstand before cracking and is

measured as the percent increase in length of the specimen before breaking. The presence of reinforcing fillers is often accompanied by an increase in stiffness and ultimate tensile strength. In rubber technology a reinforcement index is defined as modulus at 300% strain divided by modulus at 100% strain. [18]]

10.4 Compression dynamics experiments

Compression tests were run on a cylindrical specimen (1.8 mm x 1.2 mm Ø) of vulcanised compound to assess the behaviour of the composite in conditions mimicking the compressive forces supported during usage. In compression dynamics, specimen is submitted to strain in the normal direction with respect to the one typical of shear tests. The output of the analysis are storage E' and loss E" dynamic moduli and their ratio tanδ. Analyses were run in strain sweep mode, three strain values were investigated while frequency and temperature remained constant. Tests were also sun in temperature sweep mode, three temperatures were investigated while frequency and strained remained constant throughout the experiment.

10.5 Swelling measurements for crosslink density

Crosslink density of vulcanised composites was esteemed by placing a specimen of vulcanised sample (10 mm x 10 mm x 1 mm) in excess toluene (25 mL) and let it reach equilibrium for 3 days at room temperature. Then, samples were retrieved from the solvent, gently tapped with paper and quickly weighed. The results of this solvent swelling test were used to evaluate the crosslink density according to the Flory-Rhener equation:

$$CD = -\frac{[ln(1 - V_R) + V_R + \chi V_R^2]}{\rho_R V_0 \left(V_R^{1/3} - \frac{V_R^2}{2}\right)}$$

where CD is the crosslink density, ρ_R the density of rubber (0.92 g·cm^{-3}), V_0 is the molar volume of the solvent (106.3 cm^3· mol^{-1} for toluene), V_R is the volume fraction of rubber in the swollen material, and χ is the Flory-Huggins polymer-solvent interaction term (0.36)· [19].

References

[1] A. Granata, D. S. Argyropoulos, *J. Agric. Food Chem.* **1995**, *43*, 1538.

[2] A. Salanti, M. Orlandi, L. Zoia, *ACS Sustain. Chem. Eng.* **2020**, *8*, 8279.

[3] A. Salanti, M. Orlandi, H. Lange, F. Ferruti, L. Zoia, *ACS Sustain. Chem. Eng.* **2022**, *10*, 11680.

[4] M. Lievonen, J. J. Valle-Delgado, M.L. Mattinen, E.L. Hult, K. Lintinen, M. A. Kostiainen, A. Paananen, G. R. Szilvay, H. Setälä, M. Österberg, *Green Chem.* **2016**, *18*, 1416.

[5] M.L. Mattinen, J. J. Valle-Delgado, T. Leskinen, T. Anttila, G. Riviere, M. Sipponen, A. Paananen, K. Lintinen, M. Kostiainen, M. Österberg, *Enzyme Microb. Technol.* **2018**, *111*, 48.

[6] M. Österberg, M. H. Sipponen, B. D. Mattos, O. J. Rojas, *Green Chem.* **2020**, *22*, 2712.

[7] A. Duval, F. Vilaplana, C. Crestini, M. Lawoko, *Holzforschung* **2016**, *70*, 11.

[8] C. Gioia, M. Colonna, A. Tagami, L. Medina, O. Sevastyanova, L. A. Berglund, M. Lawoko, *Biomacromolecules* **2020**, *21*, 1920.

[9] M. H. Sipponen, H. Lange, M. Ago, C. Crestini, *ACS Sustain. Chem. Eng.* **2018**, *6*, 9342.

[10] N. Majoul, S. Aouida, B. Bessaïs, *Appl. Surf. Sci.* **2015**, *331*, 388.

[11] ASTM, *Stand. Pract. Lap Shear Adhes. Fibre-Reinf. Plast. FRP Bond. West Conshohocken PA U. S.* **2001**.

[12] I. Ribca, M. E. Jawerth, C. J. Brett, M. Lawoko, M. Schwartzkopf, A. Chumakov, S. V. Roth, M. Johansson, *ACS Sustain. Chem. Eng.* **2021**, *9*, 1692.

[13] R. A. Sheldon, *Green Chem.* **2007**, *9*, 1273.

[14] J. Andraos, *Green Process. Synth.* **2019**, *8*, 324.

[15] D. Barana, S. D. Ali, A. Salanti, M. Orlandi, L. Castellani, T. Hanel, L. Zoia, *ACS Sustain. Chem. Eng.* **2016**, *4*, 5258.

[16] S. R. Khimi, K. L. A. Pickering, *J. Appl. Polym. Sci.* **2014**, *40008*, 1.

[17] M. Guaita, F. Ciardelli, E. P. La Mantia, *Fondamenti di scienza dei polimeri*, Edizioni N., **2006**.

[18] J. Fröhlich, W. Niedermeier, H. D. Luginsland, *Compos. Part A Appl. Sci. Manuf.* **2005**, *36,* 449.

[19] R. Joseph, K. E. George, D. J. Francis, K. T. Thomast, *Int. J. Polym. Mater.* **1987**, *12*, 29.

RESULTS AND DISCUSSION

11 Study of the chemical compatibilisation of lignin with rubber and evaluation of the effects on the mechanical performances of elastomeric composites

11.1 Lignin mechanochemical functionalisation

Aiming at compatibilising lignin with rubber to enhance the mechanical performances of the resulting composites, different non-conventional approaches targeting the hydroxyl groups of lignin were evaluated, in particular esterification was investigated. In order to prove the applicability of those synthetic routes to lignin with different structural features, herbaceous alkaline and softwood kraft lignins were selected as subject of study (Table 4).

Table 4. Analysis of herbaceous alkaline lignin and softwood kraft lignin by GPC and quantitative ^{31}P NMR spectroscopy experiments.

Properties	Herbaceous alkaline lignin	Softwood kraft lignin
Molecular weight characteristics		
M_n / g mol^{-1}	1900	2800
M_W / g mol^{-1}	4600	6300
PDI	2.4	2.2
Hydroxyl group content / mmol g^{-1}		
Aliphatic-OH	3.11	1.60
S-type and condensed phenolic –OH	0.61	1.37
G- type phenolic -OH	0.59	1.58
H - phenolic -OH	0.31	0.15
Total phenolic -OH	1.51	3.10
Carboxylic acids	0.70	0.50

Among non-conventional synthetic strategies, enzymatic catalysis was regarded as an appealing methodology having the advantage over alternative chemical processes of being environmentally friendly, occurring under rather mild conditions and potentially targeting reactive groups in chemo-, regio- or stereoselective ways.[1] Kraft lignin could be functionalised by lipase-assisted transesterification of acyl donors.[2] Similarly, studies performed on cellulose[2] suggested for the possibility to address lignin aliphatic hydroxyls by lipase-catalysed transesterification with vinyl acetate in different conditions including pure aqueous and mixed organic solvent/aqueous media. In that investigation, experiments

evidenced a low acetyl extent (0.16 wt %) in reactions run in aqueous buffer solution on solid cellulose. Conversely, when cellulose was dissolved in a dimethyl sulfoxide/paraformaldehyde mixture, it was possible to obtain higher conversion yields (7.87 wt % acetyl content). Considering such evidences, aiming at the functionalisation of lignin with vinyl acetate as activated acyl donor, a mixture of DMSO and water was studied as possible reaction media capable of solubilising lignin and vinyl acetate and preserving the enzymatic activity of lipase from *Aspergillus niger*.[3] Experiments were devoted to study the effect of the sequence of addition of the reactive species on the reaction outcome. In particular, attempts included: a) the pre-solubilisation of herbaceous alkaline lignin in DMSO, followed by the addition of aqueous phosphate buffer at pH 7, vinyl acetate and enzyme; b) the solubilisation of lignin and acyl donor in DMSO and the addition of the enzyme dispersed in a phosphate buffer at pH 7. Temperature was maintained at 40±5 °C under magnetic stirring and the progress of the reaction was evaluated at 24, 48 and 72 h by FT-IR/ATR spectra. No significant difference in the signals was observed between the substrate and the reaction product, proving the inefficacy of the treatment in functionalising alkaline lignin. Those results were ascribed to the prevailing of hydrolytic reactions in the presence of water[4] and led to the choice of running reactions in the solid state. More specifically, mechanochemistry in planetary ball mill was studied as a potential way to functionalise lignin. This approach looked particularly appealing for the possibility to prevent or at least limit hydrolytic processes, overcome solubility restrictions and reduce the use of solvents.[5] Mechanoenzymatic esterification of β-*O*-4' lignin model compounds was reported to selectively functionalise primary alcohols in good to high yields, preserving phenols and potentially maintaining antioxidant properties.[5] Attracted by the possibility to specifically target one kind of hydroxyl groups and preserve lignin antioxidant properties, the same conditions reported for lignin model compounds were applied to alkaline lignin. More specifically, lignin was submitted to a mechanochemical transesterification with vinyl acetate as activated acyl donor catalysed by lipase B from *Candida antarctica*, immobilised on Immobead. The treatment failed in functionalising lignin, as revealed by FT-IR/ATR analysis.

The enzymatic catalysis under such conditions did not produce the expected results and suffered from the impossibility to recover the enzyme at the end of the reaction and reuse it. So, alkaline catalysis was considered as a possible alternative to induce lignin functionalisation with a mechanochemical approach. Guo *et al.*[6] reported the mechanochemical transesterification of organosolv lignin catalysed by KOH. In that study, methyl oleate was chosen as acyl donor and 25 % of hydroxyl groups were reported to be converted. Similarly, other methyl esters were expected to display the same results when reacted with herbaceous alkaline and softwood kraft lignin. In particular, methyl methacrylate was selected because of its abundancy, commercial relevance and the possibility to functionalise lignin with an activated double bound which could react during the vulcanisation of rubber compounds and grant for a covalent grafting

of the lignin-based filler to the elastomeric matrix. Even though the reaction conditions were similar to the ones reported in literature,[6] including a methyl ester, *i.e.*, methyl methacrylate, as acyl donor and a hydroxide of an alkali metal, *i.e.*, NaOH, as activator, no conversion was detected by FT-IR/ATR analysis. The starting material was recovered even when the experiment was repeated with the optimised procedure (discussed below) comprising the pre-treatment of lignin with sodium hydroxide and the following addition of methyl methacrylate.

Activated acyl donors were consequently deemed intriguing to induce mechanochemical hydrophobisation or functionalisation with a group reactive during vulcanisation. Such a chemical modification of lignin could be achieved by using acyl chlorides or acyclic anhydrides, which were discarded in the present study due to the drawbacks connected to the use of halogenated chemicals and poor atom efficiency.[7,8] More specifically, the acylation process *via* transesterification of enol esters was investigated for the possibility to efficiently run reactions with mild catalysis, without release of acidic by-products, in the presence of poor nucleophiles including hindered alcohols.[9,10] The driving force for the formation of the desired ester relies on the release of an enol as the leaving group which easily tautomerises to the corresponding ketoform, leaving no free nucleophile and making the reaction irreversible, as illustrated in Scheme 5.[8,11]

The direct mixing of alkaline lignin with a model enol ester as acyl donor, *i.e.*, vinyl acetate, and a base, *i.e.*, NaOH and Na_2CO_3, in a planetary ball mill for 2h at 500 rpm did not result in any modification of the substrate, as elucidated by FT-IR/ATR spectroscopy. The unsuccessful outcome of the reaction was ascribed to the base-catalysed conversion of the ester into a poorly reactive carboxylic acid prior to the reaction with lignin. A pre-treatment of lignin for 30 min at 500 rpm with a base was thus performed before the addition of the activated acyl donor. This step was required to convert the hydroxy groups of lignin into alkoxides which could act as nucleophiles towards the acyl donor. An extra quantity of base was required to deprotonate carboxylic acids present in lignin. Then, the acyl donor was added, and the reaction mixture was further milled for 4h at 500 rpm. The product was recovered by acidic precipitation (HCl 0.1 M) and washed with excess water for the neutralisation of lignin, removal of salts and residual unreacted acyl donor. This optimised procedure is depicted in Scheme 5.

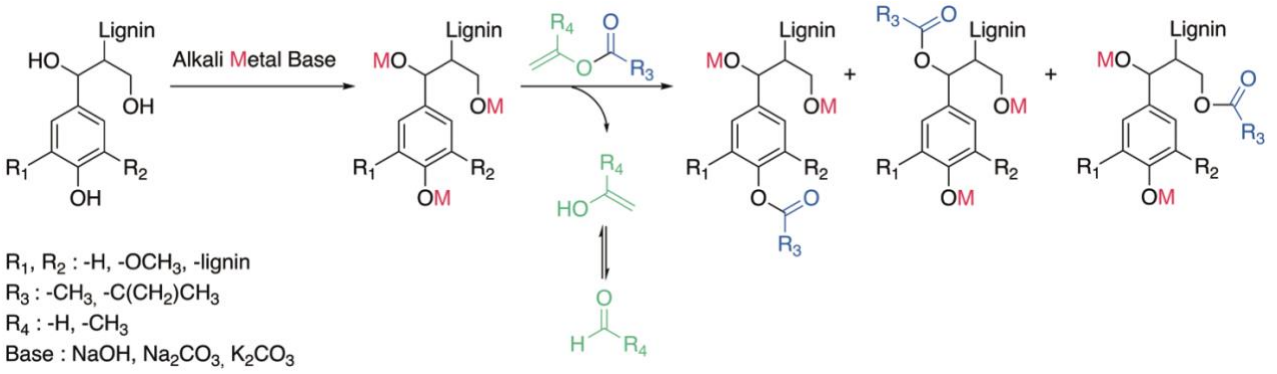

Scheme 5. Reaction scheme for the mechanochemical functionalisation of lignin with enol esters as acyl donors.

FT-IR/ATR spectroscopy provided a qualitative confirmation for the efficacy of the pre-treatment of different lignin types, *i.e.*, herbaceous alkali and softwood kraft lignins, with a hydroxide of an alkali metal, *i.e.*, NaOH, as a base, performed either in the solution state, *i.e.*, dissolution of lignin in water in the presence of NaOH followed by lyophilisation, or in the ball mill, followed by the addition of an enol ester as acyl donor, *i.e.*, vinyl acetate.

Infrared spectra showed an increase in intensity for peaks typical of carbonyl and carboxyl functions, appearance of bands related to the newly created ester bond and decrease in intensity of signals associated to hydroxyl functionalities, as detailed in Table 5 and illustrated in Figure 15 and Figure 19.

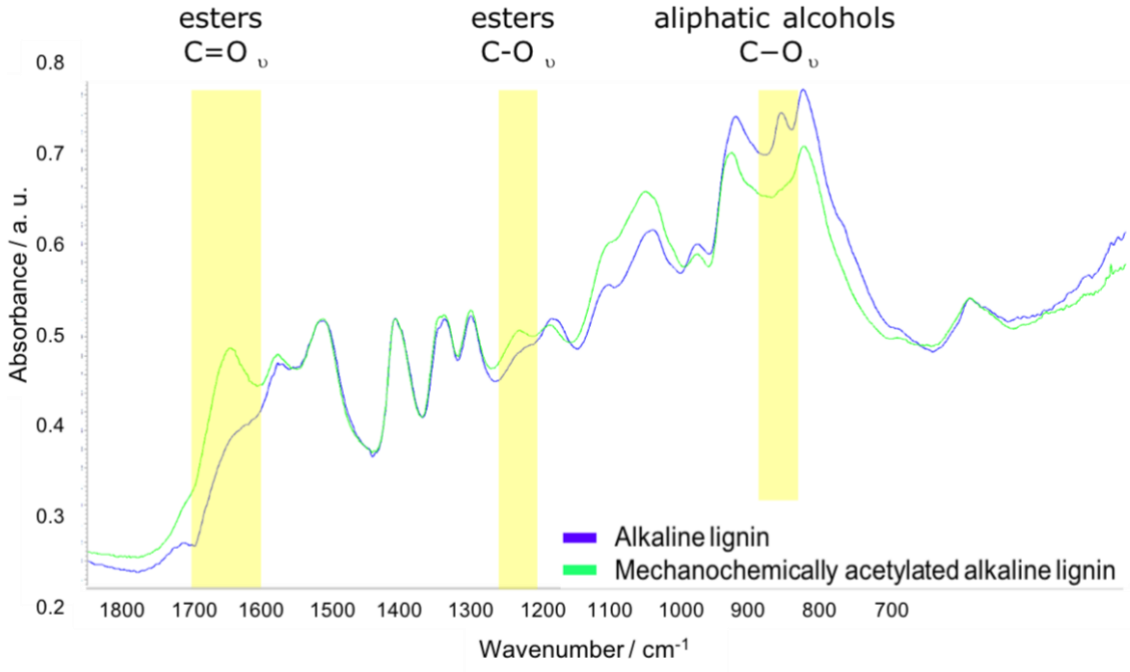

Figure 15. FT-IR / ATR spectrum for alkaline lignin and its derivative acetylated by mechanochemical transesterification with vinyl acetate as acyl donor and sodium hydroxide as alkaline activator.

Table 5. FT-IR/ATR typical bands for lignin. In bold are highlighted the diagnostic signals which account for the desired functionalisation with vinyl acetate and vinyl methacrylate as acyl donors.

Wavenumber/cm^{-1}	Observed bond roto-vibration
3400	O−H stretching
2900	C−H stretching of alkyl groups
2650	COOH
1740	C=O carbonyl groups of aliphatic esters; increment in intensity
1695–1720	unconjugated C=O groups of carbonyl and carboxylic groups
1700	C=O stretching in α,β-unsaturated esters; observed only in case of functionalisation with vinyl methacrylate
1630	C=C stretching; observed only in case of functionalisation with vinyl methacrylate
1595 and 1505	aromatic skeletal vibrations
1460 and 1430	C−H deformation in methyl or methylene groups and aromatic ring stretching
1370	C−H bending of acetyl -CH_3
1320	C−O stretching of the syringyl units (not in KL lignin)
1290	CH_3 vibration
1265	C−O stretching of guaiacyl unit
1200–1250	C−O ester band; appearing of the peak
1215	C−O stretching of phenolic functionalities and aromatic ethers; decrement in intensity
1150 and 1115	C−H in-plane deformations of guaiacyl and syringyl units
1025	C−O stretching of primary aliphatic alcohols and ethers
950	CH_3 rocking
850 and 830	Out of plane vibration modes connected to C−H bonds of guaiacyl and syringyl units
810	C=CH_2 stretching; observed only in case of functionalisation with vinyl methacrylate

Of particular interest was the increment in intensity of the 1740 cm^{-1} band related to the C=O stretching of esters which partially overlapped with the 1695–1720 cm^{-1} band associated with the C=O stretching

of carbonyl and carboxyl functionalities originally present in lignin. The absorbance of this peak could be normalised with respect to the one of the 1505 cm^{-1} band which was associated to aromatic skeleton vibrations and whose intensity proved unaffected by functionalisation. Such a normalisation provided a semi-quantitative evaluation of the extent of esterification, allowing for a quick screening of the best reaction conditions in the phase of process optimisation.

A quantitative estimation of the functionalisation degree was provided by ^{31}P NMR according to a well-established procedure.[12] This approach consisted in the dissolution of the sample in due solvent (a mixture of pyridine and deuterated chloroform), addition of an internal standard and phosphitylation of aliphatic, phenolic and carboxyl groups of lignin (Scheme 4). This procedure provided an indirect proof of the functionalisation of those groups by detecting the decrement in intensity of the corresponding signals. ^{1}H NMR spectroscopy offered a direct tracing of the effective conversion of those groups and incorporation of the functionalising agent in the structure of lignin, as discussed below.

Untreated lignin, milled lignin, lignin milled in the presence of a base and lignin treated with acyl donor in the absence of a base, after acidic precipitation and freeze-drying, shared the same intensity of the bands at 1740 cm^{-1} and at 1505 cm^{-1} in IR spectroscopy and the same hydroxyl groups content in ^{31}P NMR spectroscopy, proving that none of these treatments was sufficient in modifying lignin and that those samples could be considered as reference. Only when active base and acyl donor were milled with lignin, those parameters experienced variations.

Once qualitatively assessed by IR spectroscopy the efficacy of the treatment with sodium hydroxide as activator and vinyl acetate as model acyl donor, the reaction time was optimised in order to obtain the maximum conversion in the shortest time. Alkaline lignin was selected as model substrate. The first screenings were run on a 200 mg scale (referred to as *small scale* in the main text), then the process was scaled up to 5 g (referred to as *large scale* in the main text) in order to produce consistent batches of functionalised lignin to be introduced as fillers in rubber composites.

^{31}P NMR offered the possibility to perform the desired evaluations, as summarised in Table 6. Mechanochemical treatment of lignin with a suitable acyl donor in the absence of base resulted in no conversion. It resulted that for both small- and large- scale procedures a 30 min pre-treatment of lignin with the alkaline activator was sufficient to obtain the conversion of ionisable groups; a longer reaction time demonstrated to have a neutral or detrimental effect on the degree of functionalisation. For the small-scale procedure, the optimised reaction time with vinyl acetate resulted to be 2 h, a longer time did not improve degree of esterification. For the large-scale process, the ideal time of treatment with the acyl donor was 4 h while longer reaction times gave no significant enhancement in the extent of conversion.

Table 6. Quantification by ^{31}P NMR of the conversion degree of aliphatic (ROH) and phenolic (PhOH) -OH groups as a function of duration of the pre-treatment of alkaline lignin with NaOH (0.6 mmol/mmol$_{COOH+PhOH+ROH}$) and of the treatment with the acyl donor (vinyl acetate, 0.8 mmol/mmol$_{PhOH+ROH}$).

Duration of the pre-treatment of lignin with NaOH / min	Duration of the pre-treatment of lignin with acyl donor / h	Residual ROH / mmol·g^{-1}	Residual PhOH / mmol·g^{-1}	Converted ROH/ %	Converted PhOH/ %
Small scale procedure					
0	4	n.a.	n.a.	ca. 0[a]	ca. 0[a]
30	4	1.96	1.34	37	11
30	2	1.93	1.34	38	11
30	1	n.a.	n.a.	< 38[a]	< 11[a]
60	2	n.a.	n.a.	ca. 38[a]	ca. 11[a]
Large scale procedure					
30	2	n.a.	n.a.	< 47[a]	< 13[a]
30	4	1.65	1.31	47	13
30	6	n.a.	n.a.	ca. 47[a]	ca. 13[a]

Once verified the efficacy of sodium hydroxide in triggering the mechanochemical esterification of alkaline lignin and individuated the ideal reaction time, a variety of acyl donors was tested on a small scale (Table 7). The qualitative evaluation of the outcome of the reaction was assessed by FT-IR/ATR.

As mentioned before, methyl methacrylate proved ineffective in functionalising both alkaline and kraft lignins in the presence of NaOH and in the optimised reaction times. Conversely, IR spectroscopy confirmed the success in using vinyl acetate as model activated acyl donor for both lignins. Followingly, attention was focused on the transesterification of kraft lignin with vinyl methacrylate with the prospect of making this industrial-scale available lignin active to vulcanisation and enhancing its reinforcing effect in rubber compounds. The transesterification with vinyl esters was driven by the release of acetaldehyde (Scheme 5. Reaction scheme for the mechanochemical functionalisation of lignin with enol esters as acyl donors.) which is, however, considered as hazardous by the European Chemical Agency (ECHA). The release of rather safer by-products would be preferable so, as a proof of concept, isopropenyl acetate was considered as an activated acyl donor for transesterification liberating acetone as by-product. IR spectroscopy demonstrated the occurring of functionalisation when kraft lignin was treated with isopropenyl acetate. The use of this acyl donor was accompanied by the release of acetone, which is safer than acetaldehyde, but did not provide lignin with the desired reactivity towards vulcanisation. There is limited commercial availability of isopropenyl α,β-unsaturated esters which could grant for the looked

for functionalisation so vinyl methacrylate was considered as the most intriguing acyl donor from a technological point of view.

Table 7. Screening by FT-IR/ ATR of the efficacy of different acyl donors in triggering the mechanochemical esterification of softwood kraft lignin in the presence of NaOH as activator.

Acyl donor	Functionalisation
Methyl methacrylate	no
Vinyl acetate	yes
Vinyl methacrylate	yes
Isopropenyl acetate	yes

Once confirmed the efficacy of the treatment with vinyl acetate as model acyl donor and individuated the ideal reaction time, attention was focused on the nature of the alkaline activator. FT-IR/ATR proved a valid qualitative tool for a quick screening of the efficacy of different bases in catalysing the introduction of the desired ester groups as mentioned before and described in Table 5.

The first attempts were devoted to the use of a hydroxide of an alkali metal, *i.e.*, NaOH, inspired by literature reporting successful oleation and succinylation of organosolv lignin in a ball mill in the presence of KOH and NaOH, respectively.[6,13] The treatment of both alkaline and kraft lignin with NaOH followed by the addition of the model acyl donor, *i.e.*, vinyl acetate, resulted in the desired functionalisation of lignin. Then, ammonium hydroxide (NH_4OH) was considered as a possible activator for the reaction. Its use was considered particularly intriguing for the possibility to prepare natural rubber (NR) masterbatches by directly mixing NR latex in ammonia with esterified lignin ammonium salt without any intermediate purification step and straightforwardly drying the material. However, even high excesses of NH_4OH were not sufficient to catalyse the desired esterification. This failing can be ascribed to the volatilisation of the base during the milling process that is always accompanied by significant heat production. Afterwards, carbonates of both alkali and alkali-earth metals, *i.e.*, sodium, potassium, and calcium, were investigated as possible activators. No functionalisation could be detected in the case of calcium carbonate, probably due to the impossibility of a divalent cation to act as a counterion for alkoxides in the solid state which are typical for the mechanochemical reactions. Conversely, both sodium and potassium carbonate proved effective in triggering the esterification of lignin. However, since sodium and potassium carbonates are weaker base than sodium hydroxide, a higher stoichiometric excess of carbonates was required to replicate similar functionalisation degrees with respect to NaOH, leading to high mass ratios of base to lignin of up to 50% (Table 12). Additionally, the neutralisation step of esterified lignin during purification was accompanied by great effervescence which was considered as a

detrimental factor when planning to further scale the process up to the hundred grams and even larger scales. For these practical considerations, most of the investigations aiming at the optimisation of the reaction parameters were conducted by considering sodium hydroxide as the preferable activator. The list of the screened bases and the corresponding reaction outcome are presented in Table 8.

Table 8. Screening by FT-IR/ ATR of the efficacy of different bases in triggering the mechanochemical esterification of softwood kraft lignin in the presence of vinyl acetate as acyl donor.

Base	**Functionalisation**
NaOH	yes
NH_4OH	no
Na_2CO_3	yes
K_2CO_3	yes
$CaCO_3$	no

Further investigations involved the use of sodium hydroxide as activator and the screening of different acyl donors as functionalising agents.

In order to prove the efficacy of this approach on different lignin types, herbaceous alkaline and softwood kraft lignin were investigated. Attention was focused on the transesterification with vinyl methacrylate of kraft lignin with the prospect of making this industrial-scale available lignin active to vulcanisation and enhancing its reinforcing effect in rubber compounds. The transesterification with vinyl esters was driven by the release of acetaldehyde which is, however, considered as hazardous by the European Chemical Agency (ECHA). The release of rather safer by-products would be preferable, and, as a proof of concept, isopropenyl acetate was hence considered as an activated acyl donor for transesterification liberating acetone as by-product. The first screenings of reaction parameters were run on a 200 mg scale (referred to as *small scale* in the main text), then the process was scaled up to 5 g (referred to as *large scale* in the main text) in order to produce consistent batches of functionalised lignin to be introduced as fillers in rubber composites.

The main parameters investigated for the optimisation of the procedure, besides reaction time (Table 6), were the stoichiometry of acyl donor and base. The degree of esterification was assessed by quantitative ^{31}P NMR spectroscopy experiments involving both herbaceous alkaline (AL) and softwood kraft lignins (SKL).

Investigations on the functionalisation of alkaline lignin with NaOH and vinyl acetate on a small scale (Table 9) evidenced that, being equal the amount of base, the percentage of converted aliphatic alcohols (ROH) and phenols (PhOH) did not vary linearly with the amount of acyl donor. Even when a high excess of acyl donor was used (2.4 $mmol_{VA}/mmol_{PhOH+ROH}$), the degree of esterification did not exceed 40 % for ROH and 20 % for PhOH. This observation was ascribed to the base-catalysed partial hydrolysis of vinyl acetate and its partial evaporation concomitant with the temperature increase associated to milling. Moreover, increasing the amount of NaOH did not result in an increment of the degree of esterification. Not all hydroxyl groups are probably kinetically not accessible due to internal H-bonding, this accounting for the observed plateau in the esterification degree. When balancing stoichiometry of reagents and degree of esterification, the optimal conditions appeared to be 0.6 $mmol_{NaOH}/mmol_{COOH+PhOH+ROH}$ and 0.8 $mmol_{VA}/mmol_{PhOH+ROH}$.

Table 9. Base and acyl donor stoichiometry, degree of conversion of aliphatic alcohols and phenols for alkaline lignin submitted to mechanochemical esterification according to the small-scale procedure.

Base stoichiometry	Acyl donor stoichiometry	Residual ROH	Residual PhOH	Converted ROH	Converted PhOH
$mmol_{NaOH}/mmol_{COOH+PhOH+ROH}$	$mmol_{VA}/mmol_{PhOH+ROH}$	$mmol \cdot g^{-1}$	$mmol \cdot g^{-1}$	%	%
0.9	2.4	1.99	1.37	36	9
0.9	0.8	2.11	1.37	32	9
0.9	0.5	2.24	1.33	28	12
0.6	0.8	1.71	1.34	45	11
0.6	0.5	1.93	1.34	38	11

Then, large-scale functionalisation of alkaline lignin with NaOH and VA was optimised (Table 10). Experimental observation led to similar conclusions as the ones driven for the small-scale process. The degree of esterification did not increase linearly with the amount of base and acyl donor, the maximum conversion degrees recorded for 0.6 $mmol_{NaOH}/mmol_{COOH+PhOH+ROH}$ and 0.8 $mmol_{VA}/mmol_{PhOH+ROH}$.

Table 10. Base and acyl donor stoichiometry, degree of conversion of aliphatic alcohols and phenols for alkaline lignin submitted to mechanochemical esterification according to the large-scale procedure.

Base stoichiometry	Acyl donor stoichiometry	Residual ROH	Residual PhOH	Converted ROH	Converted PhOH
$mmol_{NaOH}$ /$mmol_{COOH+PhOH+ROH}$	$mmol_{VA}$ /$mmol_{PhOH+ROH}$	$mmol \cdot g^{-1}$	$mmol \cdot g^{-1}$	%	%
0.9	0.8	196	134	37	11
0.9	0.5	205	134	34	11
0.9	0.3	199	140	36	7
0.6	0.8	165	131	47	13
0.6	0.5	199	133	36	12

In literature, milling lignin in the presence of large excess of NaOH, *i.e.*, 1–10 equivalents, was reported to provoke lignin degradation into fragments with lower molecular weight.[14] Gel permeation chromatography allowed verifying that the optimal procedure here presented did not resulted in any degradation of lignin. Analyses confirmed that the optimised reaction conditions did not significantly affect the molecular weight distribution of lignin and did not cause its degradation (Figure 16 and Table 11). The sharp peak at low molecular weight was associated to residual unreacted reagents.

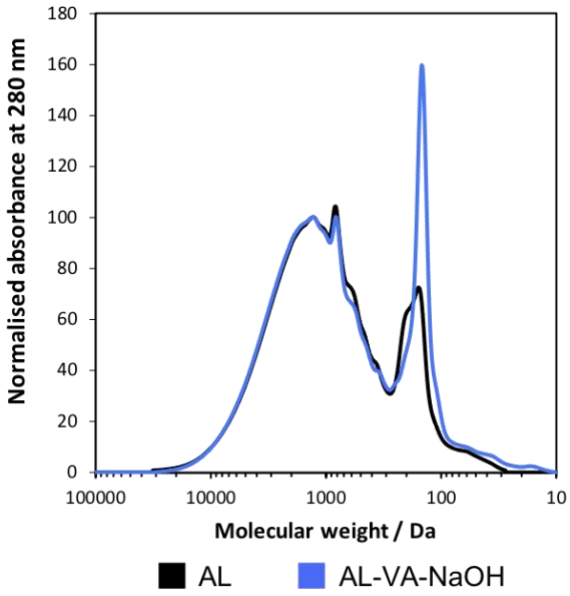

Figure 16. GPC traces for AL and AL treated with 0.6 equiv. of NaOH and 0.8 equiv. of vinyl acetate (VA).

Table 11. Molecular weight distribution assessed by GPC for alkaline lignin and lignin treated with 0.6 equiv. of NaOH and 0.8 equiv. of vinyl acetate (VA).

Sample	M_n / $g \cdot mol^{-1}$	M_w/ $g \cdot mol^{-1}$	PDI
Alkaline lignin	1900	4600	2.4
Alkaline lignin treated with NaOH and VA, optimised procedure	1800	4200	2.3

The same screenings were performed on softwood kraft lignin in order to prove the applicability of mechanochemical esterification to different lignins and to further proceed with this lignin for the development of innovative bio-based fillers for rubber compounds (Table 12). Kraft lignin is industrially available both as dried powder and as wet powder with a solid content of 40-70 %. The latter results more economically convenient since the extensive drying of lignin is energy demanding. It was demonstrated that a preliminary drying of lignin resulted in higher esterification degrees. However, in order to better simulate industrial conditions, the optimisation of the mechanochemical esterification was run on a moist kraft lignin cake (55 % solid content). As evidenced for alkaline lignin, also for KL the extent of functionalisation did not vary linearly with base and acyl donor quantities, but it reached it optimum for 0.7 equiv. of NaOH and 0.7 equiv. of VA. When sodium carbonate was tested as possible alkaline activator, in order to obtain results comparable to those of NaOH, it was necessary to resort to higher stoichiometric amount of base since sodium carbonate is a weaker base compared to sodium hydroxide. However, the seeked esterification degrees were obtained when a high excess of Na_2CO_3 was used, reaching a mass ratio of 50 % of Na_2CO_3 over lignin. Even if Na_2CO_3 would have been preferable to NaOH Moreover, the neutralisation of lignin salt with 0.1 M HCl during the purification step was associated to high effervescence which rendered the process challenging to be scaled up.

Table 12. Base and acyl donor stoichiometry, degree of conversion of aliphatic alcohols and phenols for softwood kraft lignin submitted to mechanochemical esterification according to the small-scale procedure.

Base stoichiometry	Acyl donor stoichiometry	Residual ROH	Residual PhOH	Converted ROH	Converted PhOH
$mmol_{NaOH}$ $/mmol_{COOH+PhOH+ROH}$	$mmol_{VA}$ $/mmol_{PhOH+ROH}$	$mmol \cdot g^{-1}$	$mmol \cdot g^{-1}$	%	%
0.9	0.8	1.09	2.17	32	30
0.9	0.7	1.14	2.36	29	24
0.7	0.7	0.83	1.71	48	45
0.7	0.4	1.07	2.17	33	30
0.7	0.3	1.10	2.42	31	22
$mmol_{Na_2CO_3}$ $/mmol_{COOH+PhOH+ROH}$	$mmol_{VA}$ $/mmol_{PhOH+ROH}$	$mmol \cdot g^{-1}$	$mmol \cdot g^{-1}$	%	%
1.0	1.2	1.02	1.92	36	38
0.8	1.0	1.49	2.88	7	7

The most promising reaction conditions were replicated in the large-scale procedure (Table 13) in order to evaluate the reproducibility of results while upscaling and to produce consistent batches of functionalised kraft lignin to be included in rubber compounds. In particular, lignin functionalised with 0.7 NaOH, 0.3 VM and 1.6 Na_2CO_3, 0.3 VM were used as reinforcing fillers, as described in the following section.

Table 13. Base and acyl donor stoichiometry, degree of conversion of aliphatic alcohols and phenols for softwood kraft lignin submitted to mechanochemical esterification according to the large-scale procedure.

Base stoichiometry	Acyl donor stoichiometry	Residual ROH	Residual PhOH	Converted ROH	Converted PhOH
$mmol_{NaOH}$ $/mmol_{COOH+PhOH+ROH}$	$mmol_{VA}$ $/mmol_{PhOH+ROH}$	$mmol \cdot g^{-1}$	$mmol \cdot g^{-1}$	%	%
0.9	0.9	1.09	2.02	32	35
0.9	0.6	1.10	2.29	31	26
$mmol_{NaOH}$ $/mmol_{COOH+PhOH+ROH}$	$mmol_{VM}$ $/mmol_{PhOH+ROH}$	$mmol \cdot g^{-1}$	$mmol \cdot g^{-1}$	%	%

0.7	1.0	0.99	2.39	38	23
0.7	0.3	1.25	2.57	22	17
$mmol_{Na_2CO_3}$ /$mmol_{COOH+PhOH+ROH}$	$mmol_{VM}$ /$mmol_{PhOH+ROH}$	$mmol \cdot g^{-1}$	$mmol \cdot g^{-1}$	%	%
1.6	0.3	1.42	2.88	11	7

Methacrylated lignin intended as filler for rubber compounds was fully characterised by FT-IR/ATR, GPC, ^{31}P NMR, and ^{1}H NMR.

Chromatography confirmed that under optimal conditions kraft lignin was not significantly degraded into smaller fragments (Figure 17 and Table 14).

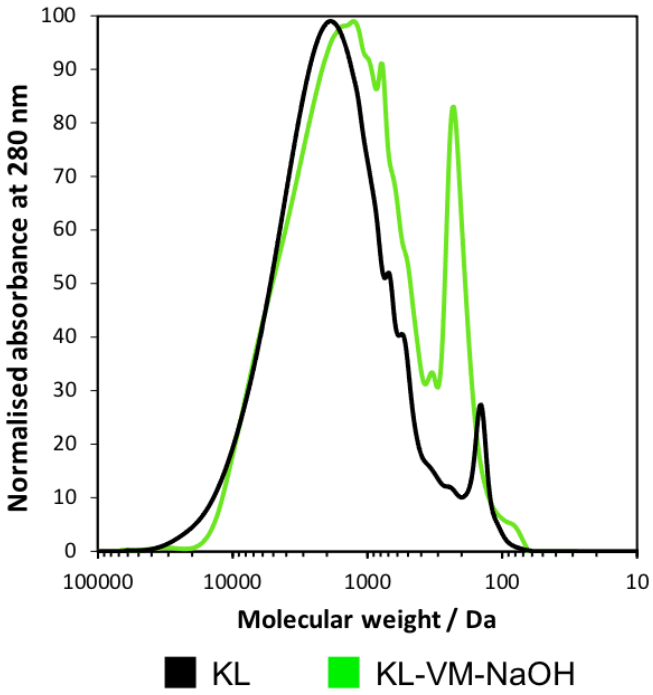

Figure 17. GPC traces for softwood kraft lignin and softwood kraft lignin treated with 0.6 equiv. of NaOH and 0.8 equiv. of vinyl methacrylate (VM).

Table 14. Molecular weight distribution assessed by GPC for alkaline lignin and lignin treated with 0.6 equiv. of NaOH and 0.8 equiv. of methacrylate (VM).

Sample	M_n/ $g \cdot mol^{-1}$	M_w/ $g \cdot mol^{-1}$	PDI
Kraft lignin	2800	6300	2.2
Kraft lignin treated with NaOH and VM, optimised procedure	2300	5200	2.3

The esterification was indirectly detected by decrement in intensity of signals related to ROH and PhOH in ^{31}P NMR. This decrease in intensity gave a quantitative evaluation of the degree of functionalisation (Figure 18).

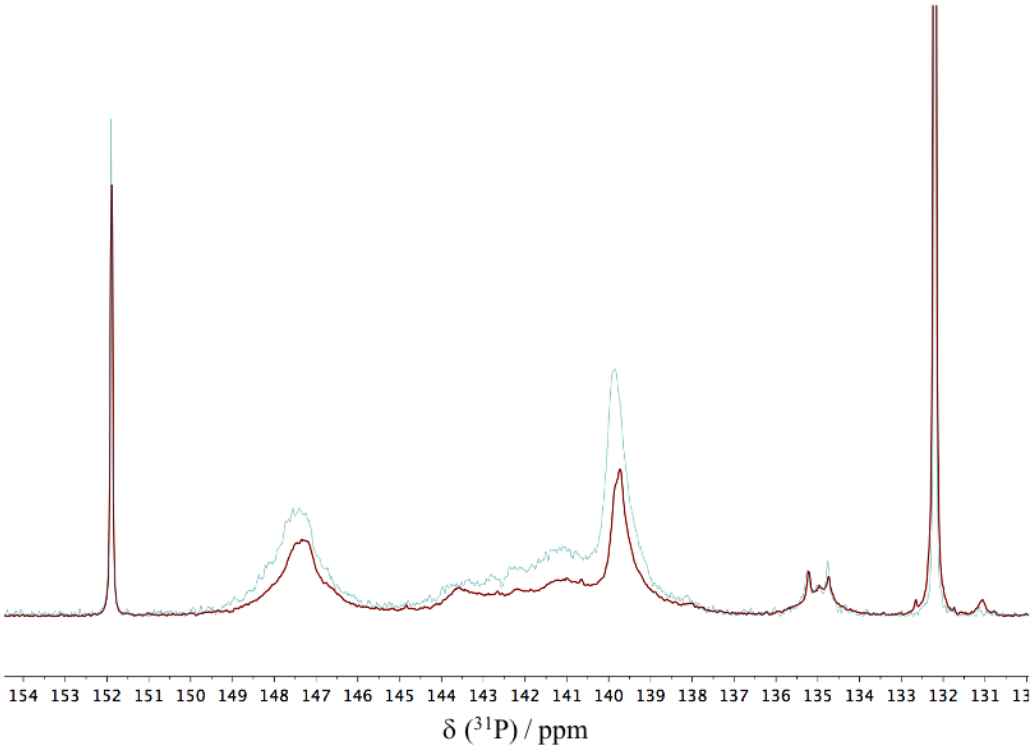

Figure 18. Superimposed ^{31}P NMR spectra for softwood kraft lignin (red line) and mechanochemically esterified softwood kraft lignin (blue line).

A direct proof of functionalisation was provided by FT-IR/ ATR and ^{1}H NMR which showed the appearance of peaks related to the presence of the methacrylic group (Figure 19, Figure 20, Figure 21). In particular, in ^{1}H NMR signals in the chemical shift range 5.6-6.2 corresponded to olefinic protons. Those peaks resulted split into two, accounting for the possibility that the methacrylic function could be bound to an aliphatic alcohol or a phenol.

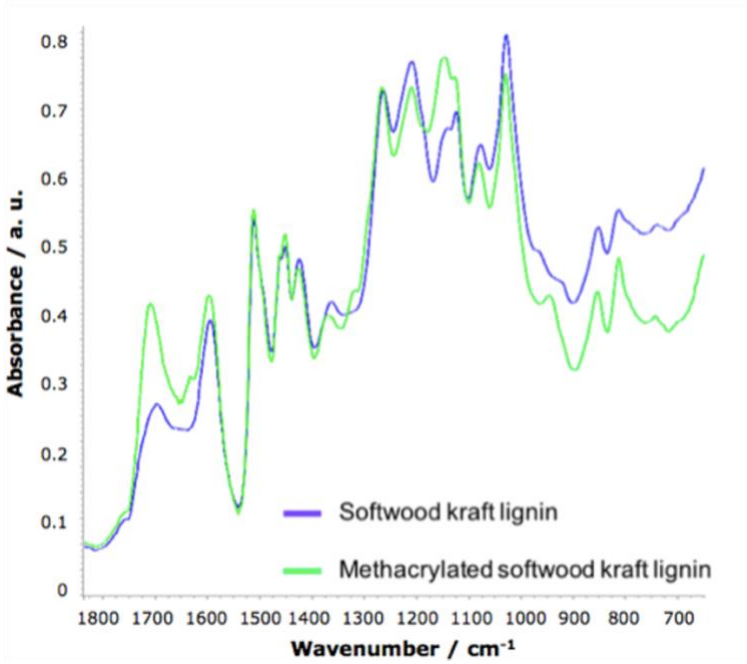

Figure 19. FT-IR / ATR spectra in the range 1825-650 cm^{-1} for KL and its corresponding methacrylated derivative.

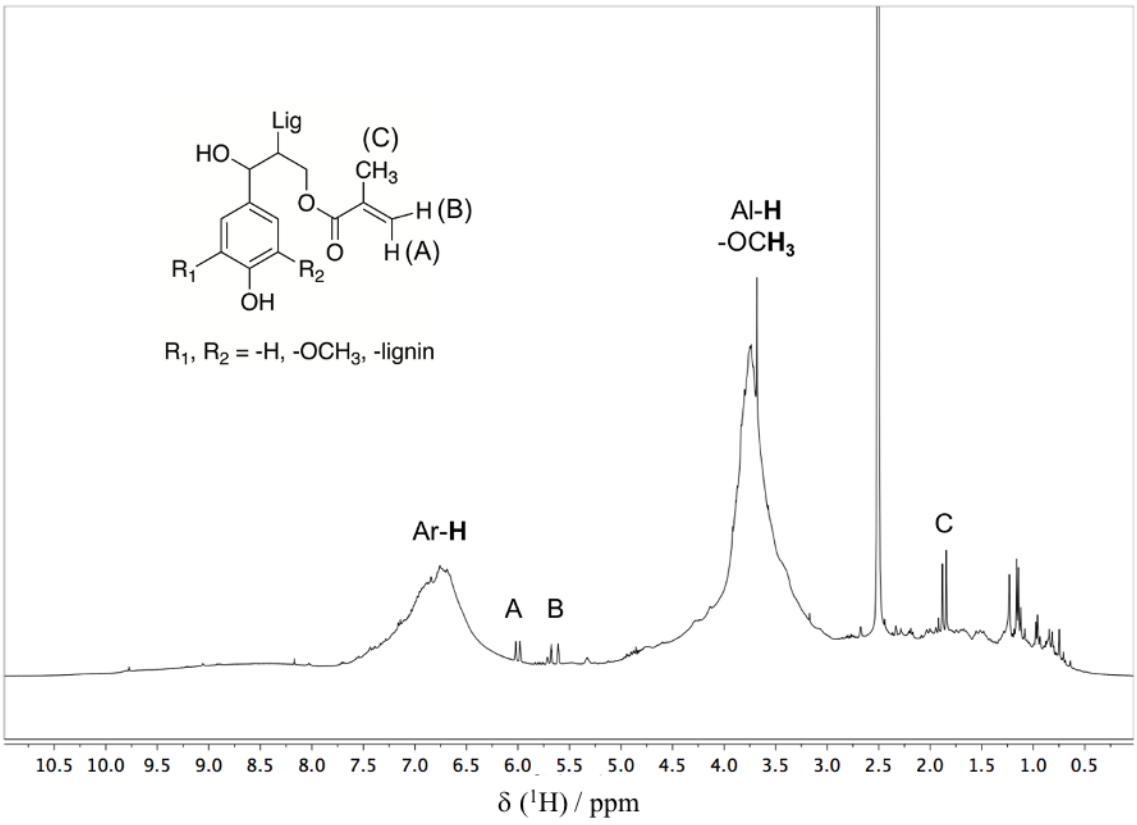

Figure 20. ^{1}H NMR spectrum in d_6-DMSO of methacrylated kraft lignin in the range 0–11 ppm.

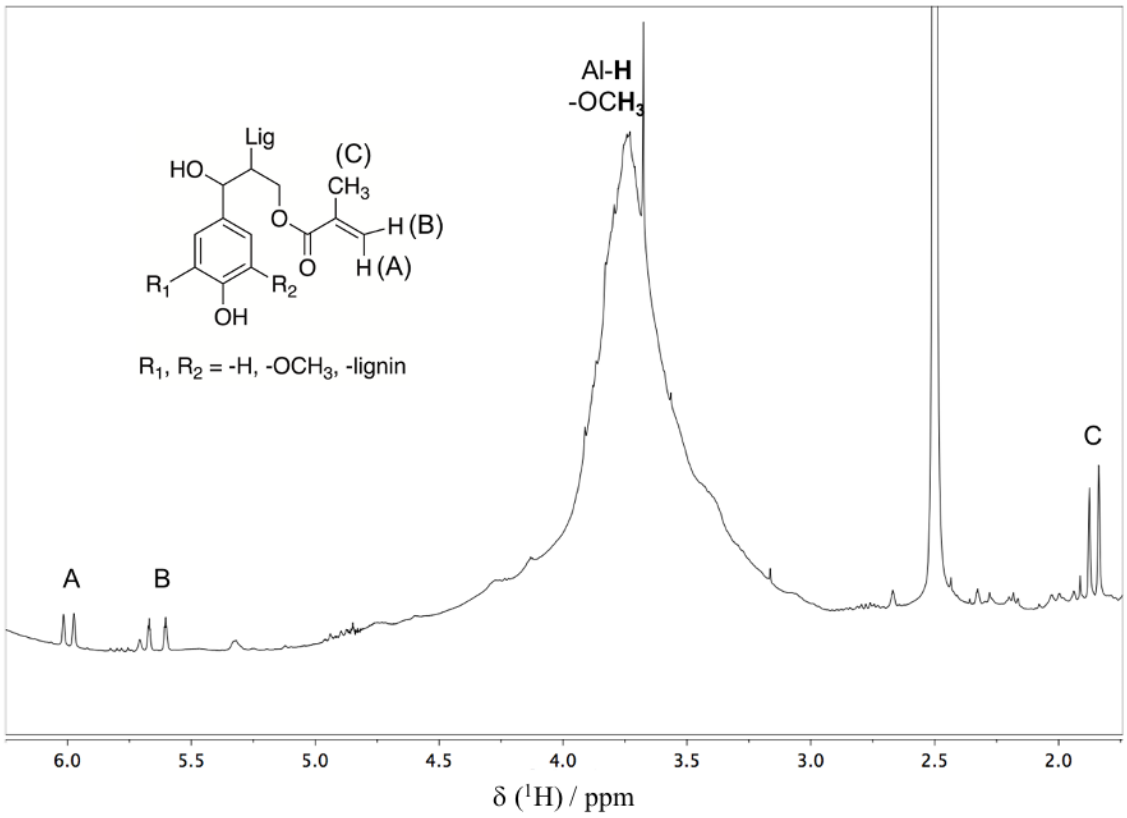

Figure 21. ^{1}H NMR spectrum in d_6-DMSO of methacrylated kraft lignin in the range 1.5-6.5 ppm.

11.2 Preparation and assessment of the mechanical performances of rubber composites including functionalised lignin

The following section is devoted to the discussion of the dynamic mechanical of composites whose preparation was described in the previous chapter. The study included the dynamic mechanical properties of vulcanised compounds, the vulcanisation kinetics, the tensile properties and the swelling behaviour.

The rheometer allowed measuring the change in the torque necessary to maintain a specific amplitude of oscillation at a given temperature. The vulcanisation curve is obtained by plotting the torque as a function of time at the curing temperature (Figure 22).

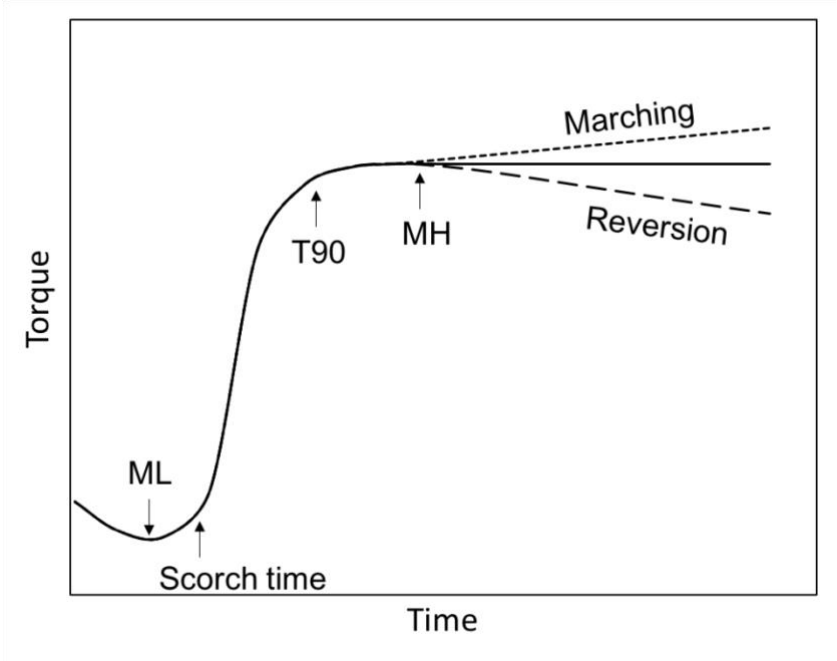

Figure 22. Typical vulcanisation curve.

Information about the vulcanisation characteristics and kinetics can be inferred by evaluating several quantities. When the sample is heated under pressure, viscosity decreases so the torque exerted on the rotor drops. The rheometer collects the minimum torque value, known as ML (moment lowest), which provides information about the rigidity of uncured rubber compound at the vulcanisation temperature. When the curing starts, the torque increases. The moment when the curing actually starts is known as scorch time and is often correlated to Ts2, the time taken by the torque to increase by 2 units above ML value. Once crosslinking has started, the item cannot be reshaped anymore, and the torque value grows till reaching the maximum value acknowledged as MH (moment highest). The difference MH - ML can be related to the extent of crosslinking and can be affected by many factors, including filler flocculation. An important parameter to be taken into account is T90, the time needed by the torque to reach 90 %

of the maximum value (MH) and it is considered as the optimal curing time. After reaching MH, the torque can either reach a plateau, decrease due to a drop in crosslinking associated to thermal ageing (reversion) or increase (marching modulus). [16]

Rubber process analysis provides information about the viscoelastic properties of compounds, data are recorded on both green and cured samples. It is possible to obtain information about processability, vulcanisation characteristics, after-cure behaviour. Disc-shaped-rubber composites (5.5 g) was inserted between two thin Mylar films (4 x 4 cm) and transferred into a heated chamber at 70 °C for 10 min. Then, strain sweep tests were performed: oscillating shear strain changed in steady steps while frequency and temperature remained constant. The instrument measured the stress associated to the applied strain. Then, the sample was cured at 170 °C for 10–15 min. Finally, the vulcanised sample was submitted to the same oscillatory tests as the green compound.

More in detail, specimens are deformed under dynamic conditions applying oscillatory strains γ following a periodic law:

$$\gamma = \gamma_0 \cdot sin\omega t$$

where $\gamma_0$is the maximum deformation and ω is the frequency in rad·s^{-1}. The ensuing stress is sinusoidal, too, and shares the same frequency. For purely elastic materials, stress is in phase with strain ($\sigma_0 = \gamma_0 G$). On the contrary, for viscous materials, strain and stress are out of phase by 90° ($\sigma_0 = \eta\dot{\gamma}$, being $\dot{\gamma} = \frac{\partial\gamma}{\partial t}$ and η the viscosity). For viscoelastic materials such as elastomers, stress and strain are out of phase by an angle $0° < \delta < 90°$ (Figure 23). As a consequence, stress for viscoelastic materials can be defined as:

$$\sigma = \sigma_0 \cdot \sin(\omega t + \delta) = \sigma_0 \cdot (\sin\delta \cdot cos\omega t + \cos\delta \cdot sin\omega t)$$

Stress can be expressed as a combination of a component in phase with strain representing stored energy (elastic or storage modulus G') and a component out of phase by 90° with deformation constituting energy dissipated as heat (viscous or loss modulus G").

$$\sigma = \gamma_0 \cdot (G' \cdot sin\omega t + G'' \cdot cos\omega t)$$

where $G' = \frac{\sigma_0}{\gamma_0}\cos\delta$; $G'' = \frac{\sigma_0}{\gamma_0}\sin\delta$; $\frac{G''}{G'} = tan\delta$; $G^* = G' + iG''$.

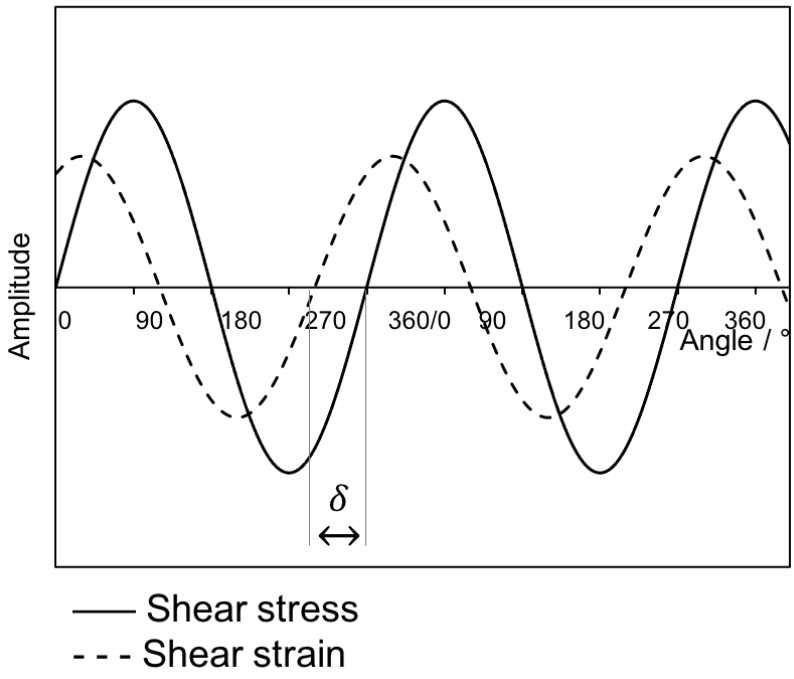

Figure 23. Dynamic viscoelastic response to shear oscillatory deformations.

Complex G^*, storage G' and loss G'' moduli, and the dumping factor $tan\delta$ are crucial values describing reinforcing mechanism of filled elastomers. In particular, $tan\delta$ denotes material dumping characteristics. It is a measure of the ratio of the energy dissipated as heat to the maximum energy stored in the material during one cycle of oscillation. The addition of reinforcing fillers to elastomeric compounds is known to deeply affect static and dynamic behaviours. The trend of complex modulus G^*as a function of dynamic deformation in filled rubber compounds is simplified as a result of four main contributions (Figure 24). *Polymer network* depends on the features of unfilled polymer and on the crosslink density. *Hydrodynamic effect* is related to strain amplification due to the presence of undeformable filler particles. *In-rubber structure* is a measure of bond and occluded rubber which is shielded from deformation, incrementing the effective concentration of filler and affecting reinforcement. *Filler network* is a measure of all filler-filler interactions. The contribution of filler network to the overall modulus drops at high deformations due to the disruption of filler agglomerates, giving rise to the well-known Payne effect. [17]]

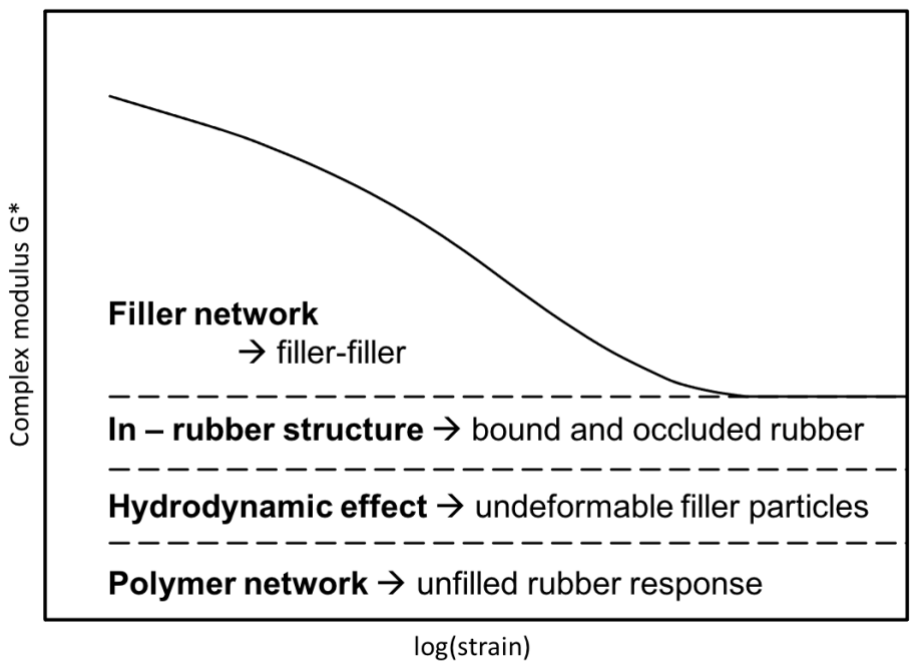

Figure 24. Ideal contributions to the complex modulus of filled elastomers.

Samples will be labelled *RR 00XX+00LL PP Z* according to the rubber blend, filler content and vulcanisation system.

RR stands for the rubber blend, specifically:

NR for natural rubber;

BR for butadiene rubber;

SBR for styrene butadiene rubber.

00XX refers to 00 phr of traditional filler:

CB for carbon black;

Si for silica.

00LL indicates 00 phr of lignin:

L for milled lignin;

LMet(NaOH) and LMet(Na_2CO_3) for lignin mechanochemically methacrylated in the presence of NaOH or Na_2CO_3 as alkaline activator.

PP accounts for the process of production of NR / lignin masterbatches:

Pr for coprecipitated masterbatches;

Dr for codried masterbatches.

Z refers to the vulcanisation system:

O for peroxides;

S for sulphur.

The unit *phr* stands for *parts per hundred rubber* and indicates the percentual mass ratio between the specific ingredient and the total rubber quantity in the formulation.

11.2.1 NR/SBR composites including lignin and silica as fillers

NR/SBR compounds were studied in order to develop tyre treads including a mixture of silica and lignin as reinforcing fillers. The presence of SBR in the elastomer, which has a relatively high glass transition temperature if compared to other common rubber used in tyre technology (*e.g.* isoprenic and butadiene rubbers), is crucial for the application in tyre treads where traction is a required performance parameter. As a first screening, peroxide-vulcanised compounds were prepared (

Table 15) in order to evaluate and exalt the reinforcing effect of lignin methacrylation considering that the activated C=C double bond is particularly reactive towards peroxides. Reference compounds (*NRSBR 50Si O* and *NRSBR 35Si O*) included silica compatibilised with a methacryloyl silane which mimicked the methacrylic functionalisation of lignin (*NRSBR 35Si+25LPrMet(NaOH) O*) and shared the same reactivity during vulcanisation. Model compounds *NRSBR 50Si O* and *NRSBR 35Si O* represent the upper and lower limits, respectively, in terms of storage modulus. While reference compound *NRSBR 50Si O* was above the percolation limit, the other model compound (*NRSBR 35Si O*) was below that value and was characterised by lower storage modulus and hysteresis. Innovative compounds (*NRSBR 35Si+25LPr O* and *NRSBR 35Si+25LPrMet(NaOH) O*) included 25 phr of either milled or methacrylated lignin in partial substitution of 15 phr of silica, this decision driven by the well-known weaker reinforcing performances of lignin compared to silica.[15]

Table 15. NR/SBR composites including lignin coprecipitated with NR, silica as co-filler, peroxide-based vulcanisation.

Components and formulation in phr	NRSBR 50Si O	NRSBR 35Si O	NRSBR 35Si+25LPr O	NRSBR 35Si+25LPrMet (NaOH) O
Styrene - butadiene rubber (BSL SLR 4630)	102.75	102.75	102.75	102.75
Natural rubber (SIR20)	25	25		
Coprecipitated NR masterbatch, 50% milled lignin			50	
Coprecipitated NR masterbatch, 50% methacrylated lignin				50
Silica (ZEOSIL 1165 MP)	50	35	35	35
γ-methacryloyl propyl triethoxy silane (TEMS)	4	2.8	2.8	2.8
Antioxidant (6PPD)	2	2	2	2
Peroxide-based vulcanising agent (LUPEROX 101XL45)	2.3	2.3	2.3	2.3
Tensile properties				
Stress at 50% deformation / MPa	1.03	0.82	0.90	0.87
Stress at 100% deformation / MPa	1.32	1.13	1.22	1.22
Stress at 300% deformation / MPa	3.63	3.37	3.31	4.36
Stress at break / MPa	14.96	8.95	10.59	12.15
Elongation at break / %	695.51	565.64	703.57	611.58
Energy/ $J \cdot cm^{-3}$	41.04	21.82	32.19	31.01
Vulcanisation kinetics (170 °C, 10 min) and dynamo-mechanical properties				
ML (moment lowest) / dN·m	5.85	3.61	4.72	4.09
MH (moment highest) / dN·m	14.89	9.68	10.27	10.69
T90 / min	11.7	11.65	11.30	11.48
TS2 / min	3.55	4.03	4.32	3.99
dG' (0.4 - 10 % deformation) / MPa	0.30	0.42	0.70	0.34
G' (at 9 % deformation) / MPa	1.33	0.52	0.63	0.96
tanδ (at 9 % deformation)	0.171	0.131	0.281	0.172

The addition of lignin (*NRSBR 35Si+25LPr O* and *NRSBR 35Si+25LPrMet(NaOH) O*) on top of silica (*NRSBR 35Si O*) was associated with an increment in both storage modulus and hysteresis. Noticeably, functionalised lignin was resulted in a higher storage modulus and lower tanδ values than milled lignin,

with the latter property reaching the same value as reference compound *NRSBR 50Si P*. Since hysteresis is connected to rolling resistance, reducing its value results in an increment in the fuel efficiency of the vehicle. Moreover, while the presence of lignin was associated to a decrease in stress at break, this parameter improved in the case of functionalisation, nearly reaching the levels of model composite *NRSBR 50Si O*. In fact, functionalisation ensured an enhanced dispersion of the filler inside the rubber matrix (with respect to milled lignin), as demonstrated by a higher ratio between stress values at 300 % and 100 % deformation.

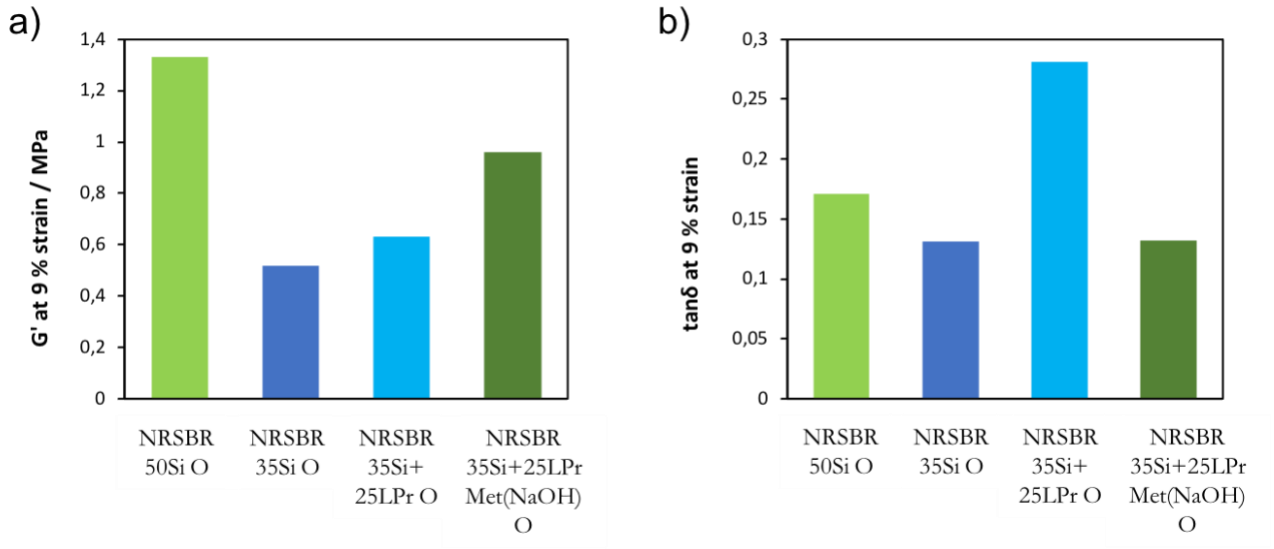

Figure 25. Storage modulus G' (a) and hysteresis tanδ (b) values at 9 % strain for NR SBR compounds vulcanised by peroxides.

NR/SBR composites containing lignin reported in

Table 16 were prepared by mixing a coprecipitated NR/lignin masterbatch with styrene-butadiene rubber and subsequently adding the other ingredients (paragraphs 9.1.1 and 9.2).

Table 16. NR/SBR composites including lignin coprecipitated with NR, silica as co-filler, sulfur-based vulcanisation.

Components and formulation in phr	NRSBR 50Si S TESPD	NRSBR 50Si S TEMS	NRSBR 35Si S	NRSBR 35Si+ 25LPr S	NRSBR 35Si+ 25LPrMet (NaOH) S	NRSBR 35Si+ 25LPrMet (Na_2CO_3) S
Styrene - butadiene rubber (BSL SLR 4630)	102.75	102.75	102.75	102.75	102.75	102.75
Natural rubber (SIR20)	25	25	25			
Coprecipitated NR masterbatch, 50% milled lignin				50		
Coprecipitated NR masterbatch, 50% methacrylated lignin					50	50
Silica (ZEOSIL 1165 MP)	50	50	35	35	35	35
γ -methacryloyl propyl triethoxy silane (TEMS)		4				
50 % bis(triethoxysilylpropyl)disulfide supported on CB (TESPD)	8		5.6	5.6	5.6	5.6
Antioxidant (6PPD)	2	2	2	2	2	2
Stearic acid	1	1	1	1	1	1
Zinc oxide	1	1	1	1	1	1
Accelerator CBS	3	3	3	3	3	3
Sulfur	1	1	1	1	1	1
Tensile properties						
Stress at 50% deformation / MPa	1.11	0.78	0.96	1.03	1.13	0.99
Stress at 100% deformation / MPa	1.64	1.09	1.40	1.45	1.58	1.36
Stress at 300% deformation / MPa	6.28	3.67	4.50	4.18	4.66	3.94
Stress at break / MPa	19.48	17.71	11.24	16.92	15.06	14.29
Elongation at break / %	599.92	696.04	534.90	749.97	794.09	750.91
Energy/ J·cm^{-3}	46.13	42.37	24.29	50.36	45.84	43.77
Vulcanisation kinetics (170 °C, 10 min) and dynamo-mechanical properties						
ML (moment lowest) / dN·m	3.76	3.04	2.96	3.67	4.05	4.22
MH (moment highest) / dN·m	14.11	12.09	10.90	10.53	11.60	23.81
T90 / min	4.56	5.89	3.98	6.19	6.06	2.63
TS2 / min	1.73	2.94	1.94	2.22	1.97	1.00
dG' (0.4 - 10 % deformation) / MPa	0.82	0.72	0.20	0.47	0.73	0.96
G' at 9 % deformation / MPa	1.21	0.91	0.84	1.06	1.21	1.89
tanδ at 9 % deformation	0.142	0.148	0.097	0.134	0.142	0.101

Sulfur-vulcanised NR/SBR composites are typically characterised by an efficient vulcanisation system comprising little amounts of sulfur and high amounts of accelerator (CBS) which produced short sulfur bridges that made the compound thermally stable and suitable for manufacturing tyre treads.

Reference compounds N*RSBR 50Si S TESPD* and *NRSBR 50Si S TEMS* (

Table 16) differed for the silane used to compatibilise silica. Composite N*RSBR 50Si S TESPD* included disulfide silane (TESPD) and displayed higher crosslink density (MH-ML) which reflected into higher rigidity (lower elongation at break), improved stress at 300 % deformation and superior storage modulus when compared to composite *NRSBR 50Si S TEMS* containing methacryloyl silane. This difference in crosslink density and overall properties was connected to the higher activity of disulfides in vulcanisation with respect to methacrylic functions. Despite these differences, the two reference compounds showed similar ultimate properties and hysteresis values, suggesting promising results for fillers, in particular lignin, compatibilised with a methacrylic function.

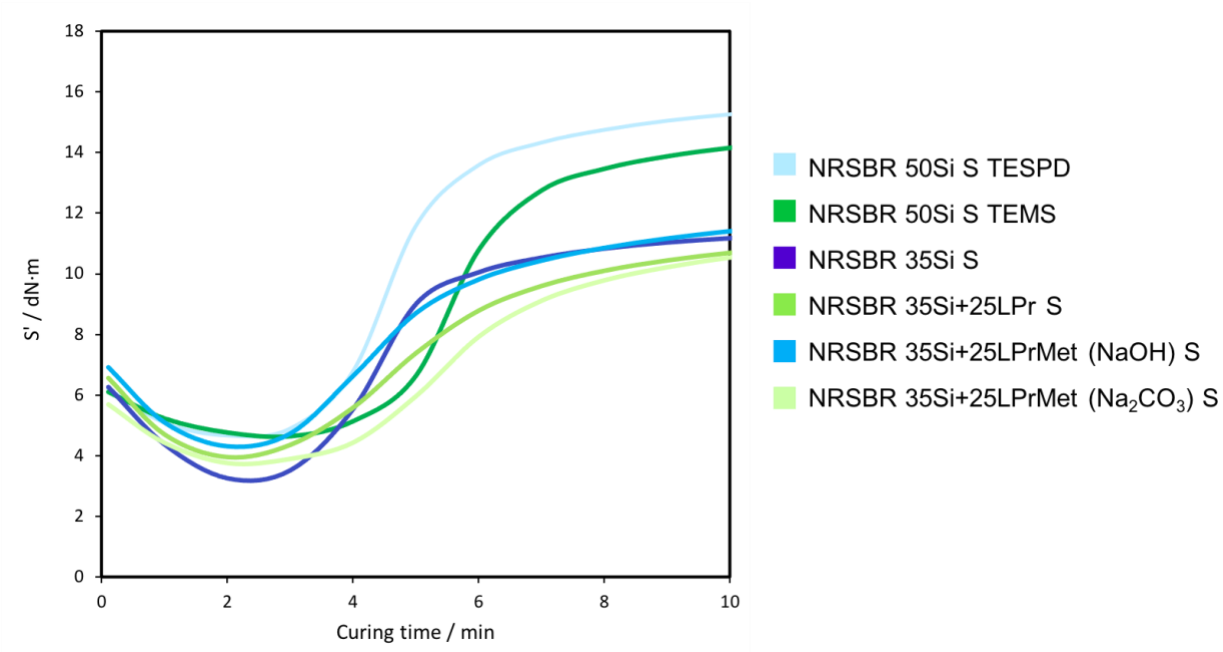

Figure 26. Vulcanisation kinetics (170 °C, 10 min) for sulphur-vulcanised NR/SBR compounds (for more details about the formulation see

Table 16).

When comparing compounds with the same silica content, the addition of either milled or methacrylated lignin (*NRSBR 35Si+35LPr S, NRSBR 35Si+25LPrMet (NaOH) S, NRSBR 35Si+25LPrMet (Na_2CO_3) S*) was associated to better values of storage modulus, stress and elongation at break than *NRSBR 35Si S*, while tanδ moderately increased. With respect to model compound *NRSBR 50Si S TESPD*, the partial substitution of silica with milled (*NRSBR 35Si+35LPr S)* or methacrylated lignin (*NRSBR 35Si+25LPrMet (NaOH) S* and *NRSBR 35Si+25LPrMet (Na_2CO_3) S*) resulted in lower rigidity (namely, increase in elongation at break) and lower stress at break. Methacrylated lignin was associated with higher storage modulus than milled lignin, confirming the efficiency of functionalisation in grafting the macromolecules of the elastomeric matrix and immobilising them. The improvement in ultimate properties and in the balance between storage modulus was particularly evident in the composite including lignin methacrylated with Na_2CO_3 catalysis (*NRSBR 35Si+25LPrMet (Na_2CO_3) S*). This compound showed faster vulcanisation kinetics than the one containing lignin methacrylated with NaOH catalysis (*NRSBR 35Si+25LPrMet (NaOH) S*). This was ascribed to a lower content in acids residual from the previous steps which could interact and partly deactivate the sulfenamidic accelerator (CBS). The increased G' values of *NRSBR 35Si+25LPrMet (Na_2CO_3) S* could be ascribed to a more efficient vulcanisation, which was confirmed by the high MH value. Additionally, *NRSBR 35Si+25LPrMet (Na_2CO_3) S* exhibited lower hysteresis than *NRSBR 35Si+25LPrMet (NaOH) S*.

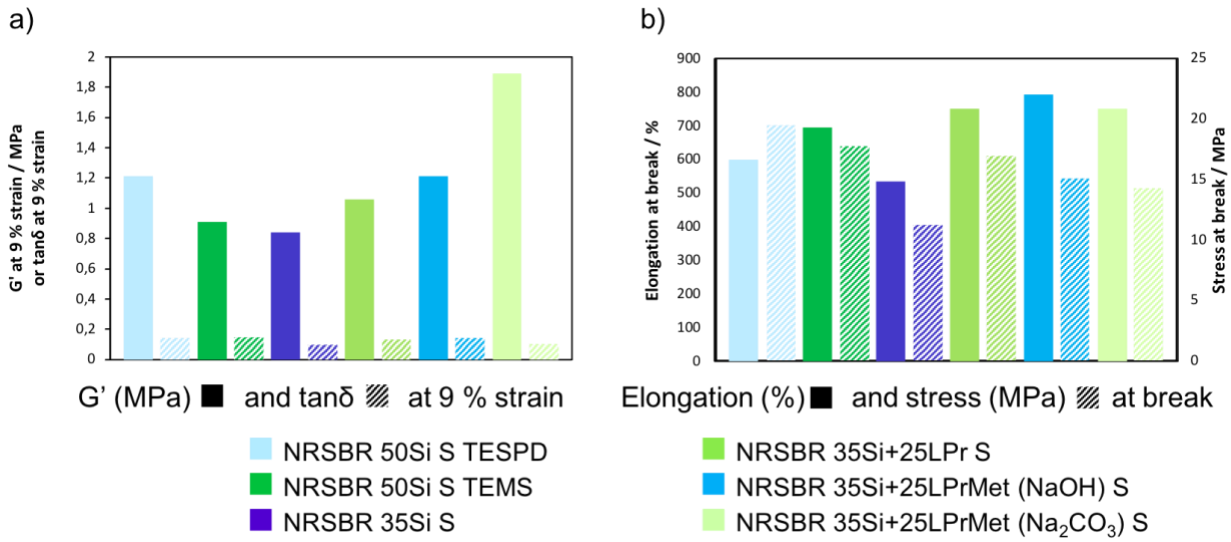

Figure 27. Storage modulus G' and hysteresis tanδ (a), elongation and stress at break (b) for sulphur-vulcanised NR/SBR compounds. For more details about the formulation see

Table 16.

NR/SBR composites containing lignin reported in Table 17 were prepared by mixing a codried NR/lignin masterbatch with styrene-butadiene rubber and subsequently adding the other ingredients (paragraphs 9.1.2 and 9.2).

Table 17. NR/SBR composites including lignin codried with NR, silica as co-filler, sulfur-based vulcanisation.

Components and formulation in phr	NRSBR 35Si S	NRSBR 35Si+25LDr S	NRSBR 35Si+25LDr Met(Na_2CO_3) S
Styrene - butadiene rubber (BSL SLR 4630)	102.75	102.75	102.75
Natural rubber (SIR20)	25		
Codried NR masterbatch, 50% milled lignin		50	
Codried NR masterbatch, 50% methacrylated lignin			50
Silica (ZEOSIL 1165 MP)	35	35	35
50 % bis(triethoxysilylpropyl)disulfide supported on CB (TESPD)	5.6	5.6	5.6
Antioxidant (6PPD)	2	2	2
Stearic acid	1	1	1
Zinc oxide	1	1	1
Accelerator CBS	3	3	3
Sulfur	1	1	1
Tensile properties			
Stress at 50% deformation / MPa	0.96	1.01	1.15
Stress at 100% deformation / MPa	1.40	1.41	1.78
Stress at 300% deformation / MPa	4.50	3.84	4.66
Stress at break / MPa	11.24	7.03	8.78
Elongation at break / %	534.90	454.59	489.72
Energy/ $J \cdot cm^{-3}$	24.29	14.89	19.91
Vulcanisation kinetics (170 °C, 10 min) and dynamo-mechanical properties			
ML (moment lowest) / dN·m	2.96	3.69	3.61
MH (moment highest) / dN·m	10.90	12.71	13.91
T30 / min	2.01	3.46	3.45
T90 / min	3.98	6.27	6.15

TS2 / min	1.94	3.19	3.20
dG' (0.4 - 10 % deformation) / MPa	0.20	0.44	0.43
G' at 9 % deformation / MPa	0.84	1.06	1.13
tanδ at 9 % deformation	0.097	0.121	0.113

The incorporation of lignin into the elastomer delayed the vulcanisation of rubber because of the radical scavenging provided by phenol groups in lignin.[16,17] The addition of lignin on top of silica (*NRSBR 35Si+25LDr S* and *NRSBR 35Si+25LDrMet(Na_2CO_3) S*) led to an increment in storage modulus and crosslink density (MH-ML) which resulted in higher rigidity with respect to *NRSBR 35Si S*. The extent of crosslink density is deeply influenced by the kind and amount of fillers, activators and accelerators used.[18] Being equal the cure package for compounds detailed in Table 17, variations in crosslink density can be ascribed to the filler-rubber interactions[19] and be rationalised by resorting to the equilibrium swelling theory developed by Flory and Rehner.[20] When cured compounds are soaked in a solvent (*i.e.*, toluene), the higher the crosslink density the lower the number of solvent molecules which can be accommodated, resulting in a relatively low swelling. The increase in filler-rubber interactions was found to be proportional to the filler content and responsible for the decrease in swelling due to the immobilisation of rubber macromolecules by the filler and the ensuing restricted motion of the elastomeric matrix. This phenomenon was particularly evident in the case of methacrylated lignin (*NRSBR 35Si+25LDrMet(Na_2CO_3) S*) which could create covalent bonds with the rubber macromolecules upon vulcanisation. The formation of strong interactions which constituted new constraints to rubber motion was responsible for the higher rigidity of lignin-containing compounds (*NRSBR 35Si+25LDr S* and *NRSBR 35Si+25LDrMet(Na_2CO_3) S*) with respect to the reference (*NRSBR 35Si S*). The crosslink density calculated by Flory-Rehner equation (paragraph 10.5) showed the same trends as the evolution of MH-ML evidenced by vulcanisation curves (Figure 28).

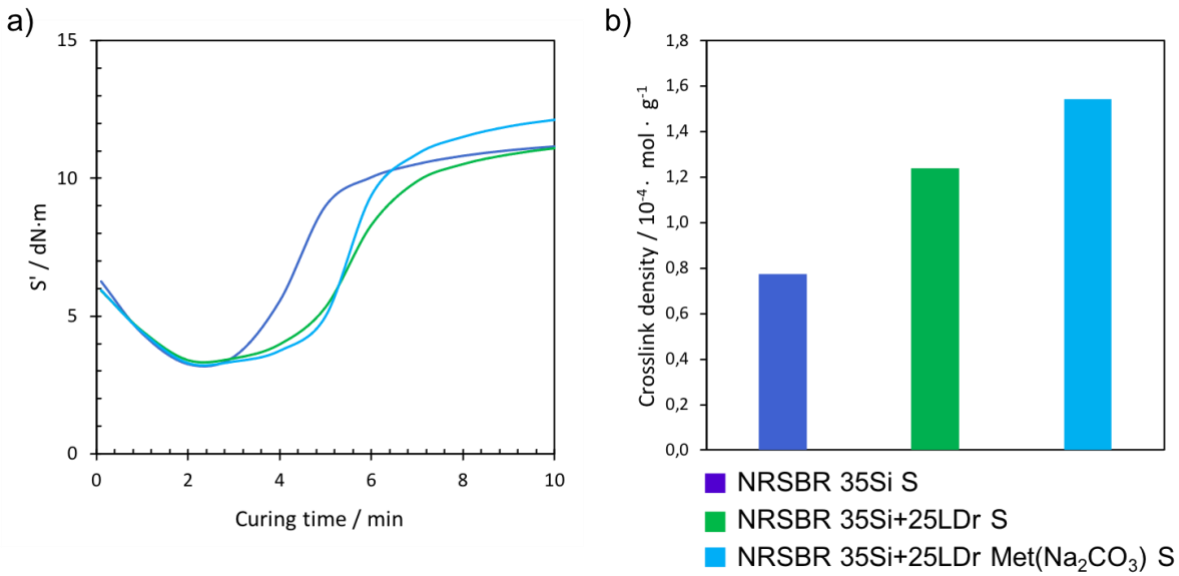

Figure 28. Vulcanisation kinetics (170 °C, 10 min, a) and crosslink density determined by swelling experiments of the cured compounds in toluene (b). For more details about the formulation see Table 17.

The addition of lignin on top of silica was also associated with an increase in tanδ which slightly improved in the case of methacrylated lignin even if not achieving the same values as silica. The compound containing methacrylated lignin (*NRSBR 35Si+25LDrMet(Na_2CO_3) S*) presented better mechanical performances than the corresponding formulation with milled lignin (*NRSBR 35Si+25LDr S*), of particular interest were the superior storage modulus, stress at 300 % deformation, stress at break, energy and lower hysteresis (Table 17).

11.2.2 NR/BR composites including lignin and silica as fillers

NR/BR composites containing lignin as a filler were prepared by mixing a coprecipitated NR/lignin masterbatch with butadiene rubber and subsequently adding the other ingredients (paragraphs 9.1.1 and 9.2).

Table 18. NR/BR composites including lignin coprecipitated with NR, silica as co-filler, peroxide-based vulcanisation.

Components and formulation in phr	NRBR 40Si O	NRBR 10Si+50LPr O	NRBR 10Si+50LPr Met(NaOH) O
Butadiene rubber (CB 25)	50	50	50
Natural rubber (SIR20)	50		
Coprecipitated NR masterbatch, 50% milled lignin		100	
Coprecipitated NR masterbatch,			100

50% methacrylated lignin			
Silica (ZEOSIL 1165 MP)	40	10	10
γ-methacryloyl propyl triethoxy silane (TEMS)	3.2	0.8	0.8
Antioxidant (6PPD)	2	2	2
Peroxide-based vulcanising agent (LUPEROX 101XL45)	2.3	2.3	2.3

Tensile properties

Stress at 50% deformation / MPa	1.08	0.89	0.85
Stress at 100% deformation / MPa	1.50	1.33	1.28
Stress at 300% deformation / MPa	5.09	5.08	5.44
Stress at break / MPa	13.84	9.91	11.08
Elongation at break / %	542.81	506.29	508.48
Energy/ $J \cdot cm^{-3}$	29.57	22.97	24.11

Vulcanisation kinetics (170 °C, 10 min) and dynamo-mechanical properties

ML (moment lowest) / dN·m	4.35	4.25	2.61
MH (moment highest) / dN·m	13.03	7.57	5.62
T30 / min	1.83	1.99	2.20
T90 / min	7.85	7.37	8.17
TS2 / min	1.36	3.83	5.15
dG' (0.4 - 10 % deformation) / MPa	0.56	0.24	0.22
G' at 9 % deformation / MPa	1.39	1.09	0.77
tanδ at 9 % deformation	0.21	0.23	0.16

Peroxide-vulcanised NR/BR composites including lignin and silica as reinforcing fillers are reported in Table 18. The partial substitution of silica with lignin (*NRBR 10Si+50LPr O* and *NRBR 10Si+50LPr Met(NaOH) O*) resulted in higher rigidity which reflected into weakly lower elongation and moderately inferior stress at break. It was also associated to a slight increment in hysteresis and decrement in modulus. The use of methacrylated lignin allowed for the decrease in hysteresis, reaching even lower values than reference compound *NRBR 40Si O*. Moreover, functionalisation was accompanied with high compatibilisation of the filler with the matrix, as shown by the low value of ML.

The compound containing functionalised lignin presented a stress at 300 % deformation to stress at 100% deformation ratio which was higher than in the other two compounds, proving a better dispersion of the filler inside the polymeric matrix and the covalent binding of lignin with rubber during vulcanisation.

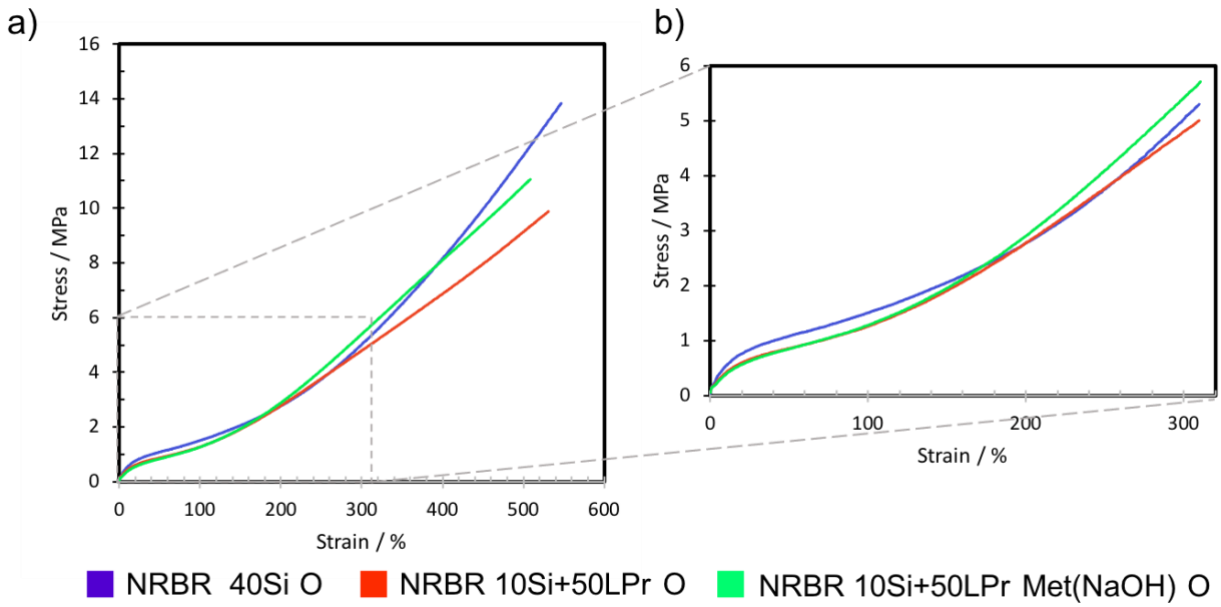

Figure 29. Stress to strain curve (a) and magnification (b) for peroxide-vulcanised NR/BR composites including lignin and silica as reinforcing fillers. For more details about the formulation, see Table 18.

Sulphur-vulcanised NR/BR composites including silica and lignin as reinforcing fillers are described in

Table 19. Those compounds were vulcanised with a system poor in accelerator and rich in sulphur content, as such having long polysulphide bridges which could withstand the strong deformations tyre sidewalls face under the working conditions.[21] Sulphur S_8 is known to be poorly soluble in dienic polymers and migrate towards the surface of the composite. In order to overcome the solubility issue, the vulcanising agent here used was oil-extended sulphur which was able to release S_8 during vulcanisation.

Table 19. NR/BR composites including lignin coprecipitated with NR, silica as co-filler, sulfur-based vulcanisation.

	NRBR 40Si S TEMS	NRBR 40Si S TESPD	NRBR 10Si+ 50LPr S	NRBR 10Si+ 50LPr Met (NaOH) S	NRBR 10Si+ 50LPr Met (Na_2CO_3) S
Components and formulation in phr					
Butadiene rubber (CB 25)	50	50	50	50	50
NR (SIR20)	50	50			
Coprecipitated NR masterbatch, 50% milled lignin			100		
Coprecipitated NR masterbatch, 50% methacrylated lignin				100	100
Silica	40	40	10	10	10
γ-methacryloyl propyl triethoxy silane (TEMS)	3.2				
50 % bis(triethoxysilylpropyl)disulfide supported on CB (TESPD)		6.4	1.6	1.6	1.6
Antioxidant (6PPD)	2	2	2	2	2
Stearic acid	2	2	2	2	2
Zinc oxide	3	3	3	3	3
Accelerator CBS	1	1	1	1	1
66 % wt oil-extended sulfur	3	3	3	3	3
Tensile properties					
Stress at 50% deformation / MPa	1.00	1.28	1.00	1.15	1.20
Stress at 100% deformation / MPa	1.44	1.96	1.53	1.71	1.81
Stress at 300% deformation / MPa	4.80	7.03	5.01	6.49	6.80
Stress at break / MPa	18.82	20.06	10.65	11.19	11.19
Elongation at break / %	693.16	617.88	522.85	464.61	464.61
Energy/ $J \cdot cm^{-3}$	50.42	51.91	24.44	24.40	24.39
Vulcanisation kinetics (170 °C, 10 min) and dynamo-mechanical properties					
ML (moment lowest) / dN·m	3.09	3.93	4.09	4.07	3.68
MH (moment highest) / dN·m	14.11	17.52	11.92	8.50	21.54
T90 / min	5.34	5.41	7.63	7.46	4.25
TS2 / min	1.57	1.06	2.27	2.93	1.89
dG' (0.4 - 10 % deformation) / MPa	0.59	0.78	0.18	0.25	0.28
G' at 9 % deformation / MPa	1.19	1.54	1.12	1.13	1.51
tanδ at 9 % deformation	0.145	0.141	0.140	0.192	0.067

Reference compounds *NRBR 40Si TEMS S* and *NRBR 40Si TESPD S* presented a different chemistry at the interface between silica and elastomer due to the different silane used for compatibilisation. Disulfide silane in *NRBR 40Si TESPD S*, provided higher reinforcement and crosslink density (MH-ML) than methacryloyl silane in *NRBR 40Si TEMS S*. However, when silica was compatibilised with a methacryloyl silane (*NRBR 40Si TEMS S*), failure properties were excellent, proving that the functionalisation of a filler with a methacrylic group could properly work in a system vulcanised with sulphur.

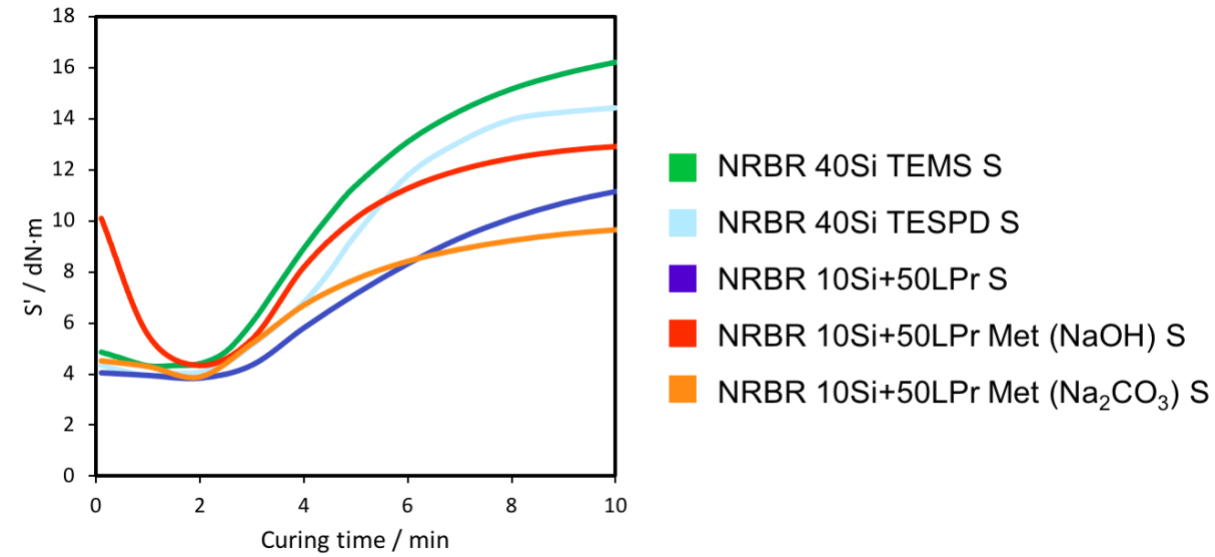

Figure 30. Vulcanisation kinetics (170 °C, 10 min) for sulfur-vulcanised NR/BR composites including silica and lignin as reinforcing fillers.

When substituting part of the silica with lignin (*NRBR 10Si+50LPr S, NRBR 10Si+50LPr Met (NaOH) S* and *NRBR 10Si+50LPr Met (Na_2CO_3) S* vs *NRBR 40Si TESPD S*), more rigid compounds were obtained. The compounds *NRBR 10Si+50LPr Met (NaOH) S* and *NRBR 10Si+50LPr Met (Na_2CO_3) S* include lignin methacrylated with the catalysis of NaOH and Na_2CO_3, respectively. The former presented a slow vulcanisation kinetics due to the residual presence of methacrylic acid as shown by ^{31}P NMR, this negatively affecting both storage modulus and hysteresis. The latter (*NRBR 10Si+50LPr Met (Na_2CO_3) S*) showed excellent hysteresis values and a storage modulus which was comparable to model compound *NRBR 40Si TESPD S*.

11.2.3 NR/BR composites including lignin and carbon black as fillers

Composites including 25 phr of carbon black and 25 phr of either milled or methacrylated lignin (*NRBR 25CB +25LPr S* and *NRBR 25CB +25LPrMet (NaOH) S*, respectively) shared the same storage modulus (Figure 31) and hysteresis while stress and elongation at break (as outlined in Table 20) improved in the presence of functionalisation.

Table 20. NR/BR composites including lignin coprecipitated with NR, carbon black as co-filler, sulfur-based vulcanisation.

Components and formulation in phr	NRBR 50CB S	NRBR 25CB + 50LPr S	NRBR 25CB + 50LPrMet (NaOH) S	NRBR 25CB +25LPr S	NRBR 25CB +25LPrMet (NaOH) S
Butadiene rubber (CB 25)	50	50	50	50	50

Natural rubber (SIR20)	50			25	25
Coprecipitated NR masterbatch, 50% milled lignin		100		50	
Coprecipitated NR masterbatch, 50% methacrylated lignin			100		50
Carbon black (N550)	50	25	25	25	25
Antioxidant (6PPD)	2	2	2	2	2
Stearic acid	2	2	2	2	2
Zinc oxide	3	3	3	3	3
Accelerator CBS	1	1	1	1	1
66 % wt oil-extended sulfur	3	3	3	3	3
Tensile properties					
Stress at 50% deformation / MPa	1.761	1.54	1.58	1.42	1.46
Stress at 100% deformation / MPa	3.29	2.59	2.62	2.53	2.65
Stress at 300% deformation / MPa	14.15	8.79	8.35	9.22	10.20
Stress at break / MPa	15.92	13.23	10.61	9.27	11.71
Elongation at break / %	326.82	443.71	395.75	305.62	343.07
Energy/ $J \cdot cm^{-3}$	22.96	28.46	21.56	13.38	18.34
Vulcanisation kinetics (170 °C, 10 min) and dynamo-mechanical properties					
ML (moment lowest) / dN·m	3.43	3.34	4.60	3.47	3.40
MH (moment highest) / dN·m	24.74	14.33	15.72	14.13	13.97
T90 / min	2.92	6.88	4.14	6.56	6.82
TS2 / min	1.20	1.02	1.15	1.46	1.50

In compounds containing 25 phr of carbon black and 50 phr of lignin (*NRBR 25CB + 50LPr S* and *NRBR 25CB + 50LPr S*), functionalisation was associated to a decrease in stress at break, an increase in hysteresis and a meaningful increment in storage modulus, which was even higher than the one of reference compound containing 50 phr of CB (*NRBR 50CB S*). However, *NRBR 25CB + 50LPr Met(NaOH) S* showed a more pronounced Payne effect than reference compound *NRBR50CB S*, suggesting that the mechanical performances drop at high strains. The storage modulus trends evidenced for those two compounds (*NRBR50CB S* and *NRBR 25CB + 50LPr* S) fell in the desired direction of reducing the content of fossil-based materials and contemporarily increasing the content in renewable materials in tyre compounds while preserving the mechanical performances.

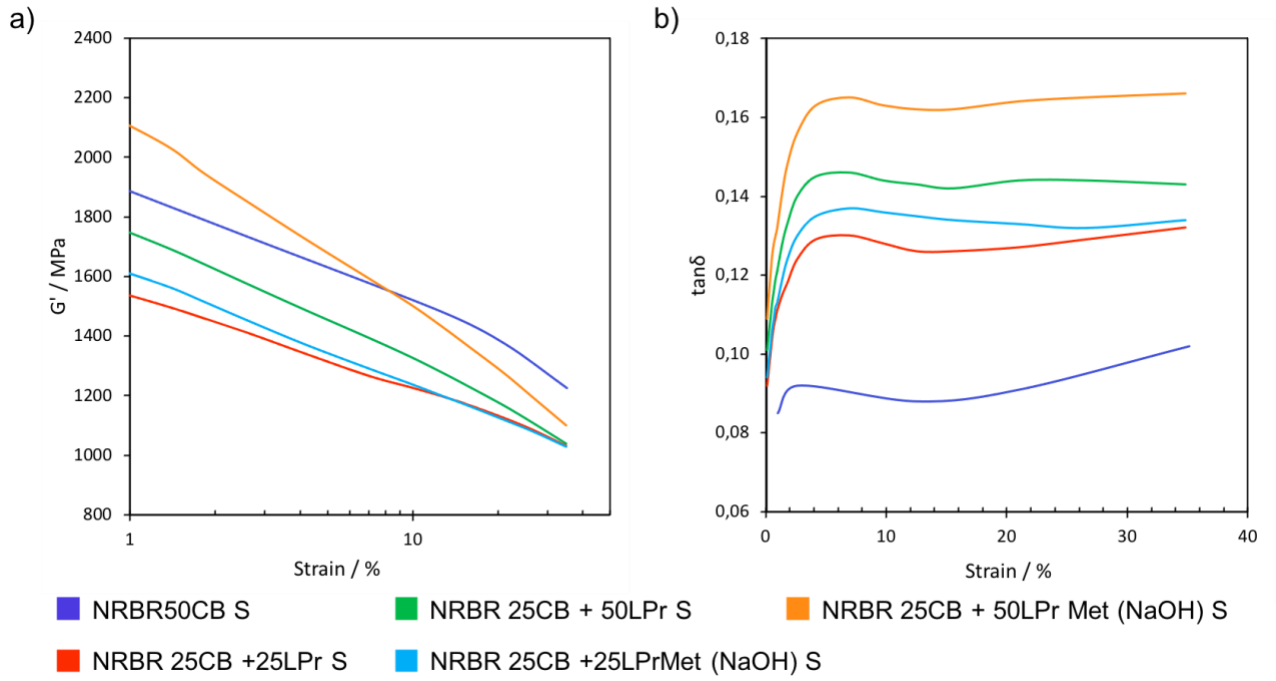

Figure 31. Storage modulus (a) and hysteresis (b) as a function of strain for NR/BR composites including lignin and carbon black as reinforcing fillers vulcanised 170 °C 15 min.

12 Study of the structural characteristics of softwood and hardwood kraft lignins and their fractions with a particular focus on phenolic group distribution as a function of molecular weight

The structural complexity of lignin is known to hamper its conversion into value-added products and the rational design of functional materials. Such structural complicacy is particular evident in kraft lignin isolated from the kraft pulping process whose harsh conditions (highly alkaline pH values and temperatures over 160 °C for several hours) alter the native structure of lignin by cleavage and successive repolymerisation of fragments. Those phenomena connected to the treatment of the biomass deeply influence the final structure of lignin inducing an increase in the variety of inter-unit bonds and distribution of molecular weights with respect to native lignin. For the rational design of functional materials, it is crucial to overcome the heterogeneity of kraft lignin structure by separating lignin into more homogeneous assemblies and deeply understanding the functional groups distribution in such fractions.

It is possible to isolate narrowly polydisperse fractions out of the starting lignin by selective solvent extraction.[9] This approach allows for the isolation of lignin fractions on the basis of their physicochemical characteristics which can be tuned by selecting the polarity and H-bond capacity of the solvent.[33,34] Among those feature which can be selected according to the nature of the solvent, there is the content in hydroxyl groups. The quantity of phenols in each fraction is of particular relevance while targeting the final properties of the materials. In fact, this parameter could be helpful for the aware choice of specific lignin fractions for a particular application, *e.g.* crosslink agents, anti-oxidants, fillers with thermal protection properties.[5,35] An innovative analytical procedure allowed verifying that isolated fractions not only had a specific phenolic content and a narrow molecular weight distribution but also were homogeneous in terms of phenol distribution alongside the molecular weight ranges.[10] Such an approach took inspiration from a previous work where the authors analysed the phenolic groups distribution as a function of molecular weight in technical lignins.[36] This evaluation could be performed by selectively and quantitatively labelling phenols with the dansyl fluorescent functionality (Scheme 6). Then, reference acetylated lignin and labelled lignin were analysed by GPC coupled to a UV-Vis (set at 280 nm) and a fluorescent detector ($\lambda_{excitation}$: 390 nm, $\lambda_{emission}$: 550 nm), respectively. This set up allowed discerning the dansyl-labelled phenols response from the lignin aromatic skeleton input and inferring information about the phenolic group distribution as a function of molecular weight (MW).

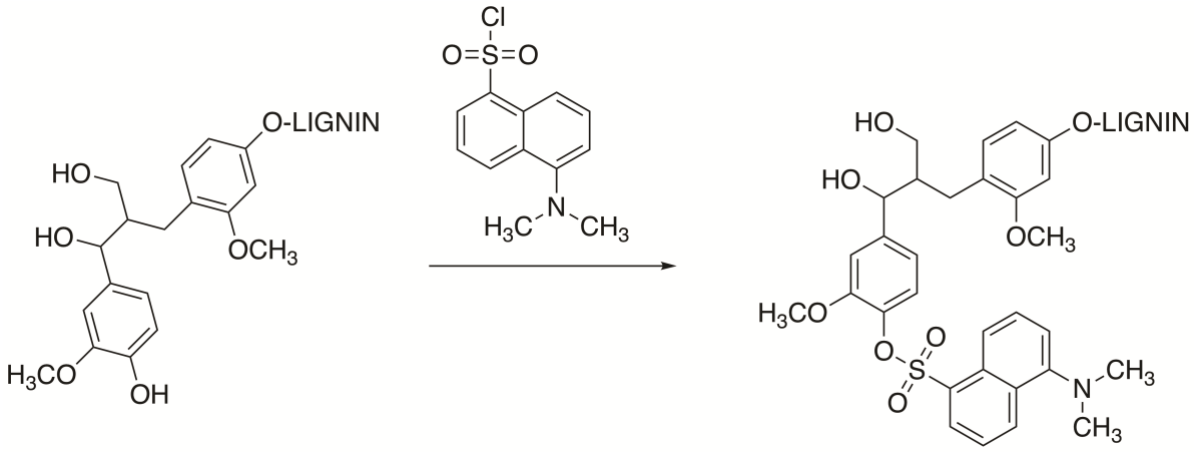

Scheme 6. Dansylation reaction for a typical β-*O*-4' structure of guaiacylic nature.

Initially, commercially available softwood kraft (SKL from local farmers) and hardwood kraft (HKL) lignin were fractionated by successive extractions with organic solvents, *i.e.*, ethyl acetate (EA), ethanol (ET), and acetone (AC), to yield thee soluble fractions, i.e., EA, ET, and AC, as well as one residual, since insoluble fraction (INS), as illustrated in Scheme 7.

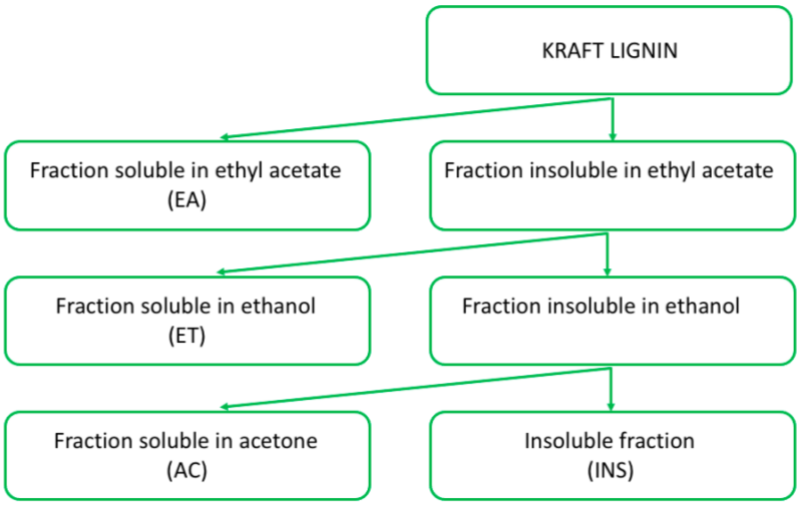

Scheme 7. Fractionation of kraft lignin by successive solvent extractions with organic solvents.

Softwood (SW) and hardwood (HW) lignin extracted by the acidolytic procedure reported in literature[37], SKL, HKL and their fractions were characterised by standard GPC after acetylation.

Chromatograms were then analysed as follows.[10]

1. In GPC chromatograms of acetylated lignin, the representative weight fraction was assessed for each specific molecular weight (MW) range b→a including >10000 g·mol^{-1}; 10000-5000 g·mol^{-1}; 5000-3000 g·mol^{-1}; 3000-2000 g·mol^{-1}; 2000–1000 g·mol^{-1}; 1000-200 g·mol^{-1}. The calculations were performed by

dividing the UV absorbance calculated over a specific MW range by the one associated to the whole MW distribution:

$$\frac{g_{lignin\ (b \rightarrow a)}}{g_{total\ lignin}} = \frac{\sum_{n=a}^{b} Abs(n)}{\sum_{n=200}^{10000} Abs(n)}$$

2. The fluorescence of the sample was corrected taking into account the effect of auto-fluorescence of lignin, related to the presence of aromatic structures like stilbenoids and phenylcumarones.

3. The UV profile of a generic dansylated sample was compared to the curve of the corresponding acetylated sample in order to estimate the variation in hydrodynamic volume of lignin after dansylation. The displacement towards higher MW influenced low MW species than the high MW ones. So, the integration range 1000-200 $g \cdot mol^{-1}$ in acetylated curves was turned into 1250-200 $g \cdot mol^{-1}$ for dansylated profiles to take into account this phenomenon. The other ranges were not submitted to any change.

4. The representative phenolic molar fraction associated to a specified molecular weight range was individuated by elaborating fluorescence signals. The same MW ranges were considered as in point 1. Since the auto-fluorescence of lignin was corrected, signals accounted only for the fluorescence of dansyl-labelled phenols. Phenolic molar fractions were calculated by dividing the fluorescence intensity calculated over a specific MW range by the one related to whole MW distribution:

$$\frac{mmol_{PhOH\ (b \rightarrow a)}}{mmol_{total\ PhOH}} = \frac{\sum_{n=a}^{b} Fluo(n)}{\sum_{n=200}^{10000} Fluo(n)}$$

Finally, the phenolic content over a specific MW range was calculated as follows:

$$\frac{mmol}{g} PhOH\ (b \rightarrow a) = \frac{mmol_{PhOH\ (b \rightarrow a)}}{g_{lignin\ (b \rightarrow a)}} = \frac{mmol_{PhOH\ (b \rightarrow a)}}{mmol_{total\ PhOH}} \cdot \frac{mmol_{total\ PhOH}}{g_{total\ lignin}} \cdot \frac{g_{total\ lignin}}{g_{lignin\ (b \rightarrow a)}}$$

where $\frac{mmol_{total\ PhOH}}{g_{total\ lignin}}$ was the quantification obtained by ^{31}P NMR analysis.

GPC chromatograms regarding softwood lignin are illustrated in Figure 32 while extraction yield and numerical results are shown in

Table 21.

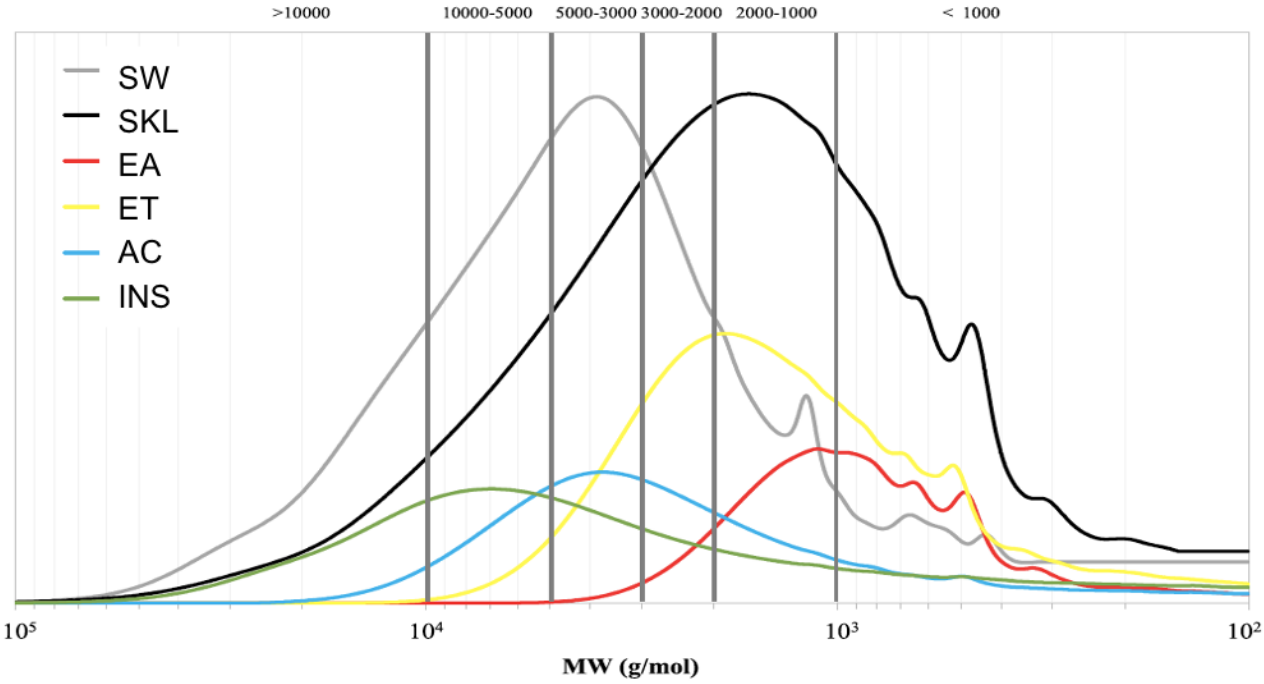

Figure 32. GPC-UV (280 nm) chromatograms of SW, SKL lignin and fractions (EA, ET, AC, INS) after acetylation. The relative intensity is normalised on the basis of extraction yields. [10]

Table 21. Fractionation yield and GPC-UV (280 nm) data of SW lignin, SKL lignin, and fractions EA, ET, AC, and INS after acetylation. [10]

	Fractionation Yield	M_n	M_w	PDI	Molecular weight ranges / g·mol^{-1}					
					< 1000	1000-2000	2000-3000	3000-5000	5000–10000	> 10000
	% wt	g·mol^{-1}			Weight fraction % wt					
SW	n.a.	5700	13500	2.37	0.11	0.13	0.15	0.24	0.23	0.14
SKL	n.a.	3350	10900	3.27	0.23	0.28	0.16	0.15	0.12	0.06
EA	0.17	1100	1550	1.38	0.48	0.41	0.09	0.02	0.00	0.00
ET	0.40	1900	2900	1.54	0.26	0.35	0.21	0.14	0.03	0.00
AC	0.20	3550	5750	1.62	0.12	0.18	0.19	0.27	0.21	0.03
INS	0.22	6600	14600	2.21	0.06	0.12	0.11	0.19	0.29	0.23

Ethyl acetate could solubilise 17 % of the starting SKL, ethanol 40 %, acetone 20 % and finally 22% of insoluble residue was recovered. SKL solvent fractions displayed a lower polydispersity than SKL, MW increased following the order EA, ET, AC and INS. Acidolytic lignin SW had lower polydispersity than SKL lignin, as expected by bond cleavage and repolymerisation which lignin fragments experience during kraft pulping. For all the samples it was possible to calculate the weight fraction of each specific MW range by resorting to equations illustrated in paragraph 6.6.

The same analytics and data elaboration were used to characterise HW lignin, HKL lignin and its fractions, as illustrated in and summarised in

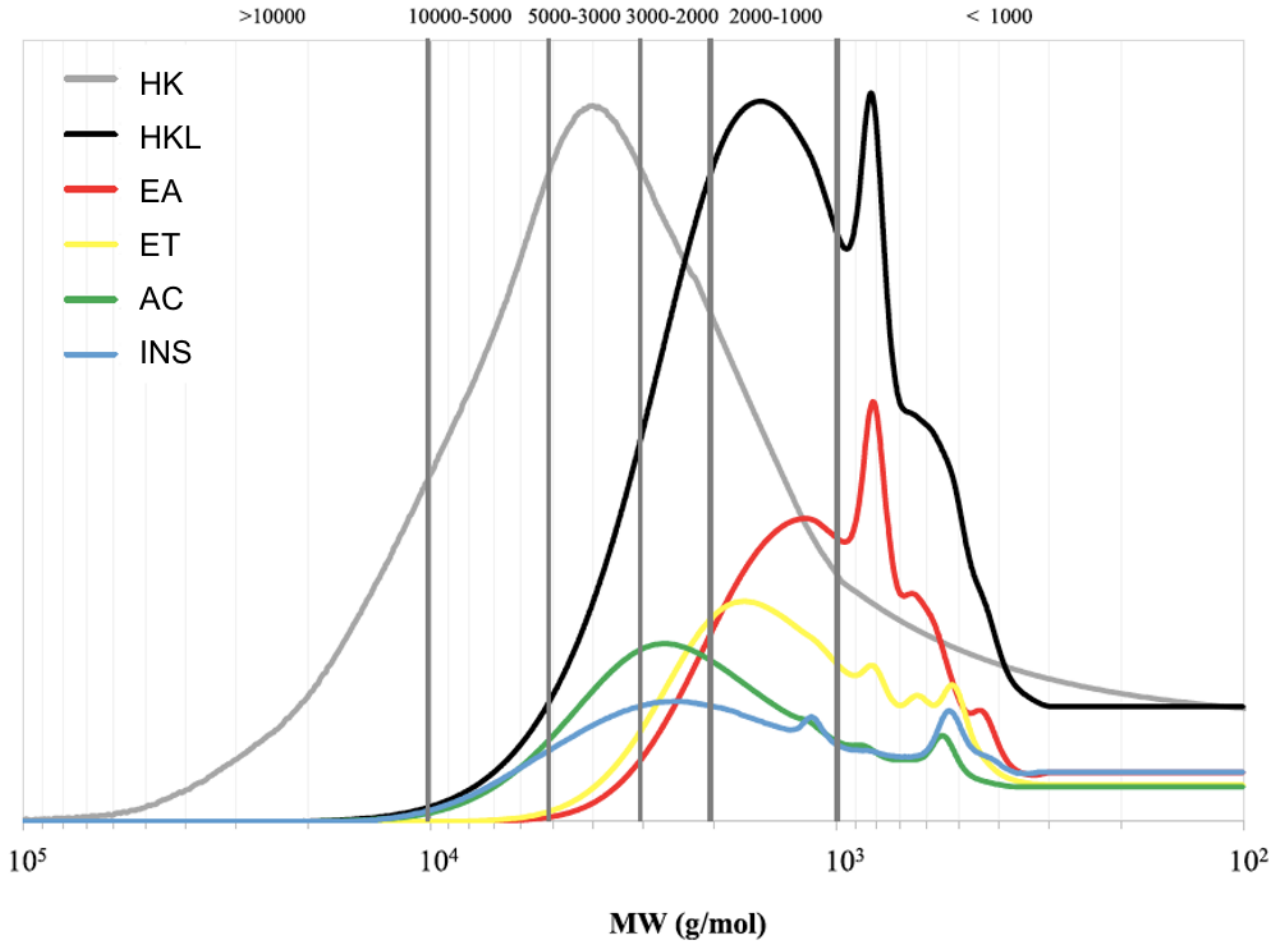

Figure 33 and **Error! Reference source not found.**.

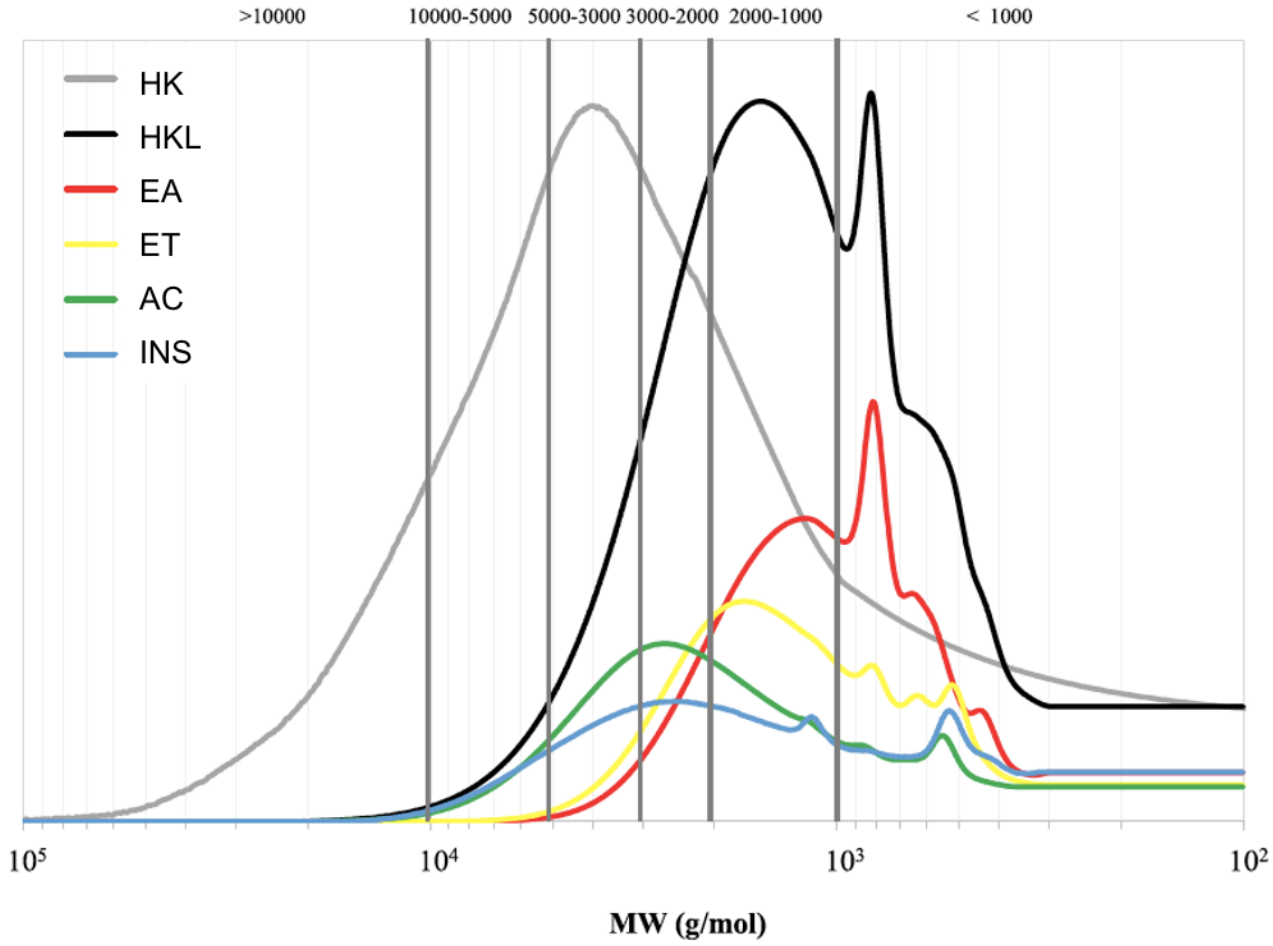

Figure 33. GPC-UV (280 nm) chromatograms of HW, HKL lignin and fractions (EA, ET, AC, INS) after acetylation. The relative intensity is normalised on the basis of extraction yields. [10]

Table 22. Fractionation yield and GPC-UV (280 nm) data of HW lignin, HKL lignin, and fractions EA, ET, AC, and INS after acetylation. [10]

					Molecular weight ranges / g·mol^{-1}					
	Fractionation Yield	M_n	M_w	PDI	< 1000	1000-2000	2000-3000	3000-5000	5000–10000	> 10000
	% wt	g·mol^{-1}			Weight fraction % wt					
HW	n.a.	4700	11930	2.54	0.08	0.17	0.17	0.27	0.22	0.10
HKL	n.a.	1685	2850	1.69	0.30	0.38	0.18	0.10	0.03	0.00
EA	0.32	1215	1700	1.40	0.42	0.44	0.12	0.03	0.00	0.00

ET	0.25	1475	2090	1.42	0.30	0.43	0.20	0.07	0.00	0.00
AC	0.23	2365	3770	1.59	0.22	0.27	0.22	0.22	0.08	0.00
INS	0.20	2470	4000	1.62	0.21	0.27	0.20	0.21	0.10	0.01

SW, SKL lignin and its fractions were successively characterised by quantitative ^{31}P NMR after phosphitylation.[9] The corresponding results are illustrated in Table 22.

Table 22. ^{31}P NMR data for SW, SKL lignin and its fractions. [10]

lignin	aliphatic -OH	condensed phenolic -OH	G-type phenolic -OH	H-type phenolic -OH	total phenolic -OH	acidic COOH
	mmol·g^{-1}					
SW	3.43	0.33	0.76	0.10	1.18	0.13
SKL	1.91	1.84	2.13	0.24	4.21	0.42
EA	0.94	1.80	2.99	0.23	5.02	0.56
ET	1.75	1.91	2.33	0.25	4.49	0.36
AC	1.91	1.97	1.80	0.26	4.03	0.38
INS	2.82	1.51	1.46	0.17	3.14	0.36

HW, HKL lignin and its fractions were fully characterised by ^{31}P NMR after phosphitylation (Table 23).

Table 23. ^{31}P NMR data for HW, HKL lignin and its fractions. [10]

lignin	aliphatic -OH	condensed phenolic -OH	G-type phenolic -OH	H-type phenolic -OH	total phenolic -OH	acidic COOH
	mmol·g^{-1}					
HW	3.62	0.95	0.65	0.07	1.60	0.24
HKL	1.02	2.12	0.71	0.10	2.93	0.38

EA	0.64	2.46	0.75	0.08	3.29	0.70
ET	0.96	2.33	0.78	0.13	3.24	0.29
AC	1.21	2.24	0.82	0.13	3.19	0.31
INS	1.30	1.59	0.57	0.07	2.24	0.28

The validity of solvent fractionation was assessed by multiplying the phenol quantifications obtained by ^{31}P NMR for EA, ET, AC and INS by the corresponding fraction yield and then summing up for each functional group. The calculated values collimated with the ones obtained experimentally for SKL and HKL. The good correlation found between calculation and experimental data confirmed the reliability of ^{31}P NMR.

Then, samples were dansylated, acetylated and analysed by GPC equipped with a fluorescence detector. The selectivity of fluorescence detector for dansyl units guaranteed that chromatograms showed the phenolic molecular weight distribution. The fluorescence of the sample was corrected taking into account the effect of auto-fluorescence of lignin, related to the presence of aromatic structures like stilbenoids and phenylcumarones.[38]

For the softwood lignin samples, chromatograms are reported in Figure 34 and numerical outputs in Table 24.

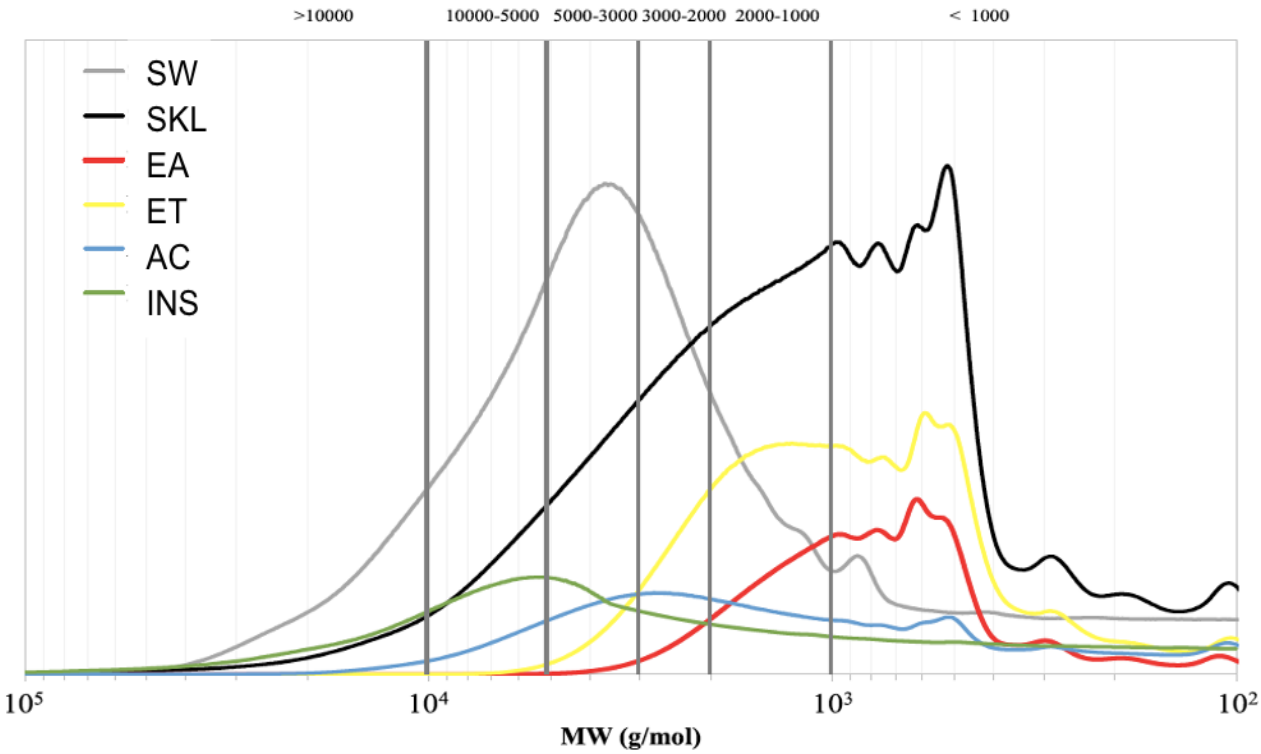

Figure 34. GPC equipped with fluorescence detector ($\lambda_{excitation}$: 390 nm, $\lambda_{emission}$: 550 nm) profiles of SW lignin, SKL lignins and its solvent fractions (EA, ET, AC, and INS) after dansylation and acetylation. The relative intensity is calculated based on fractionation yields. [10]

Table 24. GPC equipped with fluorescence detector data for SW lignins dansylated and acetylated. [10]

					Molecular weight ranges / g·mol^{-1}					
	Aromatic OH fractionation yield	M_n	M_w	PDI	< 1000	1000-2000	2000-3000	3000-5000	5000–10000	> 10000
	% wt	g·mol^{-1}			Absolute phenolic molar fraction mol/mol					
SW	n.a.	4800	10300	2.14	0.14	0.13	0.15	0.27	0.21	0.10
SKL	n.a.	2850	8450	6.20	0.36	0.25	0.13	0.12	0.09	0.04
EA	0.21	980	1450	1.48	0.59	0.33	0.07	0.01	0.00	0.00
ET	0.43	1600	2900	1.85	0.40	0.30	0.16	0.11	0.03	0.00
AC	0.20	2500	6000	2.37	0.19	0.22	0.19	0.22	0.15	0.04
INS	0.16	7400	17200	3.61	0.12	0.16	0.13	0.20	0.25	0.14

The relative molar fractions of phenols were calculated from the absolute ones by multiplying the absolute value of EA, ET, AC and INS samples by the corresponding phenol fractionation yield shown in Table 24. The results of such calculations are reported in Figure 35.

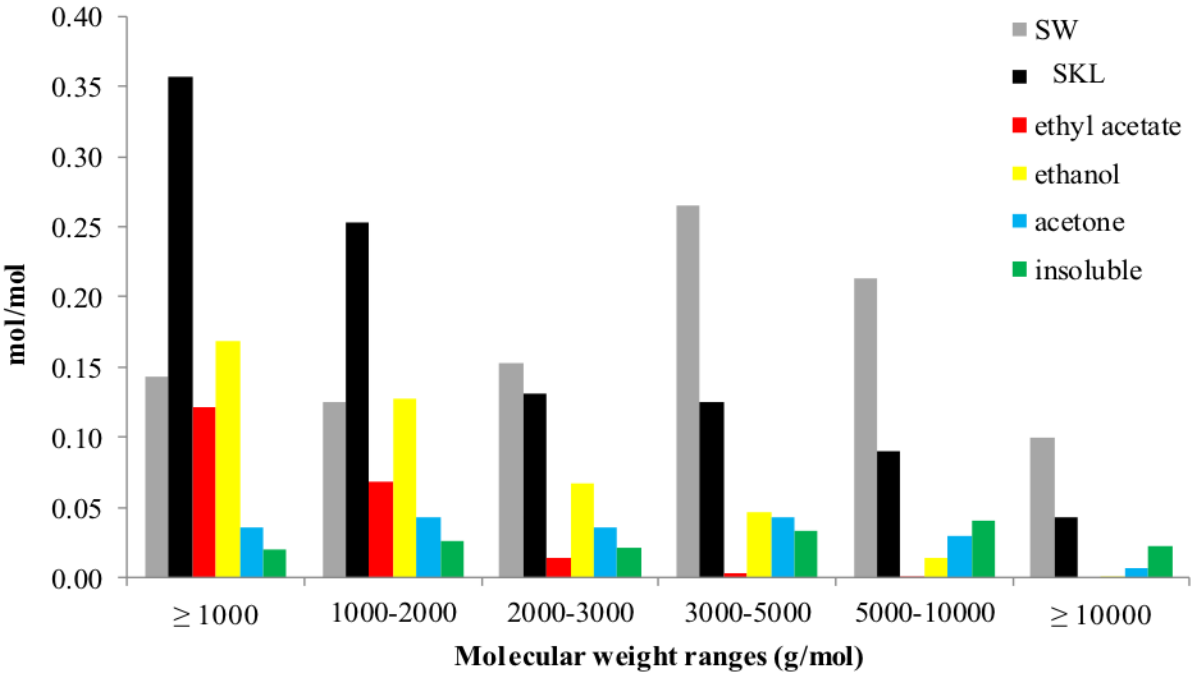

Figure 35. Relative molar fraction of phenols in mol/mol, for SKL lignin and solvent fractions EA, ET, AC, and INS of specific molecular weight ranges. [10]

The molar fractions of phenols for each specific MW range were calculated according to the equations discussed in paragraph 6.6. The validity of the data was confirmed by summing up all the relative phenolic molar fractions of a specific MW range for each fraction and comparing the result obtained for the molar phenol fractions of original SKL. The accordance with the calculations endorsed the validity of the data.

The same approach was applied to HW, HKL lignin and its fractions which were analysed by GPC equipped with a fluorescent detector. Chromatograms are shown in Figure 36 and numerical results are reported in Table 25.

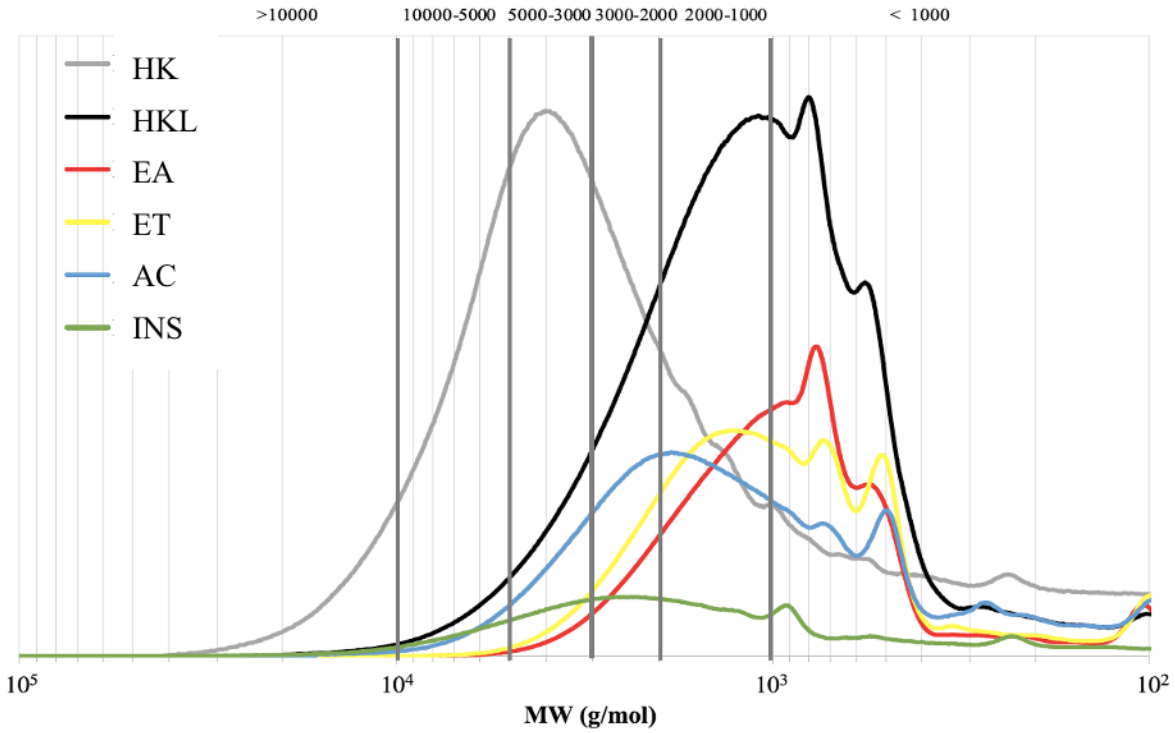

Figure 36 GPC equipped with fluorescence detector ($\lambda_{excitation}$: 390 nm, $\lambda_{emisssion}$: 550 nm) profiles of HW lignin, HKL lignin and its solvent fractions (EA, ET, AC, and INS) after dansylation and acetylation. The relative intensity is calculated based on fractionation yields. [10]

Table 25. GPC equipped with fluorescence detector data for HW lignins dansylated and acetylated. [10]

	Aromatic OH fractionation yield	M_n	M_w	PDI	Molecular weight ranges / g·mol^{-1}					
					< 1000	1000-2000	2000-3000	3000-5000	5000–10000	> 10000
	% wt	g·mol^{-1}			Absolute phenolic molar fraction mol/mol					
HW	n.a.	3650	7670	2.10	0.08	0.17	0.17	0.30	0.22	0.06
HKL	n.a.	1800	3000	1.67	0.33	0.39	0.17	0.08	0.02	0.00
EA	0.36	1110	1460	1.32	0.44	0.42	0.12	0.01	0.00	0.00
ET	0.27	1370	1960	1.43	0.33	0.43	0.17	0.06	0.00	0.00
AC	0.25	2390	3250	1.36	0.25	0.33	0.21	0.15	0.05	0.00
INS	0.15	2600	4950	1.90	0.21	0.31	0.21	0.18	0.09	0.00

The data of weight fraction and molar fractions of phenols for all the MW ranges were used to estimate a molecular weight range-dependent quantification of phenolic groups in terms of $mmol_{PhOH}/g_{fraction}$, as explained in paragraph 6.6 and illustrated in Table 26 for SW lignins and Table 27 for HW lignins.

Table 26. Estimations of phenol content in mmol/g for the SW lignin, SKL lignin, and solvent fractions EA, ET, AC, and INS of the specific molecular weight ranges >10000, 10000-5000, 5000-3000, 3000-2000, 2000–1000 and <1000 g/mol. [10]

lignin	Molecular weight ranges / g·mol^{-1}					
	< 1000	1000-2000	2000-3000	3000-5000	5000–10000	> 10000
	Aromatic OH content / mmol·g^{-1}					
SW	1.47	1.18	1.22	1.29	1.10	0.85
SKL	6.46	3.85	3.43	3.40	3.29	2.63
EA	6.17	4.01	3.81	3.87	n.a.	n.a.
ET	6.79	3.85	3.36	3.52	3.18	n.a.
AC	6.26	4.94	4.04	3.22	2.95	4.36
INS	6.78	4.14	3.78	3.30	2.66	1.90

Table 27. Estimations of phenol content in mmol/g for the HW lignin, HKL lignin, and solvent fractions EA, ET, AC, and INS of the specific molecular weight ranges >10000, 10000-5000, 5000-3000, 3000-2000, 2000–1000 and <1000 g/mol. [10]

lignin	Molecular weight ranges / g·mol^{-1}					
	< 1000	1000-2000	2000-3000	3000-5000	5000–10000	> 10000
	Aromatic OH content / mmol·g^{-1}					
HW	1.75	1.65	1.72	1.94	1.67	1.00
HKL	3.31	2.97	2.72	2.24	2.39	n.a
EA	3.45	3.18	3.25	1.43	n.a	n.a
ET	3.56	3.25	2.78	2.81	3.05	n.a
AC	3.66	3.91	3.07	2.20	2.06	n.a
INS	2.20	2.55	2.35	1.95	1.95	n.a

The molecular weight polydispersity for HKL lignin was quite low and comparable to the one of its solvent-extracted fractions (**Error! Reference source not found.**). Moreover, the phenol distribution as a function of molecular weight for starting HKL lignin and its fractions proved narrowly polydisperse. These observations suggested that solvent fractionation for such a lignin was not a powerful tool to tune the properties of lignin and select fractions with peculiar characteristics which could find specific applications.

Acidolytic lignin SW showed a higher phenolic content in the lower MW ranges than in higher MW ranges. It was also characterised by an overall more homogeneous phenolic distribution than SKL lignin, without any peaking of phenolic content at low MW values and severe depletion at high MWs. Such evidences suggested that acidolytic SW lignin was less degraded than SKL lignin with respect to the native

lignin *in planta*. The opposite could be observed for SKL lignin, which showed a more heterogeneous phenolic distribution than SW lignin, as expected by bond cleavage and repolymerisation which lignin fragments experience during kraft pulping. Together with the data regarding polydispersity, SKL was suspected to be degraded if compared to what is expected for native lignin *in planta*.[32]

In SKL samples, solvent extraction proved effective in isolating fractions with a narrow molecular weight polydispersity. Additionally, SKL lignin fractions EA, ET and AC proved to have a more homogeneous phenolic molecular weight distribution in the range >1000 than the native SKL lignin, confirming that solvent extraction was effective in isolating more monodisperse fractions with a more homogeneous phenolic content with respect to the starting lignin. The evaluation of the phenol content in different molecular weight ranges could provide helpful information when aiming at valorising lignin. Solvent fractionation demonstrated to reduce polydispersity in terms of both molecular weight and phenol distribution. Interestingly, SKL-EA sample was composed for 50 % of a fraction with MW<1000 (

Table 21) and a phenol content of around 6 mmol g^{-1} (Table 26). Those values fit with oligomeric lignin structures (dimers, trimers and tetramers) with one phenol per aromatic unit. Such characteristics made SKL ethyl acetate soluble fraction particularly promising when planning to valorise lignin in contests where a high phenol content plays a crucial role for thermal protection, functionalisation, etc.[5,35,39,40]

All the considerations regarding the phenol content as a function of molecular weight led to the emerging of some structural trends illustrated in Figure 37.

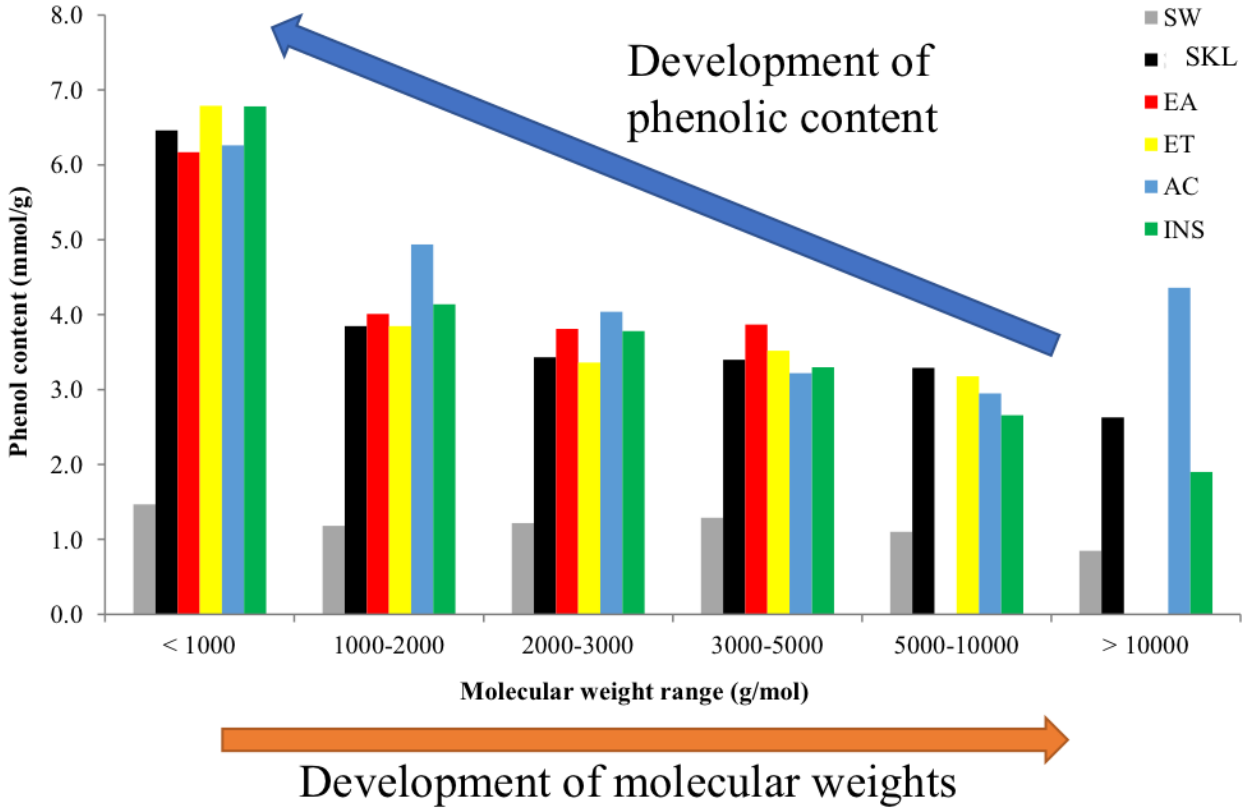

Figure 37. Trends emerging from the structural data as determined on the basis of GPC-analysis of dansylated/acetylated SW lignins and ^{31}P NMR spectroscopy. [10]

The trends were consistent with what can be expected on the basis of literature detailing the structural features of SKL.[41] Solvent extraction could help select certain structural characteristics on a preferable but not super-selective manner but it did not manage to completely exclude some specific structural motifs in isolated fractions. The gradual change in solvent polarity and H-bonding capacity led to the expected increment in MW from EA to AC, with the highest values for INS. That increase was accompanied by a decrease in phenol content. All those observations, along with data for M_n, M_w and PDI were consistent with the interpretation of SKL lignins being rather binary mixtures of macromolecules with a low MW, relatively highly condensed structures and high phenolic content, *i.e.* EA, ET, and AC fractions, and macromolecules with relatively high MW, low amounts of condensed structures and low phenolic content, *i.e.*, the INS fraction.[32]

13 Study of the synthesis and modification of lignin nanoparticles and evaluation of the effects on the mechanical performances of rubber nanocomposites

13.1 Synthesis, modification and characterisation of lignin nanoparticles

Lignin nanoparticles (LNPs) are a new frontier in the field of nanomaterials which is driving more and more attention, aiming at the development of novel functional materials based on renewable feedstocks.

Nanomaterials proved to show unique properties related to their high surface area[42] while their interactions depend on the surface chemistry. Lignin nanoparticles (LNPs) may find application in a large variety of fields including nanomedicine, UV-blockers, antioxidants, reinforcement of polymers, electrodes.[13,43–45] However, lignin structural heterogeneity makes the production of nanomaterials challenging. The most studied approaches reported in literature for the formation of lignin nanoparticles include solvent shifting, pH shifting, crosslinking polymerisation. Among those ones, solvent shifting seemed promising for the possibility to recycle organic solvent used to solubilise lignin before the polarity shift induced by the addition of water provoked the self-assembly of lignin into spherical nanoparticles due to minimisation of surface energy.[46]

Among the solvent shifting methods, an early work[47] reported the preparation of spherical nanoparticles by dissolving lignin into an organic solvent, *i.e.*, tetrahydrofuran (THF), and slowly exchanging with water by dialysis. The process led to the formation of smooth spherical LNPs with an average hydrodynamic diameter between 200-500 nm which could be tuned by varying the initial concentration of the lignin solution in THF. Successive investigations[48] evidenced the possibility to submit LNPs to intraparticle crosslinking by treatment with laccase. This approach sounded intriguing for the reinforcement of LNPs in order to make them stable under the physical stresses they would experience while included in elastomeric composites for tyres. Moreover, the possibility to induce an intraparticle crosslinking could lead to the dimensional stabilisation of such nanoparticles in both acidic and alkaline media, allowing for the homogeneous dispersion of LNPs in NR latex stabilised with ammonia (pH 10.5).

First of all, LNPs were synthesised by dissolving industrially available softwood kraft lignin (SKL, commercially named BIOPIVA™ 200 from UPM, Finland) in THF at a concentration of 0.2 % wt. Then the solution was filtered to remove possible insoluble residues (75 % m/m yield) and introduced into a dialysis bag which was soaked in excess, periodically replaced deionised water (ten times the volume of lignin solution in THF) for 24 h. LNPs were formed during this slow solvent exchange which resulted in

diluted water suspensions (nearly 0.1 % wt) at pH ca. 4.5 with negligible traces of organic solvent.[48] THF could be recovered from the washing waters by evaporation under reduced pressure and reutilised for the formation of new batches of LNPs. Such LNPs showed an average hydrodynamic diameter around 60 nm at pH 4.5, as determined by DLS, as well as a smooth surface and spherical morphology, as evidenced by SEM (Figure 38a). However, such LNPs obtained by solvent shift were held together only by physical interactions and swelled at pH 10.5, while preserving their spherical morphology (Figure 38b) probably due to the deprotonation of carboxyl and phenolic groups in alkaline conditions resulting in electrostatic repulsion and larger hydrodynamic radius.[49]

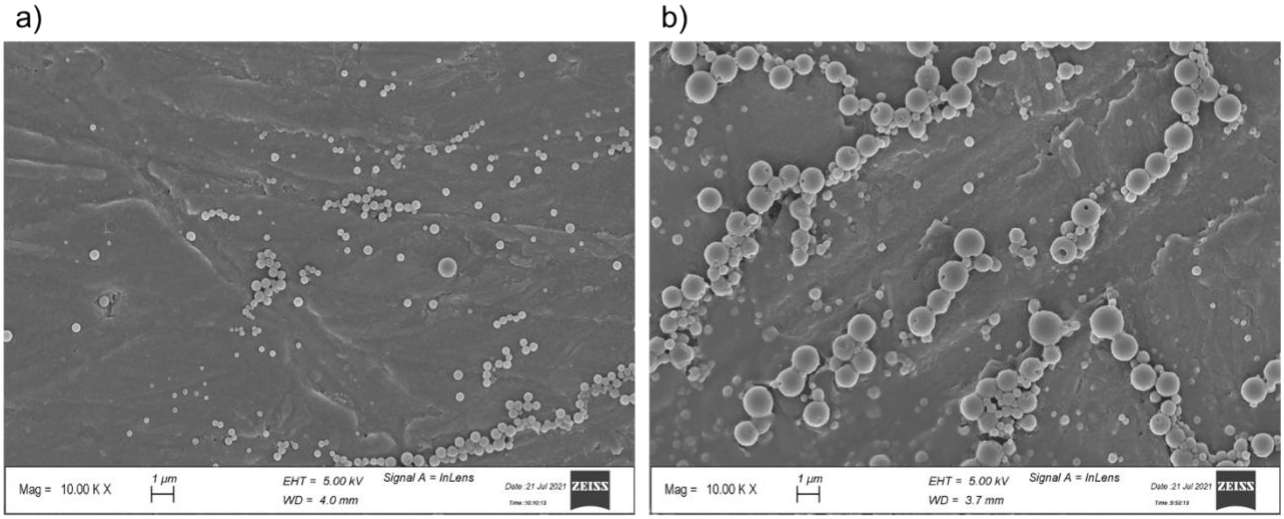

Figure 38. SEM images for air-dried LNPs obtained by solvent exchange via dialysis at pH 4.5 (a) and 10.5 (b).

In order to improve nanoparticle dimensional stability and increase their rigidity, the introduction of new chemical bonds was taken into account. The treatment of LNPs in the disperse state (approx. 0.1 % wt) at pH 4.5 (suitable for enzyme activity) with high redox potential laccase (oxidoreductase) from *Trametes versicolor* (13.0 nkat·mg^{-1}) exploited the formation of phenoxy radicals and coupling for the generation of new covalent bonds. The proposed reaction mechanism is reported in Scheme 8.

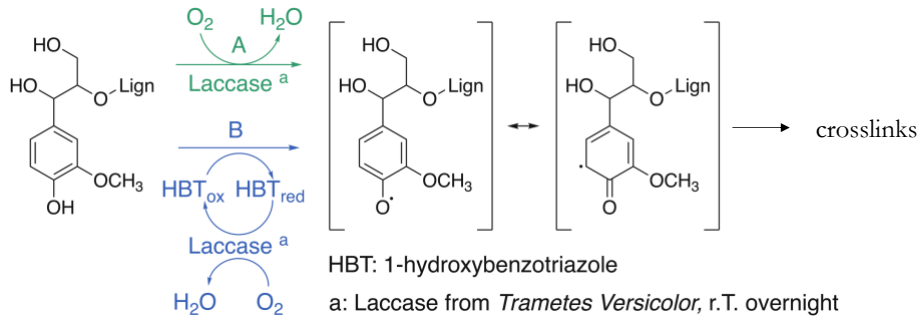

Scheme 8. Scheme for enzymatic crosslinking of lignin in the presence and absence of HBT as redox mediator.

The enzymatic treatment proved effective in crosslinking as confirmed by molecular weight increase detected by GPC (Figure 39 and Table 28). The chromatogram evidenced the disappearance of the peaks

related to low molecular weight (MW) fractions. As described in literature,[13,50,51] during nanoprecipitation of lignin induced by solvent polarity shift, low MW fractions result to be preferentially localised on the surface of LNPs. The vanishing of the peaks related to such oligomers in the chromatograms was ascribed to the interactions with the enzyme which were restricted to the surface of LNPs[52] and probably left the core unaffected. LNPs treated with laccase in such a diluted dispersion (approx. 0.1 % wt) proved to be intraparticle crosslinked, as demonstrated by the retaining of the dimensions at pH 4.5 (detected by DLS, Figure 40). Higher suspension concentrations would have led to interparticle crosslinking with the loss of the original nanosize of LNPs.[48]

Aiming at an extensive crosslinking, enzymatic treatment was then assisted by 1-hydroxybenzotriazole (HBT) as a redox mediator, which in literature was reported to trigger the polymerisation of lignin (4 % $mmol_{HBT}/mmol_{PhOH}$).[53] The smaller size of HBT if compared to the enzyme was believed to help the formation of radicals also in the core on the basis of the shuttle function of HBT, removing the surface restrictions to the enzymatic treatment. However, all experiments involving different amounts of HBT (5, 15 and 35 % $mmol_{HBT}/mmol_{PhOH}$) led to a moderate decrease in MW, probably due to the prevalence of oxidation on radical coupling. Once radical species are formed, these can undergo different reactions in competition with each other, resulting in overall polymerisation or depolymerisation.[54] The use of HBT in the present conditions could hence not enhance the desired internal crosslinking of LNPs and its use was associated to a partial degradation of the molecular structure.

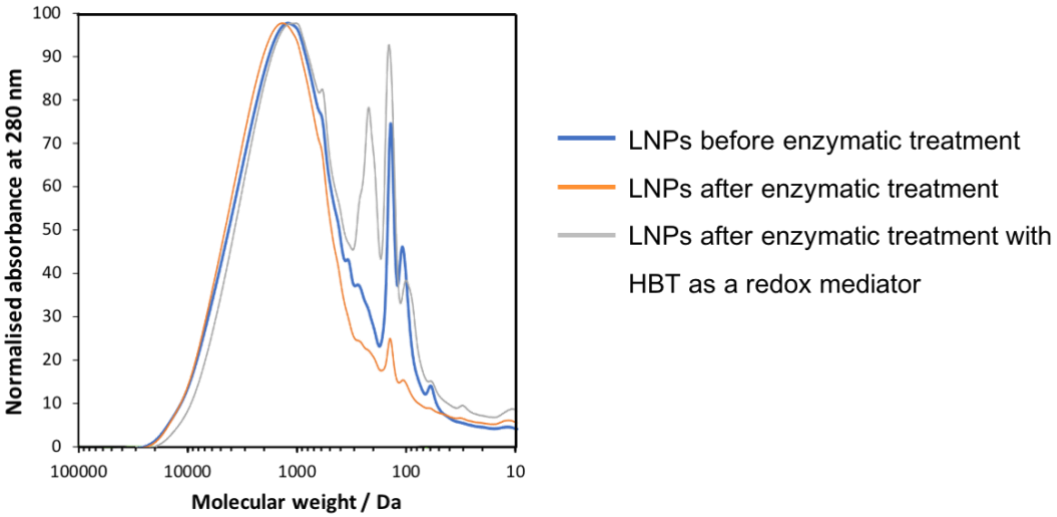

Figure 39. GPC traces for LNPs and LNPs treated with laccase in the absence and presence of HBT as redox mediator.

Table 28. Molecular weight distributions of LNPs before enzymatic treatment and LNPs treated with laccase in the absence and presence of HBT as redox mediator.

Sample	M_n / g mol^{-1}	Mw / g mol^{-1}	PDI
LNPs before enzymatic treatment	3200	9100	2.9
LNPs after enzymatic treatment	3500	9000	2.6
LNPs after enzymatic treatment with HBT as redox mediator	2500	7100	2.9

The dimensional stability of LNPs in a pH range between 4.5 and 10.5 was investigated. The morphology of LNPs resulted spherical at the extremes of the pH range as evidenced by SEM (Figure 38). Such morphological considerations, along with the dimensional studies by DLS, allowed for the calculation of the swelling ratio of LNPs when exposed to alkaline pH (10.5) in comparison with the native acidic pH of the suspension (4.5), as illustrated in the following equation:

$$S = \frac{V_{pH\ 10.5} - V_{pH\ 4.5}}{V_{pH\ 4.5}}$$

where S is the swelling ratio, $V_{pH\ 4.5}$ and $V_{pH\ 10.5}$ are the average volumes of LNPs at pH 4.5 and 10.5, respectively, calculated for spherical nanoparticles using the hydrodynamic radius detected by DLS (Figure 40).

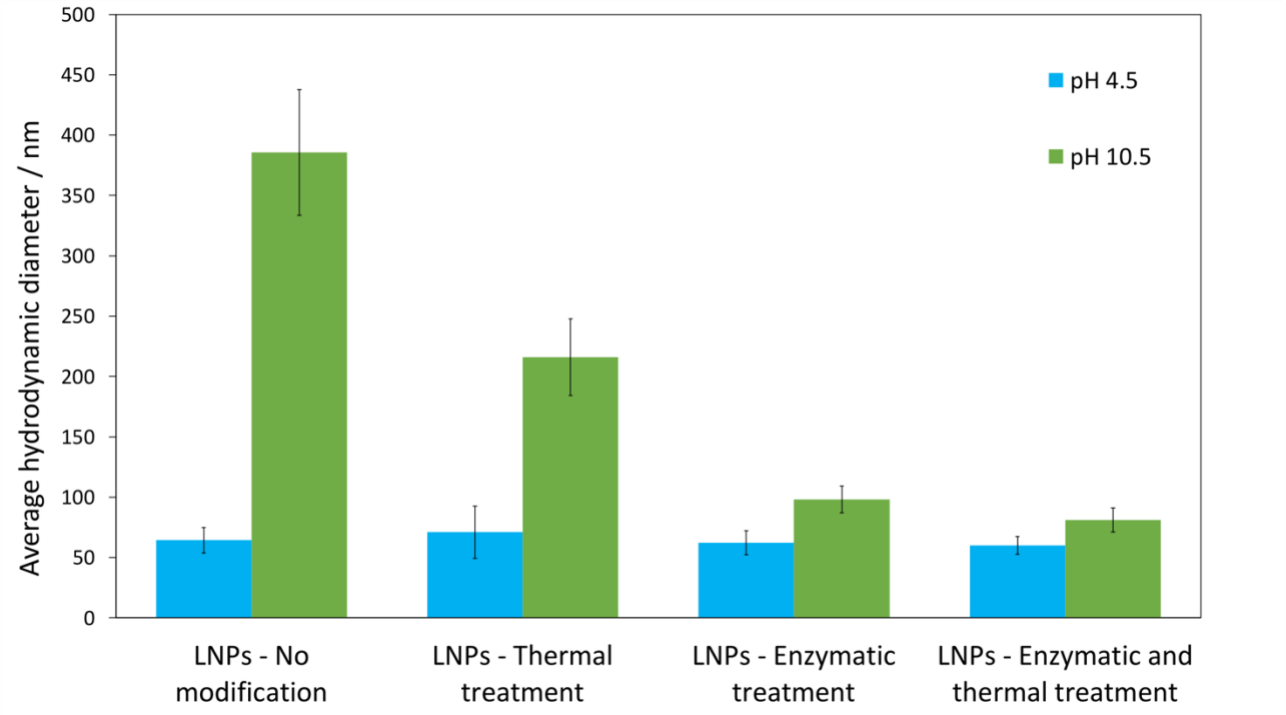

Figure 40. Average hydrodynamic diameter measured by DLS at pH 4.5 and 10.5 for LNPs henceforth described and the relative swelling ratio.

Untreated LNPs were stabilised only by physical interactions and swelled at pH 10.5, probably due to the deprotonation of carboxyl and phenolic groups in alkaline conditions resulting in electrostatic repulsion and larger hydrodynamic radius.[49] Swelling could be partially limited by heating LNPs in the dispersion state at 80 °C, 10 min. Such a relative dimensional stability after a simple thermal treatment was already observed in literature[55] and was detailed in Table 29. The crosslinking associated to the enzymatic procedure proved intraparticle as demonstrated by the dimensional constancy of LNPs at pH 4.5. The enzymatic process, especially when followed by the thermal treatment, exceptionally improved the dimensional stability of LNPs in basic conditions, the new covalent bonds reinforced LNPs and contributed to limiting the swelling induced by ionisation at alkaline pH.

Table 29. Swelling ratios for LNPs when exposed to alkaline pH (10.5) in comparison with the native acidic pH of the suspension (4.5).

Type of LNPs	LNPs - no modification	LNPs - thermal treatment	LNPs - enzymatic treatment	LNPs - enzymatic and thermal treatment
Swelling ratio	215	27	3	1

Nanodimensions were preserved even in alkaline environment, making reinforced LNPs suitable for the dispersion in NR latex stabilised by ammonia. Nanosized particles are known to display a higher reinforcing effect than microparticles in elastomeric matrixes due to the high surface area of those nanoobjects which could immobilise a larger fraction of the macromolecules of the matrix. The effectiveness of filler-matrix interactions is also conditioned by the reciprocal chemical compatibility of the two components. So, the possibility to combine the nanodimension, covalent reinforcement and functionalisation of LNPs sounded intriguing. Lignin was functionalised by the mechanochemical esterification procedure described in the previous section with NaOH as activator and vinyl acetate as acyl donor. Then, nanoparticles were formulated and submitted to enzymatic intraparticle crosslinking. The corresponding average hydrodynamic diameters and swelling ratios are reported in Figure 41 and Table 30.

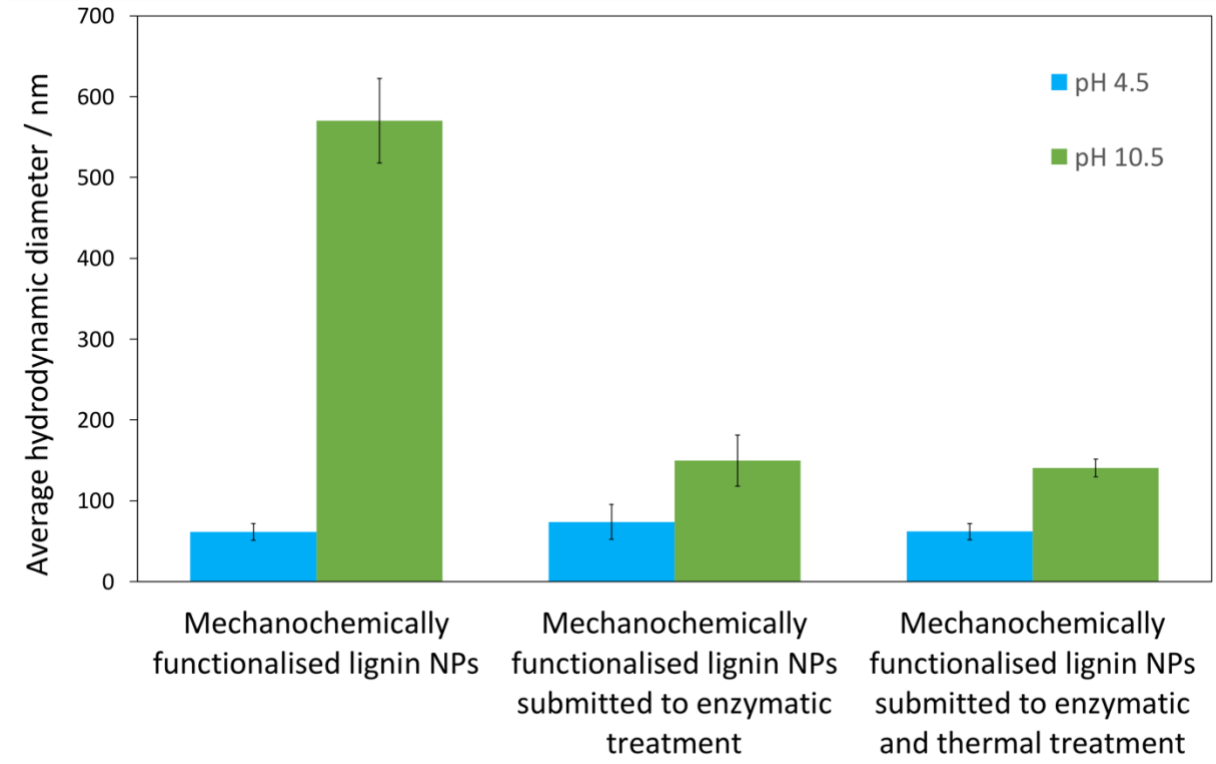

Figure 41. Average hydrodynamic diameter measured by DLS at pH 4.5 and 10.5 for LNPs realised combining mechanochemical functionalisation and nanoformulation and the relative swelling ratio.

Table 30. Swelling ratios for LNPs realised combining mechanochemical functionalisation and nanoformulation when exposed to alkaline pH (10.5) in comparison with the native acidic pH of the suspension (4.5).

Type of LNPs	LNPs form mechanochemically functionalised lignin	LNPs from mechanochemically functionalised lignin - enzymatic treatment	LNPs from mechanochemically functionalised lignin - enzymatic and thermal treatment
Swelling ratio	795	11	7

DLS data at acidic pH (4.5) showed the intraparticle nature of enzymatic crosslinking. The comparison of dimensional data acquired at pH 4.5 and 10.5 by DLS evidenced an exceptionally high swelling ratio for LNPs prepared from mechanochemically modified lignin. Those observations could be supported by the loss of H-bond capacity experienced by esterified hydroxyl groups. The partial esterification of those functionalities reduced the number of H-bonds which could hold together the macromolecules constituting LNPs and contrast swelling. Additionally, the swelling ratio resulted higher for LNPs from functionalised lignin than for LNPs from unmodified lignin, even after enzymatic and thermal treatment (for comparison see Table 29 and Table 30). This phenomenon could be explained by a less extensive crosslinking when part of hydroxyl groups was esterified and could not participate in the crosslinking process. However, crosslinking proved effective in drastically reducing alkaline-induced swelling in the case of esterified lignin. Nevertheless, the approach of nanoformulating esterified lignin did not guarantee any control on the localisation of esters, either on the surface or in the inner part of LNPs. It was essential that active groups were exposed on the surface to obtain reinforcing fillers which could chemically graft to the rubber matrix during vulcanisation. The investigation of the mechanism of lignin nanoprecipitation became crucial to set up a procedure to selectively obtain a surface functionalisation of LNPs. Due to the small size of LNPs, the reactivity of LNPs is largely defined by the nature of surface-exposed functional groups.[56] Additionally, the reinforcement of LNPs consumed relatively high amounts of enzyme (7.7 % mass of enzyme / mass of lignin), which could not be recovered at the end of the process. So, an alternative reinforcing procedure should be implemented to avoid or at least reduce wastes. Moreover, nanoprecipitation assisted by dialysis required long times and high excesses of water, and it resulted in LNP suspensions with an extraordinarily high dilution (nearly 0.1 % wt) when compared to the concentration needed (around 7 % wt) for mixing lignin with natural rubber latex.[57] As a result, the setup of a surface specific functionalisation of LNPs should be accompanied by an easily scalable process of nanoformulation which would require shorter times and would result in more concentrated suspensions with respect to the dialysis-based approach. Recent literature reported a rapid nanoprecipitation of lignin including the poring of a non-solvent, *i.e.,* water, into a lignin solution in water

and water-miscible organic solvent, or *vice versa*.[58] LNPs instantaneously formed upon solvent mixing and a spherical morphology was obtained due to minimisation of surface energy.[59] The process would result in a four-fold increase in the concentration of LNP suspensions with respect to the dialysis-based procedure, reducing the solvent requirements and energy demands associated to the needed concentration of the dispersion. Aggregation phenomena were observed in literature when trying to further increase the concentration.[48]

As mentioned before, the rational design of functional materials is hampered by the structural complexity of softwood kraft lignin (SKL) which was selected for its availability at industrial scale. Solvent extraction could help overcome the structural heterogeneity of SKL by isolation of nearly monodisperse fractions and simultaneous modulation of hydroxyl groups as a function of the polarity and H-bond capacity of the solvent.[34,60] Investigations regarding nanoprecipitation corroborated a molecular weight (MW) driven mechanism with a preferential localisation of high MW fractions in the inner part of LNPs and low MW fractions on the surface.[13,50,51] This evidence was taken into account for the setup of a covalent surface-specific functionalisation of LNPs consisting in the isolation of low and high MW fractions of SKL (BIOPIVA™ 200 from UPM, Finland) by solvent extraction, specific functionalisation of the low MW constituent and recombination with the corresponding high MW component for the synthesis of LNPs, aiming at recovering and valorising the whole starting material.[61] Besides, taking advantage of the mechanism of nanoprecipitation, alkaline stable, internally crosslinked LNPs were prepared by functionalising high MW fractions isolated by solvent extraction, recombining them with the matching low MW fractions and thermally curing such LNPs.

The procedure included a preliminary single-step solvent extraction for the isolation of low and high MW fractions which were optionally individually etherified with epichlorohydrin[39] (Scheme 9) and recombined according to their original mass proportions (Scheme 10).

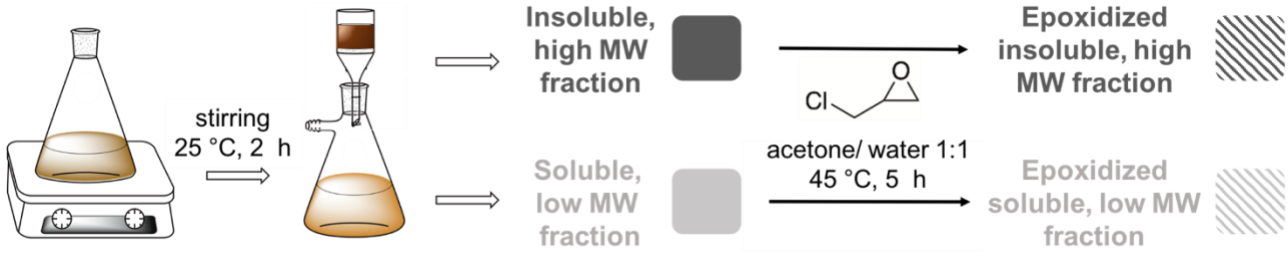

Scheme 9. Single-step solvent fractionation of SKL followed by etherification of the fractions with epichlorohydrin. [61]

SKL was firstly extracted with green organic solvent of different polarity, *i.e.*, ethyl acetate (EtOAc) and ethanol (EtOH), aiming at the isolation of low and high MW fractions through a single-step solvent

fractionation. Solubilisation yield, MW and PDI augmented when increasing the polarity and H-bond capacity of the solvent (Figure 42 and

Table 31).[60] More in detail, by extraction with EtOAc it was possible to isolate a more homogeneous soluble fraction with a lower PDI with respect to the procedure with EtOH. When compared to insoluble fractions, soluble components isolated with both solvents presented low MW and remarkably higher phenolic end groups which were consistent with the presence of smaller polymeric chains with respect to insoluble fractions.[32] The content in carboxylic acids decreased while the number of aliphatic alcohols increased with incrementing the MW of fractions (

Table 31). This general trend in SKL solvent fractionation had been previously reported in literature.[62–64]

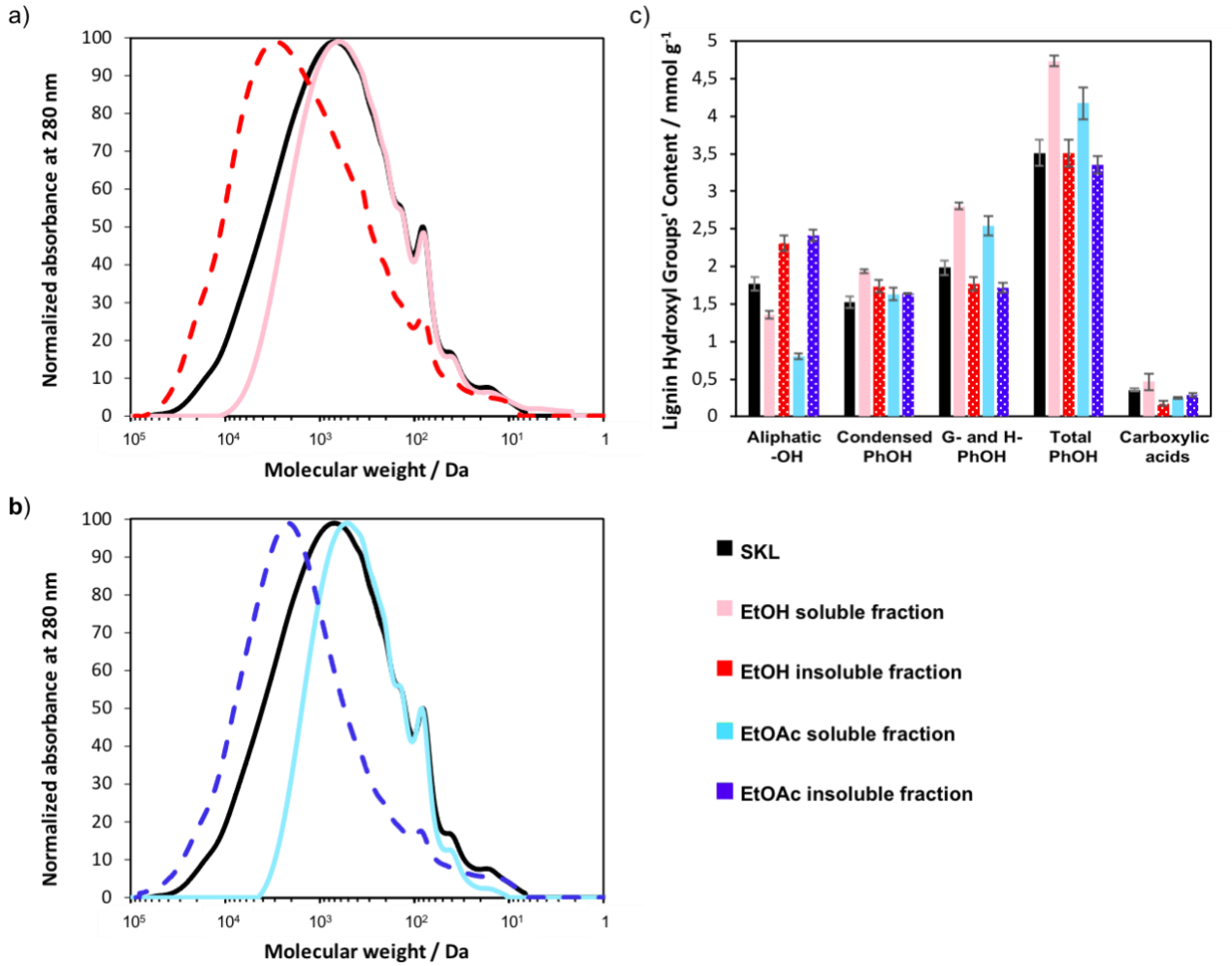

Figure 42. GPC traces of different fractions of SKL from ethanol (a) and ethyl acetate (b) treatment, and quantitative ^{31}P NMR spectroscopy experiments (c). [61]

Table 31. Analysis of different fractions of SKL by extraction yield, GPC and quantitative ^{31}P NMR spectroscopy experiments.[61]

Properties	SKL	Sol_{EtOH}	Ins_{EtOH}	Sol_{EtOAc}	Ins_{EtOAc}
extraction yield / % m/m	100	56	44	36	64
Molecular weight characteristics					
M_n / g mol^{-1}	2100	1100	3700	700	4000
M_W / g mol^{-1}	6700	3300	9000	1300	12400
PDI	3.3	3.0	2.4	1.8	3.2
Hydroxyl group content / mmol g^{-1}					
Aliphatic-OH	1.86	1.36	2.31	0.80	2.41
Condensed phenolic -OH	1.53	1.93	1.74	1.63	1.64
G- and H- phenolic-OH	1.98	2.80	1.77	2.54	1.72
Total phenolic-OH	3.87	4.73	3.51	4.17	3.35
Carboxylic acids	0.35	0.46	0.18	0.25	0.29

Then, SKL and its fractions were etherified with epichlorohydrin following a standard procedure.[39] IR spectroscopy confirmed the effectiveness of the treatment. In particular, diagnostic signals of the functionalisation included the decrement in the intensity of bands related to phenols (O-H stretching at 1370 cm^{-1}) and appearance of signals typical of epoxy groups (920 cm^{-1}), as illustrated for Sol_{EtOAc} and the corresponding epoxidised derivative in Figure 43.

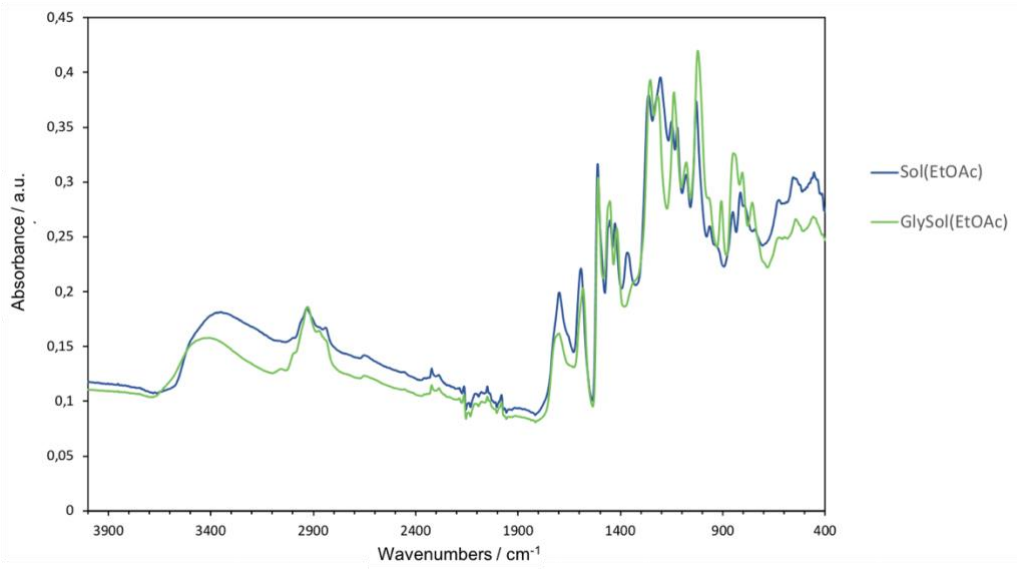

Figure 43. FT-IR/ATR spectrum of Sol_{EtOAc} and the corresponding glycidyl-derivative $GlySol_{EtOAc}$. [61]

LNPs were prepared by a procedure recently reported in literature. [58] After dissolving lignin into a 3:1 % wt mixture of water-miscible organic solvent, *i.e.*, acetone, and water, excess water was added as antisolvent and spherical LNPs formed instantaneously. Then, the organic solvent was recovered by evaporation under reduced pressure and a stable aqueous nanodispersion was obtained. Aiming at the valorisation of the whole starting material, LNPs were synthesised by recombining epoxidised insoluble fractions with the corresponding soluble portion and, *vice versa*, epoxidised soluble fractions with the related insoluble component (Scheme 10). LNPs in the dispersed state were thermally cured in a sealed vial .at 105 °C for 16 h.[62]

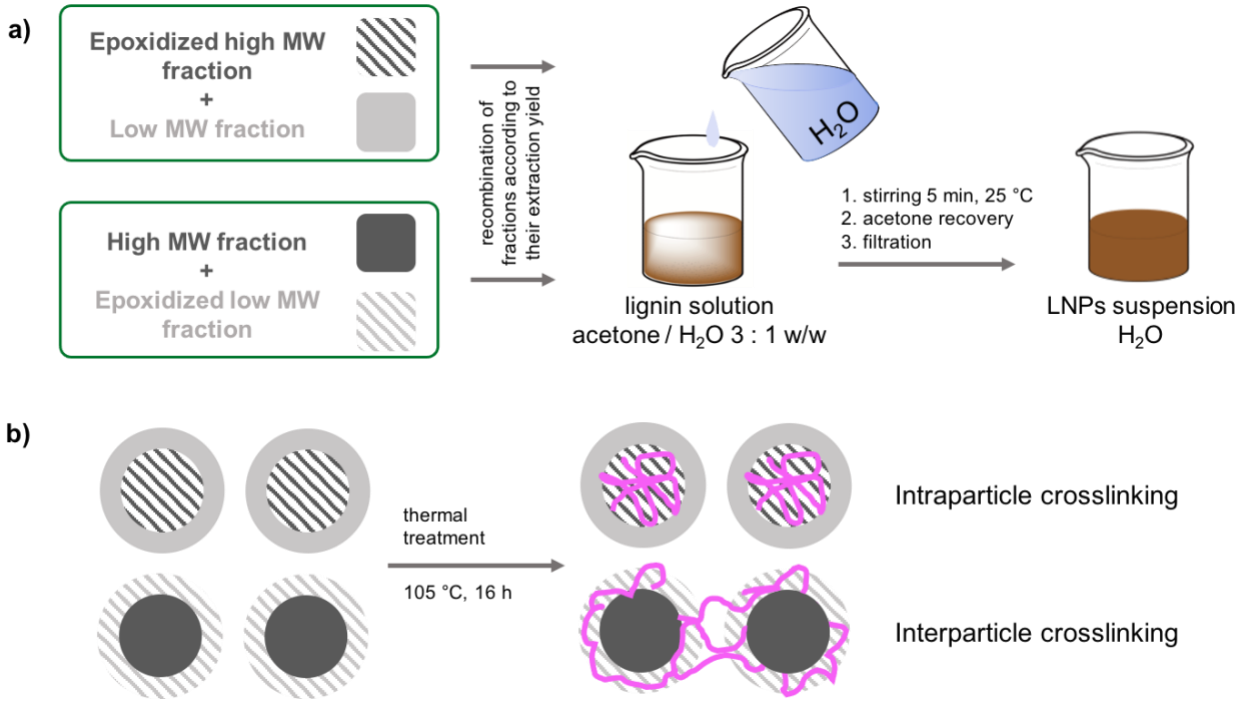

Scheme 10. Synthesis of LNPs by nanoprecipitation (a) and schematic depiction of LNP structure and crosslinking before and after thermal treatment (b). [61]

After thermal treatment, regular LNPs, NPs from epoxidised SKL, and NPs obtained by merging the unmodified insoluble (Ins) and the epoxidised soluble (GlySol) lignin fractions proved colloidally stable at room temperature (Figure 45a). After thermal treatment, regular LNPs presented no significant variations in particle size. Conversely, NPs prepared from epoxidised SKL and GlySol+Ins evidenced an increase in dimensions (Figure 45b), which is probably ascribable to thermally initiated ring-opening reactions. The most remarkable dimensional increment was observed for LNPs from epoxidised SKL, followed by NPs including epoxidised soluble, low MW fractions (GlySol). In those cases, upon thermal treatment dispersions turned visibly unstable. This observation was imputable to the thermally induced crosslinking of epoxy groups, which was corroborated by the disappearance of the diagnostic bands

associated to epoxy groups in FT-IR/ATR spectra (Figure 44). Contrariwise, NPs including epoxidised high MW fractions faced a significantly lower extent of interparticle reactions, so they stayed disperse with an average hydrodynamic diameter inferior to 400 nm.

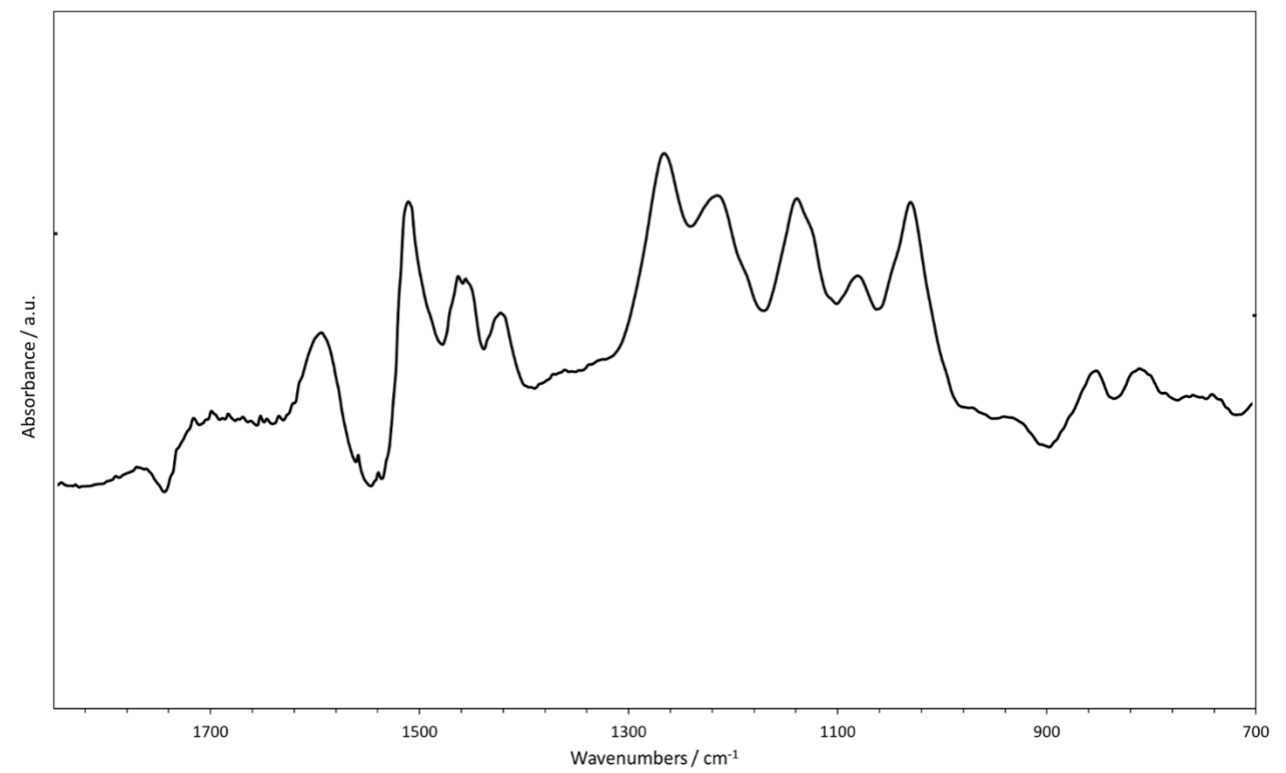

Figure 44. FT-IR / ATR spectrum of Ins_{EtOAc} + $GlySol_{EtOAc}$ LNPs after thermal treatment. [61]

The dimensional variation observed for GlySol+Ins LNPs led to conclude that epoxidised low MW fractions preferentially located on the surface of LNPs and that thermal curing triggered intraparticle crosslinking, as portrayed in Scheme 10b. With respect to LNPs resulting from fractions extracted in ethanol, particles derived from fractionations in ethyl acetate, *i.e.*, $GlySol_{EtOAc}$+Ins_{EtOAc} LNPs, faced a superior degree of interparticle crosslinking, as echoed by the extent of the dimensional increment experienced after thermal curing. The experimental higher degree of crosslinking experienced by LNPs from ethyl acetate extraction was credited to the highly selective isolation of a narrowly polydisperse, low MW fraction[10,36] which, after etherification with epichlorohydrin, specifically localised on the outer surface of LNPs. This explanation was consistent with the MW-dependent nanoprecipitation mechanism reported in literature.[13] Contrariwise, ethanol could extract a soluble fraction with a broad MW distribution. In $GlySol_{EtOH}$+Ins_{EtOH} LNPs, the functionalised ethanol-soluble fraction was believed to distribute in a comparably unspecific manner partly on the surface and partly in the core of LNPs, resulting in a less marked intraparticle crosslinking and dimensional increment.

SEM images (Figure 45c and d) confirmed that the spherical morphology of LNPs was preserved even after the thermal treatment. The SEM pictures of thermally cured $GlySol_{EtOAc}$+Ins_{EtOAc} LNPs, allowed inferring a superficial crosslinking by considering a three-dimensional structure and piling up of LNPs. Such supraparticle structures were not detected in the images regarding the same LNPs before the thermal treatment, consenting to exclude simple aggregation of ripening effects which could have led to similar observations.

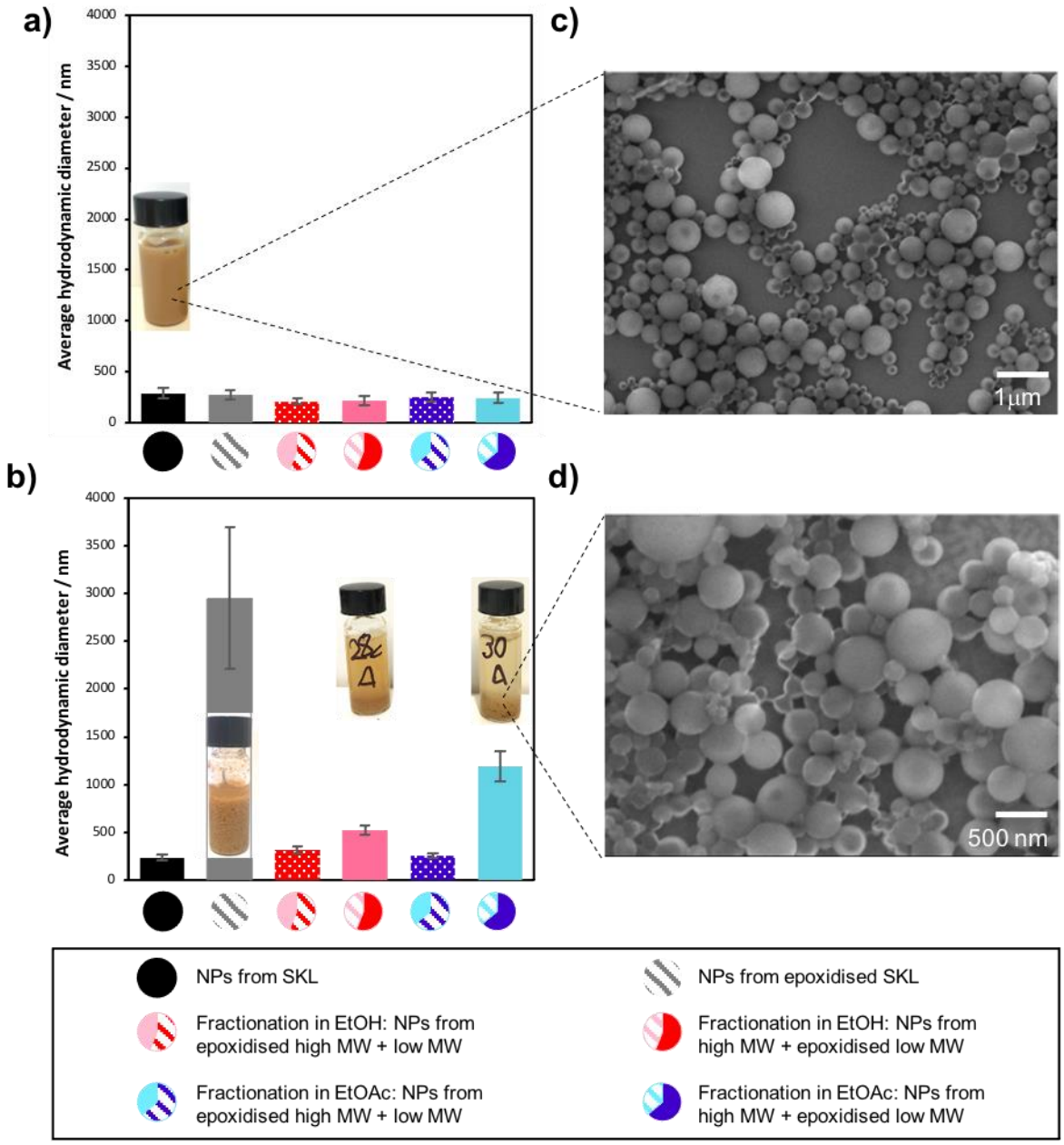

Figure 45. Analysis of hydrodynamic diameter by DLS before (a) and after (b) thermal curing. SEM images of air-dried LNPs (c) and thermally cured LNPs (d). [61]

Thermally cured LNPs prepared from epoxidised insoluble and unmodified soluble fractions, *i.e.*, Sol+GlyIns LNPs, presented peculiar characteristics. Sol_{EtOAc}+$GlyIns_{EtOAc}$ LNPs showed no evident dimensional variation after thermal curing, as was observed for LNPs from unmodified SKL. This evidence suggested that epoxidised insoluble fraction (GLyIns) was localised in the inner part of LNPs and that thermally induced crosslinked confirmed by FT-IR/ATR (Figure 46) was restricted to the internal parts of LNPs.

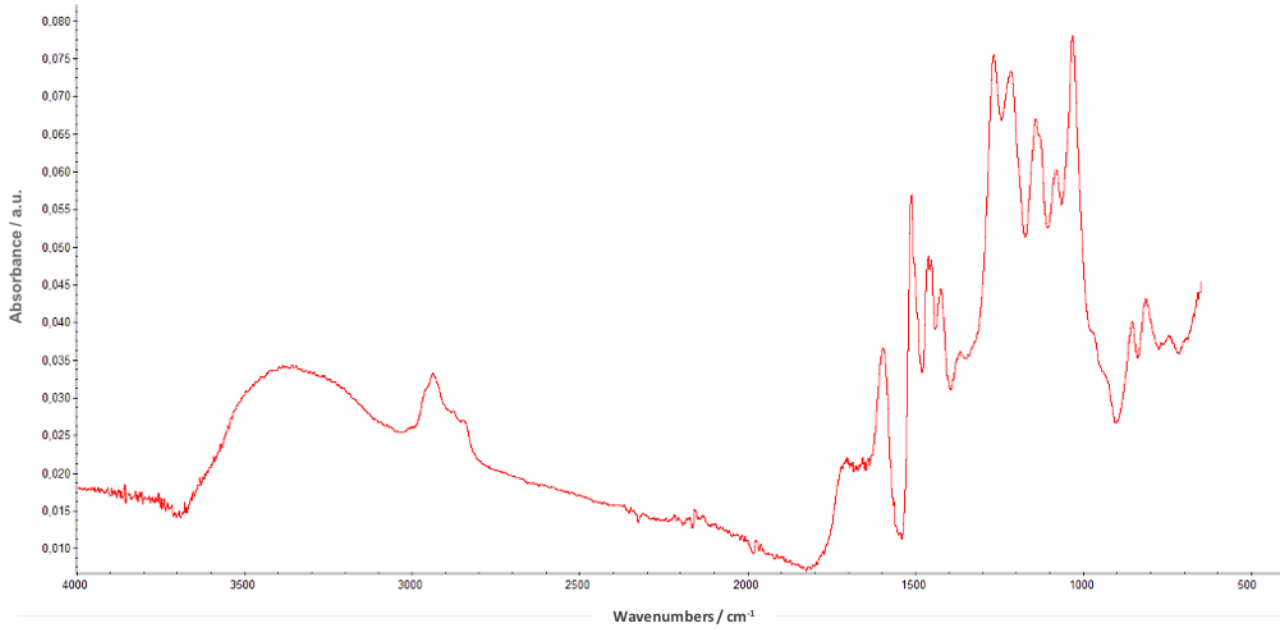

Figure 46. FT-IR / ATR spectrum of $GlyIns_{EtOAc}$ + Sol_{EtOAc} LNPs after thermal treatment. [61]

This internal reinforcement resulted in a high dimensional stability of those LNPs up to pH 12 (Figure 47). On the contrary, the modest dimensional increment presented by thermally cured Sol_{EtOH}+$GlyIns_{EtOH}$ LNPs was ascribed to the scarce selectivity of ethanol extraction which allowed isolating two fractions with poorly dissimilar MWs. Ethanol extracted fractions presented a rather feeble driving force in specifically localising either on the surface or in the core of LNPs during the MW-dependent nanoparticle formation process. As a result, $GlyIns_{EtOH}$ could expose part of the reactive epoxy groups on the surface, resulting in a modest interparticle crosslinking and dimensional increment.

The well-known alkaline-induced swelling of LNPs related to the polyelectrolyte nature of lignin[65] was observed for thermally treated SKL NPs. Contrariwise, thermally cured Sol+GlyIns LNPs showed a high dimensional stability in alkaline conditions, *i.e.*, pH 12, with respect to the same cured LNPs in acidic conditions, *i.e.,* pH 4.5. The covalent crosslinking endowed Sol+GlyIns LNPs with dimensional stability in alkaline conditions, as such unlocking the possibility for covalent surface functionalisation of internally stabilised LNPs. The invariance in size during the exposure to alkaline environments made these particles

intriguing for their mixing in NR latex stabilised by ammonia for the production of NR masterbatches filled with LNPs.

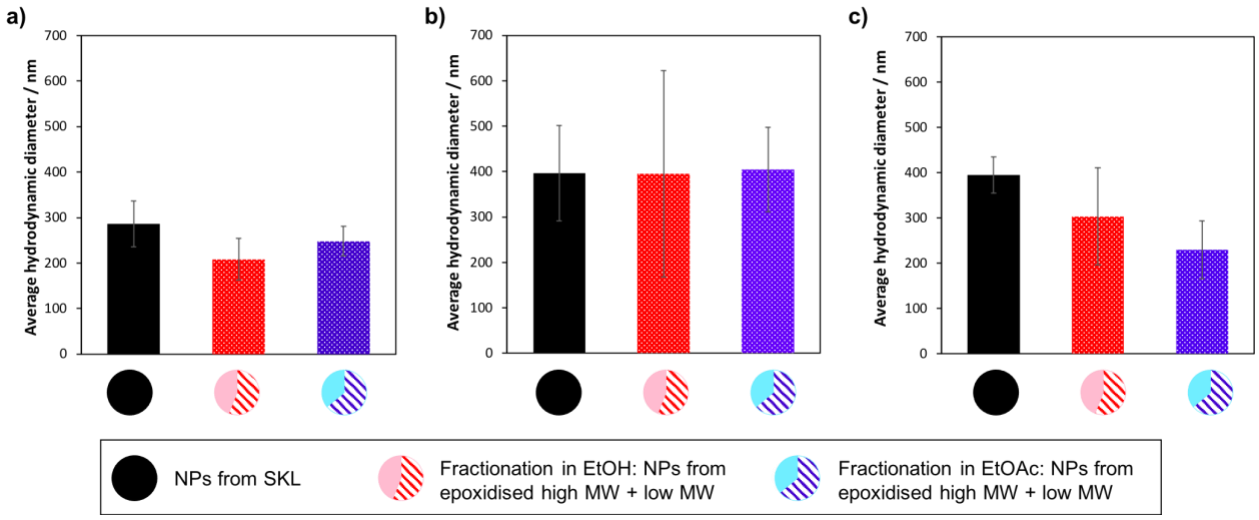

Figure 47. Analysis of hydrodynamic diameter of LNPs by DLS at pH 4.5 (a) and at pH 12 before (b) and after (c) thermal curing at 105 °C. [61]

The possibility to limit functionalisation of lignin to high or low MW fractions in accordance with the targeted properties conformed to the principles of green chemistry related to minimisation of waste and derivatisation. Additionally, LNPs with a surface-specific covalent functionalisation, could find various applications including adsorbents, flocculants and sensors.[66] Bio-based adhesives are attracting attention as a sustainable alternative to traditional fossil-based materials. In this field, lignin is under investigation as adhesive for both soft and hard substrates. Recent literature[67] evidenced the role of confined evaporation-induced self-assembly of nanolignin and non-covalent interactions between adhesive and substrate to obtain glues with good performances. Investigations focused on the possibility to use surface-functionalised LNPs as waterborne adhesives for aminated glass (Scheme 11). Common microscope glass slides were functionalised with (3-aminopropyl)triethoxysilane (APTES) to expose amino groups on the surface of the substrate. This functional group could afford a covalent binding to LNPs presenting an epoxidised surface, which were added in the dispersion state according to a procedure reported in literature for a direct comparison.[67] Among all the LNPs hitherto described, $GlySol_{EtOAc}$+Ins_{EtOAc} LNPs proved the most effective in terms of intraparticle crosslinking, corroborating the desired location of epoxy groups on the surface of LNPs where they could induce intraparticle crosslinking and covalent binding of those LNPs to the surface of aminated glass substrates. So, $GlySol_{EtOAc}$+Ins_{EtOAc} LNPs were elected for shear adhesive tests and compared to regular SKL NPs.

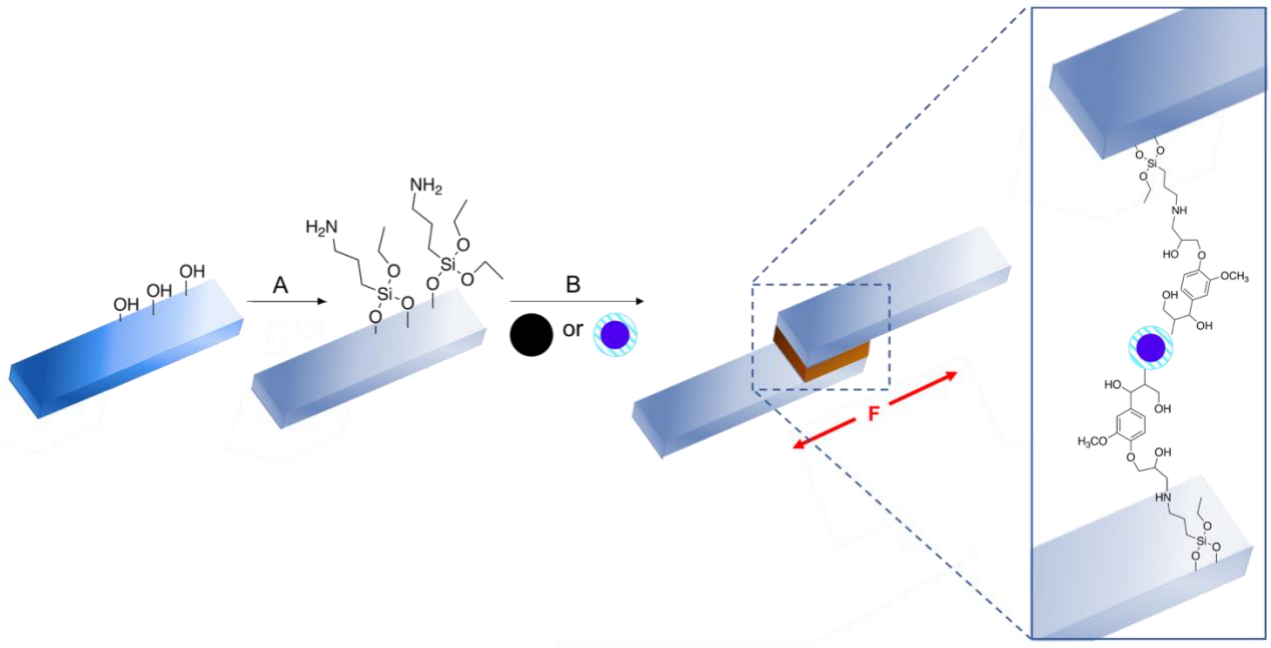

Scheme 11. Surface functionalisation of glass slides and application of LNP-based adhesives. A. Amination of glass slides. 1. (3-aminopropyl)triethoxysilane, *i*PrOH / H_2O, 95:5 (v/v), 25 °C, overnight; 2. *i*PrOH / H_2O washing. B. 1. Deposition of 0.43 % (% wt) LNP aqueous dispersions (black: SKL, blue: $GlySol_{EtOAc}$+Ins_{EtOAc}) and junction of aminated glass slides; 2. Thermal treatment, 105 °C, 16 h. [61]

An even distribution of LNPs on glass joints was macroscopically evident and any accumulations of materials at the edges of the joints was evident (Figure 48a), contrarily to what was observed for organosolv lignin NPs on bare glass.[67] After the breaking of the joint during the in-plane test, SEM images (Figure 48d and e) showed that LNPs piled up in the junction, revealing the centrality of particle-particle interactions. Moreover, after joint disruption, both glass slides proved covered by LNPs, proving that a durable particle-substrate interaction was well maintained and that failure point was at the particle-particle level. Remarkably, $GlySol_{EtOAc}$+Ins_{EtOAc} LNPs showed double adhesive strength compared to regular SKL (ultimate shear strengths of 5.1 ± 0.8 MPa and 2.4 ± 0.2 MPa, respectively) on aminated glass. This result was expected on account of the surface chemistry which permitted the covalent binding of surface-epoxidised LNPs to the support upon thermal treatment (Scheme 11).

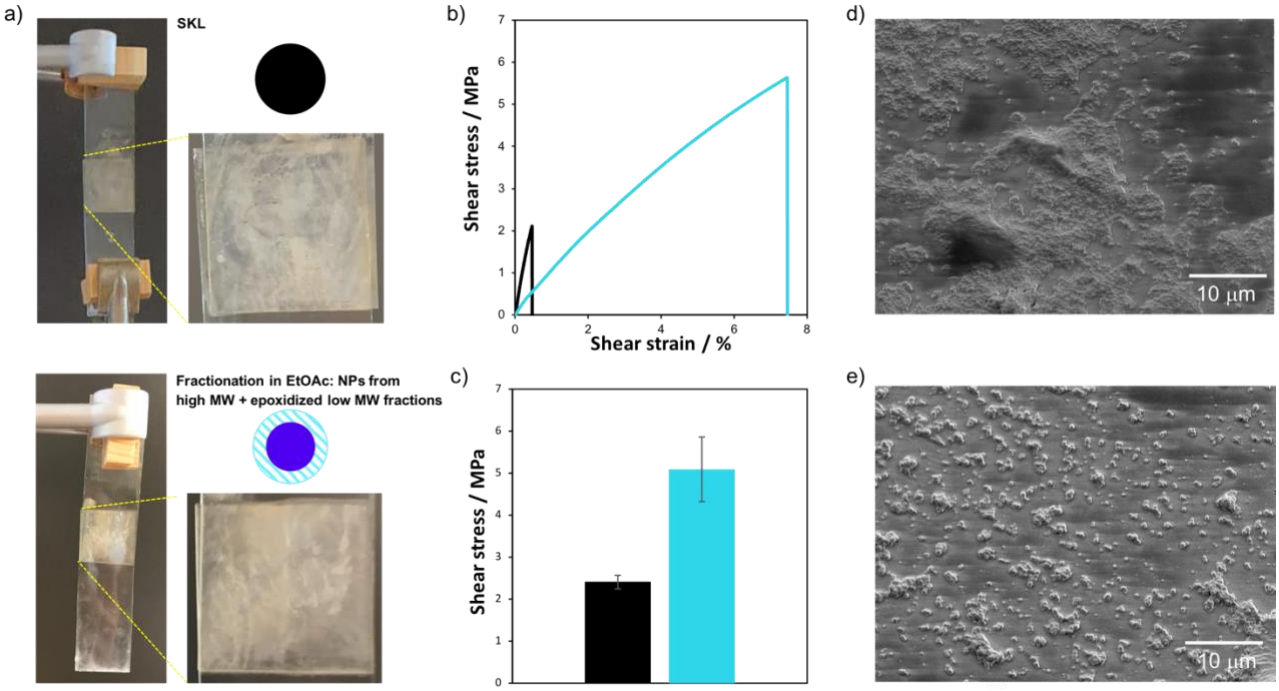

Figure 48. Images of LNPs glass joints and schematic depiction of LNPs used as adhesives (a). Stress to strain curves of glass joints using different LNP aqueous dispersions (black: SKL NPs, light blue: $GlySol_{EtOAc}$+Ins_{EtOAc} NPs) obtained by the tensile testing machine (b). Ultimate tensile strength evaluated in the lab by applying a load to the jointed glass slides (c). Scanning electron microscopy images of joints ruptured after tensile test for adhesives based on SKL NPs (d) and $GlySol_{EtOAc}$+Ins_{EtOAc} NPs (e). [61]

The comparison of shear strength of adhesives (Table 32) prepared from LNP suspensions of similar concentration evidenced that SKL NPs on aminated glass performed 20 times better than organosolv lignin NPs on pristine glass.[67] This observation could be attributed to the higher interactions energies between amines and lignin with respect to lignin and hydroxyl groups on pristine glass surfaces. SKL NPs touched the lower limit of strength individuated by ASTM-D4690 standard for urea-formaldehyde adhesives.[68] Outstandingly, $GlySol_{EtOAc}$+Ins_{EtOAc} LNPs performed even better on aminated glass as ascribed to the covalent binding between amino groups exposed on glass surface and epoxy groups located on the surface of LNPs (Scheme 11). A rather low interface loading of $GlySol_{EtOAc}$+Ins_{EtOAc} LNPs was able to outclass a thousand fold concentration of wood adhesives prepared from lignin formulated with epoxide-based crosslinkers.[69] The same intraparticle crosslinked LNPs also outperformed intraparticle-crosslinked hybrid bisphenol A / diglycidyl ether-modified lignin NPs as wood adhesives which needed a relatively high concentration of NPs.[62] An innovative adhesive based on water-soluble epoxidised lignin crosslinked with LNPs[70] required a thousand times higher interfacial loading to reach a shear strength which doubled the one of $GlySol_{EtOAc}$+Ins_{EtOAc} LNPs. While taking into consideration other bio-based adhesives for glass, LNPs on aminated glass gave similar results to chitin-amyloid

mixtures[71] and chitin nanocrystals[72] on pristine glass. Regular SKL NPs showed a shear strength of the same magnitude as CNCs with a more material-efficient way in terms of interfacial loading.[73]
The recombination of epoxidised ethyl acetate soluble fraction with unmodified ethyl acetate insoluble fraction resulted in high-performance nanoparticle adhesives which conformed to the principle of green chemistry as for the reduction of functionalising agents and for the recovery of the whole starting material.

Table 32. Comparison of the shear strength of diverse bio-based adhesives reported in literature. [61]

Reference	Material	Support	Interface loading / kg m^{-2}	Shear strength / MPa
Present work	SKL NPs	aminated glass	$3.2 \cdot 10^{-4}$	2.4 ± 0.2
Present work	$GlySol_{EtOAc}$+Ins_{EtOAc} LNPs	aminated glass	$3.2 \cdot 10^{-4}$	5.1 ± 0.8
[67]	organosolv NPs	pristine glass	$3.2 \cdot 10^{-4}$	0.110 ± 0.037
[69]	lignin with epoxide-based crosslinkers	wood	$4 \cdot 10^{-1}$	2.2 ± *n.a.*
[62]	intraparticle-crosslinked hybrid bisphenol A / diglycidyl ether-modified lignin NPs	wood	$1 \cdot 10^{-1}$	4.0 ± 0.8
[70]	crosslinked water-soluble epoxidised lignin / LNPs	wood	$3 \cdot 10^{-1}$	13 ± *n.a.*
[71]	chitin-amyloid mixtures	pristine glass	$2.6 \cdot 10^{-4}$	1.4 ± 0.4
[72]	chitin nanocrystals	pristine glass	$8.0 \cdot 10^{-4}$	5.26 ± *n.a.*
[73]	CNCs	pristine glass	$2.2 \cdot 10^{-2}$	4.7 ± 0.7

The environmental impact of these innovative bio-based adhesives was assessed. A particular focus was dedicated to the case of $GlySol_{EtOAc}$+Ins_{EtOAc} LNPs and the comparison with LNPs from epoxidised SKL (GlySKL NPs) which would show the same superficial functionalisation and result in comparable interparticle crosslinking performances, and thus expected similar adhesive behaviour upon thermal curing (105 °C, 16 h). The *E*-factor[74] was considered as a simple metric for the environmental assessment of those adhesives. Moreover, the solvent demand was computed as an independent metric and excluded from the calculations of *E*-factor due to the different processing required for the treatment of solvents and non-volatile wastes. The two indicators could give only an approximative estimation of the environmental impact without taking into consideration toxicity issues and energy demand.

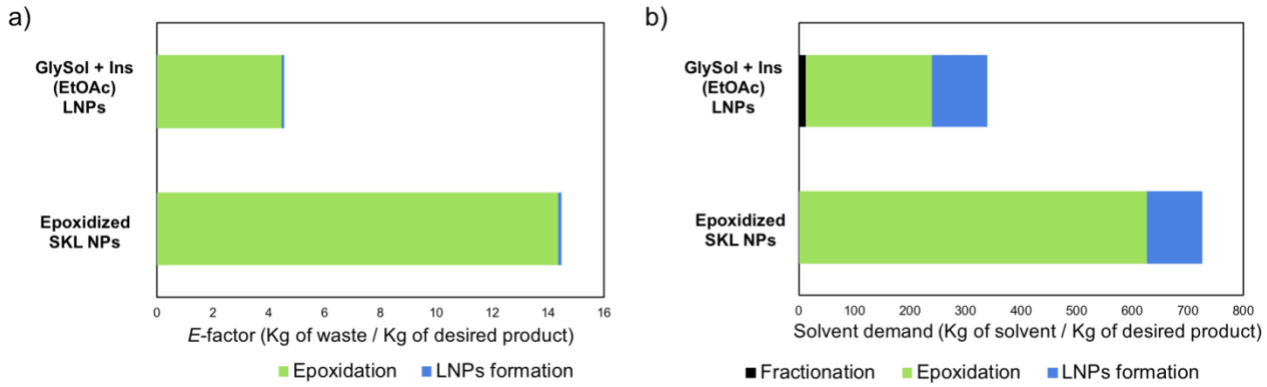

Figure 49. Contributions of fractionation, epoxidation and LNPs formation steps to the overall *E*-factor calculated excluding solvents (a) and solvent demand (b) for the formation of fully epoxidised SKL NPs and GlySol+Ins (EtOAc) LNPs. [61]

The estimation of the impact of each step to the total values of *E*-factor and solvent demand (Figure 49) followed equations reported in literature.[75–79] This method highlighted the contribution of fractionation, epoxidation and LNP formulation on the *E*-factor and solvent demand of the whole process. As for $GlySol_{EtOAc}$+Ins_{EtOAc} LNPs, solvent extraction was accompanied by a quantitative recovery of the starting material, so it did not have impact on the calculation of *E*-factor while the solvent, *i.e.*, EtOAc, counted for the estimation of the solvent demand. The distinction of the metrics into the single contributions of each stage evidenced the outstanding impact of epoxidation, which included excess epichlorohydrin and low concentration for the progress of the reaction. The epoxidation of the sole soluble fraction allowed reducing the quantity of functionalised material from 100% to 36%, as such drastically diminishing the *E*-factor and solvent demand associated to this stage. The strong diminution of solvent demand related to epoxidation more than compensated the solvent consumption related to fractionation, which was needed for $GlySol_{EtOAc}$+Ins_{EtOAc} LNPs but not for GlySKL NPs. As a result, the preparation of $GlySol_{EtOAc}$+Ins_{EtOAc} LNPs proved to have a better environmental impact regarding *E*-factor and solvent demand with respect to the formation of GlySKL NPs.

13.2 Preparation and assessment of the mechanical performances of rubber composites including lignin nanoparticles

Polymer nanocomposites have recently gained more and more attention owing to noteworthy improvements in diverse composite properties.[76–80] The nanoscale dimensions of the filler is known to induce elevated interfacial contacts between filler and matrix leading to a higher fraction of immobilised polymer and resulting in a synergistic enhancement in the performances of the compound which are superior to those of the individual components. Recent studies in literature showing promising results for the introduction of nanofillers in elastomeric composites[81,82] stimulated the development of diverse nanolignins as possible reinforcing fillers for rubber compounds.

The following section is devoted to the discussion of the dynamic mechanical characterisation of composites whose preparation was described in the previous chapter. The study included the dynamic mechanical properties of vulcanised compounds, the vulcanisation kinetics, the tensile properties and compression dynamics of cured composites.

Samples will be labelled according to the filler content as follows:

- *00CB+00L* refers to compounds comprising *00* phr of traditional filler, *i.e.* carbon black (*CB*), *00* phr of milled lignin (*L*) mixed in the form of a slurry with NR latex for the preparation of a 50 % wt NR masterbatch obtained by codrying;
- *00CB+00L(NH$_4$OH)* refers to compounds comprising *00* phr of traditional filler, *i.e.* carbon black (*CB*), *00* phr of milled lignin (*L*) mixed in the form of an alkaline solution (the base was sodium hydroxide, *NH$_4$OH*) with NR latex for the preparation of a 50 % wt NR masterbatch obtained by codrying;
- *00CB+00LNP* refers to compounds comprising *00* phr of traditional filler, *i.e.* carbon black (*CB*), *00* phr of diverse lignin nanoparticles (*LNP*) which could be: *Small* (150 nm of hydrodynamic diameter), *Large* (350 nm of hydrodynamic diameter), *GlyIns* (prepared by recombining lignin soluble and epoxidised insoluble fractions after fractionation in ethyl acetate), *GlySol* (prepared by recombining lignin insoluble and epoxidised soluble fractions after fractionation in ethyl acetate).

The unit *phr* stands for *parts per hundred rubber* and indicates the percentual mass ratio between the specific ingredient and the total rubber quantity in the formulation.

13.2.1 NR composites including diverse nanolignins as filler

Internal compounds for tyres containing nanolignins of diverse dimensions, *i.e.*, small and large LNPs with an average hydrodynamic diameter of 150 and 350 nm, respectively, produced as described in paragraph 8.2.5, with mechanical stability, *i.e.*, internally crosslinked $GlyIns_{EtOAc}$+Sol_{EtOAc} LNPs, or with networking capabilities, *i.e.*, interparticle crosslinked Ins_{EtOAc}+$GlySol_{EtOAc}$ LNPs, as monofillers were prepared in order to investigate the technological merits and limitations of such particles as reinforcing materials. Rubber composites were prepared by blending natural rubber latex with the suitable lignin dispersed or dissolved in aqueous media and drying the mixture at 45 °C for approximately 60 h. It was observed that the drying process resulted in an inhomogeneous material, with dusty sediment on the bottom and a brownish, polymeric film on the surface. Such a separation can be ascribed to partial lignin dispersibility in the rubber latex, limited colloidal stability of the system or segregation of a lignin fraction with a reduced compatibility with rubber. Such a material was finally mixed in a twin screw extruder with additional natural rubber and the other ingredients of the compound, according to the formulation recipes reported in

Table 33. SEM images evidenced that LNPs retained their size when mixed with latex stabilised by ammonia (Figure 50).

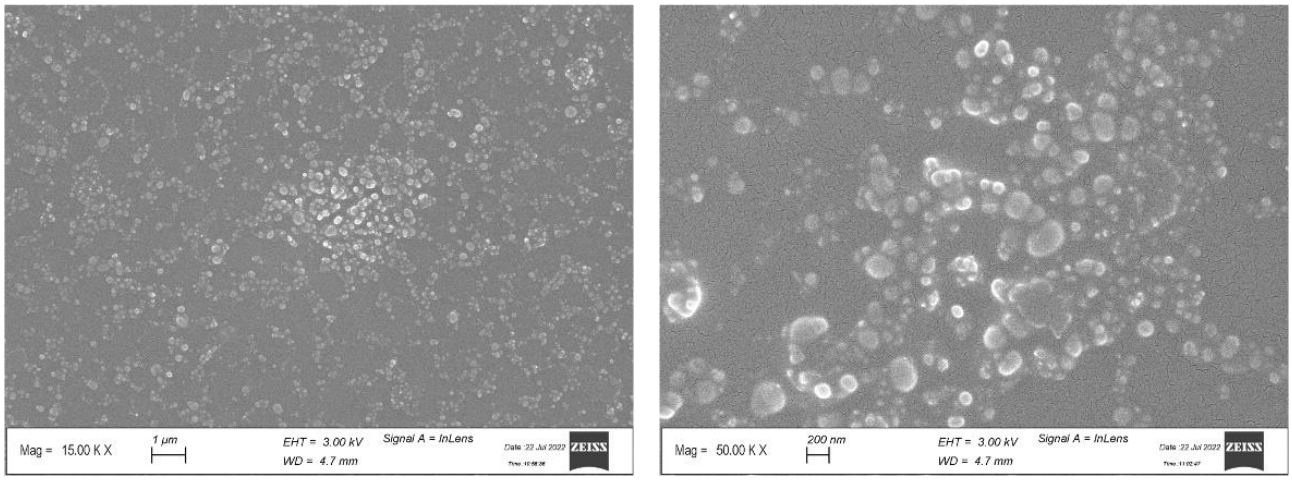

Figure 50. SEM images for dried masterbatches of natural rubber including 100 phr of large LNPs (350 nm of average hydrodynamic diameter).

Table 33. NR composites including nanolignin codried with NR as filler.

Components and formulation in phr	NR 50L (NH_4OH) S	NR 50L S	NR 50LNP Small S	NR 50LNP Large S	NR 50LNP GlyIns S	NR 50LNP GlySol S
Natural rubber (SIR20)	50	50	50	50	50	50
Codried NR masterbatch, 50% small LNPs			100			
Codried NR masterbatch, 50% large LNPs				100		
Codried NR masterbatch, 50% large LNPs EpoIN					100	
Codried NR masterbatch, 50% large LNPs EpoOUT						100
Codried NR masterbatch, 50% unmodified lignin	100					
Codried NR masterbatch, 50% unmodified lignin dissolved in ammonia		100				
Antioxidant (6PPD)	2	2	2	2	2	2
Stearic acid	2	2	2	2	2	2
Zinc oxide	4	4	4	4	4	4
Accelerant TBBS	1.8	1.8	1.8	1.8	1.8	1.8
66 % wt oil-extended sulfur	4	4	4	4	4	4
Tensile properties						
Stress at 300% deformation / Stress at 100% deformation	2.20	2.05	2.54	2.63	2.86	2.84
Stress at 50% deformation / MPa	0.36	0.41	0.47	0.37	0.37	0.35
Stress at 100% deformation / MPa	0.96	1.03	1.20	0.97	1.01	0.94
Stress at 300% deformation / MPa	1.04	1.32	1.77	1.35	1.61	1.46
Stress at break / MPa	3.08	2.71	4.51	3.55	4.61	4.14
Elongation at break / %	12.88	11.20	12.83	12.79	9.87	13.17
Energy/ $J \cdot cm^{-3}$	594.68	568.75	559.57	557.51	459.5	564.85
Vulcanisation kinetics (170 °C, 10 min) and dynamo-mechanical properties						
ML (moment lowest) / dN·m	1.66	1.67	1.60	1.60	1.96	1.88
MH (moment highest) / dN·m	8.75	8.79	10.72	9.19	11.69	10.77
T90 / min	2.88	2.49	2.95	2.84	3.13	3.29
TS2 / min	1.51	1.63	1.35	1.51	1.43	1.58
dG' (0.4 - 10 % deformation) / MPa	0.16	0.18	0.16	0.16	0.15	0.13
G' at 9 % deformation / MPa	0.710	0.801	0.792	0.707	0.776	0.682
tanδ at 9 % deformation	0.061	0.045	0.065	0.051	0.057	0.058

Compression dynamics

23 °C, 1 Hz	E' / MPa	3.624	4.189	4.342	3.723	3.546	3.210
	Tanδ	0.039	0.027	0.049	0.028	0.043	0.051
23 °C, 10 Hz	E' / MPa	3.764	4.276	4.541	3.835	3.705	3.388
	Tanδ	0.046	0.030	0.058	0.038	0.053	0.061
23 °C, 100 Hz	E' / MPa	3.924	4.359	4.784	3.974	3.898	3.597
	Tanδ	0.091	0.068	0.102	0.081	0.095	0.104
70 °C, 1 Hz	E' / MPa	3.678	4.209	4.309	3.798	3.619	3.233
	Tanδ	0.037	0.032	0.047	0.032	0.040	0.044
70 °C, 10 Hz	E' / MPa	3.798	4.315	4.486	3.907	3.755	3.377
	Tanδ	0.036	0.027	0.044	0.028	0.039	0.044
70 °C, 100 Hz	E' / MPa	3.936	4.415	4.679	4.029	3.919	3.550
	Tanδ	0.052	0.040	0.059	0.044	0.058	0.063
100 °C, 1 Hz	E' / MPa	3.782	4.313	4.406	3.942	3.689	3.342
	Tanδ	0.036	0.033	0.044	0.030	0.036	0.038
100 °C, 10 Hz	E' / MPa	3.901	4.415	4.570	4.046	3.817	3.473
	Tanδ	0.037	0.031	0.045	0.027	0.038	0.040
100 °C, 100 Hz	E' / MPa	4.030	4.506	4.747	4.142	3.965	3.620
	Tanδ	0.048	0.040	0.055	0.041	0.054	0.056

Two different compounds were taken as reference for the systems including lignin as monofiller. *NR 50L S* was prepared from a masterbatch obtained by mixing NR latex with an aqueous slurry of unmodified micrometric lignin, while *NR 50L (NH_4OH) S* derived from a masterbatch achieved by blending NR latex with a solution of unmodified lignin in ammonia. Compared to the former and all the innovative compounds, the latter showed a fast vulcanisation kinetics (T90) which led to extraordinarily low hysteresis and other anomalous values. These features were ascribed to residual ammonia in the masterbatch which could have acted as additional accelerant during vulcanisation. For all the above-mentioned reasons, *NR 50L (NH_4OH) S* proved not to be suitable as reference for all the 'example' composites which will be henceforth compared to *NR 50L S*.

Small and large LNPs (*NR 50LNPSmall S* and *NR 50LNPLarge S*) dispersed better in the elastomeric matrix than micrometric lignin (*NR 50L S*) as proved by the high ratios between stresses at 300% and 100% deformation. The three composites shared the same elasticity, by elongation at break. If compared with the other two compounds, small LNPs were associated to higher crosslink density (Figure 51) which impacted on the high stress at break of the composite. Small LNPs allowed for an enhanced reinforcement with respect to micrometric lignin and large LNPs (surface area of 4.1 $m^2 \cdot g^{-1}$), which was expected for small nanofillers which are known to have a higher specific surface area (surface area of

11.0 $m^2 \cdot g^{-1}$) with respect to larger particles, as such having more interactions with the macromolecules of the polymeric matrix whose motions resulted restricted and guaranteeing a high fraction of immobilised rubber. While small LNPs showed similar hysteresis to *NR 50L S*, large LNPs displayed the same reinforcement as the reference compound but extraordinarily low hysteresis (Figure 51).

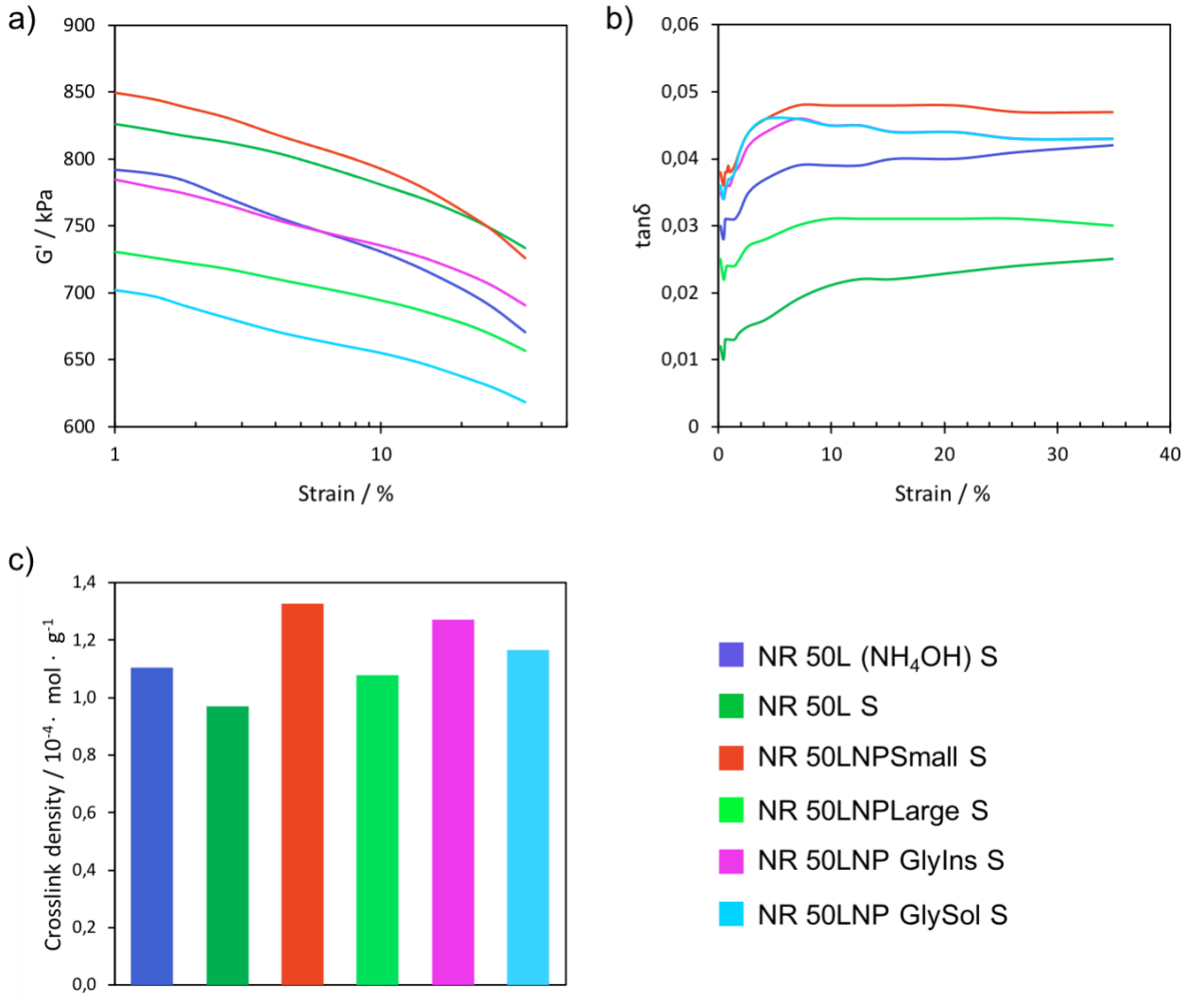

Figure 51. Storage modulus (a) and hysteresis (b) as a function of strain, crosslink density determined by swelling experiments (c) for NR compounds including nanolignin as fillers and the corresponding reference compounds-

Along with the static performances, the analysis of the dynamic properties was conducted by exposing the cured compounds to cyclic alternating compressions at diverse temperatures (23, 70 and 100 °C) and deformation frequencies (1, 10, 100 Hz) which could simulate the working conditions of tyres on the road. Noteworthy, at every tested temperature and frequency, small LNPs exhibited a dynamic modulus (E') which was 10-20% higher than in the cases of micrometric lignin and large LNPs.

Subsequently, micrometric lignin was compared to thermally treated $GlyIns_{EtOAc}$+Sol_{EtOAc} LNPs and Ins_{EtOAc}+$GlySol_{EtOAc}$ LNPs which were prepared according to the methodology described in paragraph 8.2. Based on the observations previously reported in paragraph 13.1, after thermal curing in the dispersed state at 105 °C for 16 h, $GlyIns_{EtOAc}$+Sol_{EtOAc} LNPs were expected to display an intraparticle crosslinking which should guarantee an enhanced stability of the particles under physical stresses related to the deformations induced during the mechanical testing of the compound. However, unlike what occurred for $GlyIns_{EtOAc}$+Sol_{EtOAc} LNPs batches produced on small scale, after thermal curing LNPs fabricated on large scale did not preserve the same average size as the starting material. The increase detected by DLS and visualised by SEM in the dimensions after thermal curing for LNPs produced in large scale (Figure 52) can be ascribed to the modifications in the synthetic procedure required for the preparation of a suitable quantity of filler for the production of a rubber compound (paragraph 8.2). In particular, epoxidation of the insoluble fraction was scaled up from 500 mg to 5 g of substrate and thermal curing was run on 7.5 % wt instead of 0.43 % wt for the LNPs dispersion used for the small scale, necessitated by the high volumes otherwise involved in the large-scale set-up in case of a linear scaling. The scale up of the epoxidation may have induced a crosslinking of the substrate during the reaction itself and a consequent increase in molecular weight. The variation in molecular weight could, however, not be detected by GPC due to the limited solubility of the GlyIns in THF. Such an event could have affected the molecular weight-driven nanoprecipitation mechanism, leading to the exposure of part of the epoxy groups on the surface of LNPs which could determine interparticle crosslinking responsible for the increase in LNP dimensions evidenced by DLS and SEM. Another possible explanation for this phenomenon could be the different dilution of the LNP dispersions during the curing step. While an intraparticle crosslinking was possible in the high dilutions typical of the small scale, the high solid content of the large scale apparently prevented the possibility for an exclusive intraparticle crosslinking and was accompanied by an interparticle crosslinking which accounted for the dimensional increase of $GlyIns_{EtOAc}$+Sol_{EtOAc} LNPs.

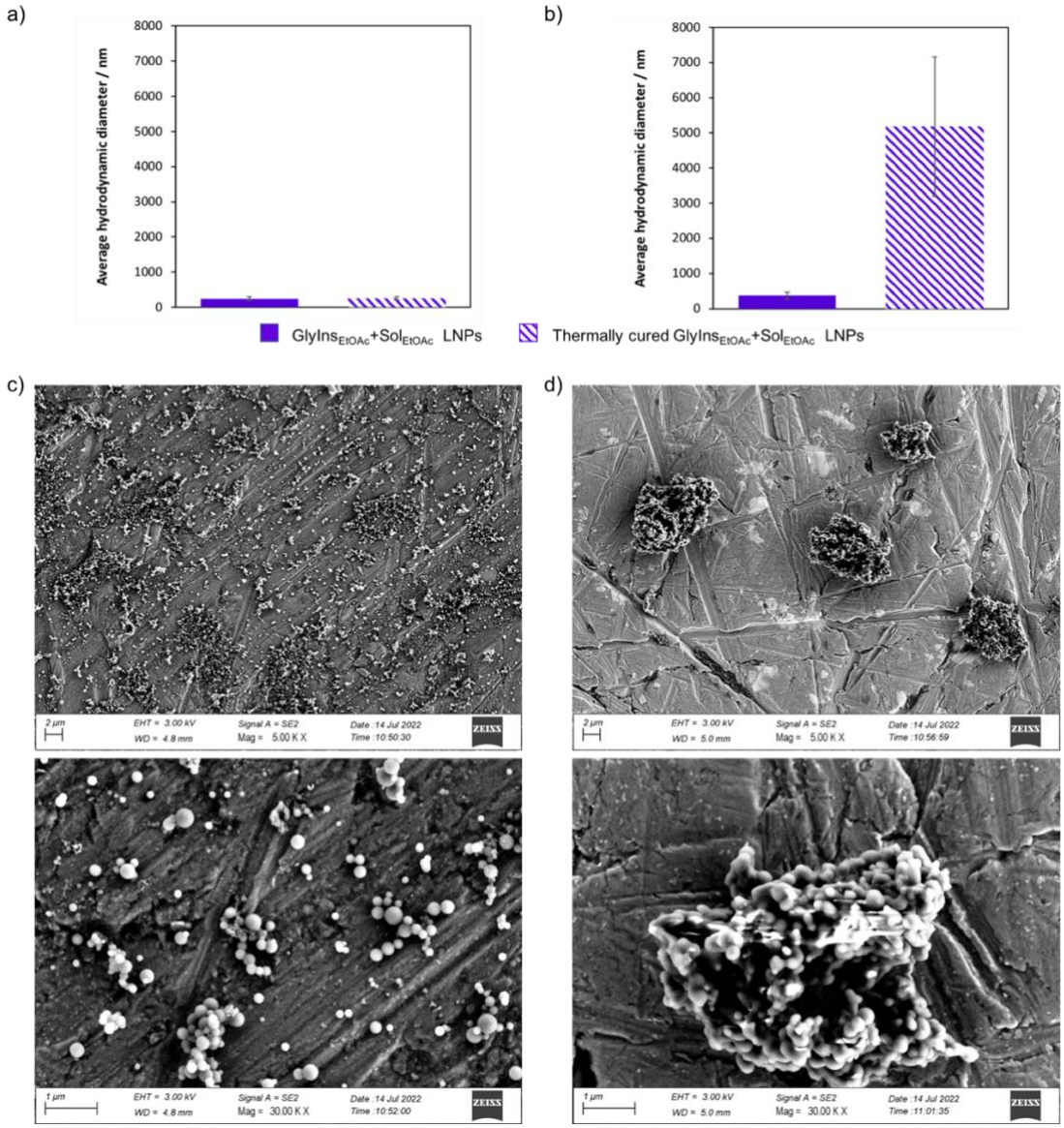

Figure 52. Dimensional analysis by DLS of GlyIns$_{EtOAc}$+Sol$_{EtOAc}$ LNPs produced on small (a) and large (b) scale before and after thermal curing (105 °C, 16 h). SEM images of thermally cured GlyIns$_{EtOAc}$+Sol$_{EtOAc}$ LNPs produced on small (c) and large (d) scale.

Parallelly, after curing, the presumed interparticle crosslinking of Ins$_{EtOAc}$+GlySol$_{EtOAc}$LNPs was expected to produce a strong filler-filler network which was hoped to induce the immobilisation of a high fraction of rubber and impart a strong reinforcement to the compound. The thermal curing of such particles resulted in an agglomeration of intraparticle crosslinked LNPs, as evidenced by DLS and SEM images (Figure 53).

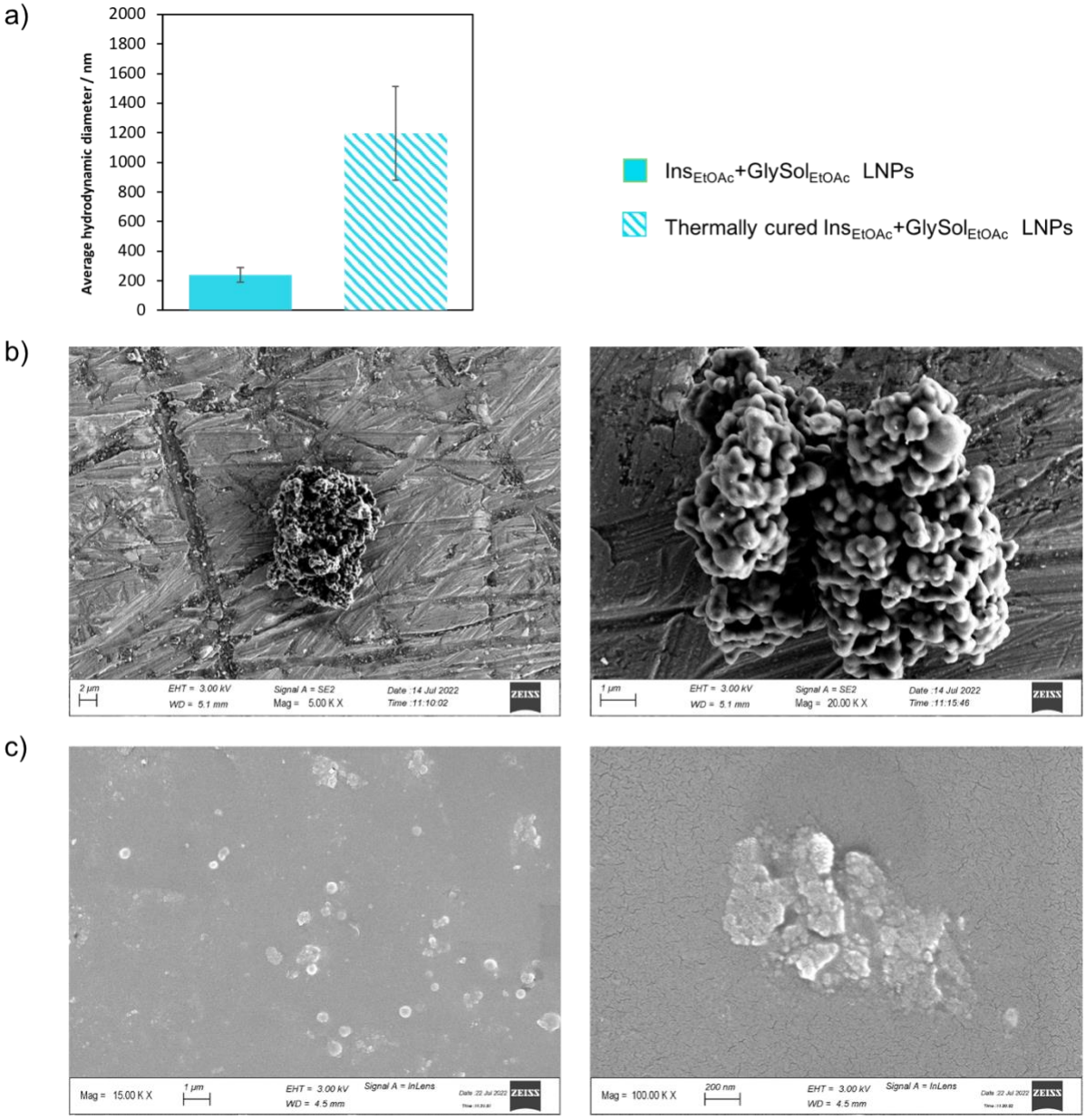

Figure 53. Dimensional analysis by DLS of Ins_{EtOAc}+$GlySol_{EtOAc}$ LNPs produced on large scale before and after thermal curing at 105 °C for 16 h (a). SEM images of thermally cured $GlyIns_{EtOAc}$+Sol_{EtOAc} LNPs produced on large scale (b). SEM images of masterbatches of natural rubber including 100 phr of thermally cured $GlyIns_{EtOAc}$+Sol_{EtOAc} LNPs (c).

Both systems of nanoparticles *NR 50LNP GlyIns S* and *NR 50LNP GlySol S* showed an enhanced dispersion in the polymeric matrix with respect to the reference compound *NR 50L S*, as shown by the high ratios between stresses at 300% and 100% deformation. Both innovative composites proved stronger than the reference which proved the better efficacy of such materials as reinforcing fillers than micrometric unmodified lignin (Figure 51). While hysteresis values were comparable in the three systems

under examination, an intriguing improvement of the storage modulus was observed only for the compound including thermally cured $GlyIns_{EtOAc}$+Sol_{EtOAc} LNPs. As for thermally crosslinked Ins_{EtOAc}+$GlySol_{EtOAc}$ LNPs, SEM images (Figure 53) showed an agglomerated morphology of micrometric size that was further confirmed by DLS (Figure 53), which did not correspond to the desired structured, necklace-like filler-filler network of nanobeads exposing a high surface area to the polymer macromolecules and guaranteeing a high number of interactions with them. As a result, such particles acted like, or even worse, than unmodified lignin and did not display the expected reinforcement. In order to take advantage of the possibility to covalently bind the spherical nanoparticles into a sort of necklace-like network, which is to the best of our knowledge something still not attempted in literature for organic nanoparticles, further studies would be needed.

The dynamic compression tests evidenced that *NR 50L S* and NR 50LNP GlyIns S shared similar dynamic modulus and hysteresis values, while *NR 50LNP GlySol S* proved not as performant as the other two compounds.

13.2.2 NR composites including carbon black and diverse nanolignins as fillers

The presence of lignin nanoparticles as monofiller in NR compounds resulted in an improvement of the mechanical performances with respect to micrometric unmodified lignin. However, LNPs were not associated to high reinforcement values considered relevant from a technological point of view, even when their content in the composite reached 50 phr. In order to obtain technologically applicable results, it was thus decided to explore the possibility to use nanolignin in association with carbon black as reinforcing filler. Such an approach was hoped to produce innovative systems with comparable or even improved mechanical performances with respect to reference compounds reinforced solely with carbon black while increasing the content of renewable materials in the composite.

The study included the evaluation of the mechanical properties of NR compounds reinforced with 50 phr of fillers (

Table 34), *i.e.*, carbon black and mixtures of different proportion of carbon black with unmodified micrometric lignin, small and large lignin nanoparticles with an average hydrodynamic diameter of 150 and 350 nm, respectively.

Table 34. NR composites including nanolignin codried with NR, carbon black as co-filler.

Components and formulation in phr	NR 50CB S	NR 40CB+ 10L S	NR 25CB+ 25L S	NR 40CB+ 10LNP Small S	NR 40CB+ 10LNP Large S	NR 25CB+ 25LNP Small S	NR 25CB+ 25LNP Large S
Natural rubber (SIR20)	100	90	75	90	90	75	75
Codried NR masterbatch, 50% small LNPs				20		50	
Codried NR masterbatch, 50% large LNPs					20		50
Codried NR masterbatch, 50% unmodified lignin		20	50				
Carbon black (N326)	50	40	25	40	40	25	25
Antioxidant (6PPD)	2	2	2	2	2	2	2
Stearic acid	2	2	2	2	2	2	2
Zinc oxide	4	4	4	4	4	4	4
Accelerant TBBS	1.8	1.8	1.8	1.8	1.8	1.8	1.8
66 % wt oil-extended sulfur	4	4	4	4	4	4	4
Tensile properties							
Stress at 300% deformation / Stress at 100% deformation	5.169	4.734	3.608	4.386	4.326	3.507	3.593
Stress at 50% deformation / MPa	1.740	1.52	1.25	1.54	1.67	1.34	1.39
Stress at 100% deformation / MPa	3.320	2.59	1.89	2.77	2.98	2.25	2.31
Stress at 300% deformation / MPa	17.160	12.26	6.82	12.15	12.89	7.89	8.3
Stress at break / MPa	25.140	20.79	17.68	23.22	22.31	20.54	19.68
Elongation at break / %	393.280	409.34	483.45	457.66	439.00	520.67	508.85
Energy/ $J \cdot cm^{-3}$	40.90	33.13	30.26	43.04	40.73	40.43	39.66
Vulcanisation kinetics (170 °C, 10 min) and dynamo-mechanical properties							
ML (moment lowest) / dN·m	2.57	1.87	1.84	2.21	2.05	1.87	1.78
MH (moment highest) / dN·m	22.00	17.78	12.55	18.58	19.02	14.54	15.21
T90 / min	2.26	2.39	2.33	2.56	2.32	2.65	2.52
TS2 / min	0.91	1.03	1.17	1.03	0.83	1.11	0.93
dG' (0.4 - 10 % deformation) / MPa	0.99	0.63	0.23	0.69	0.74	0.24	0.30
G' at 9 % deformation / MPa	1.487	1.225	0.957	1.279	1.365	0.982	1.086
tanδ at 9 % deformation	0.109	0.084	0.056	0.094	0.094	0.064	0.075

Compression dynamics

23 °C, 1 Hz	E' / MPa	5.321	4.617	3.808	4.825	5.101	4.156	4.209
	Tanδ	0.104	0.075	0.049	0.088	0.092	0.060	0.083
23 °C, 10 Hz	E' / MPa	5.662	4.857	3.978	5.119	5.410	4.373	4.512
	Tanδ	0.115	0.089	0.063	0.101	0.109	0.075	0.095
23 °C, 100 Hz	E' / MPa	6.083	5.175	4.202	5.490	5.825	4.656	4.871
	Tanδ	0.166	0.142	0.112	0.152	0.162	0.125	0.144
70 °C, 1 Hz	E' / MPa	4.992	4.328	3.668	4.502	4.748	4.016	3.990
	Tanδ	0.085	0.067	0.052	0.075	0.082	0.060	0.072
70 °C, 10 Hz	E' / MPa	5.234	4.525	3.838	4.730	4.993	4.211	4.224
	Tanδ	0.092	0.070	0.054	0.080	0.081	0.056	0.077
70 °C, 100 Hz	E' / MPa	5.557	4.768	4.036	5.019	5.276	4.422	4.517
	Tanδ	0.108	0.087	0.070	0.096	0.103	0.078	0.095
100 °C, 1 Hz	E' / MPa	5.193	4.514	3.837	4.655	4.813	4.094	4.051
	Tanδ	0.075	0.058	0.046	0.067	0.075	0.053	0.065
100 °C, 10 Hz	E' / MPa	5.393	4.672	3.970	4.842	5.027	4.270	4.241
	Tanδ	0.078	0.060	0.048	0.069	0.075	0.053	0.069
100 °C, 100 Hz	E' / MPa	5.641	4.856	4.133	5.056	5.254	4.447	4.473
	Tanδ	0.091	0.074	0.060	0.082	0.090	0.067	0.083

The substitution of 10 phr of carbon black (*NR 50CB S*) with the same amount of lignin (*NR 40CB+10L S*, *NR 40CB+10LNPSmall S* and *NR 40CB+10LNPLarge S*) resulted in an increase in the elongation at break and a decrease in the stress at break which however improved in the case of LNPs (*NR 40CB+10LNPSmall S* and *NR 40CB+10LNPLarge S*) which nearly reached the same values as reference compound containing pure CB. In LNP-based composites, the strain energy density, the energy required to deform the material corresponding to the area under the load strain-stress curve, was similar to if not even higher than the same parameter in reference compound reinforced solely with carbon black. While the partial replacement of carbon black was connected to a decrease in the crosslink density, the nanometric size of LNPs was associated to an improvement of this parameter. Remarkably, the combination of 40 phr of CB with 10 phr of either small or large LNPs resulted in a higher reinforcement. Nanolignin was associated to a noteworthy reduction in Payne effect with respect to pure CB and micrometric lignin, resulting in mechanical properties which did not drop under strong deformations. Both shear (G') and compression (E') moduli showed the same trend, improving from micrometric lignin to small LNPs, finally reaching the highest values for both large LNPs and carbon black. Outstandingly, the dynamic tanδ related to the composite containing large LNPs experienced smaller variations with temperature if compared to the other compounds under investigation, proving a little dependence of the mechanical behaviours on the working temperature.

The content of renewable materials in rubber compounds was further increased by replacing half of the carbon black with the corresponding amount of unmodified micrometric lignin (*NR 25CB+25L S*), small (*NR 25CB+25LNPSmall S*) and large (*NR 25CB+25LNPLarge S*) LNPs. The energy density was similar for composites including pure carbon black and LNPs, while it was lower in the case of unmodified lignin. The presence of LNPs was associated with a higher elongation at break with respect to pure CB and CB-unmodified lignin blends. The dispersion of the fillers inside the elastomeric matrix (estimated by the ratio between the stresses at 300 % and 100 % deformation) was excellent for the reference compound reinforced with pure CB while it was 30 % lower for lignin-containing composites, probably due to the mutual interactions between lignin and carbon black which are not as ideal as the CB-CB ones. Stress at break decreased when partially replacing CB with lignin, however it upgraded in the case of LNPs nearly reaching the same values as reference compound containing pure CB. The shear storage modulus G' increased from micrometric lignin to small LNPs and then to large LNPs, reaching its maximum with pure CB. Interestingly, the E' compression modulus of composites reinforced with LNPs-CB blends resembled the one of *NR 50CB S* and their hysteresis was even lower, this leading to an overall improvement of mechanical performances of composites while increasing the content of bio-based materials.

References

[1] D. E. Hall, J. C. Moreland, *Rubber Chem. Technol.* **2001**, *74*, 525.

[2] Group Industrial Plan sustainability targets.

[3] N. A. Mohamad Aini, N. Othman, M. H. Hussin, K. Sahakaro, N. Hayeemasae, *Front. Mater.* **2020**, *6*.

[4] P. Frigerio, L. Zoia, M. Orlandi, T. Hanel, L. Castellani, *BioResources* **2014**, *9*, 1387.

[5] D. Barana, S. D. Ali, A. Salanti, M. Orlandi, L. Castellani, T. Hanel, L. Zoia, *ACS Sustain. Chem. Eng.* **2016**, *4*, 5258.

[6] D. K. Setua, M. K. Shukla, V. Nigam, H. Singh, G. N. Mathur, *Polym. Compos.* **2000**, *21*, 988.

[7] M. Paravidino, U. Hanefeld, *Green Chem.* **2011**, *13*, 2651.

[8] F. A. Carey, R. J. Sundberg, *Advanced Organic Chemistry: Part A: Structure and Mechanisms*, Springer Science & Business Media, **2007**.

[9] A. Tagami, C. Gioia, M. Lauberts, T. Budnyak, R. Moriana, M. E. Lindström, O. Sevastyanova, *Ind. Crops Prod.* **2019**, *129*, 123.

[10] A. Salanti, M. Orlandi, H. Lange, F. Ferruti, L. Zoia, *ACS Sustain. Chem. Eng.* **2022**, *10*, 11680.

[11] A. Papon, K. Saalwächter, K. Schäler, L. Guy, F. Lequeux, H. Montes, *Macromolecules* **2011**, *44*, 913.

[12] S. Beisl, A. Miltner, A. Friedl, *Int. J. Mol. Sci.* **2017**, *18*, 1244.

[13] M. H. Sipponen, H. Lange, M. Ago, C. Crestini, *ACS Sustain. Chem. Eng.* **2018**, *6*, 9342.

[14] K. M. Koeller, C.-H. Wong, *Nature* **2001**, *409*, 232.

[15] K. Yang, Y.-J. Wang, *Biotechnol. Prog.* **2003**, *19*, 1664.

[16] M. J. Alston, R. B. Freedman, *Biotechnol. Bioeng.* **2002**, *77*, 641.

[17] U. T. Bornscheuer, R. J. Kazlauskas, *Hydrolases in Organic Synthesis: Regio- and Stereoselective Biotransformations*, John Wiley & Sons, **2006**.

[18] U. Weißbach, S. Dabral, L. Konnert, C. Bolm, J. G. Hernández, *Beilstein J. Org. Chem.* **2017**, *13*, 1788.

[19] X. Guo, X. Junna, M. P. Wolcott, J. Zhang, *ChemistrySelect* **2016**, *1*, 3449.

[20] X. Zhao, Y. Zhang, M. Yang, Z. Huang, H. Hu, A. Huang, Z. Feng, *Polymers* **2018**, *10*, 907.

[21] J. Otera, *Chem. Rev.* **1993**, *93*, 1449.

[22] M. Habulin, Ž. Knez, *J. Mol. Catal. B Enzym.* **2009**, *58*, 24.

[23] A. Granata, D. S. Argyropoulos, *J. Agric. Food Chem.* **1995**, *43*, 1538.

[24] X. Guo, J. Xin, J. Huang, M. P. Wolcott, J. Zhang, *Polymer* **2019**, *183*, 121859.

[25] T. Kleine, J. Buendia, C. Bolm, *Green Chem* **2013**, *15*, 160.

[26] J. Liu, H.-F. Liu, L. Deng, B. Liao, Q.-X. Guo, *J. Appl. Polym. Sci.* **2013**, *130*, 1736.

[27] H. Wang, W. Liu, J. Huang, D. Yang, X. Qiu, *Polymers* **2018**, *10*, 1033.

[28] P. Ghosh, S. Katare, P. Patkar, J. M. Caruthers, V. Venkatasubramanian, K. A. Walker, *Rubber Chem. Technol.* **2003**, *76*, 592.

[29] F. Bueche, *J. Appl. Polym. Sci.* **1961**, *5*, 271.

[30] D. Y. Kim, J. W. Park, D. Y. Lee, K. H. Seo, *Polymers* **2020**, *12*, 2020.

[31] H. J. Kim, G. R. Hamed, *Rubber Chem. Technol.* **2000**, *73*, 743.

[32] C. Crestini, H. Lange, M. Sette, D. S. Argyropoulos, *Green Chem.* **2017**, *19*, 4104.

[33] O. Sevastyanova, M. Helander, S. Chowdhury, H. Lange, H. Wedin, L. Zhang, M. Ek, J. F. Kadla, C. Crestini, M. E. Lindström, *J. Appl. Polym. Sci.* **2014**, *131*.

[34] M. Gigli, C. Crestini, *Green Chem.* **2020**, *22*, 4722.

[35] H. Sadeghifar, D. S. Argyropoulos, *ACS Sustain. Chem. Eng.* **2015**, *3*, 349.

[36] A. Salanti, M. Orlandi, L. Zoia, *ACS Sustain. Chem. Eng.* **2020**, *8*, 8279.

[37] A. Salanti, L. Zoia, M. Orlandi, F. Zanini, G. Elegir, *J. Agric. Food Chem.* **2010**, *58*, 10049.

[38] B. Albinsson, S. Li, K. Lundquist, R. Stomberg, *J. Mol. Struct.* **1999**, *508*, 19.

[39] C. Gioia, G. Lo Re, M. Lawoko, L. Berglund, *J. Am. Chem. Soc.* **2018**, *140*, 4054.

[40] L. Zoia, A. Salanti, P. Frigerio, M. Orlandi, *BioResources* **2014**, *9*, 6540.

[41] A. Duval, F. Vilaplana, C. Crestini, M. Lawoko, *Holzforschung* **2016**, *70*, 11.

[42] T. Xu, N. Zhang, H. L. Nichols, D. Shi, X. Wen, *Mater. Sci. Eng. C* **2007**, *27*, 579.

[43] Q. Lu, M. Zhu, Y. Zu, W. Liu, L. Yang, Y. Zhang, X. Zhao, X. Zhang, X. Zhang, W. Li, *Food Chem.* **2012**, *135*, 63.

[44] G. Milczarek, O. Inganäs, *Science* **2012**, *335*, 1468.

[45] S. Beisl, A. Friedl, A. Miltner, *Int. J. Mol. Sci.* **2017**, *18*, 2367.

[46] F. Xiong, Y. Han, S. Wang, G. Li, T. Qin, Y. Chen, F. Chu, *Ind. Crops Prod.* **2017**, *100*, 146.

[47] M. Lievonen, J. J. Valle-Delgado, M.-L. Mattinen, E.-L. Hult, K. Lintinen, M. A. Kostiainen, A. Paananen, G. R. Szilvay, H. Setälä, M. Österberg, *Green Chem.* **2016**, *18*, 1416.

[48] M.-L. Mattinen, J. J. Valle-Delgado, T. Leskinen, T. Anttila, G. Riviere, M. Sipponen, A. Paananen, K. Lintinen, M. Kostiainen, M. Österberg, *Enzyme Microb. Technol.* **2018**, *111*, 48.

[49] G. Tamura, Y. Shinohara, A. Tamura, Y. Sanada, M. Oishi, I. Akiba, Y. Nagasaki, K. Sakurai, Y. Amemiya, *Polym. J.* **2012**, *44*, 240.

[50] I. V. Pylypchuk, P. A. Lindén, M. E. Lindström, O. Sevastyanova, *ACS Sustain. Chem. Eng.*

2020, *8*, 13805.

[51] I. V. Pylypchuk, A. Riazanova, M. E. Lindström, O. Sevastyanova, *Green Chem.* **2021**, *23*, 3061.

[52] S. R. Saptarshi, A. Duschl, A. L. Lopata, **2013**, 12.

[53] E. Nugroho Prasetyo, T. Kudanga, L. Østergaard, J. Rencoret, A. Gutiérrez, J. C. del Río, J. Ignacio Santos, L. Nieto, J. Jiménez-Barbero, A. T. Martínez, J. Li, G. Gellerstedt, S. Lepifre, C. Silva, S. Y. Kim, A. Cavaco-Paulo, B. Seljebakken Klausen, B. F. Lutnaes, G. S. Nyanhongo, G. M. Guebitz, *Bioresour. Technol.* **2010**, *101*, 5054.

[54] C. Cui, H. Sadeghifar, S. Sen, D. S. Argyropoulos, **2013**, 23.

[55] T. Leskinen, M. Smyth, Y. Xiao, K. Lintinen, M.-L. Mattinen, M. A. Kostiainen, P. Oinas, M. Österberg, *Nord. Pulp Pap. Res. J.* **2017**, *32*, 586.

[56] T. Zou, N. Nonappa, M. Khavani, M. Vuorte, P. Penttilä, A. Zitting, J. J. Valle-Delgado, A. M. Elert, D. Silbernagl, M. Balakshin, M. Sammalkorpi, M. Österberg, *J. Phys. Chem. B* **2021**, *125*, 12315.

[57] D. Barana, S. D. Ali, A. Salanti, M. Orlandi, L. Castellani, T. Hanel, L. Zoia, *ACS Sustain. Chem. Eng.* **2016**, *4*, 5258.

[58] M. Österberg, M. H. Sipponen, B. D. Mattos, O. J. Rojas, *Green Chem.* **2020**, *22*, 2712.

[59] F. Xiong, Y. Han, G. Li, T. Qin, S. Wang, F. Chu, *Ind. Crops Prod.* **2016**, *83*, 663.

[60] V. Ponnuchamy, O. Gordobil, R. H. Diaz, A. Sandak, J. Sandak, *Int. J. Biol. Macromol.* **2021**, *168*, 792.

[61] F. Ferruti, I. Pylypchuk, L. Zoia, H. Lange, M. Orlandi, A. Moreno, M. H. Sipponen, *Green Chem.* **2023**.

[62] T. Zou, M. H. Sipponen, A. Henn, M. Österberg, *ACS Nano* **2021**, *15*, 4811.

[63] V. Passoni, C. Scarica, M. Levi, S. Turri, G. Griffini, *ACS Sustain. Chem. Eng.* **2016**, *4*, 2232.

[64] A.-S. Jääskeläinen, T. Liitiä, A. Mikkelson, T. Tamminen, *Ind. Crops Prod.* **2017**, *103*, 51.

[65] M. B. Agustin, P. A. Penttilä, M. Lahtinen, K. S. Mikkonen, *ACS Sustain. Chem. Eng.* **2019**, *7*, 19925.

[66] A. Moreno, M. H. Sipponen, *Mater. Horiz.* **2020**, *7*, 2237.

[67] S. Beisl, J. Adamcyk, A. Friedl, H. Ejima, *Colloid Interface Sci. Commun.* **2020**, *38*, 100306.

[68] ASTM, *ASTM D4690, Standard Specification for Urea-Formaldehyde Resin Adhesives*, **2012**.

[69] R. Jingxian Li, J. Gutierrez, Y.-L. Chung, C. W. Frank, S. L. Billington, E. S. Sattely, *Green Chem.* **2018**, *20*, 1459.

[70] K. A. Henn, S. Forssell, A. Pietiläinen, N. Forsman, I. Smal, P. Nousiainen, R. P. B. Ashok,

P. Oinas, M. Österberg, *Green Chem.* **2022**.

[71] L. G. Greca, K. J. D. France, J. Majoinen, N. Kummer, O. I. V. Luotonen, S. Campioni, O. J. Rojas, G. Nyström, B. L. Tardy, *J. Mater. Chem. A* **2021**, *9*, 19741.

[72] H. Liu, Y. Feng, X. Cao, B. Luo, M. Liu, *ACS Appl. Mater. Interfaces* **2021**, *13*, 11356.

[73] B. L. Tardy, J. J. Richardson, L. G. Greca, J. Guo, H. Ejima, O. J. Rojas, *Adv. Mater.* **2020**, *32*, 1906886.

[74] R. A. Sheldon, *Green Chem.* **2007**, *9*, 1273.

[75] J. Andraos, *Green Process. Synth.* **2019**, *8*, 324.

[76] S. Thomas, R. Stephen, *Rubber nanocomposites: preparation, properties, and applications*, John Wiley & Sons, **2010**.

[77] M. Abdalla, D. Dean, D. Adibempe, E. Nyairo, P. Robinson, G. Thompson, *Polymer* **2007**, *48*, 5662.

[78] S. Thomas, H. J. Maria, *Progress in rubber nanocomposites*, Woodhead Publishing, **2016**.

[79] G. Momen, M. Farzaneh, *Rev Adv Mater Sci* **2011**, *27*, 1.

[80] G. Kortaberria, L. Solar, A. Jimeno, P. Arruti, C. Gomez, I. Mondragon, *J. Appl. Polym. Sci.* **2006**, *102*, 5927.

[81] A. Rangan, M. V. Manjula, K. G. Satyanarayana, R. Menon, *Biodegrad. Green Compos.* **2016**, 167.

[82] L. Cao, J. Huang, J. Fan, Z. Gong, C. Xu, Y. Chen, *Polym. Rev.* **2022**, *62*, 549.

CONCLUSIONS

Rubber compounds need reinforcing fillers to enhance their mechanical properties. Effective bio-based reinforcing fillers for tyre applications were produced as an alternative to conventional, environment-threatening fossil-based materials. The goal was developing tyre compounds minimising impacts on people and environment while maximising performances, with a particular focus on storage modulus and hysteresis, respectively related to mechanical strength and rolling resistance. In particular, the possibility to develop different materials form softwood kraft lignin was investigated. This resource was selected for its availability at industrial scale and its high, yet underexploited, potentialities. Its incorporation in an elastomeric matrix could not be straightforward due to the limited compatibility between lignin and rubber. It was necessary to enhance filler-matrix interactions to detect an improvement in the mechanical performances.

An innovative mechanochemical procedure was set up for the chemical modification of lignin. Mechanochemistry allowed running reactions in the solid state, avoiding organic solvents, limiting work-up procedures and reducing wastes with respect to wet chemistry syntheses. In particular, aliphatic alcohols and phenols in lignin were esterified in the presence of a base as activator and enol ester as acyl donor. The study of the role of the activator evidenced the need for an alkaline compound to trigger the desired functionalisation. In the tested experimental conditions, a hydroxide or carbonate of alkali metals was required to deprotonate acidic hydoxyl groups in lignin, while bases of alkaline earth metals proved ineffective. This observation could be ascribed to the inefficiency of divalent cations to act as a counterion for lignin alkoxides in the solid state. The employment of enol esters instead of more conventional acyl donors, *i.e.*, anhydrides and acyl chlorides, was associated to a high atom efficiency and the avoidance of halogenated reagents. The release of an enol, which easily tautomerised to the corresponding ketoform, constituted the driving force for the formation of the desired ester and rendered the reaction irreversible. In screening efforts, methyl esters proved ineffective since their use was not associated to the release of any good leaving group. The use of enol esters, particularly vinyl and isopropenyl esters, was accompanied by the functionalisation of the targeted groups, reaching 35 % of conversion. This procedure gave the desired functionalisation in two types of lignin, *i.e.*, herbaceous alkaline and softwood kraft lignin. In both cases the mechanochemical treatment was not associated to any degradation of the starting material, lignin was not broken down in lower molecular weight fragments. These evidences demonstrated that this innovative synthetic procedure could be applied to lignin with different botanical source and isolation process without significantly compromising their integrity. The procedure was consequently scaled up to a 5 g scale to obtain consistent batches for the production of rubber composites.

The mechanical performances of innovative NR/SBR and NR/BR compounds were investigated. In all compounds, dynamic mechanical tests evidenced that methacrylation ensured an enhanced compatibilisation, hence, dispersion of lignin inside the elastomeric matrix with respect to milled lignin. Methacrylation of lignin was also associated to an increased stiffness and resistance to solvent swelling with respect to composites void of functionalised lignin. These phenomena were connected to a restriction in polymer chain dynamics of the rubber layers in direct contact with the filler. These observations confirmed that methacrylated lignin was covalently bound to rubber molecules during vulcanisation. In particular, NR/SBR compounds were studied in order to develop tyre treads including a mixture of silica and lignin as reinforcing fillers. In the case of peroxide-vulcanised composites, functionalised lignin, when associated to silica, was accompanied by higher storage modulus and lower hysteresis values than milled lignin, the latter property reaching the same value as reference compound including silica as unique filler. However, peroxide-based vulcanisation is not as technologically relevant as the sulphur-based one. In sulphur-vulcanised compounds, methacrylated lignin in association with silica was correlated to higher storage modulus than milled lignin. The addition of lignin on top of silica was also associated with an increase in hysteresis which slightly improved in the case of methacrylated lignin with respect to milled lignin even if not achieving the same performances as silica. NR/BR compounds including lignin as reinforcing fillers were studied for their possible application for tyre sidewalls. In peroxide-vulcanised formulations, functionalised lignin associated to silica was correlated to improved tensile properties and hysteresis. In sulphur-cured composites, methacrylated lignin in combination with and partial substitution to carbon black was accompanied by a noteworthy increment in storage modulus, however joined by an increment in hysteresis.

The structural complexity of lignin required a deeper investigation of its structure and a refinement. The heterogeneity of lignin was overcome by solvent extraction. A combination of quantitative ^{31}P NMR and GPC equipped with fluorescent detector allowed defining crucial structural characteristics of hardwood and softwood kraft lignins and their fractions. The analytical procedure allowed for a deep insight on lignin structure with a particular focus on phenolic group distribution as a function of molecular weight without resorting to extremely expensive laboratory equipment. The method assessed the homogeneity of phenolic distribution as a function of molecular weight in fractions isolated by solvent extraction. These analyses proved that the extraction procedure was effective in isolating groups of macromolecules which were homogeneous in terms of phenol distribution alongside the molecular weight ranges.

Insights into correlations between molecular weight characteristics and phenolic group content, or more generally hydroxyl group content, represents a prerequisite for insightful lignin valorisations. The results obtained in the structural investigation evidence the importance of solvent extraction of softwood kraft lignin for isolating fractions with specific molecular weight ranges and phenolic group distribution. This approach was exploited in an applicative fashion in the development of lignin nanoparticles (LNPs) with tuneable properties. The aim was to use those lignin nanoparticles as reinforcing agents for rubber compounds, taking advantage of the high mechanical reinforcement associated to the nanodimensions of the filler. After single-step solvent extraction of softwood kraft lignin, high and low molecular weight fractions were separately epoxidised. LNPs were prepared by nanoprecipitation induced by solvent polarity shift in a material-efficient way so that the whole starting material was recovered and valorised. LNPs obtained by recombining the epoxidised high MW fraction and the corresponding low MW fraction proved dimensionally stable under alkaline conditions after thermal curing, endorsing the hypothesis that epoxidised high MW fractions constituted the core of LNPs obtained by nanoprecipitation. The dimensional stability of those internally crosslinked LNPs in alkaline conditions sounded promising for their mixing with natural rubber latex stabilised by ammonia for the production of rubber compounds. By the same recombinational approach, LNPs with a surface-specific covalent functionalisation were prepared by merging the epoxidised low MW fraction and the corresponding high MW fraction. Upon thermal curing, these LNPs experienced interparticle crosslinking which sounded intriguing for the possibility to develop structured reinforcing fillers for rubber compounds. Interparticle-crosslinked nanoparticles exhibited competitive adhesive performances for aminated glass. The inclusion of lignin nanoparticles in rubber composites is an explored field of research. For this reason, model NR composites including LNPs were studied for possible applications for tyre internal compounds. LNPs of different dimensions, *i.e.*, 150 and 350 nm of hydrodynamic diameter, were investigated. LNPs proved to preserve their size when mixed with rubber latex. When used as unique fillers, small and large LNPs dispersed better in the elastomeric matrix than micrometric lignin. Small LNPs were accompanied with improved reinforcement with respect to micrometric lignin and large LNPs. This result was in agreement with the higher surface area of those particles compared to the other ones as such having more interactions with the macromolecules of the polymeric matrix whose motions resulted restricted and guaranteeing a high fraction of immobilised rubber. While small LNPs showed similar hysteresis to micrometric lignin, large LNPs displayed the same reinforcement as the compound including micrometric lignin but extraordinarily low hysteresis. The scale up of the production of intra- and inter-particle crosslinked LNPs did not succeed due to the higher concentrations required during the realisation of the scale. While internally cured LNPs displayed higher storage modulus than micrometric lignin, intraparticle-crosslinked LNPs resulted in a micrometric agglomerate which exhibited the same

mechanical effects as micrometric lignin in rubber composites. LNPs as unique fillers did not ensure the high reinforcement values relevant from a technological point of view. The partial substitution of CB with LNPs was associated to a noteworthy reduction in Payne effect with respect to pure CB and micrometric lignin, resulting in mechanical properties which did not drop under strong deformations. Interestingly, the compression modulus of composites reinforced with LNPs-CB blends resembled the one of pure-CB compounds and their hysteresis was even lower, this leading to an overall improvement of mechanical performances of composites while increasing the content of bio-based materials.

In conclusion, the chemical modification of lignin with groups reactive to vulcanisation proved useful in improving the storage modulus of rubber compounds when modified lignin partially replaced silica or carbon black. However, in those systems the hysteresis values were higher than in elastomeric composites including only traditional fillers. Insightful generated innovative nanolignin with tunable inter- and intralinking possibilities gave intriguing results when partially replacing carbon black, enhancing the mechanical properties of compounds while incrementing the content of bio-based materials. The two approaches could be combined to obtain nanolignins functionalised at the surface with groups active to vulcanisation, with the aim of further increasing the content of renewable materials at the expense of fossil-based ones while improving the mechanical performances of elastomeric compounds.